



HAL
open science

Contribution of kinetic electrons in Tokamak plasmas

Charles Ehrlacher

► **To cite this version:**

Charles Ehrlacher. Contribution of kinetic electrons in Tokamak plasmas. Plasma Physics [physics.plasm-ph]. Université Paris Saclay (COMUE), 2018. English. NNT: 2018SACLX033 . tel-01891837

HAL Id: tel-01891837

<https://pastel.hal.science/tel-01891837>

Submitted on 10 Oct 2018

HAL is a multi-disciplinary open access archive for the deposit and dissemination of scientific research documents, whether they are published or not. The documents may come from teaching and research institutions in France or abroad, or from public or private research centers.

L'archive ouverte pluridisciplinaire **HAL**, est destinée au dépôt et à la diffusion de documents scientifiques de niveau recherche, publiés ou non, émanant des établissements d'enseignement et de recherche français ou étrangers, des laboratoires publics ou privés.



Contribution des électrons cinétiques dans les plasmas de Tokamak

Thèse de doctorat de l'Université Paris-Saclay
préparée à l'École Polytechnique

École doctorale n°572 Ondes et Matières (EDOM)
Spécialité de doctorat: Physique des Plasmas

Thèse présentée et soutenue à Palaiseau, le 12 juillet 2018, par

Charles Ehrlacher

Composition du Jury :

M. Étienne GRAVIER Professeur, Université de Lorraine	Président
M. Peter BEYER Professeur, Université d'Aix-Marseille	Rapporteur
M. Étienne GRAVIER Professeur, Université de Lorraine	Rapporteur
M. Pierre MOREL Docteur, École Polytechnique – LPP	Examineur
M. Jean-Marcel RAX Professeur, École Polytechnique	Directeur de thèse
M. Yanick SARAZIN Docteur, CEA – IRFM	Co-Directeur de thèse
Mme Virginie GRANDGIRARD Docteur, CEA – IRFM	Responsable CEA

Remerciements

Tout d'abord, je souhaiterais remercier chaleureusement M. Jean-Marcel Rax qui m'a accueilli à bras ouverts dans le monde de la fusion, que j'ai eu le plaisir d'avoir en tant que professeur de master 2 et qui a accepté de diriger cette thèse. Ses enseignements et son livre formidable m'ont accompagné et, j'en suis sûr, m'accompagneront tout au long de ma vie scientifique.

Je tiens à exprimer toute ma gratitude à Yanick Sarazin et Virginie Grandgirard, dont j'ai pu d'abord apprécier le talent pédagogique comme professeurs, et qui ont accepté d'encadrer ce travail de thèse. Leurs grandes qualités scientifiques et humaines, leur enthousiasme pour la recherche et leur grande disponibilité m'ont beaucoup apporté au cours de ces années. Je souhaiterais remercier également Xavier Garbet pour le temps qu'il a consacré, en particulier pour le travail sur la contribution des électrons piégés à l'amortissement des GAMs que je n'aurais jamais pu effectuer seul, et les nombreuses discussions que nous avons eues. Je voudrais aussi témoigner ma reconnaissance à Philippe Ghendrih pour son soutien et ses conseils durant la thèse.

Je suis très reconnaissant envers Peter Beyer et Étienne Gravier d'avoir accepté de rapporter ce travail, ainsi qu'à Pierre Morel d'avoir bien voulu faire partie du jury.

Enfin, je souhaiterais remercier les autres chercheurs avec qui j'ai eu le plaisir d'échanger, en particulier Guilhem Dif-Pradalier, Guillaume Latu, Alessandro Biancalani, Alberto Bottino, Chantal Passeron, Éric Nardon, Nicolas Fedorczak, Guido Ciraolo, Rémi Dumont ainsi que les autres chercheurs de l'IRFM.

L'IRFM est un endroit exceptionnel pour effectuer un doctorat et la bonne ambiance qui y règne y est pour beaucoup! Mes remerciements s'adressent à tous les doctorants, stagiaires et postdocs que j'ai eu le plaisir de côtoyer, notamment les jeunes Peter, Adrien, Anastasia, Camille, Elisabetta, Guillaume, Nicolas, Pierre-Antoine, les moins jeunes Alberto, Axel, Camille, Cristian, Damien, Davide, Jae-Heon, Julien, les Laurents, Ling Feng, Nicolas le footeux, Nicolas l'autre footeux, Olivier, Sarah, et les vénérables Alexandre, Claudia, David, Didier, Étienne, Fabien, François, Hugo, Jean-Baptiste, Jorge, Romain, Thomas, Yuuichi. Sans eux, ce séjour en Provence aurait eu une tout autre saveur.

Enfin, je souhaiterais témoigner toute ma reconnaissance à Océane Gewirtz, Jean-Marie Bourgeois, ainsi qu'à toute l'équipe franco-chinoise de l'IFCEN pour l'excellent accueil et leurs chaleureux encouragements pour finir ce travail de thèse en parallèle des enseignements. Un petit clin d'œil à mes camarades physiciens, notamment Damien qui m'a patiemment supporté... soutenu au cours de cette année et Yunhua qui a été un bon compagnon d'arme pendant les soirées et week-ends de travail.

Mes parents et ma sœur Virginie, m'ont toujours soutenu, que ce soit avant ou pendant ce travail de thèse. J'aimerais les en remercier tous les trois du fond du cœur.

À mes parents,

À ma sœur Virginie.

Contents

Résumé	9
Abstract	11
Introduction	13
1 Particle trajectories & gyrokinetics	19
1.1 Tokamak configuration	20
1.1.1 Torus and canonical coordinates	20
1.1.2 Geometry of the magnetic field	22
1.2 Particle trajectories	24
1.2.1 Derivation of particle velocity	24
1.2.2 Derivation of the Angle-Action coordinates from the motion invariants	27
1.2.3 Characteristics of trapped particles	30
1.3 Gyrokinetic description of a plasma	36
1.3.1 The gyrokinetic model	37
1.3.2 Presentation of some properties of the GYSELA code	39
1.4 Calculation of the particle density in gyrokinetics	42
1.4.1 Link between particles and gyro-centres	42
1.4.2 Expression of the particle density	44
2 Kinetic Electrons in GYSELA	45
2.1 Ion turbulence with adiabatic electrons	45
2.1.1 Quasi-neutrality with adiabatic electrons	46
2.1.2 Limits of the adiabatic electrons approach - Need for kinetic electrons	50
2.2 Quasi-neutrality with kinetic electrons	51
2.3 Filter for (deeply) trapped electrons	54
2.3.1 The advantage of a filter	54
2.3.2 Quasi-neutrality with kinetic filter for electrons	54
2.3.3 Implementation of the kinetic filter for electrons in GYSELA	56
2.4 GYSELA quasi-neutrality solver	59
2.4.1 Normalized quasi-neutrality equation for full kinetic electrons	59

2.4.2	Normalized quasi-neutrality equation for trapped kinetic electrons	61
2.5	Introduction of a pure density source term in GYSELA	65
3	Role of trapped electrons to GAM damping	69
3.1	Dispersion relation of GAM	71
3.1.1	Vlasov equation	71
3.1.2	Linear solution of the Vlasov equation	72
3.1.3	Quasi-electroneutrality	73
3.2	Trajectories and hamiltonian components	75
3.2.1	Trajectories using angle-action variables	75
3.2.2	Fourier components of the hamiltonian	75
3.2.3	Passing particles	76
3.2.4	Trapped particles	77
3.3	Real part of the dispersion relation	78
3.4	GAM damping	80
3.4.1	Contribution of ions to GAM damping	80
3.4.2	Contribution of electrons to GAM damping	81
3.5	Rosenbluth-Hinton test with kinetic electrons	89
3.5.1	Numerical convergence tests with GYSELA	90
3.5.2	Dependence on the radial wave number $k_r \rho_i$	94
3.5.3	Dependence on the mass ratio m_i/m_e	95
3.5.4	Dependence on the safety factor q	96
3.5.5	Dependence on the temperature ratio $\tau_e = T_e/T_i$	96
3.5.6	Conclusion	98
4	Study of the ITG-TEM instability	99
4.1	The ITG and TEM instability	100
4.1.1	Drift wave and interchange mechanisms	100
4.1.2	Dispersion relation in presence of density and temperature gradients	103
4.1.3	Dispersion relation of ITG and TEM	106
4.2	Linear ITG-TEM simulations	112
4.2.1	Parameters used and type of the instability in a linear simulation	112
4.2.2	Numerical study to determine the maximum time step	113
4.2.3	Dependence of the growth rate and pulsation with the toroidal wavenumber	115
4.2.4	Dependence of the growth rate and the pulsation with the ion temperature gradient	116
4.2.5	Normalisation of the value of ρ^* in GYSELA to fit the one in GT5D	119
4.3	Method for non-linear simulations	121
4.3.1	The so-called ω_H mode: a signature of the electrostatic model	122
4.3.2	The aligned coordinates method: a way to reduce the toroidal discretization	123
4.4	First results of non-linear simulations	130
4.4.1	Potential structure	130

4.4.2	Energy conservation	131
4.4.3	Energy transfer between the electric wave and particles	133
4.5	Conclusion	140
Conclusion		141
Appendices		145
A Appendices of chapter 1		147
A.1	Expression of the intrinsic angle θ^*	147
A.2	Change of coordinates from particle to gyrocentre	149
A.2.1	Canonical change of coordinates for \bar{f} : $(\mathbf{q}_{gy}, \mathbf{p}_{gy})$ to $(\mathbf{q}_{GC}, \mathbf{p}_{GC})$	149
A.2.2	Particle versus gyrocentre distribution functions	152
A.3	Expression of the polarization density $n_{s,pol}$	153
B Appendices of chapter 2		157
B.1	Adiabatic particle transport	158
B.2	Computation of $n_{e\mathcal{R}}$	159
B.3	Normalized QN for adiabatic electrons	162
B.3.1	How to overcome the difficulty due to $\langle \phi \rangle_{FS}$ term ?	163
B.3.2	Numerical solving of the quasi-neutrality equation	164
C Appendices of chapter 3		169
C.1	Saturation limit	169
C.2	Angle action variables	170
C.3	Electron Lagrangian using angular variables	172
C.4	Trapped electron Lagrangian	174
C.4.1	Trapped electron Lagrangian for a $\sin \theta$ GAM perturbation	174
C.4.2	Explicit calculation of the electron Lagrangian	175
C.5	Damping rate estimation	177
C.6	Form of the density perturbation to get a sinusoidal potential	178
D Appendices of chapter 4		179
D.1	Conservation equations	179
D.1.1	Matter conservation	179
D.1.2	Energy conservation	181
D.2	The ω_H mode and the kinetic Alfvén wave	184
D.3	Aliasing and Nyquist frequency	185
D.4	Kinetic electrons close to resonance surfaces	186

Résumé

Les plasmas de fusion par confinement magnétique sont le siège d'instabilités qui développent des structures turbulentes d'échelles milli- à centi-métriques. Le transport qui en résulte contrôle le temps de confinement de l'énergie et, in fine, les performances énergétiques. Dans les régimes de confinement non améliorés, c'est une turbulence à l'échelle ionique qui domine ce transport. Cette turbulence est portée par les ions, mais également par une certaine classe d'électrons, ceux qui sont piégés dans les miroirs locaux du champ magnétique. Il est de fait important de prendre en compte leur dynamique, d'autant plus qu'ils sont également responsables du transport de matière. L'objectif de la thèse consiste à étudier l'impact des électrons d'une part, sur l'amortissement des "Geodesic Acoustic Modes" (GAM) d'une part, et sur la croissance linéaire des modes de turbulence "Ion Temperature Gradients" (ITG) et "Trapped Electron Modes" (TEM) d'autre part. Les GAMs sont des oscillations à la fréquence acoustique du potentiel électrique moyen sur les surfaces magnétiques. Ils interagissent de façon critique avec la micro-turbulence au travers notamment de leur couplage au mouvement des particules énergétiques du plasma. Les ITG et TEM représentent les 2 classes d'instabilités électrostatiques dominantes dans le cœur des plasmas de tokamak. Elles sont à ce titre supposées contrôler le transport turbulent de cœur. Cette étude est donc une étape préliminaire pour la prédiction du transport turbulent en prenant en compte l'influence des électrons. Le cadre approprié pour décrire cette turbulence est la théorie dite "gyrocinétique", qui procède d'une réduction de l'espace des phases de 6 dimensions (6D) à $4D + 1$ invariant par une moyenne sur le mouvement rapide cyclotronique. Le problème auto-consistant couple l'équation gyrocinétique pour chaque espèce (ions et électrons) aux équations de Maxwell. Le développement de ce modèle cinétique, construit comme une extension autonome du code GYSELA dont la version de base donne une réponse adiabatique aux électrons, consiste à ajouter le traitement de la fonction de distribution des électrons. Leur prise en compte est coûteuse du point de vue des ressources numériques. Trois stratégies sont envisagées pour réduire ce coût: (i) considérer des "électrons lourds", (ii) filtrer les électrons et ne retenir que ceux qui sont piégés, et (iii) adapter les coordonnées pour découpler les dynamiques parallèle (rapide) et transverse (lente) au champ magnétique.

Après une présentation du modèle gyrocinétique et des caractéristiques du code GYSELA, nous présentons le modèle des électrons adiabatiques tel qu'il est implémenté dans GYSELA et introduisons deux nouveaux modèles: le modèle "Full Kinetic Electrons"

dans lequel les électrons sont considérés comme une espèce cinétique et sont traités de la même façon que les ions et le modèle "Trapped Kinetic Electrons" dans lequel seuls les électrons piégés sont cinétiques, les électrons passants reçoivent quant à eux un traitement adiabatique. On constate que les électrons engendrent un sur-amortissement des GAM lié à une interaction résonante entre la fréquence de rebond de certains électrons piégés et celle des GAMs. Cet amortissement dépend du rapport de masse électron-ion et évolue en $(m_i/m_e)^{-1/2}$. Pour les simulations linéaires sur l'instabilité d'interchange, on retrouve que les modes ITG sont dominants sur les modes TEM pour des forts gradients de température ionique et vice versa, à profil de température électronique fixé. Un accord satisfaisant est obtenu avec le code gyrocinétique GT5D dont les résultats viennent d'être publiés. Enfin, nous proposons quelques méthodes pour construire des cas non linéaires qui permettront d'étudier l'influence des électrons cinétiques sur le transport turbulent.

Abstract

Instabilities, within fusion plasmas by magnetic confinement, develop turbulent structures with milli-centimetric scales. The resulting transport impacts the energy confinement time and, ultimately, the energy performance. In unimproved confinement regimes, ion-scale turbulence generally dominates this transport. This turbulence is carried by the ions, but also by a certain class of electrons, those trapped in the local mirrors of the magnetic field. Taking into account their dynamics is important, especially since they are also responsible for particle transport. The aim of this thesis is to study the impact of electrons on the damping of "Geodesic Acoustic Modes" (GAM) on the one hand and the linear growth of the turbulence modes "Ion Temperature Gradients" (ITG) and "Trapped Electron Modes" (TEM) on the other hand. GAMs are oscillations at the acoustic frequency of the average electric potential on magnetic surfaces. They interact critically with micro-turbulence, particularly through their coupling to the motion of energetic particles in the plasma. ITG and TEM represent the 2 classes of dominant electrostatic instabilities in tokamak core plasmas. As such, they are supposed to control turbulent transport in the core. This study is therefore a preliminary step for the prediction of turbulent transport while taking into account the influence of electrons. The appropriate framework for describing this turbulence is the so-called "gyrokinetic" theory, which proceeds from a 6 dimensions (6D) to $4D + 1$ phase space reduction invariant by an average of the fast cyclotron motion. The self-consistent problem couples the gyrokinetic equation for each species (ions and electrons) to the Maxwell equations. The development of this kinetic model, built as an autonomous extension of the GYSELA code whose basic version gives an adiabatic response to electrons, consists in adding the treatment of the electron distribution function. Taking kinetic electrons into account is costly numerically. Three strategies are envisaged to reduce this cost: (i) consider "heavy electrons", (ii) filter electrons so as to keep only the trapped ones, and (iii) adapt the coordinates to decouple the parallel dynamics (fast) and the transverse one (slow) to the magnetic field.

After a presentation of both the gyrokinetic model and some characteristics of the GYSELA code, we expose the adiabatic electrons model as it is implemented in GYSELA and introduce two new models: the "Full Kinetic Electrons" model in which electrons are treated kinetically in the same way as the ions and the "Trapped Kinetic Electrons" model in which only the trapped electrons are kinetic, the passing electrons receiving an adiabatic treatment. It is found that electrons generate an over-damping of the GAM

explained by a resonant interaction between the bounce frequency of some trapped electrons and that of the GAMs. This damping depends on the electron-ion mass ratio and evolves as $(m_i/m_e)^{-1/2}$. For linear simulations on interchange instability, we find that the ITG modes are dominant over the TEM modes for large ion temperature gradients and vice versa, at finite electron temperature gradient. A satisfying agreement is obtained with the gyrokinetic code GT5D whose results have just been published. Finally, we give some suggestions for future simulations to build non linear cases that could enable to study the influence of kinetic electrons on turbulent transport.

Introduction

Making fusion by magnetic confinement operable on an industrial scale requires that the power coming from the fusion reactions exceeds by a large amount the one needed to keep the fusion reactions alive (external heating of the plasma, power supply to generate the magnetic field configuration). Self heating of the plasma, the so-called "ignition", requires that the heating power coming from the fusion-born α particles balances the power losses. These latter are governed by radiative processes (mainly synchrotron and Bremsstrahlung) and by heat transport across the insulating magnetic configuration. This ignition criterion described by J. D. Lawson [58, Lawson 1957] depends on several parameters of the plasma, including the density n and temperature T of the various species in presence as well as a parameter τ_E called the energy confinement time given by the ratio of the total thermal energy of the plasma divided by the lost power. This criterion of ignition comes down to the triple product which states (for $T_i \in [10 \text{ keV}, 20 \text{ keV}]$):

$$n T_i \tau_E \geq 3 \cdot 10^{21} \text{ keV.s.m}^{-3}$$

We want to know which of these parameters can be changed in order to satisfy this criterion.

- T_i must be high enough for charged nuclei to overcome the Coulomb barrier, at least via the tunnel effect, hence allowing fusion reactions.
- n increases the number of fusion reactions but is limited in fusion reactors by macroscopic instabilities beyond a threshold density called the Greenwald density, which depends on the plasma current. [43, Greenwald 2002]
- τ_E is limited by the losses, including the transport of particles and energy from the core to the edge of the tokamak.

The transport limiting τ_E tends to bring down the temperature of the centre, hence preventing the fusion reactions from taking place. An important part of the research effort is dedicated to increasing τ_E . The energy confinement time can be increased by improving the plasma confinement, i.e. by reducing the level of matter and energy transport from the core to the edge of the tokamak. In the absence of perturbation on the electromagnetic field, the question of particle trajectories in a tokamak is an axisymmetric problem. There are therefore three motion invariants and in this frame the particles are confined. However, the sources of particles and energy as well as the

high density and temperature gradients imply that the system is out of equilibrium. This generates instabilities as well as large particle and energy fluxes, hence breaking the invariance of the system above a certain threshold. These fluxes are dominated by two contributions:

- The **neoclassical transport** which accounts for the enhancement of collisional transport due to large scale particle trajectories in the toroidal magnetic configuration of controlled fusion devices. In the weak collisional regime which characterizes hot fusion plasmas, the neoclassical transport coefficient scales as $\chi_{\text{neo}} \sim q^2 \varepsilon^{-3/2} \chi_{\text{coll}}$ where q stands for the safety factor and $\varepsilon = r/R_0$ stands for the inverse of the aspect ratio [28, Estève 2015]. Besides, a good estimation of the classical transport coefficient is $\chi_{\text{coll}} \sim \rho_i^2 \nu_{\text{coll}}$ with ρ_i the ion Larmor radius and ν_{coll} the collision frequency. For ITER, we have $q \simeq 3$ and $\varepsilon \simeq 1/6$ which leads to an increase of the magnitude of the transport coefficient by a factor 100.
- The **turbulent transport** which is related to the fluctuations of the electric potential. These fluctuations break two invariants of motion: first, the electric and magnetic fields \mathbf{E} and \mathbf{B} vary in time as well as the scalar and vector potentials ϕ and \mathbf{A} . The energy is therefore not invariant in time. Second, fluctuations break the axisymmetry of the tokamak, and consequently, the toroidal kinetic momentum is no more an invariant of the system.

The breaking of the three invariants results in a large transport¹ due in particular to the high density and temperature gradients within the tokamak: as an example, in Tore Supra, the temperature of the ions in the core plasma reaches a few keV. That corresponds to $T_{\text{core}} \sim 150$ MK and $T_{\text{edge}} \sim 300$ K in the edge of the plasma, the minor radius being equal to $a = 0.7$ m. It appears that the understanding of transport mechanisms, particularly turbulent transport is essential for controlled magnetic fusion.

It has been shown that electrons, and in particular those trapped in the magnetic configuration of the tokamak, can have a contribution to turbulent transport comparable to that of ions [60, 19, 77, 6, Liewer 1985, Dannert 2005, Waltz 2007, ITER Physics Basis 2007]. The main objective of this thesis is to evaluate the impact of electrons on two tokamak modes, namely the Geodesic Acoustic Modes (GAM) and the Ion Temperature Gradient instability (ITG) which is driven by ion temperature gradients. In the latter case, we also see the transition where the electron modes become dominant, particularly the Trapped Electron Mode (TEM). This study is carried on in a gyrokinetic model describing each species using a distribution function defined on a 5D-space : 3 dimensions for position and 2 dimensions for velocity. The tool at our disposal for this study is the GYSELA code which will be described further.

¹Especially the turbulent one which is much bigger than the neoclassical transport for standard scenarios where transport barriers are not taken into account

Chapters 1 and 2 introduce the models of electrons used in this study:

In chapter 1, we first introduce the tokamak magnetic geometry that we use in this study. An overview of the particle trajectories is done in which we see that the helical motion of charged particles can be decomposed into three parts: one parallel to the magnetic field and two transverse to the magnetic field that result from the Laplace force applied to the charged particle. The first transverse component is the cyclotron motion: the charged particle turns around magnetic field lines. The second transverse contribution results from the inhomogeneities of the magnetic field, constraining the particle to drift from the magnetic field lines. Besides it is seen that particles can be sorted into two classes regarding their trajectories : the trapped and passing particles. The orbit of trapped particles has the shape of a banana with a radial width which is large compared to the Larmor radius. Therefore this kind of particles is believed to play a major role in radial transport and some characteristics of trapped particles are recalled such as the bounce and precession motion. A brief description of the gyrokinetic model is then made and it is seen in this model how the equations of Vlasov and Poisson transform into the gyrokinetic and quasi-neutrality equations. The code GYSELA describing this model is then presented. GYSELA is a gyrokinetic, global, full- f , flux-driven code that considers a model with adiabatic electrons. It appears in particular that this code has many assets but requires huge numerical resources to launch long simulations. We see later that this point is critical when adding kinetic electrons. Eventually some basis of the gyrokinetic theory is presented and in particular, the notion of gyrocentre associated to a particle is defined. In particular, it is possible to decompose the particle density into two parts: the density of gyrocentres which can be computed directly from the distribution function of gyrocentres and a residual called the polarisation density which is computed directly from the electric potential and is essential whenever one wants to write properly the quasi-neutrality equation.

In chapter 2, we expose the adiabatic electrons model as it is implemented in GYSELA. However, we see that this model does not take into account neither particle transport nor the influence of electrons on turbulence. Therefore a new model is developed in which we introduce another distribution function to describe electrons kinetically. Nevertheless, such a description where both ions and electrons are kinetic requires to reduce the time step as well as the radial and poloidal steps by a factor $(m_i/m_e)^{1/2}$ each. For deuterium ions, that means that a given simulation launched with kinetic electrons will be $3600^{3/2} \sim 10^5$ times more costly than an equivalent simulation using the adiabatic electrons model. To reduce the cost of the full kinetic electron simulation, we arbitrarily reduce the mass ratio m_i/m_e . Doing so however, the kinetic behaviour of passing electrons is greatly modified from reality on the contrary to trapped electrons whose precession pulsation is independent from the mass ratio. Therefore to circumvent this problem, we introduce a third hybrid model where trapped electrons are treated kinetically and passing electrons are considered adiabatic. The three electron models are respectfully called the Adiabatic Electron, Full Kinetic Electron and Trapped Kinetic

Electron models. Eventually, the theoretical form a pure density source would take with kinetic electrons is derived.

Chapters 3 and 4 tackle the impact of kinetic electrons on the plasma behaviour:

In chapter 3, the impact of kinetic electrons on Geodesic Acoustic Modes is studied. These modes are important for at least two reasons: first, their evolution is studied in benchmarks. In our case, these tests were extended to kinetic electrons. Second, these modes play a role on turbulence and fast particles transport [17, 82, Conway 2011, Zarzoso 2013]. We provide an analytical model in which we recover the dispersion relation of GAMs from the gyrokinetic and quasi-neutrality equations. From this equation, both the ion and electron contributions for the expression of the GAM pulsation and damping rate are derived and a comparison with numerical simulations then follows. It appears that the GAM pulsation is not modified much in the presence of kinetic electrons. However, the GAM damping rate is tremendously increased for large values of the safety factor. This over-damping is due to a coupling between the bouncing modes of trapped electrons and the GAM, the former retrieving the energy stored in the latter. One important result is that the damping rate evolves with the mass ratio as $(m_i/m_e)^{-1/2}$. However, some problems have been encountered to predict analytically the correct scaling in safety factor and electron temperature of the GAM damping rate.

In chapter 4, the impact of kinetic electrons on the Ion Temperature Gradient (ITG) and the Trapped Electron Modes (TEM) instabilities is exposed. First, the ITG and TEM are described as particular cases of the general drift wave and interchange mechanisms and the dispersion relation for both ITG and TEM is given. Second, linear numerical simulations are launched while keeping only one toroidal mode. In these simulations, the density and temperature gradients in the tokamak are set for both ions and electrons such that the ITG and TEM instabilities are triggered. Only the initial unstable phase where the toroidal modes of the electric potential grow exponentially is studied here. It is observed that whenever the ion temperature gradient is reduced while maintaining a fixed electron temperature profile, the sign of the poloidal pulsation changes abruptly. The sign of the poloidal pulsation being a signature of an ion or electron mode, the sign change means that we have found the transition between ITG and TEM modes. This result is confirmed by looking at the energy transfer between particles and the electric wave. We recover the fact that in a ITG-dominated regime, the instability is mostly fuelled by the ions of the plasma whereas in the case of a TEM-dominated regime, the electrons fuel the instability. Eventually, a case where several toroidal modes are kept is built for future turbulent transport studies. It is constructed as follows: first, some modes are filtered to prevent the development of the so-called ω_H mode. This mode is the low β response of the kinetic Alfvén wave and is a signature of an electrostatic model. It should not appear in an electromagnetic model and we prefer to remove it for its appearance is concomitant with a large spurious radial transport that is not physical. Second, we use the aligned coordinate method thoroughly explained in [45, 57, Hariri

2013, Latu 2018] which consists in computing the plasma quantities along magnetic field lines. The gradients in this direction being very small, it is possible to choose a very loose discretization in that direction, thus reducing the numerical cost. This will be crucial to carry out future non-linear simulations. Finally, we present the first non-linear results obtained with kinetic electrons.

Chapter 1

Particle trajectories and gyrokinetic theory in a tokamak

The confinement of the plasma requires the presence of a particular magnetic geometry provided by the tokamak coils and the plasma currents. This magnetic field interacts with the charged particles. The resulting Laplace force prevents the particles from leaving the plasma box. Several machines have been developed, including the tokamak and the stellerator to achieve this [48, Helander 2012]. The purpose of this chapter is to describe the configuration of a tokamak of circular section like Tore Supra and to derive the resulting motion of the charged particles of the plasma.

First, we describe the geometry of the magnetic field imposed by such a tokamak and we see that the plasma in this configuration remains close to a tokamak equilibrium in which fluid quantities are homogeneous on every flux surface. Subsequently, we show that the motion of the charged particles immersed in such a field can be decomposed into a motion parallel to the field lines, a cyclotron rotation around these, and a perpendicular drift motion which slightly shifts the orbits of the particles from their associated flux surface. We then introduce the gyrokinetic model which allows one to reduce the studied phase space from 6 dimensions (3 of space, 3 of velocity) to 5 dimensions. This reduces the numerical cost of the simulations. In this model, we study a new physical object, the gyrocentre, which is obtained by decoupling the fast gyromotion of particles from the slow perpendicular motion of gyrocentres. Finally, it can be seen that the densities of particles and gyrocentres are not equal, their difference being the polarization density.

1.1 Tokamak configuration

In this work, we study a tokamak with the shape of a torus of circular section, characterized by a major radius R_0 and a minor radius a . We define the inverse of the aspect ratio as $\varepsilon_0 = a/R_0$. The toroidal direction is defined as the blue one on Fig.1.1, and the poloidal direction as the red one. We first introduce the set of torus coordinates to describe the tokamak geometry and the set of canonical coordinates which is adapted to describe the geometry of the magnetic field. Secondly, we give the expression of the magnetic field in the canonical coordinates and then an approximated expression in the torus coordinates. The geometry of magnetic field as well as the set of coordinates used in tokamaks are well described in [47, Hazeltine 2003].

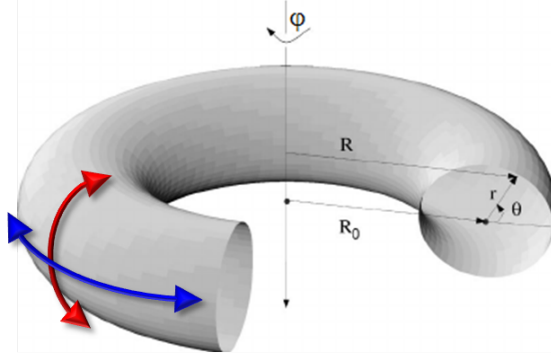


Figure 1.1: Poloidal (in red) and toroidal (in blue) angles (resp. θ and φ) and the torus coordinates (r, θ, φ) .

1.1.1 Torus and canonical coordinates

The torus coordinates are defined as the set of the three coordinates (r, θ, φ) shown on Fig.1.1 with r the minor radius, θ the poloidal angle and φ the toroidal angle. The poloidal and toroidal magnetic fluxes are defined respectively as:

$$\Phi_T \equiv \iint \mathbf{B} \cdot d\mathbf{S}_T = \int_0^r dr' \int_0^{2\pi} r' d\theta B_\varphi$$

$$\Phi_P \equiv \iint \mathbf{B} \cdot d\mathbf{S}_P = \int_0^R dR' \int_0^{2\pi} R' d\varphi B_\theta$$

and represented on Fig.1.2. The magnetic field lines wrap around the surfaces of constant poloidal flux. To simplify the expression of the magnetic field \mathbf{B} , it is convenient to define a new set of canonical coordinates (x_1, x_2, x_3) which are defined from the symmetries of \mathbf{B} .

- First, the magnetic field \mathbf{B} wraps around the magnetic surfaces of constant poloidal flux Φ_P . The coordinate x_1 is taken as a surface label. We choose $x_1 = \psi \equiv \Phi_P/2\pi$.

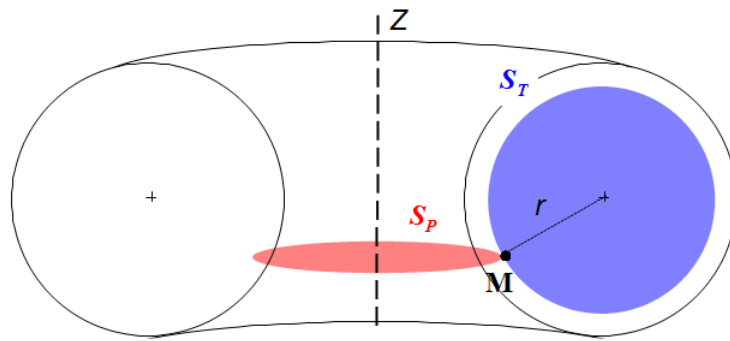


Figure 1.2: Poloidal (in red) and toroidal (in blue) flux sections.

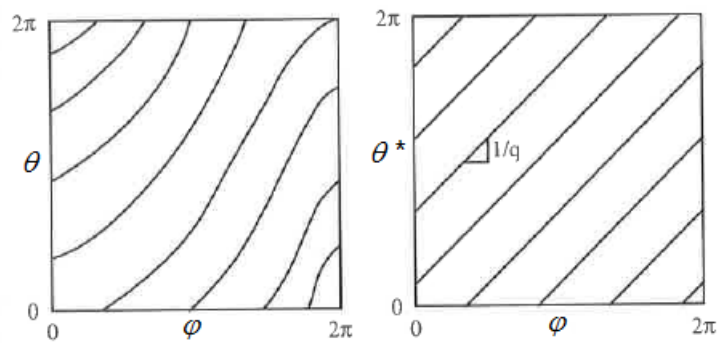


Figure 1.3: Magnetic field lines on a flux surface using (a) torus coordinates and (b) canonical coordinates.[47, Hazeltine 2003]

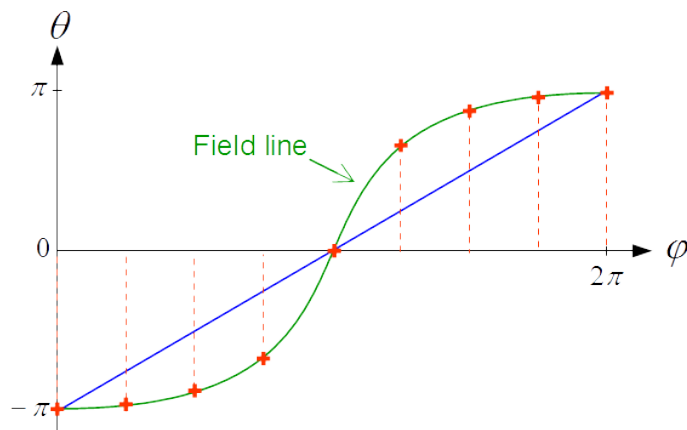


Figure 1.4: Poloidal discretization while following a magnetic field line.

- Due to the axisymmetry of the problem around the tokamak axis¹, we choose $x_3 = \varphi$ the geometric toroidal angle².
- We choose the last coordinate $x_2 = \theta^*$ called the intrinsic angle and defined so that in the set of canonical coordinates $(\psi, \theta^*, \varphi)$ the magnetic field lines are represented within each flux surface $\psi = \text{cst}$ by straight lines (shown on Fig.1.3) of equation:

$$\left. \frac{d\varphi}{d\theta^*} \right|_{FL} = \frac{\mathbf{B} \cdot \nabla \varphi}{\mathbf{B} \cdot \nabla \theta^*} \equiv q(\psi) \text{ safety factor} \quad (1.1)$$

Here the safety factor q depends on ψ only and characterizes the helicity of the magnetic field lines. It should be noted that condition (1.1) fully determines the angle θ^* once the coordinates ψ, φ are set.

We introduce the contravariant base $(\nabla\psi, \nabla\theta^*, \nabla\varphi)$ associated with the canonical coordinates $(\psi, \theta^*, \varphi)$ ³. A derivation to express the intrinsic angle θ^* from the poloidal angle θ is made in Appendix A.1. This set of coordinates is well adapted to express the magnetic field rigorously. In this coordinate system, the local helicity of the magnetic field lines is larger (q_{loc} is weaker) on the low field side than on the high field side (because $B \propto 1/R$). As a result, the θ^* coordinate has more grid points (for a given $\Delta\varphi$) on the high field side than on the low field side (see Fig.1.4). However, as the turbulence is ballooned, we look for a high number of grid points in the low field side, i.e. the opposite. This is why it is ultimately not this coordinate system that has been retained in GYSELA.

1.1.2 Geometry of the magnetic field

The currents in the poloidal coils and in the plasma induce a potential vector which can be written as:

$$\mathbf{A} = \frac{1}{2\pi} [\Phi_P \mathbf{e}_\varphi + \Phi_T \mathbf{e}_\theta] \quad (1.2)$$

where Φ_P and Φ_T correspond respectively to the poloidal and toroidal magnetic fluxes. The corresponding magnetic field can be written in the form:

$$\mathbf{B} = I(\psi) \nabla\varphi + \nabla\varphi \wedge \nabla\psi \quad (1.3)$$

where $I(\psi) = (R/2\pi) \nabla\theta^* \wedge \nabla\Phi_T$ is a function of ψ only, with $\psi = \Phi_P/2\pi$.

It is useful to have an expression of the magnetic field in the torus coordinates (r, θ, φ) . In this model, we make the hypothesis that the magnetic flux surfaces are nested concentric tori with circular section. This means that r can be taken as a magnetic surface

¹In reality, because of the finite number of toroidal coils, the magnetic field is not perfectly axisymmetric.

²A geometric angle can be defined as: placed at a constant distance of the rotation axis, the length of the arc traveled is proportional to the angle of rotation.

³By definition, each of the vector $\nabla\alpha$ in the base $(\nabla\psi, \nabla\theta^*, \nabla\varphi)$ is normal to the surface $\alpha = \text{cste}$. Moreover, $|\nabla\alpha| = 1/R_\alpha$ where R_α is the curvature radius of the coordinate line along the coordinate α .

label. The magnetic field lines wrap around these tori and can be decomposed into a toroidal field B_φ , and a poloidal field B_θ .

$$\mathbf{B} = B_\theta \mathbf{e}_\theta + B_\varphi \mathbf{e}_\varphi \quad (1.4)$$

where we have introduced $(\mathbf{e}_r, \mathbf{e}_\theta, \mathbf{e}_\varphi)$ a normalized basis of the torus coordinates. We make here the approximation $\theta^* \simeq \theta$ so that:

$$q(r) \simeq \left. \frac{d\varphi}{d\theta} \right|_{FL} = \frac{\mathbf{B} \cdot \nabla \varphi}{\mathbf{B} \cdot \nabla \theta} = \frac{r B_\varphi}{R B_\theta} \quad (1.5)$$

This approximation holds in the limit $\varepsilon = r/R_0 \rightarrow 0$. Ampère's law used on a toroidal circle states that:

$$B_\varphi \cdot R = B_0 \cdot R_0 = \mu_0 I_0 \quad (1.6)$$

where B_0 is the toroidal magnetic field at $R = R_0$ and I_0 is the total current in the poloidal coils. From equations (1.5) and (1.6) the expressions of the toroidal and poloidal magnetic fields are easily obtained and it comes:

$$\mathbf{B} = B_0 \frac{R_0}{R} \left[\frac{r}{qR} \mathbf{e}_\theta + \mathbf{e}_\varphi \right] \quad (1.7)$$

In the whole manuscript, we place ourselves in this last model and use the torus coordinates.

1.2 Particle trajectories

The theory of orbits in tokamaks has been widely discussed in several books and articles ([55, 61, 68, 72, Kruskal 1958, Littlejohn 1983, Rax 2012, Sarazin 2013]). First, the trajectories of charged particles are presented, based on the derivation in [72, Sarazin 2013]. Second, we introduce the angle-action set of variables which is well suited to describe the motion of these particles. Finally, some important characteristics of a particular class of particles, those trapped in the magnetic well present in the parallel direction, are derived.

1.2.1 Derivation of particle velocity

In the presence of an electromagnetic field (\mathbf{E}, \mathbf{B}) a particle of charge e and mass m follows the equation of Newton:

$$m \frac{d\mathbf{v}}{dt}(\mathbf{x}, t) = e(\mathbf{E}(\mathbf{x}, t) + \mathbf{v}(\mathbf{x}, t) \wedge \mathbf{B}(\mathbf{x}, t)) \quad (1.8)$$

where $\mathbf{x}(t)$ stands for the position of the particle at time t . It is useful to decompose the magnetic field as $\mathbf{B}(\mathbf{x}, t) = \langle \mathbf{B} \rangle + \tilde{\mathbf{B}}(\mathbf{x}, t)$. We have $\langle \mathbf{B} \rangle = J \cdot \mathbf{B}$, where J stands for the gyroaverage operator defined in Eq.(1.58). This term is replaced at order 0 in $(\rho_c/R)^2$ by the magnetic field $\mathbf{B}(\mathbf{x}_{GC}, t)$ evaluated at the position of the guiding centre. Within the adiabatic theory, this perturbation remains small compared to $\mathbf{B}(\mathbf{x}_{GC}, t)$. The perpendicular dynamics is dominated by a helical trajectory around the magnetic field lines – called the cyclotron motion – which is characterized by a pulsation ω_c , the cyclotron pulsation, and a perpendicular radius ρ_c , the Larmor radius. The adiabatic theory is verified only if two conditions are satisfied:

- **Temporal condition:** The magnetic field or the cyclotron frequency ω_c remains fairly constant during the cyclotron period τ_c i.e. the variation of ω_c over the duration τ_c of a complete cyclotron turn is very small compared to ω_c :

$$\tau_c \frac{d\omega_c}{dt} \ll \omega_c \Leftrightarrow \frac{1}{\omega_c} \frac{d\omega_c}{dt} \ll \omega_c \Leftrightarrow \frac{d \ln(\omega_c)}{dt} \ll \omega_c \Leftrightarrow \frac{d \ln(B)}{dt} \ll \omega_c \quad (1.9)$$

- **Spatial condition:** The value of the magnetic field seen by a particle remains almost the same on a cyclotron turn i.e. the Larmor radius ρ_c is very small compared to the characteristic length of variation of the magnetic field $L_{\nabla B}$:

$$\rho_c \ll L_{\nabla B} \Leftrightarrow \rho_c \left| \frac{\nabla B}{B} \right| \ll 1 \Leftrightarrow \rho_c \nabla \ln B \ll 1 \quad (1.10)$$

These conditions are satisfied for strongly magnetized systems, such as the tokamak. We introduce $(\mathbf{b}, \mathbf{n}_1, \mathbf{n}_2)$ an orthonormal basis attached to the particle with \mathbf{b} the normalized vector parallel to the magnetic field. The motion of such a particle can be decomposed in three different parts as we will see.

Cyclotron motion

In the absence of an electric field, and with a uniform and constant magnetic field \mathbf{B}_0 , Eq.(1.8) becomes:

$$m \frac{d\mathbf{v}}{dt}(\mathbf{x}, t) = e \mathbf{v}(\mathbf{x}, t) \wedge \mathbf{B}_0 \quad (1.11)$$

As \mathbf{B}_0 is uniform, the projection of this equation on the parallel axis gives $d_t v_{\parallel} = 0$. Furthermore, the projection of Eq.(1.11) on the two perpendicular directions, \mathbf{n}_1 and \mathbf{n}_2 , gives the following system:

$$\begin{cases} \frac{dv_{c1}}{dt} = \frac{eB_0}{m} v_{c2} \\ \frac{dv_{c2}}{dt} = -\frac{eB_0}{m} v_{c1} \end{cases} \quad (1.12)$$

where the index c refers to the cyclotron motion. The integration of sytem (1.12)⁴ gives the following form for the cyclotron motion:

$$\mathbf{x}_c(t) = v_{\parallel} t \mathbf{b} + \underbrace{\rho_c (\cos(\omega_c t) \mathbf{n}_1 + \sin(\omega_c t) \mathbf{n}_2)}_{\rho_c} \quad (1.13)$$

where the cyclotron pulsation ω_c and the Larmor radius ρ_c are defined as

$$\omega_c = \frac{eB_0}{m} \quad ; \quad \rho_c = \left| \frac{v_c}{\omega_c} \right| \quad (1.14)$$

We introduce the thermal velocity v_{th} and the thermal Larmor radius, which are good guess to get an order of magnitude of v_c and ρ_c , and are defined as

$$v_{th} = \sqrt{\frac{T}{m}} \quad ; \quad \rho_{th} = \left| \frac{v_{th}}{\omega_c} \right| \quad (1.15)$$

with T the temperature. For a temperature $T = 10$ keV and a magnetic field $B_0 = 5$ T the magnitude of the following quantities is given

	v_{th}	ω_c	ρ_{th}
Deuterium	$6.9 \cdot 10^5$ m/s	$0.24 \cdot 10^9$ Hz	2.9 mm
Electrons	$4.2 \cdot 10^7$ m/s	$0.88 \cdot 10^{12}$ Hz	48 μ m

The trajectory due to the term ρ_c is called the cyclotron motion. In a tokamak, particles have a helicoidal motion along the magnetic field lines of radius ρ_c and of wavelength $v_{\parallel}(2\pi/\omega_c)$. However the gradients and curvature of the magnetic field, as well as the transverse electric field introduce transverse drifts.

⁴This integration is made easily by considering $v_{c1} + v_{c2}$ and $v_{c1} - v_{c2}$ as the two unknowns of the system.

Transverse drifts

Taking into account the decomposition of the magnetic field $\mathbf{B}(\mathbf{x}, t) = \langle \mathbf{B} \rangle + \tilde{\mathbf{B}}(\mathbf{x}, t)$ discussed below Eq.(1.8) and decomposing the velocity as $\mathbf{v} = \langle \mathbf{v} \rangle + \tilde{\mathbf{v}}$ with $\langle \mathbf{v} \rangle \equiv \oint \mathbf{v} \frac{d\varphi_c}{2\pi}$, Eq.(1.8) leads, for each species s , to the following system:

$$m_s \frac{d\langle \mathbf{v} \rangle}{dt} = e_s \left\{ \langle \mathbf{E} \rangle + \langle \mathbf{v} \rangle \wedge \mathbf{B}_G + \langle \tilde{\mathbf{v}} \wedge \tilde{\mathbf{B}} \right\} \quad (1.16)$$

$$m_s \frac{d\tilde{\mathbf{v}}}{dt} = e_s \left\{ \tilde{\mathbf{E}} + \tilde{\mathbf{v}} \wedge \mathbf{B}_G + \langle \mathbf{v} \rangle \wedge \tilde{\mathbf{B}} + \tilde{\mathbf{v}} \wedge \tilde{\mathbf{B}} - \langle \tilde{\mathbf{v}} \wedge \tilde{\mathbf{B}} \right\} \quad (1.17)$$

where the notation $\mathbf{B}_G = \mathbf{B}(\mathbf{x}_{GC}, t)$ has been used. The term $\tilde{\mathbf{v}} \wedge \mathbf{B}_G$ is dominant in Eq.(1.17) and this equation reduces at lowest order as:

$$m_s \frac{d\tilde{\mathbf{v}}}{dt} = e_s \tilde{\mathbf{v}} \wedge \mathbf{B}_G \quad (1.18)$$

This equation has the same form as Eq.(1.11): we recover the fact that the fast dynamics is mainly dominated by the cyclotron motion discussed in section 1.2.1.

In the averaged motion equation (1.16), the term $\langle \tilde{\mathbf{v}} \wedge \tilde{\mathbf{B}} \rangle$ needs to be calculated. It can be shown (see [72, Sarazin 2013]) that this term reduces to:

$$\langle \tilde{\mathbf{v}} \times \tilde{\mathbf{B}} \rangle = -\frac{\mu_s}{e_s} \nabla B$$

where $\mu_s \equiv e_s \omega_c \rho_c^2 / 2$ is the adiabatic invariant. Equation (1.16) can then be recast as:

$$m_s \frac{d\langle \mathbf{v} \rangle}{dt} = e_s \left(\langle \mathbf{E} \rangle + \langle \mathbf{v} \rangle \wedge \mathbf{B}_G \right) - \mu_s \nabla B_G \quad (1.19)$$

We can decompose the velocity $\langle \mathbf{v} \rangle = v_{\parallel} \mathbf{b} + \mathbf{v}_{G\perp}$ with $\mathbf{b} \equiv \mathbf{B}/B$. The projection Eq.(1.19) onto the transverse plane yields:

$$m_s \left. \frac{d\mathbf{v}_{G\perp}}{dt} \right|_{\perp} + m_s \left. \frac{dv_{\parallel}}{dt} \right|_{\perp} = e_s \left(\langle \mathbf{E} \rangle_{\perp} + \langle \mathbf{v} \rangle \wedge \mathbf{B} \right) - \mu_s \nabla_{\perp} B \quad (1.20)$$

We call ω a characteristic pulsation of the drift motion. The term $\left. \frac{d\mathbf{v}_{G\perp}}{dt} \right|_{\perp}$ is of order $\frac{\omega}{\omega_c} \mathbf{v}_{G\perp}$. The transverse drift is an averaged process which appears at the time scale $\omega \sim v_{\parallel}/R \ll \omega_c$. The contribution of this term is therefore negligible at leading order.

The term $\left. \frac{dv_{\parallel}}{dt} \right|_{\perp}$ can be developed as:

$$\left. \frac{dv_{\parallel}}{dt} \right|_{\perp} = v_{\parallel} \left. \frac{d\mathbf{b}}{dt} \right|_{\perp} = v_{\parallel}^2 \nabla_{\parallel} \mathbf{b} = v_{\parallel}^2 \frac{\mathbf{N}}{R}$$

with $d_t \mathbf{b} = (v_{\parallel}/R) \mathbf{N}$ where \mathbf{N} stands for the normal unit vector of the Frenet frame, R being the associated radius of curvature which corresponds to the major radius. Taking Eq.(1.20) $\wedge \mathbf{B}$, the transverse drift velocity in the adiabatic limit reads, at lowest order:

$$\mathbf{v}_{G\perp} = \mathbf{v}_E + \mathbf{v}_{D\nabla, s} + \mathbf{v}_{DC, s} = \frac{\langle \mathbf{E} \rangle \wedge \mathbf{B}}{B^2} + \frac{\mathbf{B}}{e_s B^2} \wedge \left[\mu_s B \frac{\nabla B}{B} + m_s v_{\parallel}^2 \frac{\mathbf{N}}{R} \right] \quad (1.21)$$

It appears that two sources of transverse drifts are dominant in tokamak plasmas, namely

- The existence of a transverse electric field \mathbf{E}_\perp . The electric drift is given by:

$$\mathbf{v}_E = \frac{\langle \mathbf{E} \rangle \wedge \mathbf{B}}{B^2} \quad (1.22)$$

- The inhomogeneities of the magnetic field, that is gradient and curvature. The associated drifts are given respectively by

$$\mathbf{v}_{D\nabla,s} = \frac{v_{c,s}^2}{2\omega_{c,s}} \frac{\mathbf{b} \wedge \nabla \mathbf{B}}{B} \quad ; \quad \mathbf{v}_{DC,s} = \frac{v_\parallel^2}{\omega_{c,s}} \frac{\mathbf{b} \wedge \mathbf{N}}{\mathcal{R}_c} \quad (1.23)$$

Besides, the term $\mathbf{b} \wedge \mathbf{N}/R \simeq \mathbf{b} \wedge \nabla \mathbf{B}/B$ in the low- β limit ($\nabla \wedge \mathbf{B} \simeq 0$ in a tokamak). The magnetic drift is then recast as:

$$\mathbf{v}_{D,s} = \frac{v_\parallel^2 + \frac{v_{c,s}^2}{2}}{\omega_{c,s}} \frac{\mathbf{b} \wedge \nabla \mathbf{B}}{B} \quad (1.24)$$

\mathbf{B} is mainly oriented in the toroidal direction. The drift is therefore parallel to the vertical axis. Moreover the sign of this drift depends on the charge of the species, hence causing a charge separation between ions and electrons within the tokamak.

Parallel dynamics

The projection of Eq.(1.8) on \mathbf{b} yields:

$$m \left(\frac{d\mathbf{v}_\parallel}{dt} + \frac{d\mathbf{v}_\perp}{dt} \right) \cdot \mathbf{b} = e (E_\parallel + \mathbf{v} \wedge \mathbf{B} \cdot \mathbf{b}) \quad (1.25)$$

In the frame of the adiabatic theory, it can be shown [72, Sarazin 2013] that averaging this equation on the cyclotron motion gives at leading order in $\varepsilon \sim \omega/\omega_c \sim \rho_c/R$ and at low β :

$$m \frac{dv_\parallel}{dt} = e \langle E_\parallel \rangle - \mu \nabla_\parallel B + mv_\parallel \mathbf{v}_E \cdot \frac{\nabla B}{B} \quad (1.26)$$

1.2.2 Derivation of the Angle-Action coordinates from the motion invariants

The Noether theorem states that each symmetry of the system is associated with an invariant [38, Goldstein 2002]. The goal here is to identify three invariants of the system. Each of these invariants is associated with a periodic direction of motion. The motion along each of these periodic directions is fully described via the introduction of an angle α_i . The calculation of the actions associated with these angles leads to the introduction of the angle-action set of coordinates $(\boldsymbol{\alpha}, \mathbf{J})$. In this set of coordinates, each action can be expressed by a combination of motion invariants. First, we find the invariants of motion, then we introduce the angle-action set of coordinates $(\boldsymbol{\alpha}, \mathbf{J})$.

Motion invariants

Magnetic moment The magnetic moment μ of a charged particle of the plasma is due to the helicoidal trajectory around its associated magnetic field line. It can be calculated by assimilating this cyclotron motion to a current loop of surface $S = \pi\rho_c^2$ and current $I = e\frac{\omega_c}{2\pi}$ with ω_c standing for the cyclotron frequency:

$$\mu = IS = \pi\rho_c^2 e \frac{\omega_c}{2\pi} = \frac{e^2 \rho_c^2 B}{2m} = \frac{mv_\perp^2}{2B} \quad (1.27)$$

In the case where the magnetic field varies little at the scales of the cyclotron motion of particles in time and space $\mathbf{B}(\mathbf{x} + \rho_c, t + 1/\omega_c) \simeq \mathbf{B}(\mathbf{x}, t)$, then the magnetic moment μ of the particles is constant in time:

$$\frac{d\mu}{dt} = 0 \quad (1.28)$$

This is the adiabatic invariance of the magnetic moment which is valid only within the framework of the adiabatic theory given by the two conditions (1.9) and (1.10).

Energy Newton equation for charged particles reads:

$$m \frac{d\mathbf{v}}{dt} = e(\mathbf{E} + \mathbf{v} \wedge \mathbf{B}) \quad (1.29)$$

Taking the scalar product with \mathbf{v} , it becomes:

$$\frac{d}{dt} \left(\frac{1}{2} m v^2 \right) = -e\mathbf{v} \cdot (\nabla\phi + \partial_t \mathbf{A})$$

In the case of static electric and magnetic fields, so that $\partial_t \mathbf{A} = 0$ and $\frac{d\phi}{dt} = \mathbf{v} \cdot \nabla\phi$, it is possible to write the conservation of the energy \mathcal{E} :

$$\frac{d\mathcal{E}}{dt} = \frac{d}{dt} \left(\frac{1}{2} m v^2 + e\phi \right) = 0 \quad (1.30)$$

Toroidal kinetic momentum The plasma is supposed to be axisymmetric in the toroidal direction. As such, the action associated to the angle φ is conserved in time. Noting P_φ this invariant and p_φ the toroidal momentum, it is calculated as:

$$\int_0^{2\pi} P_\varphi d\varphi = \int_0^{2\pi R} p_\varphi \cdot dl_\varphi = \int_0^{2\pi} (m v_\varphi + e A_\varphi) R d\varphi$$

The system being axisymmetric in φ , it becomes:

$$P_\varphi = m R v_\varphi + e R A_\varphi$$

Furthermore, using Stokes' theorem, it is possible to rewrite the last term as:

$$R A_\varphi = \frac{1}{2\pi} \int \mathbf{A} \cdot d\mathbf{l}_\varphi = \frac{1}{2\pi} \int \mathbf{B} \cdot d\mathbf{S}_{pol} \equiv \psi$$

Eventually, the expression of the invariant P_φ , called toroidal kinetic momentum, associated with the axisymmetric toroidal angle φ takes the form:

$$P_\varphi = m R v_\varphi + e\psi \quad (1.31)$$

Review of motion invariants The particle dynamics is characterized by three invariants:

- The mechanic energy $\mathcal{E} \equiv \frac{1}{2}mv^2 + e\phi$ for constant electric and magnetic fields.
- The magnetic moment μ so that $\mu B \equiv \frac{1}{2}mv_{\perp}^2$ within the adiabatic limit.
- The toroidal kinetic momentum $P_{\varphi} \equiv mRv_{\varphi} + e\psi$ for axisymmetric plasma in φ .

Angle-Action coordinates

One seeks to construct a set of canonical coordinates using the three invariants of the motion previously found. We introduce the Hamiltonian H of the system. H can be decomposed into a constant equilibrium value $H_{eq}(\mathbf{J})$ on each flow surface and a perturbation $\tilde{H} = H - H_{eq}$. We seek a set of angle-action coordinates $(\boldsymbol{\alpha}, \mathbf{J})$ that satisfies the Hamilton equations and such that the actions \mathbf{J} remain constant⁵. Besides, the conservation of the action via the change of coordinate imposes:

$$\int_{\Gamma} \mathbf{J} \cdot d\boldsymbol{\alpha} = \int_{\Gamma} \mathbf{p} \cdot d\mathbf{x} \quad (1.32)$$

With this set of coordinates, for $i \in [1, 2, 3]$ the canonical equations are given by:

$$\begin{cases} \dot{\alpha}_i &= \frac{\partial H_{eq}}{\partial J_i} \equiv \Omega_i \\ \dot{J}_i &= -\frac{\partial H_{eq}}{\partial \alpha_i} = 0 \end{cases} \quad (1.33)$$

where Ω_i stands for the pulsation associated to the angle α_i . To construct the angle-action coordinates, one begins by looking for the symmetries of the system so as to decompose the general trajectory of the particles into 3 periodic parts, each associated with one of the motion invariants (or a combination of these).

- In the conditions of adiabaticity given by Eq.(1.9) and (1.10), the angle φ_c can be considered as a cyclic coordinate. The set of coordinates associated with this motion is fixed as $\alpha_1 = \varphi_c$ and J_1 is given by Eq.(1.32) and becomes:

$$2\pi J_1 = \int_0^{2\pi} mv_c \rho_c d\varphi_c \quad \longrightarrow \quad J_1 = \frac{m}{e} \mu \quad (1.34)$$

- Due to the toroidal axisymmetry of the problem, the toroidal motion is cyclic with respect to the angle φ . The set of coordinates associated with this motion is $\alpha_3 = \varphi$ and $J_3 = P_{\varphi}$ where P_{φ} stands for the toroidal kinetic momentum derived in Eq.(1.31)

⁵ This is a direct consequence from the fact that H_{eq} depends only on \mathbf{J} :

$$\frac{dJ_i}{dt} = -\frac{\partial H_{eq}}{\partial \alpha_i} = 0 \quad \Rightarrow \quad J_i = \text{constant}$$

- Although the trajectories of the so-called "passing" particles projected in the poloidal plane have a circle-like shape, this is not the case for all particles, especially the trapped ones that exhibit poloidal trajectories with the shape of a banana. The angle α_2 associated with the poloidal motion of the particles is constructed so that after an angle 2π the particle has returned to its starting point. Such an angle can be seen as equal to $\alpha_2 = 2\pi s_\theta/L_\theta$ with s_θ the poloidal projection of the curvilinear abscissa and L_θ the total distance travelled in a period of the poloidal motion. With this definition, the link between α_2 and θ is given by $\theta = \theta_0 \sin \alpha_2$. The associated action is given by:

$$2\pi J_2 = \int_0^{2\pi} (mv_\theta + eA_\theta) dl_\theta \quad (1.35)$$

This approach is particularly important when one wants to express the Hamiltonian of the system: the equilibrium part of the Hamiltonian H_{eq} depends on the actions only, whereas the perturbed part \tilde{H} depends on both the angle and action coordinates.

1.2.3 Characteristics of trapped particles

The expressions of the invariants, introduced in part 1.2.1, enable to sort particles in different classes. To do so, we recall the expression of the energy H of a particle of mass m , parallel velocity v_\parallel and magnetic moment μ in the absence of electric potential:

$$H = \frac{1}{2}mv_\parallel^2 + \mu B(r, \theta) \simeq \frac{1}{2}mv_\parallel^2 + \mu B_0(1 - \varepsilon \cos \theta) \quad (1.36)$$

When moving along the magnetic field lines, the gyrocentre explores the poloidal variations of the magnitude of the magnetic field $B(r, \theta) \simeq B_0 R_0/R$ with $R = R_0 + r \cos \theta$ the major radius, the subscript "0" referring to quantities on the magnetic axis. It follows that particles having $H < \mu B_{max}(r)$ with $B_{max}(r)$ the maximum magnitude of the magnetic field on a poloidal turn will be reflected in the parallel direction when entering the high field region of the tokamak. Thus, the particles can be sorted (at least) in two different classes whose orbits are shown on Figure 1.5:

- $|v_\parallel| > 0$ for all θ : the particle explores the whole poloidal domain. The particle is said to be **passing**.
- $|v_\parallel| = 0$ for a particular value $\theta = \theta_0$: the particle bounces back before having made a full poloidal turn. The particle is said to be **trapped**.

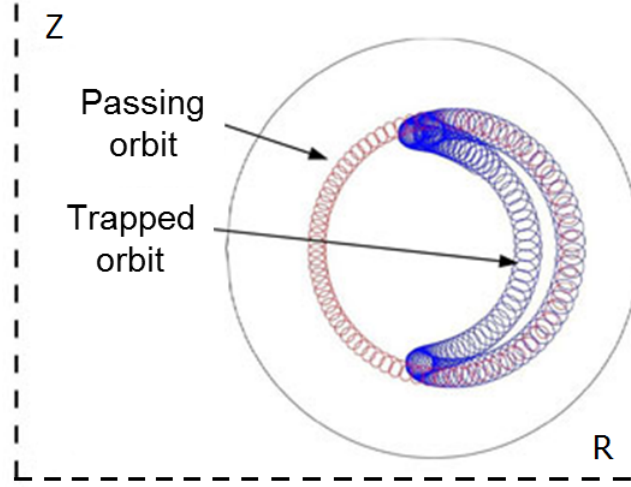
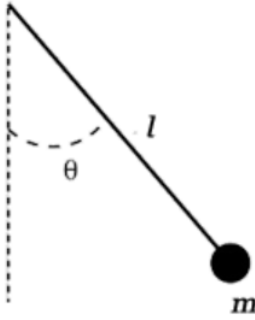


Figure 1.5: Trapped and passing orbits.

This system is analogous to the pendulum model represented beside and whose total energy H_{pend} reads:

$$H_{pend} = \frac{1}{2}ml^2\dot{\theta}^2 + mgl(1 - \cos \theta) \quad (1.37)$$



- The parallel kinetic energy $\frac{1}{2}mv_{\parallel}^2$ of the particle is analogous to the kinetic energy of the pendulum $\frac{1}{2}ml^2\dot{\theta}^2$
- The perpendicular kinetic energy μB is analogous to the potential energy of the pendulum $mgl(1 - \cos \theta)$

First, a condition is set for a particle to be trapped. Then, some characteristics of the trapped particles are derived such as the fraction of trapped particles, the shift of the trajectory from the associated magnetic field line also called the banana width δ_b and the bounce pulsation ω_b .

Trapping condition

A particle is trapped in the magnetic well when its energy H is such that $H \leq \mu B_{max}$. In that case, the expression of the energy (1.36) gives:

$$\frac{1}{2}mv_{\parallel}^2 + \mu B(r, \theta) \leq \mu B_{max}(r) \quad (1.38)$$

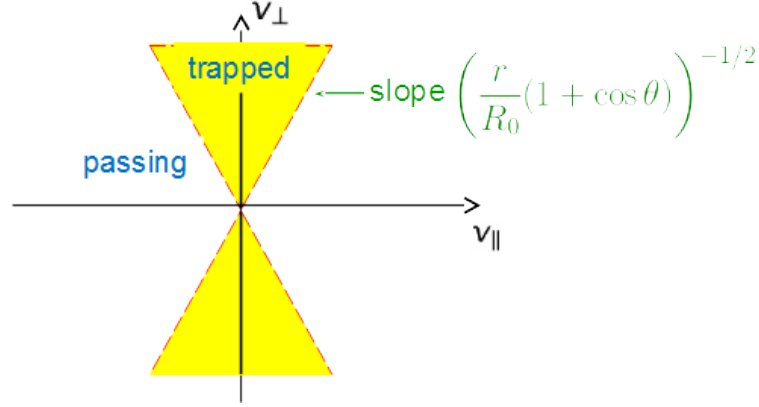


Figure 1.6: Trapping domain: the particles inside the yellow cone are trapped, the others are passing.

Taking into account that $\mu B = \frac{1}{2}mv_{\perp}^2$, Eq.(1.38) can be expressed as a trapping condition depending on the particle velocity:

$$\left| \frac{v_{\parallel}}{v_{\perp}} \right| \leq \sqrt{\frac{B_{max}(r)}{B(r, \theta)} - 1} = \tau_t(r, \theta) \quad (1.39)$$

The magnetic field is expressed as $B(r, \theta) \simeq B_0 / (1 + \varepsilon \cos \theta)$, with $\varepsilon = r/R_0$ the inverse aspect ratio. The maximum value of the magnetic field for a fixed value of ε is then $B_{max}(r) = B_0 / (1 - \varepsilon)$. Therefore, the trapping condition Eq.(1.39) becomes:

$$\left| \frac{v_{\parallel}}{v_{\perp}} \right| \leq \sqrt{\frac{1 + \varepsilon \cos \theta}{1 - \varepsilon} - 1} \simeq \sqrt{\varepsilon(1 + \cos \theta)} \quad (1.40)$$

where the second expression is approximated in the limit $\varepsilon \ll 1$. The position of the particle in velocity space $(v_{\parallel}, v_{\perp})$ sets whether the particle is trapped or passing. The trapped domain is given by a cone of equation (1.39) and represented on Fig.1.6.

Trapped fraction of particles

Let us introduce the fraction of trapped particles α_t . By definition:

$$\alpha_t(\mathbf{x}, t) = \frac{n^{trapped}(\mathbf{x}, t)}{n(\mathbf{x}, t)} = \frac{2\pi \int_0^{\infty} v_{\perp} dv_{\perp} \int_{-v_{\perp}\tau_t(r, \theta)}^{+v_{\perp}\tau_t(r, \theta)} dv_{\parallel} f(\mathbf{x}, \mathbf{v}, t)}{2\pi \int_0^{\infty} v_{\perp} dv_{\perp} \int_{-\infty}^{+\infty} dv_{\parallel} f(\mathbf{x}, \mathbf{v}, t)} \quad (1.41)$$

Here the integration domain for the trapped particle is $2\pi \int_0^{\infty} v_{\perp} dv_{\perp} \int_{-v_{\perp}\tau_t(r, \theta)}^{+v_{\perp}\tau_t(r, \theta)} dv_{\parallel}$ which is consistent with the previous condition $\left| \frac{v_{\parallel, max}}{v_{\perp}} \right| = \tau_t(r, \theta)$. In the case of a Maxwellian distribution function centred on an average velocity of 0 in the parallel and

perpendicular directions: $f_{eq}(\mathbf{x}, \mathbf{v}, t) = n_{eq} (2\pi v_{th}^2)^{-3/2} \exp\left(-\left(v_{\parallel}^2 + v_{\perp}^2\right)/2v_{th}^2\right)$, expression (1.41) becomes:

$$\begin{aligned} \alpha_t &= 2\pi \int_0^{\infty} v_{\perp} dv_{\perp} \int_{-v_{\perp}\tau_t(r,\theta)}^{+v_{\perp}\tau_t(r,\theta)} dv_{\parallel} \frac{1}{(2\pi v_{th}^2)^{3/2}} \exp\left(-\frac{v_{\parallel}^2 + v_{\perp}^2}{2v_{th}^2}\right) \\ &= \frac{2\pi}{(2\pi v_{th}^2)^{3/2}} \int_0^{\infty} v_{\perp} dv_{\perp} \exp\left(-\frac{v_{\perp}^2}{2v_{th}^2}\right) \int_{-v_{\perp}\tau_t(r,\theta)}^{+v_{\perp}\tau_t(r,\theta)} dv_{\parallel} \exp\left(-\frac{v_{\parallel}^2}{2v_{th}^2}\right) \end{aligned} \quad (1.42)$$

Besides when $\varepsilon \rightarrow 0$ then $\tau_t \rightarrow 0$, and we can assume that $\exp\left(-v_{\parallel}^2/2v_{th}^2\right) \simeq 1$ on the interval $[-v_{\perp}\tau_t, +v_{\perp}\tau_t]$. Thus α_t becomes:

$$\alpha_t = \frac{4\pi\tau_t(r, \theta)}{(2\pi v_{th}^2)^{3/2}} \int_0^{\infty} v_{\perp}^2 dv_{\perp} \exp\left(-\frac{v_{\perp}^2}{2v_{th}^2}\right)$$

After a change of variable $u = v_{\perp}/\sqrt{2}v_{th}$, it comes:

$$\alpha_t = \tau_t(r, \theta) 4\pi^{-1/2} \int_0^{\infty} u^2 \exp(-u^2) du$$

Knowing that $\int_0^{\infty} u^2 \exp(-u^2) du = \sqrt{\pi}/4$, the trapped particle fraction becomes:

$$\alpha_t \xrightarrow{\varepsilon \rightarrow 0} \tau_t(r, \theta) \quad (1.43)$$

An estimation of the θ average of this fraction $\bar{\alpha}_t(r) = \frac{1}{2\pi} \int_{-\pi}^{\pi} \alpha_t(r, \theta) d\theta$ can be computed. Using the simplified expression of τ_t given by Eq.(1.40) and of α_t given by Eq.(1.43), it comes for $\varepsilon \rightarrow 0$:

$$\bar{\alpha}_t \underset{\varepsilon \rightarrow 0}{\sim} \frac{1}{2\pi} \int_0^{2\pi} \sqrt{\varepsilon(1 + \cos\theta)} d\theta = \frac{2\sqrt{2\varepsilon}}{\pi} \quad (1.44)$$

For typical values of $\varepsilon = 0, 1$, the value of the fraction of trapped particles is $\bar{\alpha}_t \simeq 0.5$.

Bounce and precession motions

As said in part 1.2.1, the transverse drifts are responsible for a shift of particle trajectories from their associated magnetic field surfaces. It results that the projections of trajectories on a poloidal surface have a circle-like shape shifted from the magnetic surfaces for passing particles, and two arcs of different radii meeting on the magnetic surface for trapped particles as shown on Fig.1.5. In addition, as the shift is not the same for the ways back and forth of the trapped particles motion, a shift appears in the toroidal direction after each bounce period of the trapped particle. This results in a precession motion for trapped particles along the toroidal angle (see Fig.1.7).

The banana width δ_b is defined as the shift of trapped particle trajectories from the associated magnetic field lines in $\theta = 0$. We also define the bounce pulsation $\omega_b = 2\pi/T_b$

where T_b is the transit/bounce time. For a passing particle, the transit time is the time needed for a particle to do a poloidal turn. For a trapped particle, the bounce time is the time needed for a particle to do a whole back and forth loop in the poloidal direction. The precession pulsation is defined as $\omega_d = 2\pi/T_d$ where T_d is the time for a trapped particle to do a toroidal turn.

The banana width δ_b can be computed knowing the conservation of the toroidal kinetic momentum $P_\varphi = mRv_\varphi + e\psi$ with $v_\varphi = \frac{B_\varphi}{B}v_\parallel \simeq v_\parallel$ in both ways back and forth of a trapped particle for $\theta = 0$. Knowing $\frac{d\psi}{dr} = -RB_\theta$ and $q(r) \simeq rB_0/RB_\theta$, it comes:

$$P_\varphi = \begin{cases} mR v_\parallel & + e\psi(r + \delta_b) \\ mR(-v_\parallel) & + e\psi(r) \end{cases} \Rightarrow \delta_b = \frac{2qm v_\parallel}{\varepsilon e B_0} \quad (1.45)$$

Besides, Eq.(1.40) gives the order $v_\parallel \sim \sqrt{2\varepsilon} v_\perp$ when $\theta = 0$. Considering thermal particles $v_\perp \simeq v_{th}$ and using the thermal Larmor radius expression ρ_{th} given in Eq.(1.15), the thermal banana width simply reduces to:

$$\delta_b \sim 2q\varepsilon^{-1/2}\rho_{th} \quad (1.46)$$

The bounce pulsation is computed from the period of the bounce/transit motion. We introduce $\pm\theta_0$ the angle of the turning points when $|v_\parallel| = 0$ (for passing particles, we take $\theta_0 = \pi$), and ε_b a parameter which equals 1 for trapped particles and 0 for passing ones. The bounce/transit period is given by:

$$\frac{2\pi}{\omega_b} = (1 + \varepsilon_b) \int_{t(\theta=-\theta_0)}^{t(\theta=+\theta_0)} dt = (1 + \varepsilon_b) \int_{-\theta_0}^{+\theta_0} \frac{qR(\theta)d\theta}{v_\parallel(\theta)} \quad (1.47)$$

where $R = R_0(1 + \varepsilon \cos \theta)$. For trapped particles, $\varepsilon_b = 1$ and v_\parallel can be approximated by condition (1.40) with v_\perp approximated by the thermal velocity v_{th} . Replacing R and v_\parallel by their θ -dependent expressions, Eq.(1.47) is recast as:

$$\frac{2\pi}{\omega_b} \simeq \frac{2qR_0}{\sqrt{\varepsilon} v_{th}} \int_{-\theta_0}^{+\theta_0} \frac{(1 + \varepsilon \cos \theta)\sqrt{1 - \varepsilon}}{\sqrt{1 + \varepsilon \cos \theta}} d\theta \quad (1.48)$$

For barely trapped particles, $\theta_0 = \pi$ and the bounce period becomes infinite, whereas for deeply trapped particles, $\theta_0 = 0$ and the bounce period becomes zero. Yet, a qualitative evaluation of ω_b can be done by doing the following approximations in Eq.(1.47): large aspect ratio limit $R = R_0$, $v_\parallel = \sqrt{2\varepsilon} v_{th}$ and $\theta_0 = \pi$. In that case, a simplified expression of the bounce pulsation is:

$$\omega_b \approx \frac{\sqrt{\varepsilon} v_{th}}{\sqrt{2qR_0}} \quad (1.49)$$

Besides, an evaluation of the ratio between the bounce and cyclotron pulsations shows that the bounce pulsation is much lower than the cyclotron pulsation:

$$\frac{\omega_b}{\omega_c} \approx \frac{\sqrt{\varepsilon} \rho_c}{q R} \ll 1$$

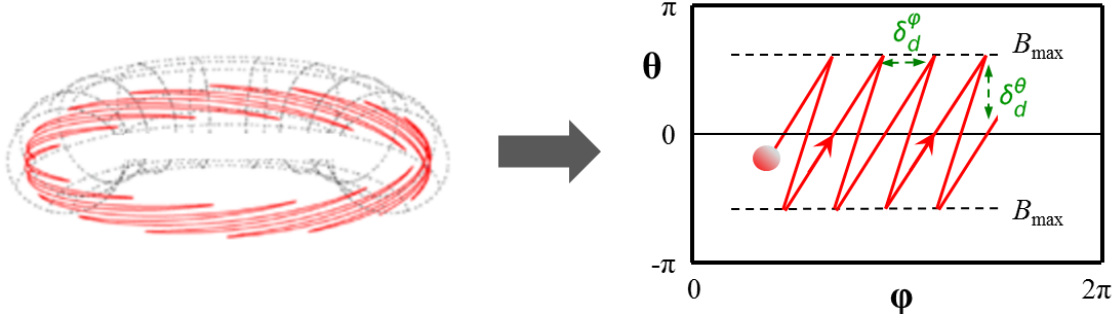


Figure 1.7: Toroidal precession of trapped particles.

Because of the radial gradients in the tokamak on the one hand and the banana width on the other hand, each way back and each way forth of the trajectory of trapped particles is done with a slightly different magnitude of the toroidal velocity. Integrated over time, this results in the existence of a toroidal precession velocity $\Delta v_{\parallel} \neq 0$. The precession velocity can be evaluated as:

$$\Delta v_{\varphi} \simeq \delta_b \left. \frac{dv_{\parallel}}{dr} \right|_{\theta=0}$$

Using Eq.(1.36) to find the expression of the parallel velocity $v_{\parallel} = \sqrt{\frac{2}{m}(H - \mu B(r, \theta))}$, it comes $\left. \frac{dv_{\parallel}}{dr} \right|_{\theta=0} \simeq \mu B_0 / m R v_{\parallel}$ in the approximation of large aspect ratio $R \simeq R_0$. It is then possible to define a precession period as the time needed for a trapped particle to do a full toroidal turn. Taking the expression of δ_b given by Eq.(1.45), this gives the following expression for the precession pulsation ω_d :

$$\omega_d = \frac{\Delta v_{\parallel}}{2\pi R} \approx \frac{q\omega_c \rho_{th}^2}{rR} \quad (1.50)$$

The ratio between the precession pulsation and the bounce pulsation is $\omega_d/\omega_b \approx \frac{q^2}{\sqrt{\epsilon}} \frac{\rho_{th}}{r} \ll 1$ where the approximation $R \simeq R_0$ has been done. Taking a safety factor $q = 2$, a temperature $T = 10$ keV, a magnetic field $B_0 = 5$ T and using ITER dimensions $R_0 = 6.2$ m and $a = 2$ m, the magnitude of the characteristics of the bounce motion at mid-radius are given here:

	δ_b	ω_b	ω_d
Deuterium	3.6 cm	$1.1 \cdot 10^4$ Hz	160 Hz
Electrons	0.59 mm	$6.8 \cdot 10^5$ Hz	160 Hz

In particular, it appears that the precession pulsation ω_d does not depend of the mass of the particle.

1.3 Gyrokinetic description of a plasma

In a plasma, two physical objects need to be described: the particles and the electromagnetic wave. On the one hand, the particles are described, in the framework of kinetic theory which is tackled in ([50, 66, Ichimaru 1973, Nicholson 1983]), by their distribution function defined in the 6D space $f(\mathbf{x}, \mathbf{v}, t)$ from which all fluid quantities can be recovered. This distribution function corresponds to the number of particles per unit volume having approximately the velocity \mathbf{v} , near the position \mathbf{x} at time t . The first fluid moments are defined as:

$$\begin{cases} n(\mathbf{x}, t) &= \int f(\mathbf{x}, \mathbf{v}, t) d^3v \\ n\mathbf{V}(\mathbf{x}, t) &= \int \mathbf{v}f(\mathbf{x}, \mathbf{v}, t) d^3v \\ \bar{\bar{P}}(\mathbf{x}, t) &= \int m(\mathbf{v} - \mathbf{V}) \otimes (\mathbf{v} - \mathbf{V})f(\mathbf{x}, \mathbf{v}, t) d^3v \\ nT(\mathbf{x}, t) &= p = \frac{1}{3}Tr(\bar{\bar{P}}) = \int m|\mathbf{v} - \mathbf{V}|^2 f(\mathbf{x}, \mathbf{v}, t) d^3v \end{cases} \quad (1.51)$$

with n the density, \mathbf{V} the fluid velocity, $\bar{\bar{P}}$ the pressure tensor, p the scalar pressure and T the temperature. On the other hand, the electromagnetic wave is described by the scalar and vector potentials $(\phi(\mathbf{x}, t), \mathbf{A}(\mathbf{x}, t))$. The equations that solve this problem are the Vlasov, the Maxwell-Gauss and Maxwell-Ampere equations. The auto-consistent problem of 5 scalar equations for 5 scalar unknowns can be written as follows:

$$\frac{df}{dt}(\mathbf{x}, \mathbf{v}, t) = 0 \quad (1.52)$$

$$\Delta\phi = -\frac{1}{\epsilon_0} \sum_s e_s n_s \quad (1.53)$$

$$\nabla \wedge \mathbf{B} = \mu_0 \mathbf{j} + \frac{1}{c^2} \frac{\partial \mathbf{E}}{\partial t} \quad (1.54)$$

with \mathbf{j} the electric current density, c the celerity of light, ϵ_0 and μ_0 the dielectric permittivity and permeability of free space respectively. This model describes fully both the particles and the electromagnetic fields of the plasma. Taking into account that in the limit $\beta \ll 1$, satisfied for a tokamak plasma, the magnetic field can be assumed to remain constant in time and that turbulent transport is dominated by its electrostatic component, two major approximations are made in our study:

- *Electrostatic approximation:* The time variations of the magnetic field are ignored. Consequently, the remaining unknowns are the distribution function f and the electric potential ϕ . Besides, the electric field reads in this approximation as $\mathbf{E} = -\nabla\phi$. This approximation should be removed when considering an electromagnetic model.
- *Gyrokinetic theory:* A change of coordinates is operated so that the fast phase of the particle motion becomes a coordinates that can be ignored. We thus operate a reduction of the phase space by eliminating the dependency over the cyclotron

angle φ_c introduced in part 1.2.2 that appeared in the Hamiltonian H describing the particle. Consequently, the new Hamiltonian \bar{H} describing the associated gyrocentre only depends of 5 variables, namely the coordinates of the gyrocentre $(\mathbf{x}_G, v_{G\parallel}, \mu)$. This description of the plasma is valid only if the difference between the two Hamiltonians $\tilde{H} = H - \bar{H}$ remains small compared to H . This is usually the case since the ratio $\tilde{H}/H \sim \rho^* \ll 1$.

In this so-called gyrokinetic model well described in [11, Brizard & Hahm 2007], the equations of the system, namely the Vlasov and Maxwell-Gauss equations, become the gyrokinetic and Poisson equations. The latter can be replaced by the quasi-neutrality equation in the limit of large wavelengths as compared to the Debye length.

First, the equations of the gyrokinetic model, namely the gyrokinetic and quasi-neutrality equations, are discussed. Second, a general description of the GYSELA code, which reproduces that model, is made.

1.3.1 The gyrokinetic model

The gyrokinetic equation

The Vlasov equation ^{6 7} (1.52) means that the distribution function f is conserved in the phase space (\mathbf{x}, \mathbf{v}) . It can be said equivalently that $f(\mathbf{X}(\mathbf{x}, t), \mathbf{V}(\mathbf{x}, t), t)$ remains constant along the trajectories so that:

$$\frac{d\mathbf{X}}{dt} = \mathbf{V} \quad \text{and} \quad \frac{d\mathbf{V}}{dt} = \frac{e}{m}(\mathbf{E} + \mathbf{V} \wedge \mathbf{B})$$

The Vlasov equation can then be developed according to its partial derivatives in position and velocity space and is recast as:

$$\frac{\partial f}{\partial t}(\mathbf{x}, \mathbf{v}, t) + \frac{d\mathbf{X}(t)}{dt} \cdot \frac{\partial f}{\partial \mathbf{x}}(\mathbf{x}, \mathbf{v}, t) + \frac{d\mathbf{V}(t)}{dt} \cdot \frac{\partial f}{\partial \mathbf{v}}(\mathbf{x}, \mathbf{v}, t) = 0 \quad (1.55)$$

The motion of the gyrocentre associated to a particle is obtained via a change of coordinates so that the fast phase of the particle motion becomes a coordinates that can be ignored (see Fig.1.8). We thus operate a reduction of phase space from 6 to 5 dimensions. We can then introduce the distribution function \bar{f} defined in the 5 dimensional phase space $(\mathbf{x}_G, v_{G\parallel}, \mu)$ and which describes the dynamics of the gyrocentres. Actually, the precise definition of a gyrocentre is a delicate matter which will be addressed in section 1.4.

⁶ This equation may be obtained by adopting a Hamiltonian approach or using the density of Klimontovich ([35, Ghendrih],[66, Nicholson 1983]).

⁷ This equation makes it possible to determine the complete evolution of f , whenever the initial conditions are set. Since macroscopic quantities such as density, pressure, energy flow are expressed as integrals of f over the velocity space, it is enough to have knowledge of the 6D-distribution function over time to know all the macroscopic data of the problem.

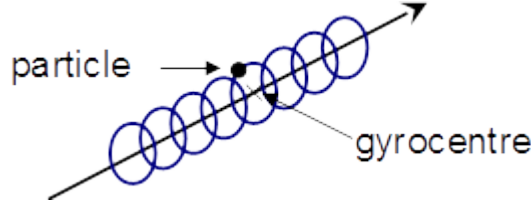


Figure 1.8: A particle motion in blue and its associated gyrocentre in black.

In the gyrokinetic model, we consider the Vlasov equation of the gyrocentres and not of the particles of the plasma. This gyrokinetic equation, whose derivation can be found in [11], is recalled here:

$$\boxed{\frac{\partial \bar{f}}{\partial t}(\mathbf{x}, v_{G\parallel}, \mu, t) + (\mathbf{v}_{G\perp} \cdot \nabla_{\perp} + v_{G\parallel} \nabla_{\parallel}) \bar{f}(\mathbf{x}, v_{G\parallel}, \mu, t) + \frac{dv_{G\parallel}}{dt} \frac{\partial \bar{f}}{\partial v_{G\parallel}}(\mathbf{x}, v_{G\parallel}, \mu, t) = 0} \quad (1.56)$$

where the evolution of the parallel velocity $v_{G\parallel}$ is given by Eq.(1.26) and the perpendicular velocity of gyrocentres $\mathbf{v}_{G\perp} = \mathbf{v}_E + \mathbf{v}_{D\nabla} + \mathbf{v}_{DC}$ reads as the sum of the electric and magnetic drifts derived respectively in Eqs.(1.22) and (1.24). In fact, Eq.(1.56) is an approximated form of the full gyrokinetic equation. A more rigorous form can be found in Eq.(5) of [40, Grandgirard 2016].

The quasi-neutrality equation

Let us rewrite Eq.(1.53) focussing only on the orders of magnitude:

$$\left| \sum_s e_s n_s \right| \simeq \varepsilon_0 k^2 |\phi|$$

The Debye length is defined as $\lambda_D = \sqrt{\varepsilon_0 T / (n_0 e^2)}$ where $n_0 \sim n_s$ stands for a typical plasma density. Poisson equation can be rewritten using the Debye length as:

$$\frac{|\sum_s e_s n_s|}{en_0} \simeq (k\lambda_D)^2 \left| \frac{e\phi}{T} \right|$$

In a tokamak plasma, the potential energy represents only a small fraction of the total energy stored in the tokamak. Actually, the ratio between potential and thermal energy is small enough to consider that the quantity $(k\lambda_D)^2 |e\phi/T| \ll 1$ for all values of k in the turbulence spectrum. Eventually, the Poisson equation is simplified in the equation of quasi-neutrality:

$$\boxed{\sum_s e_s n_s = 0} \quad (1.57)$$

1.3.2 Presentation of some properties of the GYSELA code

GYSELA (GYrokinetic SEmi-LAgrangian) is a numeric code solving the gyrokinetic model presented earlier composed of the gyrokinetic equation coupled with the equation of quasi-neutrality. This code is full- f (regarding the gyrokinetic equation), global, flux-driven, semi-Lagrangian. Some properties of this code, widely detailed in [40, Grandgirard 2016] and [1, Abiteboul 2012], are recalled hereafter.

Physical assumptions

The following key approximations have been made:

- *Circular magnetic flux surfaces*: The magnetic flux surfaces are nested concentric torus with circular section. The magnetic field lines \mathbf{B} wrap around these torus and their analytical expression is chosen as the simplified expression obtained in Eq.(1.7):

$$\mathbf{B} = B_0 \frac{R_0}{R} \left[\frac{r}{qR} \mathbf{e}_\theta + \mathbf{e}_\varphi \right]$$

- *Adiabatic electrons*: The electrons are supposed to follow a Boltzmann response which is at equilibrium with the electric potential. This assumption is no longer valid for turbulence developing on an electron scale, such as the Electron Temperature Gradients modes. Alternative models, where electrons are considered as a kinetic species, are the core of this PhD thesis.

Full- f regarding the gyrokinetic equation

Gyrokinetic codes can be sorted in two families regarding the treatment of the distribution function: those using the full- f method and those using the δf method. In the δf method [20, Denton 1995], the distribution function is decomposed as $f(t) = f_{eq} + \delta f(t)$ with f_{eq} a prescribed equilibrium profile that can be taken as a Maxwellian and δf a perturbation to this equilibrium that is let free to evolve in time. However, the back reaction of turbulent transport on the background equilibrium is not accounted for in this method. In the full- f method which is the one adopted in GYSELA, the whole distribution function is first initialized to an equilibrium profile and then let free to evolve in time. In a tokamak, the system is maintained out of equilibrium by particles and energy sources and sinks. It is therefore necessary to add in the code the source terms associated with the transported quantities (energy and particles in the case of kinetic electrons).

Global

A scale separation $k_\parallel qR \sim k_\perp \rho_i$ results from the strong anisotropy between the direction parallel to the magnetic field, characterized by weak density and temperature gradients, and the transverse directions. Some codes, called "flux-tube" ([25, Dorland 2000],[12, Candy 2003]) take advantage of this scale ordering and simulate a volume aligned on a magnetic field line and of small poloidal section. These local models enable to reduce

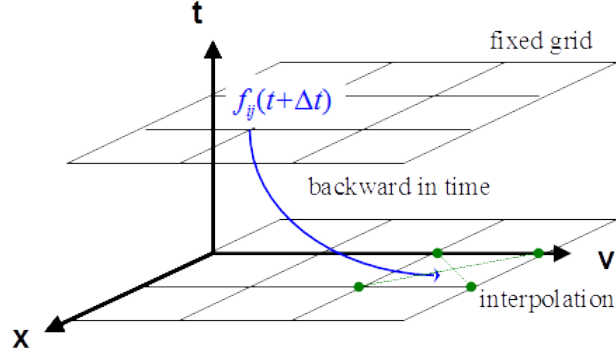


Figure 1.9: Scheme of the semi-lagrangian model.[1, Abiteboul 2012]

significantly the cost of simulations compared to other codes which simulate the whole plasma domain. However, such codes simulate only the evolution of small scales, the mean density and temperature profile being assumed to remain uniform. GYSELA is a "global" code which simulates the whole tokamak domain with a small radius belonging to an interval $[r_{min}, r_{max}]$, where r_{min} and r_{max} are chosen in the interval $[0, a]$.

Semi-Lagrangian

The specificity of this code is that it uses a semi-Lagrangian approach: the distribution function $f(\mathbf{x}, \mathbf{v}, t)$ evolves on a fixed grid in the phase space (\mathbf{x}, \mathbf{v}) , like Eulerian schemes. We assume the knowledge of the distribution function at each grid point x_i at time t . We are looking for its value at each grid point at time $t + \Delta t$. For this, we use the invariance of the distribution function along the characteristics (Lagrangian approach): the value of f at the grid point (x_j, v_j) at time $t + \Delta t$ is equal to its value at time t at the grid point (x'_j, v'_j) found by following backward in time the trajectories from $t + \Delta t$ to t . This foot of the characteristic is generally not a grid point. The value of f at this point is then obtained by interpolation (by cubic splines in GYSELA), using the knowledge of f in all the neighbouring grid points at the instant t (Fig. 1.9).

Gyroaverage operator

The gyrokinetic model uses some quantities that have to be averaged over the cyclotron motion. Let G be any function of the position \mathbf{x} . Noting φ_c the gyroangle, ρ_c the Larmor radius and \mathbf{x}_{GC} the guiding centre position associated to the particle position \mathbf{x} , the gyroaverage of G is given by the expression:

$$J.G(\mathbf{x}) = \left\{ \oint_0^{2\pi} \frac{d\varphi_c}{2\pi} e^{\rho_c \cdot \nabla} \right\} G(\mathbf{x}_{GC}) \quad (1.58)$$

J is called the gyroaverage operator. Besides, it can be noted that:

$$\oint_0^{2\pi} \frac{d\varphi_c}{2\pi} e^{\rho_c \cdot \nabla} = \oint_0^{2\pi} \frac{d\varphi_c}{2\pi} \sum_{n=0}^{\infty} \frac{(\rho_c \cdot \nabla)^n}{n!} = \oint_0^{2\pi} \frac{d\varphi_c}{2\pi} \sum_{n=0}^{\infty} \frac{(\rho_c \cdot \nabla)^{2n}}{(2n)!}$$

At the lowest order in $k_{\perp} \rho_c$, i.e. keeping only the first term $n = 0$, this integral is equal to 1. Therefore, at the lowest order, we have: $\langle \dots \rangle_{\varphi_c} \sim \dots(\mathbf{x}_{GC})$. In the case fluctuations of the various quantities are characterized by wavelengths that are large compared to the Larmor radius $k_{\perp} \rho_c \ll 1$, then J can be approximated to:

$$J_0(k_{\perp} \rho_c) \simeq \frac{1}{1 + (k_{\perp} \rho_c)^2 / 4}$$

This form of J is a Padé approximation.

Construction of an "equilibrium" distribution function from the averaged density and temperature profiles

The evolution of the distribution function is governed by the Boltzmann equation

$$\frac{df}{dt}(\mathbf{x}, \mathbf{v}, t) = \mathcal{C}(f) \quad (1.59)$$

where \mathcal{C} stands for the collision operator. However, it is not possible to find a stationary equilibrium which at the same time belongs to the kernel of the collision operator⁸ and is a function of the motion invariants, seen in part 1.2.2, only (except for the case where all density, average velocity and temperature profiles are flat). For this reason, it is difficult to find a true axisymmetric equilibrium, which is the purpose of the neoclassical theory.

In GYSELA, we introduce a Maxwellian distribution function constructed from averaged density and temperature profiles defined for any time t . Thus, we introduce the "equilibrium" density $n_{eq}(r, t) = \langle n(\mathbf{x}, t) \rangle_{FS}$ and temperature $T_{eq}(r, t) = \langle T(\mathbf{x}, t) \rangle_{FS}$, chosen independent of θ and φ ⁹, where the average on a magnetic flux surface of constant r is defined as:

$$\langle \dots \rangle_{FS} = \frac{\iint \frac{d\theta d\varphi}{\mathbf{B} \cdot \nabla \theta} \dots}{\iint \frac{d\theta d\varphi}{\mathbf{B} \cdot \nabla \theta}} \quad (1.60)$$

Here the designation "equilibrium" is abusive for these quantities do not depend on the motion invariants only. From these profiles, we can also define an "equilibrium" distribution function as:

$$f_{eq}(r, \theta, v_{\parallel}, \mu, t) = \frac{n_{eq}(r, t)}{[2\pi k_B T_{eq}(r, t)/m]^{3/2}} \exp \left\{ -\frac{\mathcal{E}_{eq}(r, \theta, v_{\parallel}, \mu, t)}{k_B T_{eq}(r, t)} \right\} \quad (1.61)$$

⁸ Boltzmann's H -theorem states that this steady state is obtained when the entropy is maximum, and when this state is reached, the solution f has a Maxwellian profile in velocity space [49, Helander 2002].

⁹In a MHD equilibrium, the ideal Euler equation reads $\mathbf{J} \wedge \mathbf{B} = \nabla p$. A consequence is $\mathbf{B} \cdot \nabla P = 0$ and the magnetic surfaces are isobar. In the case of a circular magnetic field, this means that P is independent of θ and φ .

with $\mathcal{E}_{eq}(r, \theta, v_{\parallel}, \mu, t) = \frac{1}{2}m(v_{\parallel} - V_{\parallel eq}(r, t))^2 + \mu B(r, \theta)$, $V_{\parallel eq}$ being the flux surface averaged parallel velocity. It can be noted here that there is no transverse component of the average velocity at lowest order. The solution of our evolution problem reads as the sum of this equilibrium function f_{eq} and a perturbation \tilde{f} :

$$f(\mathbf{x}, \mathbf{v}, t) = f_{eq}(r, \theta, \mathbf{v}, t) + \tilde{f}(\mathbf{x}, \mathbf{v}, t) \quad (1.62)$$

1.4 Calculation of the particle density in gyrokinetics

In the gyrokinetic model, we aim to describe the particle trajectories in a 5-dimensional space $(\mathbf{x}, v_{\parallel}, \mu)$. As particles evolve in the 6-dimensional space of positions and velocities (\mathbf{x}, \mathbf{v}) , two physical objects associated with each particle are introduced: the guiding-centre and the gyrocentre. The guiding-centre evolves in the 6-dimensional space (\mathbf{x}, \mathbf{v}) . Its trajectory is obtained by removing the cyclotronic motion to the particle's trajectory. The gyrocentre is then obtained by doing a phase space reduction to the 5 dimensions $(\mathbf{x}, v_{\parallel}, \mu)$. The objective here is to express the fluid moments, and in particular the density, as a function of the distribution function of the gyrocentres \bar{f} .

1.4.1 Link between particles and gyro-centres

The first step to take in order to derive the link between $f_s(\mathbf{x}, \mathbf{v}, t)$ and $\bar{f}_s(\mathbf{x}_{gy}, \mathbf{v}_{gy}, t)$ is to define correctly the various distribution functions used in this work.

- f is the distribution function of particles (of a given species), so that $n(\mathbf{x}) = \int f(\mathbf{x}, \mathbf{v}) d^3\mathbf{v}$ represents the density of particles at position \mathbf{x} .
- f_{GC} is the distribution function of guiding centres (associated with the previous particles), so that $n_{GC}(\mathbf{x}_{GC}) = \int f_{GC}(\mathbf{x}_{GC}, \mathbf{v}_{GC}) d^3\mathbf{v}_{GC}$ represents the density of guiding centres at position \mathbf{x}_{GC} . It is important to see that $n_{GC}(\mathbf{x}) \neq n(\mathbf{x})$ as one may see on Fig.1.10.
- \bar{f} is the distribution function of gyrocentres, so that $\bar{n}(\mathbf{x}_{gy}) = \int \bar{f}(\mathbf{x}_{gy}, \mathbf{v}_{gy}) d^3\mathbf{v}_{gy}$ represents the density of gyrocentres at position \mathbf{x}_{gy} .

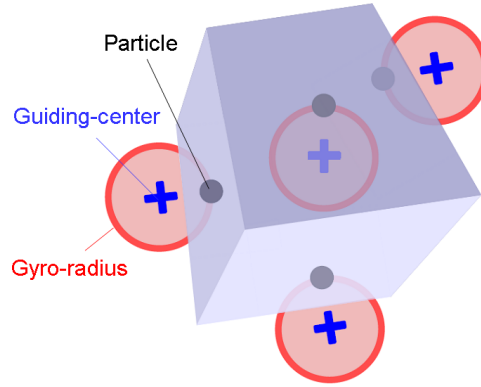


Figure 1.10: Difference between the particle and guiding-centre densities.[72, Sarazin 2013]

The coordinates of a guiding centre can be deduced from the coordinates of the particle by averaging its trajectory on a cyclotronic period: $\mathbf{x}(t) - \mathbf{x}_{GC}(t) = \rho_c$. The coordinates of a gyrocentre will be deduced from the coordinates of the guiding centre. We want the gyrocentres be defined in a 5 dimension space and we will see later which are the properties defining this new object. The aim of introducing these new coordinates is to simplify the description of the system, by gaining some degrees of liberty to describe the system (which means less parameters to compute in a numerical code).

The important point to notice is that these *three different distribution functions describe the same physical reality*. For each particle, there is only one guiding centre and one associated gyrocentre. Thus, it is natural to find the same value of the distribution function in coordinates associated with each type of item considered. Consequently, the distribution function of particles f evaluated at the position of the particles (\mathbf{x}, \mathbf{v}) is equal to the distribution function of guiding centres f_{GC} evaluated at the position of the guiding centres $(\mathbf{x}_{GC}, \mathbf{v}_{GC})$ and to the distribution function of gyro-centres \bar{f} evaluated at the position of the gyro-centres $(\mathbf{x}_{gy}, \mathbf{v}_{gy})$ (cf. [11, Brizard 2007]):

$$f(\mathbf{x}, \mathbf{v}) = f_{GC}(\mathbf{x}_{GC}, \mathbf{v}_{GC}) = \bar{f}(\mathbf{x}_{gy}, \mathbf{v}_{gy}) \quad (1.63)$$

The problem that occurs here is that the quasi-neutrality equation is a constraint on the particle densities of the different species s of the plasma, which can be expressed as integrals of the different f_s . But the gyrokinetic approach uses and computes only the distribution function of gyrocentres \bar{f}_s . Thus it is necessary to insert a link between the values of f and \bar{f} evaluated at the same point. Another point to state is that in the end, the physical quantities, like density, should be expressed in the real space \mathbf{x} . This fixes the choice of coordinates used when the link between both distribution functions is made. This change of coordinates from particle to gyrocentre is tackled in Appendix A.2. This eventually leads to the following relation between f and \bar{f} :

$$f(\mathbf{x}, \mathbf{v}, t) = e^{-\rho_c \cdot \nabla} \bar{f}(\mathbf{x}, \mathbf{v}_{GC}, t) + \frac{e}{B} \{ \phi(\mathbf{x}, t) - \bar{\phi}(\mathbf{x}_{gy}, t) \} e^{-\rho_c \cdot \nabla} \partial_\mu \bar{f}(\mathbf{x}, \mathbf{v}_{GC}) \quad (1.64)$$

It is now possible to express the density of particle using only the distribution function of gyrocentres \bar{f} .

1.4.2 Expression of the particle density

Guiding-centers and electric potential contributions

Equation (1.64) provides the relationship between the particle density n_s and the guiding-center density n_{Gs} :

$$\begin{aligned} n_s(\mathbf{x}, t) &= \int d^3\mathbf{v} e^{-\rho_c \cdot \nabla} \bar{f}_s(\mathbf{x}, \mathbf{v}_{GC}, t) \\ &+ \int d^3\mathbf{v} \frac{e_s}{B} \{ \phi(\mathbf{x}, t) - \bar{\phi}(\mathbf{x}_{gy}, t) \} e^{-\rho_c \cdot \nabla} \partial_\mu \bar{f}_s(\mathbf{x}, \mathbf{v}_{GC}) \end{aligned} \quad (1.65)$$

The first integral on the right hand side corresponds to the gyro-center density $n_{G,s}(\mathbf{x}, t)$. Using the gyro-average operator J (see Eq.(1.58)), and writing $\mathcal{J}_v = (2\pi B_{\parallel}^*/m_s)$ as the Jacobian in the velocity space, it gives:

$$n_{G,s}(\mathbf{x}, t) = \int \mathcal{J}_v d\mu dv_{G\parallel} J. \bar{f}_s(\mathbf{x}, \mathbf{v}_{GC}, t) \quad (1.66)$$

The last integral on the right hand side is the polarization density $n_{pol,s}$. Besides, the averaged value of ϕ on the gyroangle reads:

$$\bar{\phi}(\mathbf{x}_{gy}, t) = \left\{ \int \frac{d\varphi_c}{2\pi} e^{\rho_c \cdot \nabla} \right\} \phi(\mathbf{x}_{GC}, t) = \left\{ e^{-\rho_c \cdot \nabla} \left(\int \frac{d\varphi_c}{2\pi} e^{\rho_c \cdot \nabla} \right) \right\} \phi(\mathbf{x}, t)$$

Further recalling that $\mathbf{x}_{gy} = \mathbf{x} - \rho_c$ and by replacing the expression of $\bar{\phi}(\mathbf{x}_{gy}, t)$ in $n_{pol,s}$, it follows:

$$n_{pol,s}(\mathbf{x}, t) = \int \mathcal{J}_v d\mu dv_{G\parallel} \frac{e_s}{B} \int_0^{2\pi} \frac{d\varphi_c}{2\pi} \left\{ e^{-\rho_c \cdot \nabla} \partial_\mu f_{eq,s}(\mathbf{x}, \mathbf{v}) [1 - e^{-\rho_c \cdot \nabla} \langle e^{\rho_c \cdot \nabla} \rangle] \phi(\mathbf{x}, t) \right\} \quad (1.67)$$

The brackets $\langle \dots \rangle$ stand for the average over the gyro-phase: $\langle \dots \rangle \equiv \int_0^{2\pi} \dots \frac{d\varphi_c}{2\pi}$.

Expression of n_{pol} in the large wavelength limit

It is useful to consider the large wavelength limit $k_{\perp} \rho_c \ll 1$ of Eq.(1.67), for which some particularly compact expression of $n_{pol,s}$ can be derived. In such a limit, one can restrict the Taylor expansion of the operator to the leading terms of the development only. Details of the calculus are given in Appendix A.3. At second order in $k_{\perp} \rho_c$, it comes:

$$n_{pol,s}(\mathbf{x}, t) \simeq \nabla_{\perp} \cdot \left(\frac{m_s n_{eq,s}}{e_s B^2} \nabla_{\perp} \phi(\mathbf{x}, t) \right) \quad (1.68)$$

Chapter 2

Accounting for kinetic electrons in GYSELA

2.1 Ion turbulence with adiabatic electrons

In the classic gyrokinetic model detailed in chapter 1, the description of the plasma requires to solve one gyrokinetic equation per kinetic species, each coupled to the others via the Maxwell-Gauss equation which, in the electrostatic limit and for wavelength scales large compared to the Debye length, reduces to the quasi-neutrality equation. The dynamics of each kinetic species, ions and electrons, is well defined in this case.

From the numerical point of view, it should be noticed that the time step needed to accurately follow the dynamics of each species should scale like $\Delta t_s \propto R_0/v_{th,s}$ ¹, with R_0 the tokamak major radius and $v_{th,s}$ the thermal velocity of species s . The ratio of the ion and electron time step is then given by:

$$\frac{\Delta t_i}{\Delta t_e} \sim \frac{v_{th,e}}{v_{th,i}} = \sqrt{\frac{m_i}{m_e}}$$

at equal temperatures with m_s the mass of species s . This ratio is of the order of 60 for deuterium ions. In the presence of both ions and electrons, to resolve the dynamics of both species, it is needed to use the smallest time step, in that case Δt_e . Using this time step in GYSELA would be too costly as far as computation time is concerned, and it would be preferable to use Δt_i as the global time step of the model.

A possibility to circumvent this problem is to assume that the electrons are adiabatic, i.e. they are at equilibrium with the ambient electric potential. In that model, only ions are supposed kinetic. This allows us to choose a relatively large time step to describe the dynamics of the plasma.

¹ Instabilities can add other constraints to Δt . E.g., the typical growth rate of ITG $\gamma \sim v_{th}/(RL_T)^{1/2}$, where L_T stands for the characteristic length of the temperature gradient, would impose $\Delta t \gamma \lesssim 1$.

The drawback of this model is that there can be no particle transport and some classes of instabilities, namely the Trapped Electron Modes (TEM), which are believed to play a major role in turbulent transport are not taken into account. In the following, the quasi-neutrality equation is first derived with the hypothesis of adiabatic electrons and then with kinetic electrons.

2.1.1 Quasi-neutrality with adiabatic electrons

The quasi-neutrality equation (1.57) reads:

$$\sum_i Z_i n_i(\mathbf{x}, t) = n_e(\mathbf{x}, t) \quad (2.1)$$

The average on a flux surface ² of this equation is $\sum_i Z_i \langle n_i \rangle_{FS} = \langle n_e \rangle_{FS}$ where $\langle \dots \rangle_{FS}$ stands for the average on a flux surface and defined in Eq.(1.60). Calling $\tilde{n}_s = n_s - \langle n_s \rangle_{FS}$, Eq.(2.1) minus its averaged value on a flux surface gives:

$$\sum_i Z_i \tilde{n}_i(\mathbf{x}, t) = \tilde{n}_e(\mathbf{x}, t) \quad (2.2)$$

It is needed to find the expressions of \tilde{n}_i and \tilde{n}_e in the adiabatic electrons model to develop this equation.

Initially, the gyrocentre distribution function \bar{f}_s for each species s is set as a Maxwellian given by Eq.(1.61):

$$\bar{f}_{s,eq}(r, \theta, \mathbf{v}, t) = \frac{\langle n_s \rangle_{FS}(r, t)}{(2\pi \langle T_s \rangle_{FS}(r, t)/m_s)^{3/2}} e^{-\frac{\mathcal{E}_s(r, \theta, \mathbf{v})}{\langle T_s \rangle_{FS}(r, t)}} \quad (2.3)$$

As it has already been said in section 1.3.2, the eq subscript is misleading: in practice, it simply refers to the fact that during the plasma evolution, the distribution function does not change much from this Maxwellian profile. Thus, we abusively call it an "equilibrium" distribution function. From Eq.(2.3), we can define the equilibrium density of gyrocentres as:

$$n_{Gi,eq}(\mathbf{x}, t) = \int J_{0i} \bar{f}_{i,eq}(\mathbf{x}, \mathbf{v}, t) d^3v$$

The difference between the densities $n_{Gi,eq}$ and $\langle n_i \rangle_{FS}$ reduces to terms in ρ_i/L_\perp where L_\perp is a typical gradient length of $\langle n \rangle_{FS}$ and $\langle T \rangle_{FS}$. A priori, we have $\rho_i \ll L_\perp$ and we can therefore assume that $n_{Gi,eq}$ remains very close to $\langle n_i \rangle_{FS}$. Taking up the expression of particle density in the previous section (Eq.(1.66) and (1.68)), it comes:

$$n_i(\mathbf{x}, t) = \int J_{0i} \bar{f}_i(\mathbf{x}, \mathbf{v}, t) d^3v + \nabla_\perp \cdot \left(\frac{m_i n_{eq,i}}{e_i B^2} \nabla_\perp \phi \right)$$

²Hereafter, we shall restrict ourselves to simplified magnetic equilibrium, made of concentric flux surfaces of circular poloidal cross section. In this case, a given flux surface is given by $r = cste$.

Consequently, the final expression of $\tilde{n}_i \simeq n_i - n_{Gi,eq}$ is:

$$\tilde{n}_i(\mathbf{x}, t) = \int J_{0i}(\bar{f}_i - \bar{f}_{i,eq}) d^3v + \nabla_{\perp} \cdot \left(\frac{m_i n_{eq,i}}{e_i B^2} \nabla_{\perp} \phi \right) \quad (2.4)$$

where the notations introduced in chapter 1 have been used.

Electrons are assumed adiabatic, i.e. they are supposed to stay at equilibrium with the electric potential. In this case, $\tilde{n}_e(\mathbf{x}, t)$ is not obtained via the electron distribution function³. The expression of the electron density using the potential is obtained via the fluid force balance for electrons. The simplified momentum conservation equation applied to electrons, reads:

$$m_e n_e \left(\frac{\partial \mathbf{u}_e}{\partial t} + (\mathbf{u}_e \cdot \nabla) \mathbf{u}_e \right) = -\nabla p_e - e n_e (\mathbf{E} + \mathbf{u}_e \wedge \mathbf{B}) \quad (2.5)$$

where the collisions have been neglected and the pressure tensor has been reduced to a scalar pressure p_e . \mathbf{E} , \mathbf{B} are respectively the electric and magnetic fields. Neglecting the electron inertia and projecting this relationship on the axis parallel to the magnetic field, only remain the terms of pressure and Coulomb force:

$$-e n_e E_{\parallel} - \nabla_{\parallel} p_e = 0 \Rightarrow \nabla_{\parallel} p_e = e n_e \nabla_{\parallel} \phi \quad (2.6)$$

Besides $p_e = n_e T_e$, and consequently $\nabla_{\parallel} p_e = n_e \nabla_{\parallel} T_e + T_e \nabla_{\parallel} n_e$. In order to know which of these two terms is dominant, we compare the parallel diffusion coefficient for energy ($D_{T,\parallel e}$), and for particles ($D_{n,\parallel e}$). These coefficients are expressed in m²/s. These diffusions are collisional processes and it is possible to express $D_{X,\parallel e} = v_{Xe}^2 / \nu$ with v_{Xe} a characteristic velocity of variation of X (between two collisions), and ν a characteristic collision frequency. The characteristic velocity which appears in the temperature diffusion is the parallel velocity of the electrons. This velocity is taken equal to the electron thermal velocity. Noting k_B the Boltzmann constant, the thermal parallel diffusion coefficient for electrons reads:

$$D_{T,\parallel e} \sim \frac{v_{th,e}^2}{\nu} \text{ with } v_{th,e} = \sqrt{\frac{3k_B T_e}{m_e}}$$

The electrons will tend to follow the quasi-neutrality, and the electron density gradients will therefore have a similar profile to the ion density gradients. Therefore, the characteristic velocity appearing in $D_{n,e}$ is the ion thermal velocity:

$$D_{n,\parallel e} \sim \frac{v_{th,i}^2}{\nu} \text{ with } v_{th,i} = \sqrt{\frac{3k_B T_i}{m_i}}$$

Supposing $T_e \sim T_i$, the ratio between the two latter coefficient gives:

$$\frac{D_{n,\parallel e}}{D_{T,\parallel e}} \sim \frac{m_e}{m_i} \ll 1 \quad (2.7)$$

³ f_e does not exist in this model.

Electrons are highly mobile, they therefore thermalize very quickly, which has the effect of smoothing the parallel temperature gradients. From relationship (2.7), it comes:

$$\frac{\nabla_{\parallel} n_e}{n_e} \gg \frac{\nabla_{\parallel} T_e}{T_e} \Leftrightarrow T_e \nabla_{\parallel} n_e \gg n_e \nabla_{\parallel} T_e$$

Eventually, $\nabla_{\parallel} p_e \simeq T_e \nabla_{\parallel} n_e$. Therefore, Eq.(2.6) becomes at leading order:

$$\frac{\nabla_{\parallel} n_e}{n_e} \simeq \frac{e}{T_e} \nabla_{\parallel} \phi \Rightarrow \nabla_{\parallel} [\ln(n_e)] \simeq \nabla_{\parallel} \left[\frac{e}{T_e} \phi \right]$$

For a perturbation satisfying $\nabla_{\parallel} \left[\frac{e}{T_e} \phi \right] = 0$, there is no electron density response $\nabla_{\parallel} [\ln(n_e)] = 0$. Therefore, when the potential is the same on the same flux surface $\phi = \langle \phi \rangle_{FS}$, it comes $\nabla_{\parallel} n_e = 0$. Consequently, the only fluctuations of the electron density which can be different from 0 are the modes $k_{\parallel} \neq 0$. In the adiabatic electron approach, we assume $\tilde{n}_e = 0$ for the modes which remain constant on a magnetic surface (for these modes $k_{\parallel} = 0$). The electron density is then equal to its equilibrium value $n_{e,eq}$. The integration of this equation gives the following expression of the adiabatic electron density n_e^{adiab} :

$$n_e^{adiab} = n_{e,eq} e^{\frac{e}{T_e} (\phi - \langle \phi \rangle_{FS})} \quad (2.8)$$

Performing a limited development of n_e^{adiab} around its equilibrium value $\phi = \langle \phi \rangle_{FS}$, we get:

$$\tilde{n}_e^{adiab} \simeq \frac{n_{e,eq} e}{T_e} (\phi - \langle \phi \rangle_{FS}) \quad (2.9)$$

Replacing the expressions of $\tilde{n}_i(\mathbf{x}, t)$ (2.4) and $\tilde{n}_e(\mathbf{x}, t)$ (2.9) in the adiabatic quasi-neutrality equation (2.2), it comes eventually:

$$\sum_i \left[Z_i \int J_{0i} \cdot (\bar{f}_i - \bar{f}_{i,eq}) \, d^3v + Z_i \nabla_{\perp} \cdot \left(\frac{m_i n_{i,eq}}{e_i B^2} \nabla_{\perp} \phi \right) \right] = \frac{n_{e,eq} e}{T_e} (\phi - \langle \phi \rangle_{FS}) \quad (2.10)$$

It states that the sum over all species of charge density fluctuations is zero.

The GYSELA code is written in normalized units based on the following normalization choices. We use SI units and a thermal energy scale in electron volts ($1 \text{ eV} = 1.6022 \cdot 10^{-19} \text{ J}$). The four fundamental dimensional normalizing quantities are: a reference ionic mass $m_0 = A_0 m_p$ [kg], a reference ionic charge $q_0 = Z_0 e$ [C], a reference magnetic induction B_0 [T] and a reference thermal energy T_0 [eV]. Here, A_0 and Z_0 are the (dimensionless) mass number and charge state of the main ion species and e the modulus of the electron charge. These quantities are used to define the reference ion cyclotron frequency ω_{c_0} , the reference thermal speed $v_{th,0}$ and the reference Larmor-radius ρ_0 as $\omega_{c_0} = \frac{Z_0 e B_0}{m_0}$, $v_{th,0} = \sqrt{\frac{T_0}{m_0}}$ and $\rho_0 = \frac{v_{th,0}}{\omega_{c_0}} = \frac{\sqrt{T_0 m_0}}{Z_0 e B_0}$. Finally, we choose the equilibrium electron density at mid radius n_0 as reference density. Physical quantities (mass, length, time, charge and density) can be recovered from the normalized quantities used in the code (denoted with a hat symbol) by choosing values for $[A_0, Z_0, B_0, T_0, n_0]$ and applying

$m_s = A_s m_p = m_0 \hat{A}_s$ with $A_s = A_0 \hat{A}_s$, $q_s = Z_0 e \hat{Z}_s$, $l = \rho_0 \hat{l}$, $t = \frac{\hat{t}}{\omega_{c0}}$ and $n_s = n_0 \hat{n}_s$. The velocities are normalized to the corresponding thermal velocities $v_{th,s0} = \sqrt{T_0/m_s}$, i.e. $v = v_{th,s0} \hat{v}_s = \frac{v_{th,s0}}{\sqrt{\hat{A}_s}} \hat{v}_s$. The main normalizations are thus $U = \frac{T_0}{Z_0 e} \hat{\phi}$, $B = B_0 \hat{B}$, $T_s = T_0 \hat{T}_s$ while $\mu_s = \frac{T_0}{B_0} \hat{\mu}_s$ with $\hat{\mu}_s = \frac{\hat{v}_{\perp s}^2}{2\hat{B}}$ and $\mu_0 \mathbf{J} = \frac{B_0}{\rho_0} \hat{\mathbf{J}}$ with $\hat{\mathbf{J}} = \hat{\nabla} \times \hat{\mathbf{B}}$. By deduction, $\mathbf{E} = E_0 \hat{\mathbf{E}}$ with $E_0 = v_{th,0} B_0$ and the normalized distribution function \hat{f}_s , which evolves in the code, is defined as $\hat{f}_s = f_s v_{th,s0}^3 / n_0$. Finally, the energy is normalized to the reference thermal energy T_0 . In what follows, all the quantities considered are normalized coordinates, but hat symbols are omitted for the sake of readability.

In Eq.(2.10), we do the following approximations : (i) equilibrium quantities are safely replaced by their initial values⁴ and (ii) $B/B_0 \simeq 1$. The normalized quasi-neutrality equation which is solved by the GYSELA code in the case of adiabatic electrons then reads:

$$\boxed{\sum_i Z_i \int J_{0i} \cdot (\bar{f}_i - \bar{f}_{i0}) d^3v + \nabla_{\perp} \cdot (A_i n_{i0} \nabla_{\perp} \phi) = \frac{n_{e0}}{T_{e0}} (\phi - \langle \phi \rangle_{FS})} \quad (2.11)$$

where the last term on the left hand side corresponds to the ion polarization density. The velocity volume element reads:

$$d^3v = \mathcal{J}_v d\mu dv_{G\parallel} \quad \text{with} \quad \mathcal{J}_v = 2\pi B_{\parallel,s}^* \quad \text{and} \quad B_{\parallel,s}^* \equiv B + A_s/Z_s v_{G\parallel} \mathbf{b} \cdot (\nabla \wedge \mathbf{b}) \quad (2.12)$$

\mathcal{J}_v is the normalized Jacobian in velocity space. J_{0i} stands for the normalized gyro-average operator defined in Eq.(1.58). In the limit of large wave lengths (as compared to the cyclotron radius ρ_c), we use the Padé development which reads in GYSELA:

$$J_{0i} = \frac{1}{1 - \frac{\rho_c^2}{4} \nabla_{\perp}^2} \simeq 1 + \frac{A_i \mu}{2Z_i^2 B} \nabla_{\perp}^2 \quad \text{with} \quad \nabla_{\perp}^2 \simeq \frac{1}{r} \partial_r (r \partial_r) + \frac{1}{r^2} \partial_{\theta}^2 \quad (2.13)$$

In GYSELA, B in Eq.(2.13) is replaced by 1. Replacing ∇_{\perp} by ik_{\perp} it comes:

$$J_{0i} \simeq 1 - \frac{A_i \mu k_{\perp}^2}{2Z_i^2}$$

n_{e0} is the constant-in-time electron density, i.e. the initial electron density profile. Indeed, assuming an adiabatic response for the electrons freezes the phase shift between density and electric potential fluctuations: it is vanishing, hence preventing any turbulent particle transport due to the electric drift. Also, the equilibrium densities satisfy the quasi-neutrality constraint, so that $\sum_i Z_i n_{i0} = n_{e0}$: there is no electric potential at equilibrium. Notice that, with these definitions, one has $\int d^3v_i \bar{f}_{i0} = n_{i0}$, with \bar{f}_{i0} the initial distribution function of species “ i ”.

⁴ This approximation is legitimate in the case of adiabatic electrons, because in this case there is no particle transport as it is verified in part 2.1.2.

2.1.2 Limits of the adiabatic electrons approach - Need for kinetic electrons

This model of adiabatic electrons has some limitations.

First, this model prevents any significant turbulent transport of matter. Indeed, the expression of the turbulent radial transport of particles Γ_r given by the perturbed part of Eq.(1.51) and averaged on a surface of constant r reads:

$$\Gamma_r = \langle \tilde{n}_e \tilde{v}_{Er} \rangle_{FS} \quad (2.14)$$

where \tilde{n}_e is given by equation (2.9) and $\tilde{v}_{Er} = E_\theta/B$ is the radial component of the electric drift velocity. The average on a flux surface is defined in Eq.(1.60). The expression of Γ_r becomes:

$$\Gamma_r = -\frac{en_{e,eq}}{rT_e} \frac{1}{\iint \frac{d\varphi d\theta}{\mathbf{B} \cdot \nabla \theta}} \iint \frac{d\varphi d\theta}{\mathbf{B} \cdot \nabla \theta} (\phi - \langle \phi \rangle_{FS}) \frac{\partial_\theta \phi}{B} \quad (2.15)$$

A full calculation of Γ_r is made in Appendix B.1. Eventually, we get in the limit $\varepsilon \ll 1$:

$$\Gamma_r \simeq -\frac{en_{e,eq}}{rT_e} \frac{\varepsilon}{4\pi^2 B} \iint d\varphi d\theta 3 \cos \theta (\phi - \langle \phi \rangle_{FS}) \partial_\theta \phi$$

It appears that Γ_r evolves as ε . Therefore no significant radial particle transport is allowed in the case of adiabatic electrons.

Second, instabilities governed by the electrons, and in particular those trapped in the local mirrors of the magnetic configuration, are not taken into account. Numerous fluid [33, Garbet 2003] and kinetic [79, Weiland 1992], [77, Waltz 2007] models show that they can carry a turbulent transport which is of the same order of magnitude as that due to the ion turbulence in certain regimes of parameters in current tokamaks. Therefore one can expect that ion turbulence, especially the Ion Temperature Gradient modes (ITG), may have a different behaviour depending on whether the electron response is set as adiabatic or kinetic. In other words, the ion turbulence transport may not be accurately computed with the hypothesis of adiabatic electrons.

For these reasons, a new model where electrons are modelled by a kinetic distribution function has been implemented. Accounting for kinetic electrons means that the distribution function of the electron gyrocentres f_e evolves in time. In this case, the electron response (first term of Eq.(2.11)) is no longer adiabatic. The quasi-neutrality condition is then modified.

2.2 Quasi-neutrality with kinetic electrons

Kinetic electrons allow for particle transport, so that the flux surface density profiles are evolving in time. The quasi-neutrality then deals with the full charge densities, and not only the fluctuating parts. From here, we use the notation f instead of \bar{f} to refer to gyrocentre distribution functions for more readability. Accounting for both gyrocentre and polarization contributions for all species, it reads as follows:

$$\sum_i Z_i \{n_{G,i} + n_{pol,i}\} = n_{G,e} + n_{pol,e} \quad (2.16)$$

where we have introduced for any species s the notations:

$$n_{G,s} = \int J_{0s} \cdot f_s(\mathbf{x}, \mathbf{v}, t) d^3v \quad ; \quad n_{pol,s} = \nabla_{\perp} \cdot \left(\frac{m_s n_{s,eq}(r, t)}{e_s B(\mathbf{x})^2} \nabla_{\perp} \phi(\mathbf{x}, t) \right) \quad (2.17)$$

In the polarization term, we have done the approximation $n_s(\mathbf{x}, t) \simeq n_{s,eq}(r, t)$ where $n_{s,eq}(r, t)$ stands for the equilibrium density, more precisely the flux surface averaged density: $n_{s,eq}(r, t) = \langle n_s(\mathbf{x}, t) \rangle_{FS}$ where $\langle \dots \rangle_{FS}$ stands for the average on a flux surface. In the present version of GYSELA, $n_{s,eq}(r, t)$ is approximated by the initial density profile n_{s0} .

Should $A_e = m_e/m_0$ be the normalized mass of electrons, m_0 being the proton mass ($A_e \approx 1/1836$), then the electron polarization density could be neglected. Also, J_{0e} could be safely approximated by 1. In GYSELA, we decide to keep it since some test simulations were performed at artificial larger values of A_e . However, for simplification purpose, we can do these approximations in the present study. Using the normalizations introduced for Eq.(2.11), the normalized full kinetic quasi-neutrality equation becomes:

$$\sum_i Z_i \{n_{G,i} + n_{i,pol}\} = \int f_e d^3v \quad (2.18)$$

where the normalized gyrocentre and polarization densities of the ions are defined by:

$$n_{G,i} = \int J_{0i} \cdot f_i d^3v \quad ; \quad n_{pol,i} = \nabla_{\perp} \cdot (A_i n_{i0} \nabla_{\perp} \phi) \quad (2.19)$$

The drawback of the formulation Eq.(2.18) is that it contains terms of very different magnitudes: the polarization contributions are much smaller than the gyrocentre densities. From Eq.(2.17), it is possible to evaluate the ratio $n_{pol,s}/n_{G,s} \sim (k_{\perp} \rho_{th,s})^2 \rho_s^* \ll 1$ where $\rho_s^* = \rho_{th}/a$. Numerical errors on the computation of gyrocentre densities may then compete with the actual values of the polarization densities. An alternative is then to subtract on both sides the same kinetic quantity, expressed in the various velocity spaces (that of the electrons and of the ions), so as to bring the magnitude of the integrals to the level of the polarization terms. The method is detailed in the following.

The kinetic quantity that is subtracted to each side of the QN equation is an anisotropic Maxwellian distribution function constructed from the actual equilibrium distribution function of the ions:

$$f_{i,eq} = \frac{n_{i,eq}}{(2\pi)^{3/2} T_{\parallel i,eq}^{1/2} T_{\perp i,eq}} \exp \left\{ -\frac{(v_{G\parallel i} - V_{\parallel i,eq})^2}{2T_{\parallel i,eq}} - \frac{\mu B}{T_{\perp i,eq}} \right\} \quad (2.20)$$

where $n_{i,eq}$, $V_{\parallel i,eq}$, $T_{\parallel i,eq}$ and $T_{\perp i,eq}$ are functions of radius and time:

$$n_{i,eq}(r, t) = \left\langle \int f_i d^3v \right\rangle_{FS} \quad (2.21)$$

$$n_{i,eq} V_{\parallel i,eq}(r, t) = \left\langle \int v_{G\parallel i} f_i d^3v \right\rangle_{FS} \quad (2.22)$$

$$n_{i,eq} T_{\parallel i,eq}(r, t) = \left\langle \int (v_{G\parallel i} - V_{\parallel i,eq})^2 f_i d^3v \right\rangle_{FS} \quad (2.23)$$

$$n_{i,eq} T_{\perp i,eq}(r, t) = \left\langle \int \mu B f_i d^3v \right\rangle_{FS} \quad (2.24)$$

One wishes to subtract the quantity

$$n_{e\mathcal{R}}(r, \theta, t) = \sum_i Z_i \int J_{0i} \cdot f_{i,eq} d^3v \quad (2.25)$$

to the right hand side of Eq.(2.18). The idea is then to construct an electron distribution function $f_{e\mathcal{R}}$ of the same form as Eq.(2.20) such that $n_{e\mathcal{R}} = \int f_{e\mathcal{R}} d^3v$. Here, $f_{e\mathcal{R}}$ is constructed as follows:

$$f_{e\mathcal{R}} = \frac{n_{e\mathcal{R}}}{(2\pi)^{3/2} T_{\parallel e,eq}^{1/2} T_{\perp e,eq}} \exp \left\{ -\frac{(v_{G\parallel e} - V_{\parallel e,eq})^2}{2T_{\parallel e,eq}} - \frac{\mu B}{T_{\perp e,eq}} \right\} \quad (2.26)$$

where $V_{\parallel e,eq}$, $T_{\parallel e,eq}$ and $T_{\perp e,eq}$ are calculated from the electron distribution function f_e computed at time t in the same way as Eqs.(2.22), (2.23) and (2.24). Conversely, the calculation of the electron density profile $n_{e\mathcal{R}}$ relies on the constraint imposed by Eq.(2.25). Appendix B.2 details how to compute $n_{e\mathcal{R}}$ when J_{0e} is considered different of 1. The quantities $\sum_i Z_i \int J_{0i} \cdot f_{i,eq} d^3v$ and $\int f_{e\mathcal{R}} d^3v$ can then be subtracted to the left and right hand sides of Eq.(2.18), respectively, which then remains unchanged. Eq.(2.18) is then replaced by:

$$\sum_i Z_i \left\{ \int J_{0i} \cdot (f_i - f_{i,eq}) d^3v + n_{pol,i} \right\} = \int (f_e - f_{e\mathcal{R}}) d^3v \quad (2.27)$$

In the current implementation of the quasi-neutrality equation with kinetic electrons in GYSELA, some simplifications are made:

- We notice that the quantity $n_{e\mathcal{R}}$ given by Eq.(2.25) depends on both r and θ . The latter dependency comes from the gyro-average operator J_0 , which exhibits a B dependency. Indeed, using the expression of the normalized gyro-average operator Eq.(2.13), $\int d^3v J_{0i} \cdot f_{i,eq}$ gives at leading order for protons, in normalized units:

$$\int d^3v J_{0i} \cdot f_{i,eq} \simeq n_i + \frac{A_i}{2Z_i^2 B^2} \nabla_\perp^2 \int d^3v \mu B f_{i,eq} \simeq n_i \left[1 + \frac{a^2}{2L_p^2} \rho_i^{*2} (1 + 2\varepsilon \cos \theta) \right]$$

with L_p the transverse pressure gradient length and $\rho_i^* = m_i T_i / (a Z_i^2 e^2 B_0^2)$ the normalized ion gyro-radius computed with B_0 . Using this rough estimate, the poloidal component of $n_{e\mathcal{R}}$ turns out to be of order $\varepsilon \rho_i^{*2} \ll 1$ as compared to the leading term, which only depends on r . Consistently, in the following, the poloidal dependency of $n_{e\mathcal{R}}$ will safely be ignored.

- We notice that the distribution functions $f_{i,eq}$ and $f_{e\mathcal{R}}$ present in Eq.(2.27) depend on time. We choose for now to get rid of this dependency. This simplification should be removed in the future.

Therefore, the quantity subtracted on each side of Eq.(2.18) reads:

$$n_{e\mathcal{R}0}(r) = \sum_i Z_i \int J_{0i} \cdot f_{i0} d^3v$$

where f_{i0} stands for the initial distribution function of ions. Besides, we write $n_{e\mathcal{R}0} = \int f_{e\mathcal{R}0} d^3v$ where $f_{e\mathcal{R}0}$ is defined by Eq.(2.26) at time $t = 0$. In that expression, we have chosen $V_{\parallel e,eq} = 0$, $T_{\parallel e,eq} = T_{\perp e,eq} = T_{e0}(r)$ with T_{e0} chosen freely. Accounting for these simplifications, the quasi-neutrality equation which is effectively solved in GYSELA reads as follows:

$$\boxed{\sum_i Z_i \left\{ \int J_{0i} \cdot (f_i - f_{i0}) d^3v + n_{pol,i} \right\} = \int (f_e - f_{e\mathcal{R}0}) d^3v} \quad (2.28)$$

2.3 Filter for (deeply) trapped electrons

2.3.1 The advantage of a filter

Light electrons have a much larger parallel speed than ions, in the typical ratio $(m_i/m_e)^{1/2}$ at equal temperatures. So as to accurately capture their dynamics, the numerical time step has then to be reduced by the same factor as compared to simulations with adiabatic electrons, i.e. $\Delta t^{KE} \sim (m_e/m_i)^{1/2} \Delta t^{AE} \ll \Delta t^{AE}$ (where KE and AE stand respectively for kinetic and adiabatic electrons). This can rapidly lead to a prohibitive increase of the amount of CPU time for a single simulation run. One way of circumventing this difficulty is to decrease artificially the mass ratio m_i/m_e in order to reduce the CPU time consumption. By doing so however, the response time scales of electrons are modified and it is therefore important to check how the behaviour of the plasma is impacted. The idea is to see on the one hand if it is possible to make additional hypotheses to circumvent the physical problems posed by an artificially low mass ratio and on the other hand if it is possible to retrieve some physics from such simulations that could be compared to the behaviour of a real plasma [12, 8, Candy 2003, Bottino 2010]:

- *Drawback*: For "heavy" passing electrons, the inertia term of Eq.(2.5) is no longer negligible. Consequently, these electrons will not have an adiabatic response, whereas "standard" electrons do. A solution is to force their adiabatic response via a filtering of passing electrons.
- *Advantage*: Little impact is expected on TEM turbulence since the TEM instability develops at frequencies of the order of $\omega_{de} \sim q\rho_{ce}^2\omega_{ce}/rR = \frac{qT_e}{eBrR}$ which is independent of m_e .

Thus the insertion of a filtering in which trapped electrons only are treated kinetically while passing electrons have an adiabatic response, would enable to study both electron turbulence and the impact of kinetic electrons on ion turbulence while ensuring that the passing electrons are correctly described. The idea is to set up a filter in the velocity space:

$$\left| \frac{v_{G\parallel}}{v_{\perp}} \right| \leq \sigma_0 \sqrt{\frac{B_{max}(r)}{B(r, \theta)} - 1} \equiv \sigma(r, \theta) \quad (2.29)$$

The filtering parameter σ_0 is a free parameter such that $0 \leq \sigma_0 \leq 1$ allowing to treat kinetically only a fraction of trapped electrons. The case $\sigma_0 = 1$ implies that all trapped electrons are supposed kinetic whereas the case $\sigma_0 = 0$ is equivalent to the adiabatic electrons case. We choose $\sigma_0 = 1$ in the following.

2.3.2 Quasi-neutrality with kinetic filter for electrons

The form of the kinetic filter applied to the electrons is greatly inspired from the one used in GT5D [51, Idomura 2016]. The gyrokinetic equation is solved for the entire dis-

tribution function of the electrons, irrespective of whether they are passing or trapped⁵. The kinetic filter is applied to the quasi-neutrality equation only. There, the density of trapped electrons only is calculated from the electron distribution function, the remaining fraction of electrons being assumed to respond adiabatically. For a centred Maxwellian, the fraction of trapped electrons α_t is simply $\alpha_t = \sigma$, with σ given by Eq.(2.29). In the following, we introduce $n_e^{trap.}$ the density of trapped electrons calculated from the electron distribution function and $n_e^{pass.}$ the density of passing electrons receiving an adiabatic treatment. The total density of electrons is the sum of those two contributions $n_e = n_e^{trap.} + n_e^{pass.}$.

The standard quasi-neutrality equation (2.18) is then replaced by the following one:

$$\sum_i Z_i \{n_{G,i} + n_{i,pol}\} = n_e^{trap.} + n_e^{pass.} \quad (2.30)$$

with

$$n_e^{trap.} = \int_{trap.} f_e d^3v \quad (2.31)$$

The integral over the trapped domain is to be taken in between the two limits $v_{G\parallel e\pm}(r, \theta, \mu) = \pm\sigma\sqrt{2\mu B/m_e}$:

$$\int_{trap.} \dots d^3v = \int_0^\infty d\mu \int_{v_{G\parallel e-}}^{v_{G\parallel e+}} \mathcal{J}_v \dots dv_{G\parallel} \quad (2.32)$$

where \mathcal{J}_v stands for the Jacobian in velocity space defined in Eq.(2.12). The normalized polarisation density of ions is given by Eq.(2.19). We assume that $\langle n_e \rangle_{FS}$ is "well" calculated, i.e. that the **flux-surface averaged** dynamics of all electrons, including passing ones, is well described for the modes $(m, n) = (0, 0)$. In that case, the normalized density of passing electrons $n_e^{pass.}$ should satisfy two conditions:

- $n_e^{pass.}$ represents the adiabatic evolution of the passing electrons, and should be proportionnal to the total adiabatic electron density n_e^{adiab} given earlier by equation (2.8):

$$n_e^{pass.} \propto n_e^{adiab} \simeq \langle n_e \rangle_{FS} \left[1 + \frac{1}{T_{e0}} (\phi - \langle \phi \rangle_{FS}) \right] \quad (2.33)$$

- The flux surface average of the density of trapped electrons should satisfy:

$$\langle n_e \rangle_{FS} = \langle n_e^{trap.} \rangle_{FS} + \langle n_e^{pass.} \rangle_{FS} \quad (2.34)$$

These constraints set the form of $n_e^{pass.}$ as:

$$n_e^{pass.} = (1 - \bar{\alpha}_t) \langle n_e \rangle_{FS} \left[1 + \frac{1}{T_{e0}} (\phi - \langle \phi \rangle_{FS}) \right] \quad (2.35)$$

⁵This point enables to treat correctly the trapping/detrapping of electrons due to collisions close to the trapped/passing limit.

where $\bar{\alpha}_t$ is the fraction of trapped electrons averaged on a flux surface:

$$\bar{\alpha}_t(r, t) = \frac{\langle n_e^{trap.} \rangle_{FS}(t)}{\langle n_e \rangle_{FS}(t)} \quad (2.36)$$

with $n_e^{trap.}$ given by Eq.(2.31). With this form of $n_e^{pass.}$, the zonal density of passing electrons is constructed so as to automatically fulfill Eq.(2.34).

So as to improve the accuracy of the numerical solution of Eq.(2.30), one can subtract the same quantity on both ion and electron sides of the equation. In practice, we can proceed as in section 2.2, and subtract the quantity $n_{e\mathcal{R}}(r, t)$ given by Eq.(2.25). The new quasi-neutrality then reads:

$$\begin{aligned} & \sum_i Z_i \left\{ \int J_{0i} (f_i - f_{i,eq}) d^3v + n_{i,pol} \right\} \\ & = \int_{trap.} (f_e - f_{e\mathcal{R}}) d^3v + n_e^{pass.} - (1 - \alpha_{t,\mathcal{R}}) n_{e\mathcal{R}} \end{aligned} \quad (2.37)$$

where $f_{e\mathcal{R}}$ and $n_{e\mathcal{R}}$ are introduced in Eqs.(2.25) and (2.26). Finally, $\alpha_{t,\mathcal{R}}$ represents the trapped fraction of density $n_{e\mathcal{R}}$. It simply reads:

$$\alpha_{t,\mathcal{R}}(r, \theta, t) = \frac{\int_{trap.} f_{e\mathcal{R}} d^3v}{n_{e\mathcal{R}}} \quad (2.38)$$

2.3.3 Implementation of the kinetic filter for electrons in GYSELA

The numerical implementation of the quasi-neutrality equation (2.37) is costly because it demands an update of the flux-surface averaged densities and temperatures present in the expressions of $f_{i,eq}$ and $f_{e\mathcal{R}}$ every time step. Therefore, we do the same approximation as the one made in Eq.(2.28), and we replace $f_{i,eq}$ and $f_{e\mathcal{R}}$ respectively by f_{i0} and $f_{e\mathcal{R}0}$, noted simply f_{e0} in the following. In this part, some approximations are done to simplify equation (2.37). Besides, we add here the electron polarisation density as well as the gyroaverage operator on the electron distribution functions since those are effectively implemented in the code. The quasi-neutrality equation then reads:

$$\begin{aligned} & - \sum_i \nabla_{\perp} \cdot (A_i \langle n_i \rangle_{FS} \nabla_{\perp} \phi) - \nabla_{\perp} \cdot (A_e \alpha_{t,eq}(r, \theta, t) \langle n_e \rangle_{FS} \nabla_{\perp} \phi) \\ & + (1 - \bar{\alpha}_t(r, t)) \frac{\langle n_e \rangle_{FS}}{T_e} (\phi - \langle \phi \rangle_{FS}) = \sum_i Z_i \int J_{0i} (f_i - f_{i0}) d^3v \\ & - \left[\int_{trap.} J_{0e} (f_e - f_{e0}) d^3v + (1 - \bar{\alpha}_t(r, t)) \langle n_e \rangle_{FS} - \int_{pass.} J_{0e} f_{e0} d^3v \right] \end{aligned} \quad (2.39)$$

with:

- $n_s(r, \theta, \varphi, t) = \int J_{0s} f_s \, d^3v + n_{s,pol}$: the density profile of species s where $n_{s,pol}$ is defined in Eq.(2.19)
- $\alpha_{t,eq}(r, \theta, t) = \int_{trap.} J_{0e} f_{e,eq} \, d^3v / \langle n_e \rangle_{FS}$: the fraction of trapped electrons at equilibrium
- $\bar{\alpha}_t(r, t) = \langle n_e^{trap.} \rangle_{FS} / \langle n_e \rangle_{FS}$: the fraction of trapped electrons averaged on a flux surface where

$$n_e^{trap.} = \int_{trap.} J_{0e} f_e \, d^3v - \nabla_{\perp} \cdot (A_e \alpha_{t,eq} \langle n_e \rangle_{FS} \nabla_{\perp} \phi)$$

This can be written in a more compact form:

$$\mathcal{L}_i \phi + \mathcal{L}_e \phi + (1 - \bar{\alpha}_t(r, t)) \frac{\langle n_e \rangle_{FS}}{T_e} (\phi - \langle \phi \rangle) = \rho_i - [\rho_e^{trap.} + \rho_e^{pass.}] \quad (2.40)$$

where

$$\begin{cases} \mathcal{L}_i \phi &= - \sum_i A_i \nabla_{\perp} \cdot (\langle n_i \rangle_{FS} \nabla_{\perp} \phi) \\ \mathcal{L}_e \phi &= - A_e \nabla_{\perp} \cdot (\alpha_{t,eq}(r, \theta, t) \langle n_e \rangle_{FS} \nabla_{\perp} \phi) \end{cases} \quad (2.41)$$

and

$$\begin{cases} \rho_i &= \sum_i Z_i \int J_{0i} (f_i - f_{i0}) \, d^3v \\ \rho_e^{trap.} &= \int_{trap.} J_{0e} (f_e - f_{e0}) \, d^3v \\ \rho_e^{pass.} &= (1 - \bar{\alpha}_t(r, t)) \langle n_e \rangle_{FS} - \int_{pass.} J_{0e} f_{e0} \, d^3v \end{cases} \quad (2.42)$$

It appears that the operator $\mathcal{L} = \mathcal{L}_i + \mathcal{L}_e$ depends both on time t and on the poloidal angle θ . These dependences are numerically costly for two reasons:

- the θ dependency of \mathcal{L} implies that (2.40) needs the 2D resolution of a Laplacian.
- the time dependency requires \mathcal{L} to be calculated at each time step.

The numerical implementation of this equation requires to make some approximations. Two levels of approximations can be distinguished: some do not change the quasi-neutrality condition much and may be kept in GYSELA. Others may change the quasi-neutrality significantly and should be removed in the future.

The θ dependency of \mathcal{L} is due to the trapped fraction $\alpha_{t,eq}$ in the electron polarisation term $\mathcal{L}_e \phi$. This last term is A_i/A_e time smaller than $\mathcal{L}_i \phi$ and the approximation $\alpha_{t,eq}(r, \theta) \rightarrow \bar{\alpha}_t(r)$ should have little impact on the quasi-neutrality equation. Moreover, we do the approximation that the averaged densities $\langle n_s \rangle_{FS}$ and the trapped fraction α_t appearing in \mathcal{L} do not vary in time. The operator \mathcal{L} is approached by the simplified operator $\tilde{\mathcal{L}}$ defined as $\tilde{\mathcal{L}} = \tilde{\mathcal{L}}_i + \tilde{\mathcal{L}}_e$ with

$$\begin{cases} \tilde{\mathcal{L}}_i \phi &= - \sum_i A_i \nabla_{\perp} \cdot (n_{i0} \nabla_{\perp} \phi) \\ \tilde{\mathcal{L}}_e \phi &= - A_e \nabla_{\perp} \cdot (\bar{\alpha}_{t0}(r) n_{e0} \nabla_{\perp} \phi) \end{cases}$$

where $n_{s0}(r) = \int f_{s0} d^3v$ is the initial radial density profile of species s , $\bar{\alpha}_{t0}(r) = \bar{\alpha}_t(r, t = 0)$ is the initial flux surface averaged trapped electron fraction. These approximations add little change to the theoretical quasi-neutrality equation and could be kept in the future version of GYSELA.

In order to make the numerical implementation of the quasi-neutrality equation easier, we assume that the averaged densities $\langle n_s \rangle_{FS}$ and the trapped fraction $\bar{\alpha}_t$ appearing in the other terms of the quasi-neutrality equation vary slowly in time and we do the approximation $\langle n_s \rangle_{FS} \rightarrow n_{s0}$ and $\bar{\alpha}_t \rightarrow \bar{\alpha}_{t0} = \langle \int_{trap} J_{0e} f_{e0} \rangle_{FS} / \langle \int J_{0e} f_{e0} \rangle_{FS}$. This last approximation should be removed in the future. Besides, doing this approximation makes the small correction term $\rho_e^{pass.} \simeq (1 - \bar{\alpha}_{t0}(r))n_{e0} - \int_{pass.} J_{0e} f_{e0} d^3v$ useless. Therefore, we choose to remove this term in the simplified form of the quasi-neutrality equation. The equation for trapped kinetic electrons in GYSELA becomes:

$$\boxed{\tilde{\mathcal{L}}_i \phi + \tilde{\mathcal{L}}_e \phi + (1 - \bar{\alpha}_{t0}(r)) \frac{n_{e0}}{T_e} (\phi - \langle \phi \rangle_{FS}) = \rho_i - \rho_e^{trap.}} \quad (2.43)$$

2.4 GYSELA quasi-neutrality solver

This part tackles the numerical implementation of the quasi-neutrality equations in GYSELA for each of the two versions of kinetic electron models: (i) the Full Kinetic Electron (FKE) and (ii) the Trapped Kinetic Electron (TKE) model. The adiabatic case is treated in Appendix B.3.

2.4.1 Normalized quasi-neutrality equation for full kinetic electrons

The normalized quasi-neutrality equation in the case of full kinetic electrons can be written:

$$-\sum_i A_i \nabla_{\perp} \cdot (n_{i0} \nabla_{\perp} \phi) - A_e \nabla_{\perp} \cdot (n_{e0} \nabla_{\perp} \phi) = \sum_i Z_i \int J_{0i} (f_i - f_{i0}) d^3v - \int J_{0e} (f_e - f_{e0}) d^3v \quad (2.44)$$

For more readability, the symbol $\hat{\cdot}$, used for normalized quantities in GYSELA in Appendix B.3, will be omitted in the following. Previous equation is equivalent to:

$$-\sum_s A_s \nabla_{\perp} \cdot (n_{s0} \nabla_{\perp} \phi) = \sum_s Z_s \int J_{0s} (f_s - f_{s0}) d^3v \quad (2.45)$$

where conversely to the previous section the s symbol stands for all species namely both ions and electrons with n_{G_s} and $n_{G_s,eq}$ respectively defined by equations:

$$\hat{n}_{G_s} = \int d\hat{\mu}_s \int \hat{\mathcal{J}}_v d\hat{v}_{G\parallel s} \hat{J}_{0s} \cdot \hat{f}_s \quad ; \quad \hat{n}_{G_s,eq} = \int d\hat{\mu}_s \int \hat{\mathcal{J}}_v d\hat{v}_{G\parallel s} \hat{J}_{0s} \cdot \hat{f}_{s,eq}$$

where the normalized equilibrium distribution function is defined as:

$$\hat{f}_{s,eq} = c_s \frac{\hat{n}_{s0}}{(2\pi\hat{T}_s)^{3/2}} \exp \left[-\frac{(\hat{v}_{G\parallel s}^2/2 + \hat{\mu}_s \hat{B})}{\hat{T}_s} \right] \quad (2.46)$$

represents the equilibrium part of the distribution function. To avoid the polar coordinate singularity in $r = 0$, Eq.(2.45) is solved on a corona $\Omega_{r_{\min}}$ defined as:

$$\Omega_{r_{\min}} = \{(r, \theta) : r_{\min} \leq r \leq r_{\max} ; 0 \leq \theta < 2\pi\} \quad (2.47)$$

Besides, taking into account boundary conditions – periodic in θ and φ and Dirichlet in radial direction – the previous equation (2.44) can be written as:

$$\left\{ \begin{array}{ll} \mathcal{L}^{\text{FKE}} \phi(r, \theta, \varphi) = \rho^{\text{FKE}}(r, \theta, \varphi) & \forall (r, \theta) \in \Omega_{r_{\min}} ; 0 \leq \varphi < L_{\varphi} \\ \phi(r_{\min}, \theta, \varphi) = \phi(r_{\max}, \theta, \varphi) = 0 & 0 \leq \theta < 2\pi ; 0 \leq \varphi < L_{\varphi} \\ \phi(r, 0, \varphi) = \phi(r, 2\pi, \varphi) & r_{\min} \leq r \leq r_{\max} ; 0 \leq \varphi < L_{\varphi} \\ \phi(r, \theta, 0) = \phi(r, \theta, L_{\varphi}) & \forall (r, \theta) \in \Omega_{r_{\min}} \end{array} \right. \quad (2.48)$$

with $\Omega_{r_{\min}}$ defined by (2.47) and

$$\mathcal{L}^{\text{FKE}} = - \sum_s A_s n_{s0}(r) \left\{ \frac{\partial^2}{\partial r^2} + \left[\frac{1}{r} + \frac{1}{n_{s0}(r)} \frac{dn_{s0}(r)}{dr} \right] \frac{\partial}{\partial r} + \frac{1}{r^2} \frac{\partial^2}{\partial \theta^2} \right\} \quad (2.49)$$

$$\rho^{\text{FKE}} = \sum_s Z_s \int J_{0s}(f_s - f_{s0}) d^3v \quad (2.50)$$

For inner boundary conditions ($r = r_{\min}$), two choices are possible, depending on if: (i) $r_{\min} > \Delta r/2$ (for a corona case), or (ii) $r_{\min} = \Delta r/2$. For the first case ($r_{\min} > \Delta r/2$), Dirichlet conditions are applied, i.e. $\tilde{\phi}_1^m = \tilde{\phi}^m(r_i = r_{\min}, \varphi) = 0$. For the second case ($r_{\min} = \Delta r/2$), we use the same strategy than the one proposed by Lai [56, Lai 2001] to overcome the $1/r$ singularity on the axis. This strategy is simply based on the fact that if r_{\min} is chosen equal to $\Delta r/2$, the term $(\frac{1}{\Delta r^2} - \frac{1}{r\Delta r})$ which appear for a standard Poisson equation is equal to 0. In our case, this strategy is applicable if and only if the radial derivative of the density profiles n_{i0} is null at $r = r_{\min}$. Using the same strategy as the one used for adiabatic electrons, namely Fourier projection in θ direction and finite differences in radial direction, leads to the following tridiagonal system $(N_1 - 1) \times (N_1 - 1)$ system:

$$\begin{pmatrix} d_1^m & u_1 & 0 & \cdots & 0 \\ l_2 & d_2^m & u_2 & 0 & \\ 0 & l_3 & d_3^m & u_3 & 0 \\ \vdots & 0 & \ddots & \ddots & \ddots \\ & & 0 & l_{N_1-2} & d_{N_1-2}^m & u_{N_1-2} \\ 0 & & & 0 & l_{N_1-1} & d_{N_1-1}^m \end{pmatrix} \begin{pmatrix} \phi_1^m \\ \phi_2^m \\ \vdots \\ \phi_{N_1-2}^m \\ \phi_{N_1-1}^m \end{pmatrix} = \begin{pmatrix} \rho_1^{\text{FKE},m} \\ \rho_2^{\text{FKE},m} \\ \vdots \\ \rho_{N_1-2}^{\text{FKE},m} \\ \rho_{N_1-1}^{\text{FKE},m} \end{pmatrix} \quad (2.51)$$

where for each $i \in [1, N_1 - 1]$

$$\begin{cases} l_i = - \left(\frac{\beta_i}{\Delta r^2} - \frac{\alpha_i}{2\Delta r} \right) \\ d_i^m = \beta_i \left(\frac{2}{\Delta r^2} + \frac{m^2}{r_i^2} \right) \\ u_i = - \left(\frac{\beta_i}{\Delta r^2} + \frac{\alpha_i}{2\Delta r} \right) \end{cases} \quad \text{with} \quad \begin{cases} \alpha_i = \sum_s K_s(r_i) \left(\frac{1}{r_i} + \frac{1}{n_{s0}(r_i)} \frac{dn_{s0}(r_i)}{dr} \right) \\ \beta_i = \sum_s K_s(r_i) \text{ and } K_s(r_i) = A_s n_{s0}(r_i) \end{cases} \quad (2.52)$$

with ρ_i^m the poloidal wave vector of $\rho_i = \sum_s [n_{G_s}(r_i, \theta, \varphi) - n_{G_s, \text{eq}}(r_i, \theta)]$ and with $\phi_{N_1}^m = 0$.

Let us notice that as for adiabatic electron case, if inner Dirichlet boundary conditions are applied, the matrix system to solve is a $(N_1 - 2) \times (N_1 - 2)$ tridiagonal system equivalent to (2.51) where first line and first column are deleted and replaced by the condition $\phi_1^m = 0$.

2.4.2 Normalized quasi-neutrality equation for trapped kinetic electrons

The normalized quasi-neutrality equation in the case of trapped kinetic electrons can be written:

$$\begin{aligned} & - \sum_i A_i \nabla_{\perp} \cdot (n_{i0} \nabla_{\perp} \phi) - A_e \nabla_{\perp} \cdot (\bar{\alpha}_{t0}(r) n_{e0} \nabla_{\perp} \phi) + (1 - \bar{\alpha}_{t0}(r)) \frac{n_{e0}}{Z_0^2 T_e} (\phi - \langle \phi \rangle_{\text{FS}}) \\ & = \sum_i Z_i \int J_{0i} (f_i - f_{i0}) d^3v - \int_{\text{trap.}} J_{0e} (f_e - f_{e0}) d^3v \end{aligned} \quad (2.53)$$

with

$$f_{s0} = \frac{n_{s0}}{(2\pi T_{s0})^{3/2}} \exp\left(-\frac{E_s}{T_{s0}}\right) \quad \text{with} \quad E_s = \frac{1}{2} v_{G\parallel s}^2 + \mu_s B(r, \theta) \quad (2.54)$$

where the radial density and temperature profiles for ions (n_{s0} and T_{s0}) are given while the radial electron temperature profile is defined with a similar form as that of the main ions with $\tau = T_{e0}(r_{\text{peak}})/T_{i0}(r_{\text{peak}})$ a prescribed constant parameter. Besides, the radial averaged gradients R/L_{T_i} and R/L_{T_e} can be set independently. The electron density n_{e0} is chosen such that the quasi-neutrality condition is fulfilled on a flux surface average, i.e

$$\left\langle \int d^3v J_{0e} f_{e0} \right\rangle_{\text{FS}} = \left\langle \sum_i Z_i \int d^3v J_{0i} f_{i0} \right\rangle_{\text{FS}}$$

Considering low electron density gradients, we assume that $J_{0e} f_{e0} \approx n_{e0} J_{0e} \hat{f}_{e0}$ with $\hat{f}_{e0} = \frac{1}{(2\pi T_{e0})^{3/2}} \exp\left(-\frac{E_e}{T_{e0}}\right)$, then n_{e0} is approximated by:

$$n_{e0}(r) = \frac{\left\langle \sum_i Z_i \int d^3v J_{0i} f_{i0} \right\rangle_{\text{FS}}}{\left\langle \int d^3v J_{0e} \hat{f}_{e0} \right\rangle_{\text{FS}}} \quad (2.55)$$

The integral on the trapped particles $\int_{\text{trap.}}$ is defined for any function $g(r, \theta, \varphi, v_{G\parallel s}, \mu_s)$ as:

$$\int_{\text{trap.}} d^3v g(r, \theta, \varphi, v_{G\parallel s}, \mu_s) = \int_0^{\mu_s^{\text{max}}} \mathcal{J}_v d\mu_s \int_{v_{G\parallel s}^-}^{v_{G\parallel s}^+} dv_{G\parallel s} g(r, \theta, \varphi, v_{G\parallel s}, \mu_s) \quad (2.56)$$

where $\mathcal{J}_v = 2\pi B_{\parallel s}^*$ is the jacobian in velocity space and where $v_{G\parallel s}^{\pm} = \pm \sigma \sqrt{2\mu_s B(r, \theta)}$ with $\sigma(r, \theta)$ ⁶ defined in Eq.(2.29). $\bar{\alpha}_{t0}$ represents the fraction of trapped electrons averaged on a flux surface at time $t = 0$, i.e $\bar{\alpha}_{t0} = \bar{\alpha}(r, t = 0)$ with $\bar{\alpha}(r, t)$ given by Eq.(2.36). As $\langle n_{e,\text{pol}} \rangle_{\text{FS}}(t = 0) = 0$ and $\langle n_{e,\text{pol}}^{\text{trap.}} \rangle_{\text{FS}}(t = 0) = 0$ then:

$$\bar{\alpha}_{t0} = \frac{\left\langle \int_{\text{trap.}} d^3v J_{0e} f_e(t = 0) \right\rangle_{\text{FS}}}{\left\langle \int d^3v J_{0e} f_e(t = 0) \right\rangle_{\text{FS}}}$$

6

$\sigma(r, \theta) = \sigma_0 \left[\frac{\varepsilon(1 + \cos \theta)}{1 - \varepsilon} \right]^{1/2}$ for $B(r, \theta) \approx \frac{B_0 R_0}{R(r, \theta)}$ with $R(r, \theta) = R_0(1 + \varepsilon \cos \theta)$ and $\varepsilon = \frac{r}{R_0}$

Equation (2.53) can be rewritten as:

$$\mathcal{L}^{\text{TKE}}\phi + (1 - \bar{\alpha}_{t0}(r)) \frac{n_{e0}}{Z_0^2 T_e} (\phi - \langle \phi \rangle_{\text{FS}}) = \rho^{\text{TKE}} \quad (2.57)$$

with

$$\rho^{\text{TKE}}(r, \theta, \varphi) = \sum_i Z_i \int J_{0i}(f_i - f_{i0}) d^3v - \int_{\text{trap.}} J_{0e}(f_e - f_{e0}) d^3v \quad (2.58)$$

and

$$\begin{aligned} \mathcal{L}^{\text{TKE}} = & - \sum_i A_i n_{i0}(r) \left\{ \frac{\partial^2}{\partial r^2} + \left[\frac{1}{r} + \frac{1}{n_{i0}(r)} \frac{dn_{i0}(r)}{dr} \right] \frac{\partial}{\partial r} + \frac{1}{r^2} \frac{\partial^2}{\partial \theta^2} \right\} \\ & - A_e n_{e0} \bar{\alpha}_{t0} \left\{ \frac{\partial^2}{\partial r^2} + \left[\frac{1}{r} + \frac{1}{n_{e0}(r)} \frac{dn_{e0}(r)}{dr} + \frac{1}{\bar{\alpha}_{t0}(r)} \frac{d\bar{\alpha}_{t0}(r)}{dr} \right] \frac{\partial}{\partial r} + \frac{1}{r^2} \frac{\partial^2}{\partial \theta^2} \right\} \end{aligned}$$

Due to the presence of the $\langle \phi \rangle_{\text{FS}}$ term in (2.53), the same strategy than the one used for adiabatic electrons (see section B.3.1) is used, i.e

1. Compute $\rho^{\text{TKE}}(r, \theta, \varphi)$ given by Eq.(2.58) and $\langle \rho^{\text{TKE}} \rangle_{\theta, \varphi}(r)$.
2. Compute $\tilde{\rho}^{\text{TKE}}(r, \theta, \varphi) = \rho^{\text{TKE}}(r, \theta, \varphi) - \langle \rho^{\text{TKE}} \rangle_{\theta, \varphi}(r)$ the RHS of equation (2.59).
3. Solve for each $\varphi \in [0, L_\varphi[$ the 2D following system (2.59) to obtain $\tilde{\phi}(r, \theta, \varphi)$:

$$\left\{ \begin{array}{ll} \left(\mathcal{L}^{\text{TKE}} + (1 - \bar{\alpha}_{t0}(r)) \frac{n_{e0}}{Z_0^2 T_e} \right) \tilde{\phi}(r, \theta, \varphi) = \tilde{\rho}^{\text{TKE}}(r, \theta, \varphi) & \forall (r, \theta) \in \Omega_{r_{\min}} \\ \tilde{\phi}(r_{\min}, \theta, \varphi) = \tilde{\phi}(r_{\max}, \theta, \varphi) = 0 & 0 \leq \theta < 2\pi \\ \tilde{\phi}(r, 0, \varphi) = \tilde{\phi}(r, 2\pi, \varphi) & r_{\min} \leq r \leq r_{\max} \end{array} \right. \quad (2.59)$$

And applied the periodic boundary conditions in φ direction to compute $\tilde{\phi}(r, \theta, \varphi = L_\varphi)$.

4. Compute $\langle \tilde{\phi} \rangle_{\text{FS}}$ and the RHS of (2.60), i.e $\langle \rho^{\text{TKE}} \rangle_{\theta, \varphi} + (1 - \bar{\alpha}_{t0}) \frac{n_{e0}}{Z_0^2 T_e} \langle \tilde{\phi} \rangle_{\text{FS}}$.
5. Solve the 1D system (2.60) to obtain $\langle \phi \rangle_{\theta, \varphi}(r)$.

$$\left\{ \begin{array}{ll} \mathcal{L}^{\text{TKE}} \langle \phi \rangle_{\theta, \varphi}(r) = \langle \rho^{\text{TKE}} \rangle_{\theta, \varphi} + (1 - \bar{\alpha}_{t0}) \frac{n_{e0}}{Z_0^2 T_e} \langle \tilde{\phi} \rangle_{\text{FS}} & \forall r \in [r_{\min}, r_{\max}] \\ \langle \phi \rangle_{\theta, \varphi}(r_{\min}) = \langle \phi \rangle_{\theta, \varphi}(r_{\max}) = 0 & \end{array} \right. \quad (2.60)$$

6. Finally, compute $\phi(r, \theta, \varphi) = \tilde{\phi}(r, \theta, \varphi) + \langle \phi \rangle_{\theta, \varphi}(r)$.

Let us notice that solving (2.59) is equivalent to solve the same kind of $(N_1 - 1) \times (N_1 - 1)$ matrix system than (2.51) system, i.e

$$\begin{pmatrix} d_1^m & u_1 & 0 & \dots & 0 \\ l_2 & d_2^m & u_2 & 0 & \\ 0 & l_3 & d_3^m & u_3 & 0 \\ \vdots & 0 & \ddots & \ddots & \ddots \\ 0 & & 0 & l_{N_1-2} & d_{N_1-2}^m & u_{N_1-2} \\ 0 & & & 0 & l_{N_1-1} & d_{N_1-1}^m \end{pmatrix} \begin{pmatrix} \tilde{\phi}_1^m \\ \tilde{\phi}_2^m \\ \vdots \\ \tilde{\phi}_{N_1-2}^m \\ \tilde{\phi}_{N_1-1}^m \end{pmatrix} = \begin{pmatrix} \tilde{\rho}_1^{\text{TKE},m} \\ \tilde{\rho}_2^{\text{TKE},m} \\ \vdots \\ \tilde{\rho}_{N_1-2}^{\text{TKE},m} \\ \tilde{\rho}_{N_1-1}^{\text{TKE},m} \end{pmatrix} \quad (2.61)$$

where for each $i \in [1, N_1 - 1]$

$$\begin{cases} l_i &= -\left(\frac{\beta_i}{\Delta r^2} - \frac{\alpha_i}{2\Delta r}\right) \\ d_i^m &= \beta_i \left(\frac{2}{\Delta r^2} + \frac{m^2}{r_i^2}\right) + (1 - \bar{\alpha}_{t0}(r_i)) \frac{n_{e0}(r_i)}{Z_0^2 T_e(r_i)} \\ u_i &= -\left(\frac{\beta_i}{\Delta r^2} + \frac{\alpha_i}{2\Delta r}\right) \end{cases} \quad (2.62)$$

with

$$\begin{cases} \alpha_i &= \sum_{s \neq e} A_s n_{s0}(r_i) \left(\frac{1}{r_i} + \frac{1}{n_{s0}(r_i)} \frac{dn_{s0}(r_i)}{dr}\right) \\ &+ A_e n_{e0}(r_i) \bar{\alpha}_{t0}(r_i) \left(\frac{1}{r_i} + \frac{1}{n_{e0}(r_i)} \frac{dn_{e0}(r_i)}{dr} + \frac{1}{\bar{\alpha}_{t0}(r_i)} \frac{d\bar{\alpha}_{t0}(r_i)}{dr}\right) \\ \beta_i &= \sum_{s \neq e} A_s n_{s0}(r_i) + A_e \bar{\alpha}_{t0}(r_i) n_{e0}(r_i) \end{cases} \quad (2.63)$$

$\tilde{\rho}_i^{\text{TKE},m}$ is the poloidal wave vector of $\tilde{\rho}^{\text{TKE}}(r_i)$ defined as $\tilde{\rho}^{\text{TKE}} = \rho^{\text{TKE}} - \langle \rho^{\text{TKE}} \rangle_{\theta, \varphi}$ where ρ^{TKE} is given by equation (2.58). The value at outer boundary is given by Dirichlet boundary condition, i.e $\tilde{\phi}_{N_1}^m = 0$.

If inner Dirichlet boundary conditions are applied instead of using Lai's strategy, the matrix system to solve is a $(N_1 - 2) \times (N_1 - 2)$ tridiagonal system equivalent to (2.61) where first line and first column are deleted and replaced by the condition $\tilde{\phi}_1^m = 0$. The

second matrix system (2.60) reads:

$$\begin{pmatrix} d_1 & u_1 & 0 & \cdots & 0 \\ l_2 & d_2 & u_2 & 0 & \\ 0 & l_3 & d_3 & u_3 & 0 \\ \vdots & 0 & \ddots & \ddots & \ddots \\ & & 0 & l_{N_1-2} & d_{N_1-2} & u_{N_1-2} \\ 0 & & & 0 & l_{N_1-1} & d_{N_1-1} \end{pmatrix} \begin{pmatrix} \langle \phi \rangle_{\theta, \varphi}(r_1) \\ \langle \phi \rangle_{\theta, \varphi}(r_2) \\ \vdots \\ \langle \phi \rangle_{\theta, \varphi}(r_{N_1-2}) \\ \langle \phi \rangle_{\theta, \varphi}(r_{N_1-1}) \end{pmatrix} = \begin{pmatrix} \Gamma_1 \\ \Gamma_2 \\ \vdots \\ \Gamma_{N_1-2} \\ \Gamma_{N_1-1} \end{pmatrix} \quad (2.64)$$

where for each $i \in [1, N_1 - 1]$, l_i and u_i are defined by (2.62) and:

$$\begin{cases} d_i = \frac{2}{\Delta r^2} \beta_i \text{ with } \beta_i \text{ defined by (2.63)} \\ \Gamma_i = \langle \rho \rangle_{\theta, \varphi}(r_i) + (1 - \bar{\alpha}_{t0}(r_i)) \frac{n_{e0}}{Z_0^2 T_e(r_i)} \langle \tilde{\phi} \rangle_{\text{FS}}(r_i) \end{cases}$$

2.5 Introduction of a pure density source term in GYSELA

Fusion tokamaks are open systems with particle and energy losses partly due to transport. For equilibrium density and temperature profiles to reach steady states, it is necessary to provide sources of particles and energy to compensate for these losses. In the gyrokinetic model we use, this can be modelled by introducing a source distribution S_s for each species s on the right hand side of the gyrokinetic equation which takes the normalized form:

$$\frac{df_s}{dt} = S_s \quad (2.65)$$

Besides, in order to control each fluid quantity, namely density, momentum, energy and vorticity, transferred to the plasma, the source S_s is decomposed into several source terms, each being a pure source of one fluid quantity. Introducing the notations S_s^n for the pure source term of gyrocentre density, $S_s^{v_{G\parallel}}$ for the pure momentum source term, $S_s^{\mathcal{E}}$ for the pure energy source term, S_s^Ω for the pure vorticity source term, the gyrokinetic equation now reads:

$$\frac{df_s}{dt} = S_s^n + S_s^{v_{G\parallel}} + S_s^{\mathcal{E}} + S_s^\Omega \quad (2.66)$$

In the adiabatic electrons model, there can be no density transport as discussed in section 2.1.2, and therefore no density source. This is no more the case in multi-species simulations with kinetic electrons, and a density source for each species s , can be added to the right hand side of the gyrokinetic equation (2.66). This section aims to give a form the pure density source term can take with kinetic electrons, the pure source terms of momentum, energy and vorticity being unchanged from the adiabatic electrons case and implemented in appendix A of the paper [73, Sarazin 2011]. It should be stressed that as f_s is the distribution function of gyrocentres, S_s acts as a source term for the gyrocentre density, momentum, energy and vorticity. In particular, S_s^n acts as a source of gyrocentres. We will see that adding a real particle source is equivalent to adding a vorticity source for gyrocentres. First, a general form of the pure density source term is given. Second some conditions implied by momentum, energy and vorticity⁷ conservations are derived. Finally, a simplified example of a pure density source term is given.

When density transport can occur, a density source $S_s^n(r, \theta, \varphi, v_{\parallel}, \mu)$ for each species s can be added to the right hand side of the gyrokinetic equation. To simplify the problem, S_s^n is taken axisymmetric in the toroidal angle φ . For all species, this source term has the same normalized form so that, between different species, S_s^n differs only by a constant factor noted S_{0s}^n . This hypothesis is based on the idea that, in velocity space, the source distribution of each species are set as Maxwellian. Consequently, the density source term takes the normalized form:

$$S_s^n = S_{0s}^n S_r(r) S_E(r, \theta, v_{\parallel}, \mu) \quad (2.67)$$

The density source term is decomposed into a fixed radial part S_r which corresponds to the radial shape of the source, and a kinetic part S_E setting the distribution of the

⁷Whenever one has the vorticity conservation, the charge conservation for particles is trivial.

source in velocity space with $\int r dr S_r(r) = 1$ and $\int S_E d^3v = 1$.

As said previously, we would like to have a density source term S_s^n which injects gyrocentres without injecting momentum, energy or vorticity. The conservations imply conditions on the form of S_E . The aim here is to express these conditions in order to eventually find a suitable form of the density source S_s^n .

S_E is developed on an orthogonal base of Hermite and Laguerre polynomials:

$$S_E = \sum_{l=0}^{\infty} \sum_{h=0}^{\infty} c_{hl} H_h(\zeta) L_l(u) e^{-\zeta^2 - u} \quad (2.68)$$

where the following definitions have been used:

$$\zeta^2 \equiv \frac{A_s v_{G\parallel s}^2}{2T_{s,srcce}} \quad ; \quad u \equiv \frac{\mu B}{T_{s,srcce}} \quad (2.69)$$

$T_{s,srcce}$ being the constant source temperature for the s species. This source temperature is independent of the species temperature in the plasma and can be set arbitrarily. To simplify the study, we suppose it to be the same for every species and is noted T_{source} . With the adopted definitions, $B_{\parallel}^* = B(1 + J_{\parallel B} \zeta)$ and $J_{\parallel B} = \sqrt{2T_{source}} J_{\parallel} / B^2$ where J_{\parallel} stands for the current parallel to the magnetic field, the integral over the velocity space reads as follow:

$$\begin{aligned} \int d^3v &\equiv \int_{-\infty}^{+\infty} dv_{G\parallel} \int_0^{+\infty} 2\pi B_{\parallel}^* d\mu \\ &= \frac{(2\pi T_{source})^{3/2}}{\sqrt{\pi}} \int_{-\infty}^{+\infty} (1 + J_{\parallel B} \zeta) d\zeta \int_0^{+\infty} du \end{aligned}$$

Let us consider a normalized source distribution $S = S_r S_E$. We now compute the integrated source of density \mathbb{S}_n , momentum $\mathbb{S}_{v_{G\parallel}}$, energy $\mathbb{S}_{\mathcal{E}}$ and vorticity \mathbb{S}_{Ω} associated with this source. By definition, these integrated sources are defined as:

$$\begin{cases} \mathbb{S}_n &= \int d^3v S_r S_E \\ \mathbb{S}_{v_{G\parallel}} &= \int d^3v v_{G\parallel} S_r S_E \\ \mathbb{S}_{\mathcal{E}} &= \int d^3v \left(\frac{v_{G\parallel}^2}{2} + \mu B \right) S_r S_E \\ \mathbb{S}_{\Omega} &= \int d^3v J_{0s} S_r S_E \end{cases} \quad (2.70)$$

The calculation of the integrated sources is made in [73, Sarazin 2011]. In the end, it comes:

$$\begin{cases} \mathbb{S}_n &= (2\pi T_{source})^{3/2} S_r [c_{00} + J_{\parallel B} c_{10}] \\ \mathbb{S}_{v_{G\parallel}} &= 2\pi^{3/2} T_{source}^2 S_r [2c_{10} + J_{\parallel B} (c_{00} + 4c_{20})] \\ \mathbb{S}_{\mathcal{E}} &= (2\pi)^{3/2} T_{source}^{5/2} S_r \left[\frac{3}{2} c_{00} + \frac{5}{2} J_{\parallel B} c_{10} + 2c_{20} + 6J_{\parallel B} c_{30} - c_{01} - J_{\parallel B} c_{11} \right] \\ \mathbb{S}_{\Omega} &= \mathbb{S}_n + \frac{\sqrt{2\pi}^{3/2} T_{source}^{5/2}}{B^2} \left\{ \nabla_{\perp}^2 [S_r (c_{00} - c_{01})] + J_{\parallel B} \nabla_{\perp}^2 [S_r (c_{10} - c_{11})] \right\} \end{cases} \quad (2.71)$$

We want our source distribution term to be a pure source of density and this implies that $\mathbb{S}_{v_{G\parallel}}$, $\mathbb{S}_{\mathcal{E}}$ and \mathbb{S}_{Ω} should be set to zero with \mathbb{S}_n being non zero. These conditions are summed up in the following system:

$$\left\{ \begin{array}{l} \text{Injection of density} \quad c_{00} + J_{\parallel B} c_{10} \neq 0 \\ \text{Conservation of momentum} \quad 2c_{10} + J_{\parallel B}(c_{00} + 4c_{20}) = 0 \\ \text{Conservation of energy} \quad \frac{3}{2}c_{00} + \frac{5}{2}J_{\parallel B}c_{10} + 2c_{20} + 6J_{\parallel B}c_{30} - c_{01} - J_{\parallel B}c_{11} = 0 \\ \text{Conservation of vorticity} \quad \nabla_{\perp}^2 [S_r(c_{00} - c_{01})] + J_{\parallel B} \nabla_{\perp}^2 [S_r(c_{10} - c_{11})] = 0 \end{array} \right. \quad (2.72)$$

$$\text{satisfied if } \left\{ \begin{array}{l} c_{00} = c_{01} = -4c_{20} \neq 0 \\ c_{10} = c_{11} = c_{30} = 0 \end{array} \right.$$

The condition of conservation of the vorticity (or charge) is very strong: no species is allowed to introduce charges into the system, which is equivalent to a conservation of particles. A less drastic condition is $\sum_s Z_s \mathbb{S}_{\Omega}^s = 0$ which imposes the overall charge conservation in the plasma. In addition, care must be taken to inject as many positive as negative charges in the space of the gyrocentres so as not to polarize the system. We must therefore satisfy the condition $\sum_s Z_s \mathbb{S}_n^s = 0$. It should be noted that as we are dealing with the gyrocentres distribution functions, these conditions imply a pure source of gyrocentre density. To insert particles, one must have $\mathbb{S}_{\Omega} \neq 0$ while having $\sum_s Z_s \mathbb{S}_{\Omega}^s = 0$ to conserve the charge globally. Finally, one can introduce pure momentum or energy sources with a similar study.

For instance, whenever we suppose $J_{\parallel B} \ll 1$, system (2.72) reduces to $c_{20} = c_{00}/2$ and $c_{10} = c_{01} = c_{11} = 0$. Then, setting arbitrary the value $c_{00} = 1/2$, it can be verified that

$$S_s^n = S_{0s}^n S_r(r) \zeta_s^2 e^{-\zeta_s^2 - u} \quad (2.73)$$

is a possible form for a simplified pure particle source term. This density source term should be added later in GYSELA. A major asset of GYSELA is the possibility to be flux-driven, i.e. to impose constant source profiles. This condition is necessary to simulate a turbulent transport regime at steady state. In the following however, we will not take into account the sources. In the linear study of section 4.2, the associated turbulent transport is negligible so that density and temperature profiles remain approximately constant. Therefore, there is no need of source terms to prevent profiles relaxation. The same remark applies for the non-linear study of section 4.4, which only explores the very beginning of the non-linear phase. Indeed, in this case, density and temperature profiles do not evolve significantly.

Chapter 3

Contribution of trapped electrons to the damping of geodesic acoustic modes (GAM)

One of the well known saturation mechanisms for the Ion Temperature Gradient (ITG) instability is the production of axisymmetric Zonal Flows (ZF) ¹ that serve to shear stabilize the instability [44, Hammett 1993],[78, Waltz 1994]. Zonal Flows are therefore an essential element to both predict and limit turbulent transport levels in tokamaks. In 1996, gyrofluid simulations were carried out in which the Zonal Flows were systematically damped [37, Glanz 1996]. Such disappearance of these axisymmetric modes would imply that ITG turbulence would severely limit confinement in tokamaks. However, in their paper published in 1998 [71, Rosenbluth 1998], Rosenbluth and Hinton have shown that by adopting a kinetic approach, these Zonal Flows are not damped in the absence of collisions. This analytical result was later confirmed by gyrokinetic codes which all notice that the potential relaxes through time towards a non-zero residual that corresponds to the Zonal Flow value.

This study has led to a new test for gyrokinetic codes called the Rosenbluth-Hinton test which consists in introducing an axisymmetric perturbation of the radial potential profile $\tilde{\phi}(r) = \tilde{\phi}_0 \sin(kr)$, and characterize its time evolution [7, Biancalani 2017]. This test provides the residual value the flow ϕ_∞ , as predicted by Rosenbluth and Hinton, and also the pulsation ω_{GAM} and damping rate γ_{GAM} of the Geodesic Acoustic Mode (GAM), which is another mode of the potential which vanishes through time. The GAM complex frequency is well documented in the particular case of a single ion species with adiabatic electrons [75, 85, 84, Sugama 2006, Zonca 1996-2008]. It usually agrees well with simulations. However adding kinetic electrons change somewhat the picture. While

¹ The Zonal Flow (ZF) and the Geodesic Acoustic Mode (GAM) are respectively the eigenmodes ($n_1 = 0, n_2 = 0, n_3 = 0$) and ($n_1 = 0, n_2 = 1, n_3 = 0$) associated to the angles ($\alpha_1 = \varphi_c, \alpha_2 \simeq \arcsin(\theta/\theta_{max}), \alpha_3 = \varphi$) from the angle-action set of variables introduced in part 1.2.2.

the residual flow and the GAM frequency are mostly unchanged [13, Chen 2003], the GAM damping rate increases significantly [83, Zhang 2010]. This is attributed to a resonance match between the GAM and the trapped electron bounce pulsations, which changes the imaginary part of the dispersion relation, while it weakly affects its real part.

The objective is to provide an analytical estimate of the trapped electrons contribution to GAM damping, which does not seem to be available in the literature. A variational formulation is used, which is close to the one used previously to study Energetic Geodesic Acoustic Modes (EGAM) [81, Zarzozo 2012]. First the known dispersion relation of GAM is recovered using this methodology. Second an analytic expression for the GAM pulsation and damping rate is derived. In particular, the contribution of trapped electrons to the GAM damping rate is computed. A comparison of the GAM pulsation and damping rate between the analytical formulas derived here and the numerical results found using the Full Kinetic Electron (FKE) model of the GYSELA code is then carried out. This study has the double objective to quantify the impact of trapped electrons on the damping of GAM and to verify and benchmark the FKE model.

3.1 Dispersion relation of GAM

We anticipate that diamagnetic effects are negligible for GAMs, i.e. we consider a plasma of electrons and hydrogenoid ions with constant density $N = N_e = N_i$, and constant electron and ion temperatures T_e and T_i .

3.1.1 Vlasov equation

The Vlasov equation reads :

$$\partial_t F(\mathbf{x}, \mathbf{p}, t) - [H, F](\mathbf{x}, \mathbf{p}, t) = S(\mathbf{x}, \mathbf{p}, t) \quad (3.1)$$

where S is a source, H the Hamiltonian, F the distribution function. The Poisson bracket is given by :

$$[H, F] = \frac{\partial H}{\partial \mathbf{x}} \cdot \frac{\partial F}{\partial \mathbf{p}} - \frac{\partial H}{\partial \mathbf{p}} \cdot \frac{\partial F}{\partial \mathbf{x}} \quad (3.2)$$

It is possible to define two Hamiltonians H and H_{eq} :

$$H = \frac{1}{2}mv_{\parallel}^2 + \mu B + e\phi(\mathbf{x}, t) \quad (3.3)$$

$$H_{eq} = \frac{1}{2}mv_{\parallel}^2 + \mu B + e\phi_{eq}$$

where ϕ stands for the electric potential. H is the hamiltonian corresponding to the distribution function F whereas H_{eq} is the hamiltonian corresponding to the distribution function at equilibrium F_{eq} . We define F_{eq} and F_H as :

$$F_{eq} = \frac{N}{(2\pi mT)^{3/2}} \exp\left(-\frac{H_{eq}}{T}\right) \quad (3.4)$$

$$F_H = \frac{N}{(2\pi mT)^{3/2}} \exp\left(-\frac{H}{T}\right) \quad (3.5)$$

where N and T are constant density and temperature. The steady equilibrium potential ϕ_{eq} will be neglected. It is possible to decompose F in two different manners :

$$F = F_{eq} + f \quad (3.6)$$

$$F = F_H + g \quad (3.7)$$

It may be interesting to write the expression of f knowing g in the saturation limit $\frac{e\phi}{T} \sim \rho^* \ll 1$ described in Appendix C.1. In that limit, it is possible to develop F_H knowing F_{eq} .²

$$F_H = F_{eq} \exp\left(-\frac{e}{T}(H - H_{eq})\right)$$

$$= F_{eq} \left[1 - \frac{e}{T}\phi + O\left(\left(\frac{e\phi}{T}\right)^2\right) \right] \quad (3.8)$$

² $O(A)$ is a functional equivalent to any functional A .

Equations (3.6) and (3.7) imply $f - g = F_H - F_{eq}$ and it comes :

$$f \simeq g - F_{eq} \frac{e}{T} \phi \quad (3.9)$$

Rewriting (3.1) using decomposition (3.7), it comes :

$$\partial_t g - [H, g] + \partial_t (F_H) - [H, F_H] = S$$

F_H only depends of H and thus, $[H, F_H(H)] = 0$. In the case $\frac{e\phi}{T} \ll 1$, equation (3.8) gives the expression of $\partial_t F_H = -F_{eq} \frac{e}{T} \partial_t \phi$. Then, an alternative formulation of the Vlasov equation is :

$$\partial_t g - [H, g] = F_{eq} \frac{e}{T} \partial_t \phi + S \quad (3.10)$$

In Appendix C.1, we prove that, in the case of the saturation limit $\frac{e\phi}{T} \ll 1$, the Hamiltonian can be replaced by its equilibrium value H_{eq} in the expression above, i.e. the Vlasov equation can be linearised :

$$\partial_t g - [H_{eq}, g] = F_{eq} \frac{e}{T} \partial_t \phi + S \quad (3.11)$$

3.1.2 Linear solution of the Vlasov equation

It is convenient to use the set of angle-action variables $(\boldsymbol{\alpha}, \mathbf{J})$ constructed in part 1.2.2, and related to the set of position/momentum coordinates (\mathbf{x}, \mathbf{p}) , to describe the non perturbed trajectories of particles. It is reminded that this set of angle-action variables satisfies :

$$\begin{aligned} \frac{d\alpha_i}{dt} &= \frac{\partial H_{eq}}{\partial J_i} = \Omega_i(\mathbf{J}) \\ \frac{dJ_i}{dt} &= -\frac{\partial H_{eq}}{\partial \alpha_i} = 0 \end{aligned}$$

where $i = (1, 2, 3)$. This is a consequence of the existence of 3 motion invariants of the unperturbed system, namely the hamiltonian H_{eq} , the magnetic moment μ , and the canonical toroidal momentum $P_\varphi = e\psi + mv_\parallel \frac{B_\varphi}{B} R$, where ψ is the poloidal flux normalized to 2π . The first angle is the cyclotron angle, and the corresponding action is proportional to the adiabatic invariant $J_1 = \frac{m}{e} \mu$. The second and third angles are related to the guiding center motion. More precisely the third angle is equal to the toroidal angle up to an offset that is a periodic function of the second angular variable α_2 . The corresponding action is the canonical toroidal momentum P_φ . The second angle describes the bounce (resp. transit) motion of trapped (resp. passing) particles. The corresponding action can be derived explicitly, but is of little use here as it can be replaced by the energy H_{eq} at given μ and P_φ .

The perturbed hamiltonian h is defined here so that $\frac{Z}{\tau} h = e\phi/T$ with Z the charge number (i.e. $Z_i = 1$ for ions and $Z_e = -1$ for electrons) and $\tau = T/T_i$ (i.e. $\tau_i = 1$ for

ions and $\tau_e = T_e/T_i$ for electrons). Thanks to the periodicity with respect to the angle and time variables, all quantities can be developed in Fourier series as :

$$g(\boldsymbol{\alpha}, \mathbf{J}, t) = \sum_{\mathbf{n}\omega} g_{\mathbf{n}\omega} \exp \{i(\mathbf{n} \cdot \boldsymbol{\alpha} - \omega t)\} \quad (3.12)$$

$$h(\boldsymbol{\alpha}, \mathbf{J}, t) = \sum_{\mathbf{n}\omega} h_{\mathbf{n}\omega} \exp \{i(\mathbf{n} \cdot \boldsymbol{\alpha} - \omega t)\} \quad (3.13)$$

Replacing this expression of g in equation (3.11), it comes for each mode (\mathbf{n}, ω) :

$$\begin{aligned} -i\omega g_{\mathbf{n}\omega} - \sum_j \left\{ \underbrace{\frac{\partial H_{eq}}{\partial \alpha_j}}_0 \frac{\partial g_{\mathbf{n},\omega}}{\partial J_j} - \underbrace{\frac{\partial H_{eq}}{\partial J_j}}_{\Omega_j} \frac{\partial g_{\mathbf{n},\omega}}{\partial \alpha_j} \right\} &= \frac{Z}{\tau} F_{eq}(-i\omega h_{\mathbf{n},\omega}) + S_{\mathbf{n},\omega} \\ -i\omega g_{\mathbf{n}\omega} + i \sum_j n_j \Omega_j g_{\mathbf{n},\omega} &= -i\omega \frac{Z}{\tau} F_{eq} h_{\mathbf{n},\omega} + S_{\mathbf{n},\omega} \end{aligned}$$

An exact solution of Eq.(3.11) is :

$$g_{\mathbf{n}\omega} = \frac{\omega \frac{Z}{\tau} F_{eq} h_{\mathbf{n}\omega} + i S_{\mathbf{n},\omega}}{\omega - \mathbf{n} \cdot \boldsymbol{\Omega} + i0^+}$$

The term $+i0^+$ is used to do an analytical extension when the real part of the denominator vanishes according to the Landau prescription. This term cannot be skipped for causality reasons. Without sources, this solution becomes :

$$g_{\mathbf{n}\omega} = \frac{\omega}{\omega - \mathbf{n} \cdot \boldsymbol{\Omega} + i0^+} \frac{Z}{\tau} F_{eq} h_{\mathbf{n}\omega} \quad (3.14)$$

3.1.3 Quasi-electroneutrality

The quasi-electroneutrality equation takes the form $\sum_{\text{species}} Z_s N_s = 0$. This equation is supposed to be satisfied at equilibrium, which implies $\sum_{\text{species}} Z_s \int d^3\mathbf{p} F_{s,eq}(\mathbf{x}, \mathbf{p}, t) = 0$. Using the decomposition of the distribution function (3.6), the quasi-neutrality constraint can be written as :

$$\sum_{\text{species}} Z_s \int d^3\mathbf{p} f_s(\mathbf{x}, \mathbf{p}, t) = 0 \quad (3.15)$$

The quasi-electroneutrality constraint can be reformulated in a "weak" form³ as :

$$\forall h^\dagger(\mathbf{x}, t), \int d^3\mathbf{x} \left\{ \sum_{\text{species}} Z_s \int d^3\mathbf{p} f_s(\mathbf{x}, \mathbf{p}, t) \right\} h^\dagger(\mathbf{x}, t) = 0 \quad (3.16)$$

³Let $A : \mathbb{R} \rightarrow \mathbb{R}$. Then, equation $\forall x, A(x) = 0 \Leftrightarrow \forall B : \mathbb{R} \rightarrow \mathbb{R}, \int A(x)B(x)dx = 0$. The last form of the equation is called the "weak" formulation of the first one.

with h^\dagger an arbitrary field. The strong formulation Eq.(3.15) can be rewritten as $\frac{\partial \mathcal{L}}{\partial h^\dagger} = 0$, where the functional \mathcal{L} is defined as :

$$\mathcal{L} = -NT_i \sum_{\text{species}} Z_s \int d\zeta f_s(\mathbf{x}, \mathbf{p}, t) h^\dagger(\mathbf{x}, t) \quad (3.17)$$

where the volume element in the phase space $d\zeta = d^3\mathbf{x} d^3\mathbf{p} = d^3\boldsymbol{\alpha} d^3\mathbf{J}$ has been introduced. Replacing f_s by its expression depending of g_s on each mode ω (Eq.(3.9)), it comes :

$$\mathcal{L}_\omega = -NT_i \sum_{\text{species}} Z_s \int d\zeta \left(-\frac{Z_s}{\tau_s} F_{s,eq} h_\omega + g_{s,\omega} \right) h_\omega^\dagger$$

For now, h_ω^\dagger is indeterminate. We wish to take for the functional \mathcal{L} the Lagrangian of the particles, ions and electrons included. To do this, we choose $h_\omega^\dagger = h_\omega^*$. Decomposing g on its linear solutions given in Eq.(3.14), the functional recasts as :

$$\begin{aligned} \mathcal{L}_\omega &= NT_i \sum_{\text{species}} \frac{Z_s^2}{\tau_s} \int d^3\mathbf{x} h_\omega h_\omega^* \\ &\quad - NT_i \sum_{\text{species}} \frac{Z_s^2}{\tau_s} \int d\zeta F_M \sum_{\mathbf{n}} \frac{\omega}{\omega - \mathbf{n} \cdot \boldsymbol{\Omega} + i0^+} h_{\mathbf{n}\omega} h_{\mathbf{n}\omega}^* \end{aligned} \quad (3.18)$$

where we have introduced $F_M = F_{eq}/N$ the Maxwellian normalized to the density. This profile is set as the same for all species. The imaginary part of the resonant integral is most easily calculated in the action/angle space, using the volume element $d\zeta = d^3\boldsymbol{\alpha} d^3\mathbf{J}$. Also the unperturbed Hamiltonian $H_{eq}(\mathbf{J})$ is a function of the actions only and $\boldsymbol{\Omega}$ is a set of resonant frequencies $\Omega_i = \frac{\partial H_{eq}}{\partial J_i}$. Since the GAM frequency is much lower than the cyclotron frequency, only $n_1 = 0$ components are kept in Eq.(3.18). This is equivalent to a gyrokinetic calculation, with an hamiltonian $H_{eq} = \frac{1}{2}mv_\parallel^2 + \mu B$. Moreover, a GAM has a toroidal wave number that is null, which implies $n_3 = 0$ since $\alpha_3 = \varphi$ up to a periodic function of α_2 . Therefore the summation should be run on n_2 integers only. We note that useful equivalent formulation of the functional is

$$\begin{aligned} \mathcal{L}_\omega &= NT_i \sum_{\text{species}} \frac{1}{\tau} \int d\zeta F_M \left[|\phi_\omega|^2 - |J_0 \cdot \phi_\omega|^2 \right] \\ &\quad - NT_i \sum_{\text{species}} \frac{1}{\tau} \int d\zeta F_M \left| \frac{\mathbf{v}_D \cdot \nabla \phi_\omega}{-i\omega} \right|^2 \\ &\quad - NT_i \sum_{\text{species}} \frac{1}{\tau} \sum_{\mathbf{n}} \int d\zeta F_M \frac{\omega}{\omega - \mathbf{n} \cdot \boldsymbol{\Omega} + i0^+} \left| \frac{\mathbf{n} \cdot \boldsymbol{\Omega}}{\omega} h_{\mathbf{n}\omega} \right|^2 \end{aligned} \quad (3.19)$$

where J_0 denote the gyroaverage operator, \mathbf{v}_D is the vertical drift velocity, and the summation over \mathbf{n} is restricted to components $n_1 = 0, n_3 = 0$.

3.2 Trajectories and hamiltonian components

In the expression of the functional, the coefficients h_ω and $h_{n_2\omega}$ are unknowns of the problem. It is therefore needed to guess the shape of these hamiltonian components depending of the poloidal structure of the potential. First, we recall the expressions of passing and trapped trajectories using the angle-action variables. Second, a guess for the hamiltonian components appearing in the Lagrangian expression (3.18) is given.

3.2.1 Trajectories using angle-action variables

The general expressions of the guiding center position and poloidal angle read :

$$\begin{aligned} r_G &= r + \hat{r} \\ \theta_G &= \epsilon_c \alpha_2 + \hat{\theta} \end{aligned}$$

where r is the minor radius of a reference magnetic surface, $\epsilon_c = 1$ (resp. 0) for passing particles. The functions \hat{r} and $\hat{\theta}$ are functions of the actions \mathbf{J} , or equivalently to the motion invariants (H_{eq}, μ, P_φ) , and periodic functions of α_2 . We will omit to mention explicitly the dependencies on the motion invariants, to simplify the notations. The functions \hat{r} and $\hat{\theta}$ can be chosen respectively as even and odd functions of α_2 . For deeply passing particles, one finds :

$$\begin{aligned} \hat{r} &= \delta_c \cos \alpha_2 \\ \hat{\theta} &= -\frac{\delta_c}{r} \sin \alpha_2 \end{aligned}$$

where

$$\begin{aligned} \delta_c &= -\frac{v_D}{\Omega_2} \\ v_D &= -\frac{mv_\parallel^2 + \mu B}{eBR_0} \\ \Omega_2 &= \frac{v_\parallel}{qR_0} \end{aligned} \tag{3.20}$$

Here δ_c is the displacement of a drift surface and is of order $q\rho_c$, where ρ_c is the gyroradius. The trajectory equations Eq.(3.20) are valid at order 1 in δ_c/r . Eq.(3.20) corresponds to a circle that is shifted horizontally by a distance δ_c from the magnetic surface.

3.2.2 Fourier components of the hamiltonian

In the following, we use the GAM electric potential ϕ in position variables normalized to the perturbed hamiltonian h in angle-action variables so that $\phi(\mathbf{x}, t) = h(\boldsymbol{\alpha}, \mathbf{J}, t)$. While keeping a single radial wave vector, the GAM electric potential is expanded in Fourier series with respect to the poloidal angle :

$$\phi_\omega(r, \theta) = \sum_{m=-\infty}^{+\infty} \tilde{\phi}_{m\omega}(K) e^{i(Kr+m\theta)} \tag{3.21}$$

First, ϕ_ω is developed around the gyrocentre position (r_G, θ_G) : $\phi_\omega(r, \theta) = J_0 \phi_\omega(r_G, \theta_G)$. Second, using the hamiltonian decomposition Eq.(3.13) of h_ω in $\boldsymbol{\alpha}$, the mode $\mathbf{n} = (0, n_2, 0)$ is given by :

$$\begin{aligned} h_{n_2\omega}(\mathbf{J}) &= \iiint_{-\pi}^{+\pi} \frac{d\alpha_1}{2\pi} \frac{d\alpha_2}{2\pi} \frac{d\alpha_3}{2\pi} \left\{ J_0 \sum_{m=-\infty}^{+\infty} \tilde{\phi}_{m\omega}(K) e^{i(Kr_G + m\theta_G)} \right\} e^{-in_2\alpha_2} \\ &= J_0 \int_{-\pi}^{+\pi} \frac{d\alpha_2}{2\pi} \sum_{m=-\infty}^{+\infty} \tilde{\phi}_{m\omega}(K) e^{i(Kr_G + m\theta_G - n_2\alpha_2)} \end{aligned}$$

Using the trajectory equations Eq.(3.20), the correspondence between Fourier and hamiltonian components is found to be :

$$h_{n_2\omega}(\mathbf{J}) = e^{iKr} J_0 \int_{-\pi}^{+\pi} \frac{d\alpha_2}{2\pi} \sum_{m=-\infty}^{+\infty} \tilde{\phi}_{m\omega}(K) e^{i[K\hat{r} + m\hat{\theta} + (\epsilon_c m - n_2)\alpha_2]} \quad (3.22)$$

As seen above $\hat{\theta}$ is of the order of $\frac{\delta_c}{r}$ for passing particles, and can therefore be neglected against $K\hat{r}$ if $K \gg \frac{m}{r}$. It is shown in Appendix C of the thesis of C. Nguyen [65, Nguyen 2009] that $\tilde{\phi}_{m\omega}(K)$ scales as $(-iK\rho_i)^m \tilde{\phi}_{0\omega}$, where $\rho_i = \frac{mv_{Ti}}{eB_0}$ is the thermal ion gyroradius. We will therefore use the following auxiliary real numbers :

$$\tilde{\phi}_{m\omega} = (-i)^m \phi_m \quad (3.23)$$

with $\phi_{-m} = \phi_m$ and

$$\eta_m = \frac{\tilde{\phi}_{m\omega}}{(-iK\rho_i)^m} = \frac{\phi_m}{(K\rho_i)^m} \sim o(1) \quad (3.24)$$

Moreover a calculation of the potential at order 2 in $K\rho_i$ guarantees a functional that is correct at 4th order. In the following we consider only the harmonics $m = 0, \pm 1, \pm 2$ consistent with a second order calculation of the potential in $K\rho_i$, i.e.

$$\phi_\omega = \phi_0 + 2\phi_1 \sin(\theta) - 2\phi_2 \cos(2\theta) + o(K^3 \rho_i^3) \phi_0 \quad (3.25)$$

that will also be written

$$\phi_\omega = \phi_0 [1 + 2K\rho_i \eta_1 \sin(\theta) - 2K^2 \rho_i^2 \eta_2 \cos(2\theta) + o(K^3 \rho_i^3)] \quad (3.26)$$

3.2.3 Passing particles

For passing particles $\epsilon_c = 1$. Replacing Eq.(3.23) in Eq.(3.22), one gets :

$$h_{n_2\omega} = i^{n_2} e^{iKr} J_0(K\rho_i) \sum_m (-1)^m J_{n_2-m}(K\delta_c) \phi_m \quad (3.27)$$

where $J_{n_2}(K\delta_c)$ is the Bessel function of index n_2 and argument $K\delta_c$, that will be written in short \bar{J}_{n_2} to avoid the confusion with the gyroaverage operator. The decomposition

of the perturbed hamiltonian can be written with both position-momentum and angle-action variables $\phi_\omega(\mathbf{x}) = h_\omega(\boldsymbol{\alpha}, \mathbf{J})$ with :

$$\begin{cases} \phi_\omega = \sum_m (-i)^m \phi_m \exp(im\theta) \\ h_\omega = \sum_{n_2} h_{n_2\omega} \exp(in_2\alpha_2) \end{cases}$$

Using the fact that $\int d^3\mathbf{x}d^3\mathbf{p}\phi_\omega\phi_\omega^* = \int d^3\boldsymbol{\alpha}d^3\mathbf{J}h_\omega h_\omega^*$ and the development of ϕ_ω around the gyrocentre position (r_G, θ_G) : $\phi_\omega(r, \theta) = J_0\phi_\omega(r_G, \theta_G)$, it can be verified that :

$$\sum_{n_2} |h_{n_2\omega}|^2 = J_0^2 \sum_m |\phi_m|^2 \quad (3.28)$$

Since δ_c is the radial shift of a drift surface relative to the reference magnetic surface, it appears that the operator \bar{J}_{n_2} is similar to the gyroaverage operator, with the gyroradius replaced by δ_c . In the limit of small wave numbers $K\delta_c \ll 1$, $J_0(K\delta_c) \simeq 1 - \frac{1}{4}K^2\delta_c^2$, and $J_{n_2}(K\delta_c) \simeq \frac{1}{n_2!} \left(\frac{K\delta_c}{2}\right)^{n_2}$ for $n_2 \neq 0$. These properties ensure a rapid convergence of the series in n_2 whenever $K\rho_i$ is small enough. We keep only the first harmonics $n_2 = 0, \pm 1, \pm 2$, consistent with a calculation at order 2 in $K\rho_i$, and therefore order 4 for the Lagrangian. The correspondence Eq.(3.27) leads to the following relations :

$$\begin{aligned} h_0 &= e^{iKr} J_0 \bar{J}_0 \phi_0 \\ h_1 &= ie^{iKr} J_0 [\bar{J}_1 \phi_0 - \bar{J}_0 \phi_1] \\ h_{-1} &= ie^{iKr} J_0 [\bar{J}_1 \phi_0 + \bar{J}_0 \phi_1] \\ h_2 &= -e^{iKr} J_0 [\bar{J}_2 \phi_0 - \bar{J}_1 \phi_1 + \bar{J}_0 \phi_2] \\ h_{-2} &= -e^{iKr} J_0 [\bar{J}_2 \phi_0 + \bar{J}_1 \phi_1 + \bar{J}_0 \phi_2] \end{aligned} \quad (3.29)$$

Setting $b = K\delta_c$, the Bessel functions are expanded as :

$$\begin{aligned} \bar{J}_0 &= 1 - \frac{b^2}{4} + \frac{b^4}{64} + o(b^6) \\ \bar{J}_1 &= \frac{b}{2} \left[1 - \frac{b^2}{8}\right] + o(b^5) \\ \bar{J}_2 &= \frac{b^2}{8} + o(b^4) \end{aligned} \quad (3.30)$$

consistent with the constraint $\bar{J}_0^2 + 2\bar{J}_1^2 + 2\bar{J}_2^2 = 1 + o(b^6)$.

3.2.4 Trapped particles

For trapped particles $\epsilon_c = 0$. Replacing Eq.(3.23) in Eq.(3.22), one gets :

$$h_{n_2\omega} = e^{iKr} J_0 \int \frac{d\alpha_2}{2\pi} \exp\{i(K\hat{r} - n_2\alpha_2)\} \left(\phi_0 + 2\phi_1 \sin \hat{\theta} - 2\phi_2 \cos 2\hat{\theta}\right) \quad (3.31)$$

For large wavelengths $K\hat{r} \ll 1$ and anticipating that only $n_2 \neq 0$ components will matter for damping, one finds

$$h_{n_2\omega} = e^{iKr} J_0 \int \frac{d\alpha_2}{2\pi} \exp(-in_2\alpha_2) \left(iK\hat{r}\phi_0 + 2\phi_1 \sin \hat{\theta} - 2\phi_2 \cos 2\hat{\theta} \right) \quad (3.32)$$

For electrons, the operator J_0 is set to unity, consistently with the expansion of the potential at order 1 in $K\rho_i$. Also the banana width is small and will be neglected as it introduces a subdominant dependence on the electron mass. Hence the hamiltonian components read

$$h_{n_2\omega} = e^{iKr} \tilde{h}_{n_2\omega} K\rho_i \phi_0 \quad (3.33)$$

where

$$\tilde{h}_{n_2\omega} = 2 \int_0^{2\pi} \frac{d\alpha_2}{2\pi} \left(\eta_1 \sin \hat{\theta} - \eta_2 K\rho_i \cos 2\hat{\theta} \right) e^{-in_2\alpha_2} \quad (3.34)$$

3.3 Real part of the dispersion relation

It turns out that the real part of the lagrangian is most easily computed by using Eq.(3.19) and the relationship

$$-i\mathbf{n} \cdot \boldsymbol{\Omega} h_{\mathbf{n}\omega} = \left[(\mathbf{v}_D \cdot \nabla + v_{\parallel} \nabla_{\parallel}) \phi_{\omega} \right]_{\mathbf{n}} \quad (3.35)$$

We introduce the dimensionless Lagrangian $\bar{\mathcal{L}} = \mathcal{L}/N_i T_i$ and its density \bar{L} defined as $\bar{\mathcal{L}} = \int d^3\mathbf{x} \bar{L}$, which can be written as

$$\begin{aligned} \bar{L} &= NT_i \sum_{\text{species}} \frac{1}{\tau} \left[|\phi_{\omega}|^2 - \left\langle |J_0 \cdot \phi_{\omega}|^2 \right\rangle \right] \\ &- NT_i \sum_{\text{species}} \frac{1}{\tau} \left\langle \left| \frac{\mathbf{v}_D \cdot \nabla \phi_{\omega}}{-i\omega} \right|^2 \right\rangle \\ &- \sum_{\text{species}} \frac{1}{\tau} \sum_{n_2} \left\langle \frac{\omega}{\omega - n_2 \Omega_2 + i0^+} \left| \left[\frac{(\mathbf{v}_D \cdot \nabla + v_{\parallel} \nabla_{\parallel}) \phi}{-i\omega} \right]_{\mathbf{n}\omega} \right|^2 \right\rangle \end{aligned} \quad (3.36)$$

where brackets indicate an average over the velocity space with a Maxwellian weight. The extremalisation of \bar{L} with respect of ϕ_1^* and ϕ_2^* allows to compute ϕ_1 and ϕ_2 as a function of ϕ_0 . The calculation will not be repeated here as it was done in [64, Nguyen 2008], using a double expansion in $K\rho_i$ and $1/q\Omega$, where $\Omega = \frac{\omega R_0}{v_{Ti}}$. Reference [64] addresses in fact the case of Beta Alfvén Eigenmode (BAE), but also covers GAMs, which is found by imposing the electrostatic limit ($\psi_{\omega} = 0$ and $\mathcal{E}_{\omega} = \phi_{\omega}$) in the notations of [64]. One then finds

$$\phi_1 = \left\{ 1 + \frac{2 + \tau_e}{q^2 \Omega^2} + o\left(\frac{1}{q^4 \Omega^4}\right) \right\} \tau_e \frac{K\rho_i}{\Omega} \phi_0 + o(K^3 \rho_i^3) \phi_0 \quad (3.37)$$

and

$$\phi_2 = - \left\{ \frac{7}{4} + \tau_e + \frac{\tau_e(2 + \tau_e)}{q^2 \Omega^2} + o\left(\frac{1}{q^4 \Omega^4}\right) \right\} \frac{\tau_e}{\Omega^2} K^2 \rho_i^2 \phi_0 \quad (3.38)$$

Terms in ϕ_1 of order $(K^3 \rho_i^3) \phi_0$ are not given here in details for simplicity, but are necessary to calculate the functional at right order. The dispersion relation $\Re(\bar{L}) = 0$ is obtained by plugging Eq.(3.37) and Eq.(3.38) into the functional Eq.(3.36). One finally gets

$$\Re(\bar{L}) = (\Lambda_1 - \Lambda_2 K^2 \rho_i^2) K^2 \rho_i^2 |\phi_0|^2 \quad (3.39)$$

where

$$\Lambda_1 = 1 - \left(\frac{7}{2} + 2\tau_e\right) \frac{1}{\Omega^2} - \left(\frac{23}{2} + 8\tau_e + 2\tau_e^2\right) \frac{1}{q^2 \Omega^4} \quad (3.40)$$

and

$$\Lambda_2 = \frac{3}{4} - \left(\frac{13}{2} + 6\tau_e + 2\tau_e^2\right) \frac{1}{\Omega^2} + \left(\frac{747}{8} + \frac{481}{8}\tau_e + \frac{35}{2}\tau_e^2 + 2\tau_e^3\right) \frac{1}{\Omega^4} \quad (3.41)$$

This expression agrees with previous calculations [85, 84, 75, 76, Zonca 1996-2008, Sugama 2006-8]. Note however that the normalizations are different: in the aforementioned works, the thermal velocity is defined as $\sqrt{2T_i/m_i}$, and the thermal gyroradius accordingly, while the GAM frequency is normalized to a transit frequency defined as $\sqrt{2T_i/m_i}/(qR_0)$.

It appears that kinetic electrons play a minor role in the GAM expression. In fact, the kinetic answer of electrons is contained in the terms in $\omega/\omega \pm \Omega_e^e$ of Eq.(3.19). Although, these terms do not impact much the GAM pulsation, it will be seen further that they must be taken into account while evaluating the damping rate.

3.4 GAM damping

Contrary to the GAM pulsation, which is not much changed whether electrons are adiabatic or kinetic, the GAM damping is believed to depend greatly of the kinetic answer of electrons [83, Zhang 2010]. The amount of exchanged energy between particles and wave is derived from the imaginary part of the Lagrangian for ions first and for electrons second. Then the associated damping rate is computed and compared to the existing theory.

3.4.1 Contribution of ions to GAM damping

The exchange of energy between particles and waves per volume and time unit is given by the relation $W = 2\omega\Im(L)$, where $\mathcal{L} = \int d^3\mathbf{x}L$. A positive value of $W > 0$ means particle heating, i.e. damping. The calculation is restricted for now to passing ions. The imaginary part of the normalized functional $\Im(\bar{L})$ is obtained, the same way as $\Re(\bar{L})$, by plugging the value of ϕ_1 Eq.(3.37) and ϕ_2 Eq.(3.38) into the functional \bar{L} Eq.(3.36). The imaginary part of the normalized functional takes the following expression:

$$\begin{aligned} \Im(\bar{L}) &= K^2 \rho_i^2 |\phi_0|^2 \left\{ \frac{1}{2} \sqrt{\frac{\pi}{2}} q^5 \Omega^3 e^{-\frac{q^2 \Omega^2}{2}} \left[1 + 2 \frac{1 + 2\tau_e}{q^2 \Omega^2} + o\left(\frac{1}{q^4 \Omega^4}\right) \right] \right. \\ &\quad \left. + \frac{K^2 \rho_i^2}{1024} \sqrt{\frac{\pi}{2}} q^9 \Omega^5 e^{-\frac{q^2 \Omega^2}{8}} \left[1 + 16 \frac{1 + \tau_e}{q^2 \Omega^2} + o\left(\frac{1}{q^4 \Omega^4}\right) \right] \right\} \end{aligned} \quad (3.42)$$

Finally the total functional is found to be:

$$\begin{aligned} \bar{L} &= K^2 \rho_i^2 |\phi_0|^2 \left\{ \Lambda_1 - \Lambda_2 K^2 \rho_i^2 \right. \\ &\quad + i \frac{1}{2} \sqrt{\frac{\pi}{2}} q^5 \Omega^3 e^{-\frac{q^2 \Omega^2}{2}} \left[1 + 2 \frac{1 + 2\tau_e}{q^2 \Omega^2} \right] \\ &\quad \left. + i \frac{1}{1024} \sqrt{\frac{\pi}{2}} K^2 \rho_i^2 q^9 \Omega^5 e^{-\frac{q^2 \Omega^2}{8}} \left[1 + 16 \frac{1 + \tau_e}{q^2 \Omega^2} \right] \right\} \end{aligned} \quad (3.43)$$

that can be compared directly to Eq.(6) of [84, Zonca 2008]. Each bracket [...] is calculated up to an error of order $\left(\frac{1}{q^4 \Omega^4}\right)$. Moving back to physical units, the density of exchanged energy per volume and time unit:

$$\begin{aligned} W_i &= \sqrt{\frac{\pi}{2}} N_i T_i \frac{v_{Ti}}{R_0} K^2 \rho_i^2 |\phi_0|^2 q^5 \Omega^4 \left\{ e^{-\frac{q^2 \Omega^2}{2}} \left[1 + 2 \frac{1 + 2\tau_e}{q^2 \Omega^2} \right] \right. \\ &\quad \left. + \frac{K^2 \rho_i^2}{512} q^4 \Omega^2 e^{-\frac{q^2 \Omega^2}{8}} \left[1 + 16 \frac{1 + \tau_e}{q^2 \Omega^2} \right] \right\} \end{aligned} \quad (3.44)$$

where the normalized frequency Ω is given by the dispersion relation $\Re(\bar{L}) = 0$.

3.4.2 Contribution of electrons to GAM damping

Reduction of the lagrangian

Deeply passing electrons contribute weakly to GAM damping because of their large velocities. This can be seen in Eq.(3.44) when applied to electrons, where the small electron to ion mass ratio in the exponential leads to a tiny value of the power exchange compared with the contribution of passing ions. However trapped electrons do contribute to GAM damping because their bounce frequency becomes small near the passing/trapped domain and meet a resonance with the GAM pulsation [13, Chen 2003]. In principle barely passing electrons may also contribute. However their contribution was found to be small numerically [13]. Let us introduce a resonant Lagrangian for the electrons (both trapped and passing)

$$\mathcal{L}_{res,e} = -N_i T_i \frac{1}{\tau_e} \sum_{n_2=-\infty}^{+\infty} \int d\zeta F_M \frac{\omega}{\omega - n_2 \Omega_2 + i0^+} |h_{n\omega}|^2 \quad (3.45)$$

The electron bounce pulsation Ω_2 scales as the electron transit frequency $\frac{v_{Te}}{qR_0}$, i.e. is much larger than the GAM pulsation. However Ω_2 becomes small near the trapped/passing boundary, thus allowing a resonance, and therefore damping. We introduce a normalized bounce pulsation

$$\Omega_b = \frac{\Omega_2 q R_0}{v_{Te}} \quad (3.46)$$

where $v_{Te} = \sqrt{T_e/m_e}$ is the electron thermal velocity. We will also make use of the scaling parameter $\sigma = q\tau_e^{-1/2} (m_e/m_i)^{1/2}$, which is proportional to the square root of the electron to ion mass ratio, hence a number that is small compared to one. The bounce frequency normalized to the ion transit frequency can then be written

$$\Omega_2 \frac{R_0}{v_{Ti}} = \frac{\Omega_b}{\sigma} \quad (3.47)$$

The resonance condition requires $\Omega_b \simeq \sigma \ll 1$.

The volume integrated energy transfer from a GAM to electrons is $\mathcal{W}_e = 2\omega \Im(\mathcal{L}_{res,e})$. We introduce a normalized Lagrangian

$$\bar{\mathcal{L}}_{res,e} = \frac{\mathcal{L}_{res,e} \tau_e}{N_i T_i K^2 \rho_i^2 |\phi_0|^2} \quad (3.48)$$

which is readily written as

$$\bar{\mathcal{L}}_{res,e} = - \sum_{n_2=-\infty}^{+\infty} \int d\zeta F_M \frac{\Omega}{\Omega - n_2 \frac{\Omega_b}{\sigma} + i0^+} \left| \tilde{h}_{n_2\omega} \right|^2 \quad (3.49)$$

To simplify the notations, we omit the explicit dependencies of the Hamiltonian on the actions and the first and third angle variables. Hence the perturbed Hamiltonian reads

$$\tilde{h}_\omega(\alpha_2) = \sum_{n_2=-\infty}^{+\infty} \tilde{h}_{n_2\omega} e^{in_2\alpha_2} \quad (3.50)$$

consistently with

$$\tilde{h}_{n_2\omega} = \oint \frac{d\alpha_2}{2\pi} \tilde{h}_\omega(\alpha_2) e^{-in_2\alpha_2} \quad (3.51)$$

We make use of the relations

$$\frac{1}{\Omega - n_2 \frac{\Omega_b}{\sigma} + i0^+} = -i \frac{\sigma}{|\Omega_b|} \int_0^{+\infty} ds \exp \left\{ i \left[\left(\sigma \frac{\Omega}{\Omega_b} - n_2 \right) \epsilon_{\parallel} + i0^+ \right] s \right\} \quad (3.52)$$

and

$$\sum_{n_2=-\infty}^{+\infty} e^{in_2 X} = \sum_{p=-\infty}^{+\infty} 2\pi \delta(X - 2\pi p) \quad (3.53)$$

where $\epsilon_{\parallel} = \text{sign}(\Omega_b)$ is the sign of the parallel velocity for passing particles, and is equal to 1 for trapped particles. This procedure, detailed in Appendix C.3, leads to the following expression of the Lagrangian

$$\begin{aligned} \bar{\mathcal{L}}_{res,e} &= 2i\pi\sigma\Omega \sum_{p=-\infty}^{+\infty} \int d\zeta \frac{F_M}{|\Omega_b|} \oint \frac{d\alpha_2}{2\pi} \tilde{h}_\omega(\alpha_2) \oint \frac{d\alpha'_2}{2\pi} \tilde{h}_\omega^*(\alpha'_2) \\ &\quad \Theta \left[\epsilon_{\parallel} (\alpha'_2 - \alpha_2 + 2p\pi) \right] \exp \left\{ i\sigma \frac{\Omega}{\Omega_b} (\alpha'_2 - \alpha_2 + 2p\pi) \right\} \end{aligned} \quad (3.54)$$

where Θ is a Heaviside function ($\Theta(x) = 1$ for $x > 0$, 0 otherwise). This expression can also be obtained by solving the Vlasov equation when using angular variables. It is reminded that $d\zeta = d^3\boldsymbol{\alpha} d^3\mathbf{J} = (2\pi)^3 d^3\mathbf{J}$ is the volume integration element in the phase space. For passing particles, this integration element contains a summation of the sign of the parallel velocity ϵ_{\parallel} . At this point it is convenient to choose $[-\pi, \pi]$ as the interval spanned by α_2 and α'_2 . For $\epsilon_{\parallel} = 1$, negative values of p do not contribute because of the Heaviside function, while for $p \geq 1$, the Heaviside function is equal to 1 - so that the Heaviside function matters only for $p = 0$. For similar reasons, only negative values of p matter when $\epsilon_{\parallel} = -1$. A convenient form of Eq.(3.54) can be obtained after a summation over the index $p \geq 1$ for $\epsilon_{\parallel} = 1$ ($p \leq -1$ for $\epsilon_{\parallel} = -1$), namely

$$\begin{aligned} \bar{\mathcal{L}}_{res,e} &= 2i\pi\sigma\Omega \int d\zeta \frac{F_M}{|\Omega_b|} \int_{-\pi}^{\pi} \frac{d\alpha_2}{2\pi} \int_{-\pi}^{\pi} \frac{d\alpha'_2}{2\pi} \\ &\quad \tilde{h}_\omega(\alpha_2) \tilde{h}_\omega^*(\alpha'_2) \exp \left\{ i\sigma \frac{\Omega}{\Omega_b} (\alpha'_2 - \alpha_2) \right\} \\ &\quad \left\{ \Theta \left[\epsilon_{\parallel} (\alpha'_2 - \alpha_2) \right] + \frac{1}{\exp \left(-2i\pi\sigma \frac{\Omega}{|\Omega_b|} \right) - 1} \right\} \end{aligned} \quad (3.55)$$

Eq.(3.55) can be considered as a workable form. Its main advantage is to avoid using explicit resonances. Also it exhibits clearly the parametric dependencies. A convenient alternative form is

$$\bar{\mathcal{L}}_{res,e} = 2i\pi\sigma\Omega \int d\zeta \frac{F_M}{\Omega_b} \int_{-\pi}^{\pi} \frac{d\alpha_2}{2\pi} \int_{\alpha_2}^{\epsilon_{\parallel}\infty} \frac{d\alpha'_2}{2\pi} \tilde{h}_\omega(\alpha_2) \tilde{h}_\omega^*(\alpha'_2) \exp \left\{ i\sigma \frac{\Omega}{\Omega_b} (\alpha'_2 - \alpha_2) \right\}$$

Notations	$\lambda = \frac{\mu B_0}{H}$	$\epsilon_b(\lambda)$	$\theta_0(\lambda)$	κ
Passing	$0 \leq \lambda \leq \lambda_{min} = \frac{1}{1+\epsilon}$	0	π	$0 \leq \kappa \leq 1$
Trapped	$\lambda_{min} \leq \lambda \leq \lambda_{max} = \frac{1}{1-\epsilon}$	1	$-\pi \leq \theta_0 \leq \pi$	$1 \leq \kappa \leq +\infty$

Table 3.1: Notations and conventions for passing and trapped particles.

where α'_2 is now a continuous integration variable that spans the interval $[\alpha_2, \epsilon_{\parallel} \infty]$. This form can be obtained in a faster way by solving the Vlasov equation in angle variable. At this point, the velocity integration has to be further detailed, to produce a more practical expression.

Quantitative estimate of GAM electron damping

The phase space density $F_M d\zeta$ in the Lagrangian Eq.(3.55) reads

$$F_M d\zeta = d\mathcal{V} \sum_{\epsilon_{\parallel}=\pm 1} d\lambda \sqrt{\frac{2}{\pi}} dv v^3 \frac{1}{|\Omega_b|} e^{-v^2} \quad (3.56)$$

where $d\mathcal{V} = 4\pi^2 R_0 r dr$ is the volume element, $\lambda = \frac{\mu B_0}{H_{eq}}$, ϵ_{\parallel} is the sign of the parallel velocity (for passing particles only), and v is a normalized velocity $v^2 = \left[\frac{1}{2} m v_{\parallel}^2 + \mu B \right] / T$. The bounce/transit pulsation reads

$$\frac{1}{|\Omega_b|} = \frac{1 + \epsilon_b}{\sqrt{2}v} \bar{\tau}(\lambda) \quad (3.57)$$

where

$$\bar{\tau}(\lambda) = \int_{-\theta_0}^{\theta_0} \frac{d\theta}{2\pi} \frac{1}{(1 - \lambda + \epsilon \lambda \cos \theta)^{1/2}} \quad (3.58)$$

Here θ_0 is the poloidal angle of a trapped particle turning point, i.e. the positive solution of $v_{\parallel}(E, \lambda, \theta) = 0$, while $\theta_0 = \pi$ for passing particles. The meaning of the notations for trapped and passing particles is given in Table 3.1. The bounce/transit frequency Ω_b has been chosen positive. It exhibits a discontinuity at the trapped/passing boundary. The reason is that a barely passing particle makes one turn in θ , i.e. 2π , while a barely trapped particle moves back and forth in the poloidal direction, and therefore spans a 4π interval in θ . It can be verified that $\int d\zeta F_M = 1$, as expected. The pitch-angle variable λ does not allow an easy handling of the singularity at the passing/trapped boundary. It is therefore useful to introduce an alternative pitch angle parameter κ defined as

$$\kappa^2 = \frac{2\epsilon\lambda}{1 - \lambda(1 - \epsilon)} \quad (3.59)$$

It appears that

$$d\lambda = \frac{4\varepsilon}{(1+\varepsilon)^2} \frac{\kappa d\kappa}{\Lambda^2(\kappa)} \quad (3.60)$$

and

$$\frac{v_{\parallel}}{v_{Te}} = \left(\frac{\varepsilon}{1+\varepsilon} \right)^{1/2} \frac{2v}{\Lambda^{1/2}(\kappa)} \left[1 - \kappa^2 \sin^2 \left(\frac{\theta}{2} \right) \right]^{1/2} \quad (3.61)$$

where

$$\Lambda(\kappa) = \frac{2\varepsilon + (1-\varepsilon)\kappa^2}{1+\varepsilon} \quad (3.62)$$

The function $\Lambda(\kappa)$ is smooth near $\kappa = 1$, with $\Lambda(1) = 1$. The bounce/transit time can be explicated in terms of the complete elliptical function of the first kind \mathbb{K} , namely

$$\bar{\tau}(\kappa) = \left(\frac{1+\varepsilon}{2\varepsilon} \right)^{1/2} \Lambda^{1/2}(\kappa) \tau(\kappa) \quad (3.63)$$

where

$$\tau(\kappa) = \frac{2}{\pi} \begin{cases} \mathbb{K}(\kappa^2) & \text{if } 0 \leq \kappa \leq 1 \\ \frac{1}{\kappa} \mathbb{K} \left(\frac{1}{\kappa^2} \right) & \text{if } 1 \leq \kappa \leq +\infty \end{cases} \quad (3.64)$$

Details on the link between the angular variable α_2 and the poloidal angle θ can be found in the Appendix C.2.

In the following only the contribution of trapped electrons is kept, since passing electrons contribute weakly to damping. Using this set of variables in the limit of large aspect ratio $\varepsilon \ll 1$, the integrand of the Lagrangian Eq.(3.55) is recast as

$$\frac{F_M}{|\Omega_b|} d\zeta = \sqrt{\frac{2}{\pi}} \frac{1}{1+\varepsilon} d\nu \sum_{\epsilon_{\parallel}=\pm 1} \frac{\kappa d\kappa}{\Lambda(\kappa)} (1+\epsilon_b(\kappa))^2 \tau^2(\kappa) v dv e^{-v^2} \quad (3.65)$$

Another important quantity that appears in the Lagrangian Eq.(3.55) is the ratio $\sigma \frac{\Omega}{|\Omega_b|}$, which reads

$$\sigma \frac{\Omega}{|\Omega_b|} = \frac{1+\epsilon_b}{2} \sqrt{1+\varepsilon} \sigma^* \tau(\kappa) \Lambda^{1/2}(\kappa) \quad (3.66)$$

For trapped electrons, and in the limit of large aspect ratio $\varepsilon \rightarrow 0$, it reduces to $\sigma \Omega / |\Omega_b| = \sigma^* \tau(\kappa) \Lambda^{1/2}(\kappa)$. The parameter σ^* , defined as

$$\sigma^* = \frac{\sigma}{\varepsilon^{1/2}} \Omega = \left(\frac{m_e}{m_i \tau_e} \right)^{1/2} \frac{q}{\varepsilon^{1/2}} \Omega \quad (3.67)$$

is the key parameter for a GAM to meet a resonance with trapped electrons. Indeed the condition $\sigma^* \simeq 1$ corresponds to the condition $\omega \simeq \omega_b$, where the bounce frequency ω_b

scales as $\frac{v\tau_e\varepsilon^{1/2}}{qR_0}$. Introducing $\bar{L}_{res,e}$ the Lagrangian per volume unit defined as $\bar{\mathcal{L}}_{res,e} = \int dV \bar{L}_{res,e}$, the Lagrangian Eq.(3.55) reads

$$\begin{aligned} \bar{L}_{res,e} = & 8i\sqrt{2\pi}\varepsilon^{1/2}\sigma^* \int_1^{+\infty} \frac{\kappa d\kappa}{\Lambda(\kappa)} \tau^2(\kappa) \int_0^{+\infty} dv v \exp(-v^2) \\ & \int_{-\pi}^{\pi} \frac{d\alpha_2}{2\pi} \int_{-\pi}^{\pi} \frac{d\alpha'_2}{2\pi} \tilde{h}_\omega(\alpha_2) \tilde{h}_\omega^*(\alpha'_2) \exp\left\{i\sigma^* \frac{\tau}{v} \Lambda^{1/2}(\alpha'_2 - \alpha_2)\right\} \\ & \left\{ \Theta(\alpha'_2 - \alpha_2) + \frac{1}{\exp(-2i\pi\sigma^* \frac{\tau}{v} \Lambda^{1/2}) - 1} \right\} \end{aligned} \quad (3.68)$$

One important consequence of Eq.(3.68) is that $\Im(\bar{L}_{res,e})$ is some function of σ^* , up to a weak dependence on the aspect ratio. Since the frequency Ω is a function of (q, τ_e) only, this means that mass scaling prescribes the dependence on safety factor q and electron to ion ratio $\tau_e = \frac{T_e}{T_i}$.

The parameter σ^* is smaller than 1 for usual plasma parameters, typically of the order of 1/10, or less. An estimate of the integral Eq.(3.68) appears to be quite difficult. Nevertheless some exact results can be derived. It is reminded that the main GAM poloidal dependence is of the form $\tilde{h}_\omega(\alpha_2) \sim \sin[\theta(\alpha_2)]$. Introducing the function $\bar{\sigma}(v, \kappa) = \sigma^* \frac{\tau(\kappa)}{v} \Lambda^{1/2}(\kappa)$, it appears that the imaginary part of the integrand in the Lagrangian Eq.(3.68) scales as $\bar{\sigma}^3$ when $\bar{\sigma} \rightarrow 0$ (see Appendix C.4.1). This yields a very small contribution to damping and can be neglected against ion damping in most conditions. However this expansion breaks down whenever $\bar{\sigma} \simeq o(1)$, i.e. close to the curve $\sigma^* \tau(\kappa) \Lambda^{1/2}(\kappa) = v$ in the phase space (v, κ) . Since σ^* is small, this requires small values of the period $\tau(\kappa)$. This situation occurs near the trapped/passing boundary $\kappa \sim 1$, where $\tau \simeq -\frac{1}{2} \ln(\kappa - 1)$. The condition $\bar{\sigma} \simeq o(1)$ is also fulfilled at small values of the velocity $v \simeq \sigma^*$. However because of the integrand in velocity that behaves as v , the contribution from low velocities is quite small (smaller than $[\sigma^*]^2$). This means that most of the integral comes from the trapped/passing boundary $\kappa \sim 1$ as it is confirmed by Fig.3.1 which shows the contribution of particles in the velocity space (v_{\parallel}, μ) . The exact calculation of Eq.(3.68) in the region $\kappa \sim 1$ is difficult. Hence we have to resort to making some approximations. One expect the bounce integrals in (α_2, α'_2) to be dominated by the turning points $(\alpha_2 = \pm \frac{\pi}{2}, \alpha'_2 \pm \frac{\pi}{2})$. The configuration that maximize the damping is such that $\alpha = \alpha' = \frac{\pi}{2}$ (see derivation in Appendix C.4.2). This procedure provides the following estimate of the imaginary part of the Lagrangian

$$\Im(\bar{L}_{res,e}) = \sqrt{2\pi}\varepsilon^{1/2}\sigma^* \mathcal{D}(\sigma^*) \int_1^{+\infty} \frac{\kappa d\kappa}{\Lambda(\kappa)} \tau^2(\kappa) \left| \tilde{h}_\omega(\theta_0(\kappa)) \right|^2 \quad (3.69)$$

where $\tilde{h}_\omega(\theta_0)$ is the value of the perturbed Hamiltonian at the bounce point when expressed in the θ variable, and $\mathcal{D}(\sigma^*)$ measures the weight of the region in the phase space where $\sigma^* \tau(\kappa) \Lambda^{1/2}(\kappa)/v > 1$. It is reminded that $\sigma^* = q\tau_e^{-1/2}\varepsilon^{-1/2}(m_e/m_i)^{1/2}\Omega$. The perturbed Hamiltonian is of the form Eq.(3.26). The normalised amplitude of the

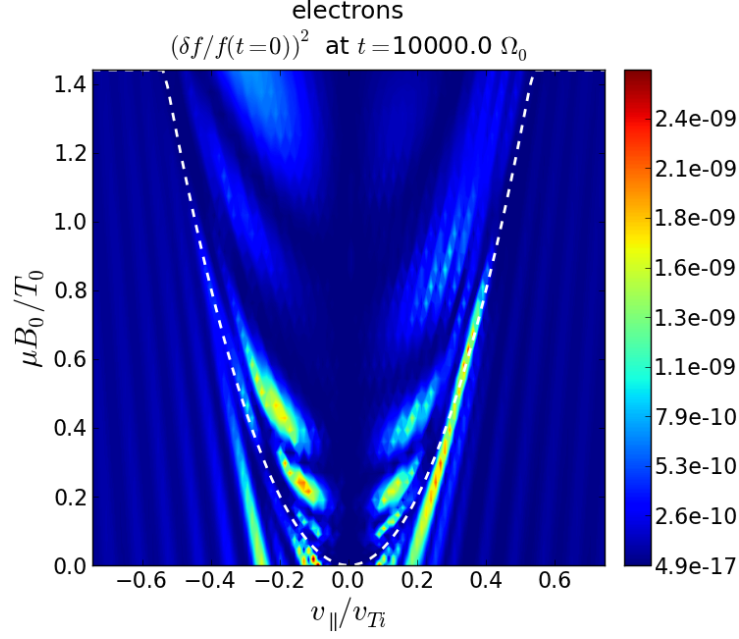


Figure 3.1: Contribution of particles to the integral Eq.(3.68) in the velocity space (v_{\parallel}, μ) . It appears that the particles located near the trapped/passing boundary (dashed white line) contribute the more.

Hamiltonian perturbation is defined as

$$\eta(\theta) = \frac{\tilde{h}_{\omega}(\theta)}{K \rho_i \phi_0} \quad (3.70)$$

In general $\eta(\theta)$ is of the form $\eta(\theta) = \eta_1 \sin(\theta) + \eta_2 \cos(2\theta)$, where from Eqs.(3.37,3.38)

$$\eta_1 = - \left\{ 1 + \frac{2 + \tau_e}{q^2 \Omega^2} \right\} \frac{\tau_e}{\Omega} \quad (3.71)$$

and

$$\eta_2 = -2 \left[\frac{7}{4} + \tau_e + \frac{\tau_e (2 + \tau_e)}{q^2 \Omega^2} \right] \frac{\tau_e}{\Omega^2} K \rho_i \quad (3.72)$$

Here the brackets [...] are calculated up to an error of order $o\left(\frac{1}{q^4 \Omega^4}\right)$. Hence the imaginary part of the Lagrangian reads

$$\Im(\bar{L}_{res,e}) \simeq G(q, \tau_e) \varepsilon^{1/2} \sigma^* \mathcal{D}(\sigma^*) K^2 \rho_i^2 |\phi_0|^2 \quad (3.73)$$

where G is a number (in the limit of large aspect ratio)

$$G(q, \tau_e) = \sqrt{2\pi} \int_1^{+\infty} d\kappa \kappa \frac{\tau^2(\kappa)}{\Lambda(\kappa)} \eta^2(\theta_0(\kappa)) \quad (3.74)$$

and $\sin\left(\frac{\theta_0}{2}\right) = \frac{1}{\kappa}$. The special case $\mathcal{D}(\sigma^*) = 1$ corresponds to the estimate based on a strong weight of bounce points, i.e. when Eq.(3.69) is exact. Since only a fraction of particles fulfill this criterion, one expects that $\mathcal{D}(\sigma^*) \leq 1$. Strictly speaking the form factor $\mathcal{D}(\sigma^*)$ depends also on ϵ , but this is a weak dependence in the limit of large aspect ratio. One important consequence of Eq.(3.73) is the dimensionless form $\mathfrak{S}(\bar{L}_{res,e})$, which offers an efficient way to probe the parametric dependencies. Since the frequency Ω and potential amplitude are functions of (q, τ_e) only, this means that the mass scaling provides a strong constraint on the dependence on safety factor q and electron to ion ratio temperature $\tau_e = T_e/T_i$.

Final expression of damping due to trapped electrons

Using Eqs.(3.48,3.73), and $W_e = 2\Omega\mathfrak{S}(L_{res,e})\frac{v_{Ti}}{R_0}$, the following expression of the power exchange between electrons and GAM is then found

$$W_e = 2G(q, \tau_e) \Omega^2 \mathcal{D}(\sigma^*) \left(\frac{m_e}{m_i}\right)^{1/2} \frac{q}{\tau_e^{3/2}} N_i T_i \frac{v_{Ti}}{R_0} K^2 \rho_i^2 |\phi_0|^2 \quad (3.75)$$

Finally the total dispersion relation with electrons is found to be $\bar{L} = 0$, where

$$\begin{aligned} \bar{L} = & K^2 \rho_i^2 |\phi_0|^2 \left\{ \Lambda_1 - \Lambda_2 K^2 \rho_i^2 + i \frac{1}{2} \sqrt{\frac{\pi}{2}} q^5 \Omega^3 e^{-\frac{q^2 \Omega^2}{2}} \left[1 + 2 \frac{1 + 2\tau_e}{q^2 \Omega^2} \right] \right. \\ & + i \frac{1}{1024} \sqrt{\frac{\pi}{2}} K^2 \rho_i^2 q^9 \Omega^5 e^{-\frac{q^2 \Omega^2}{8}} \left[1 + 16 \frac{1 + \tau_e}{q^2 \Omega^2} \right] \\ & \left. + i G(q, \tau_e) \mathcal{D}(\sigma^*) \left(\frac{m_e}{m_i}\right)^{1/2} \frac{q}{\tau_e^{3/2}} \Omega \right\} \quad (3.76) \end{aligned}$$

It is reminded that

$$\Lambda_1 = 1 - \left(\frac{7}{2} + 2\tau_e\right) \frac{1}{\Omega^2} - \left(\frac{23}{2} + 8\tau_e + 2\tau_e^2\right) \frac{1}{q^2 \Omega^4} \quad (3.77)$$

and

$$\Lambda_2 = \frac{3}{4} - \left(\frac{13}{2} + 6\tau_e + 2\tau_e^2\right) \frac{1}{\Omega^2} + \left(\frac{747}{8} + \frac{481}{8}\tau_e + \frac{35}{2}\tau_e^2 + 2\tau_e^3\right) \frac{1}{\Omega^4} \quad (3.78)$$

A rough estimate of the damping rate due to electrons is obtained by fitting the parenthesis in the real part of the dispersion relation by $1 - \frac{\Omega_0^2}{\Omega^2}$, where Ω_0 is the zero of $\Re[\bar{L}(\Omega_0)] = 0$ (see Appendix C.5). A perturbative calculation then provides the normalised damping rate

$$\frac{R_0 \gamma}{v_{Ti}} \simeq \frac{1}{2} G(q, \tau_e) \mathcal{D}(\sigma^*) \left(\frac{m_e}{m_i}\right)^{1/2} \frac{q}{\tau_e^{3/2}} \Omega_0^2 \quad (3.79)$$

Using $\eta(\theta) = \eta_1 \sin(\theta)$, with η_1 given by Eq.(3.71), the following results are found

$$G(q, \tau_e) = 0.69 \left(1 + \frac{2 + \tau_e}{q^2 \Omega_0^2}\right)^2 \frac{\tau_e^2}{\Omega_0^2} \quad (3.80)$$

and

$$\boxed{\frac{R_0 \gamma}{v_{Ti}} \simeq 0.34 \left(1 + \frac{2 + \tau_e}{q^2 \Omega_0^2}\right)^2 q \tau_e^{1/2} \mathcal{D}(\sigma^*) \left(\frac{m_e}{m_i}\right)^{1/2}} \quad (3.81)$$

where Ω_0 is a function of q and τ_e , and $\sigma^* = \frac{q}{\tau_e^{1/2} \varepsilon^{1/2}} \left(\frac{m_e}{m_i}\right)^{1/2}$. It is stressed here that the expression Eq.(3.81) is exact, though the weight function $\mathcal{D}(\sigma^*) \leq 1$ is unknown at this stage. Nevertheless this formulation greatly constrains the dependencies on q , τ_e and m_e/m_i , as anticipated. Hence a way to check this expression is to perform first a scan on one parameter to determine the function $\mathcal{D}(\sigma^*)$, and then check the variation with respect to the other parameters. Previous simulations indicate that the damping rate due to trapped electrons scales as $(m_e/m_i)^{1/2}$ [7, Biancalani 2017]. This suggests that $\mathcal{D}(\sigma^*)$ is constant and close to $\mathcal{D}(\sigma^*) \simeq 1.0$. If so, Eq.(3.81) can then be used to test other dependencies, in particular on τ_e and q .

3.5 Rosenbluth-Hinton test with kinetic electrons

We take an axisymmetric form of the potential ϕ_{00} , the indices '00' referring to the wave number 0 both in the poloidal and toroidal directions (θ, φ) . The system quickly evolves to produce a potential structure composed of a ZF part and a GAM part [80, 84, Winsor 1968, Zonca 2008]. The evolution of the mode ϕ_{00} can be decomposed into two parts: a transient part which is governed by Landau damping and vanishes after a pseudo-periodic state and a residual part which is undamped in the absence of collisions, hence remaining constant. After the reorganization phase, the axisymmetric part of the potential evolution shown on Fig.3.2 takes the form :

$$\phi_{00}(r, t) = \{ \phi_{00}(t = \infty) + (\phi_{00}(t = 0) - \phi_{00}(t = \infty))e^{-\gamma_{GAM}t} \cos(\omega_{GAM}t) \} F(r) \quad (3.82)$$

where :

- F is the radial profile of the potential supposed to remain constant in time.
- $\phi_{00}(t = \infty)$ is the residual part of the potential when time becomes infinite. It corresponds to the value predicted by Rosenbluth and Hinton [71, Rosenbluth 1998]:

$$\frac{\phi_{00}(t = \infty)}{\phi_{00}(t = 0)} = \frac{1}{1 + 1.6 \frac{q^2}{\sqrt{\epsilon}}} \quad (3.83)$$

- ω_{GAM} is the pulsation of the oscillations of the GAM damping.
- γ_{GAM} is the damping rate of the GAM damping.

In this part, ω_{GAM} and γ_{GAM} are fitted in the models AE and FKE developed in chapter 2 and compared to the analytical predictions and the results obtained by other gyrokinetic codes.

We consider a plasma in a circular concentric tokamak configuration, similar to the one used in [7, Biancalani 2017], with $R_0 = 1.3$ m, $a = 0.13$ m and $\rho^* = 1/160$. We use a flat profile for the ion and electron equilibrium densities $n_{i,eq}$ and $n_{e,eq}$, the temperatures $T_i = T_e$ and the safety factor $q = 3.5$. Besides, the plasma is chosen to be hydrogen-like with a mass ratio $m_i/m_e = 1600$. We add an initial perturbation \tilde{n}_i to the equilibrium density profile taken for the ions so that we get an axisymmetric perturbation of the potential profile $\tilde{\phi}_{00}(r, t = 0) = \tilde{\phi}_{00,0} \sin(k_r r)$.

First, a convergence test is done on the time step and the full time length of the simulation to retrieve the GAM pulsation and damping rate. Second the dependency with the safety factor and the radial structure of the initial perturbation of these two parameters is looked at and a comparison between the AE and FKE models is carried out. Finally, the dependence on the mass ratio m_i/m_e is done. It appears that the GAM pulsation is not much changed with kinetic electrons, whereas the GAM damping rate depends heavily of kinetic electrons due to the resonance of GAM with trapped electrons modes explained in part 3.4.2. In particular we retrieve the dependency $\gamma_{GAM} \propto (m_i/m_e)^{1/2}$.

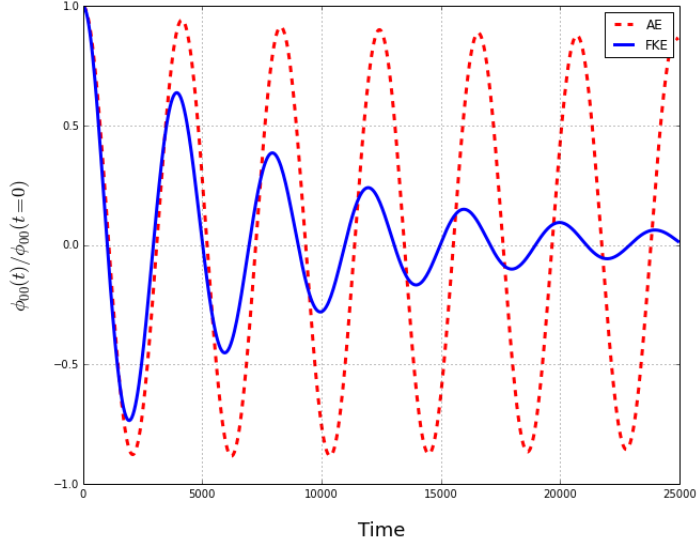


Figure 3.2: Evolution of the axisymmetric component of the potential for the adiabatic (red dashed line) and full kinetic (blue full line) electrons models.

3.5.1 Numerical convergence tests with GYSELA

The convergence scan proposed for GYSELA code has been performed with the same parameters as described in previous section. This corresponds for GYSELA to $L_r = 160/\rho_i$ with $\rho_i = \sqrt{T_i/m_i}/\Omega_i$ and an aspect ratio $1/\varepsilon = R/a = 10$. Density and temperature profiles are flat and normalized to 1. A flat safety factor is taken equal to 2 for the following tests. Electrons are considered adiabatic. In GYSELA, due to its full- f character, the initial condition is performed on the distribution function f_s and consists of an equilibrium distribution function $f_{s,eq}$ added to a perturbation \tilde{f}_s , namely $f_s = f_{s,eq} + \tilde{f}_s$. Then, the electrostatic potential $\phi(r, \theta, \varphi)$ is computed at time $t = 0$ by solving the quasi-neutrality equation. In the present test, the perturbation part \tilde{f}_s reads $\tilde{f}_s = f_{s,eq} g(r)$ with $g(r) = -\frac{1}{r} (k_r \cos(k_r r) - k_r^2 r \sin(k_r r))$ where $k_r = (k + 1)\pi/L_r$ with $k \in \mathbb{N}$. The corresponding radial profile of the zonal component $\phi_{00}(r) \sim \sin(k_r r)$ is plotted in Figure 3.3 (black line) for $k = 1$ as it is shown in Appendix C.6.

In the GYSELA code, the 5D space $(r, \theta, \varphi, v_{\parallel}, \mu)$ is uniformly discretized with $N_r \times N_{\theta} \times N_{\varphi}$ points in the 3D real space and $N_{v_{\parallel}} \times N_{\mu}$ points in the 2D velocity space (with N_x the number of points in x direction). This mesh grid is fixed in time with $r \in [0, L_r]$, $\theta \in [0, 2\pi]$, $\varphi \in [0, 2\pi]$, $v_{\parallel} \in [-\alpha v_{T_i}, \alpha v_{T_i}]$ and $\mu \in [0, L_{\mu}]$. Due to the toroidal axisymmetry of the test the number of toroidal points N_{φ} is fixed to $N_{\varphi} = 8$. A comparison (not presented here) with $N_{\varphi} = 16$ has shown really good agreement with $N_{\varphi} = 8$. Simulations with $N_{\varphi} = 4$ would be probably close to those with $N_{\varphi} = 8$ but are not possible in the code due to parallelization constraints. This technical constraint could be removed. However simulations with so little number of points in toroidal direction are

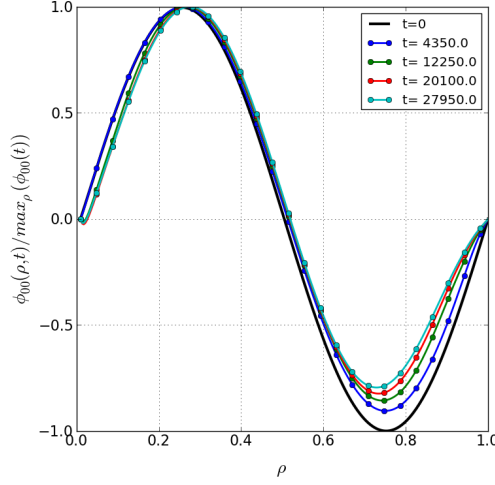


Figure 3.3: Time evolution of the radial profile of the zonal component ϕ_{00} for the initial time (black line) and 4 different times ($t = 4350 \Omega_i^{-1}$, $t = 12250 \Omega_i^{-1}$, $t = 20100 \Omega_i^{-1}$ and $t = 27950 \Omega_i^{-1}$). ρ is the normalized radial position, i.e $\rho = (r - r_{\min})/L_r$.

not standard simulations, so choice has been made to run with $N_\varphi = 8$ and to postpone the required modification of the code for now. The maximum of velocity normalized to its thermal value in parallel velocity space is fixed at $\alpha = \frac{v_{\parallel \max}}{v_{th,i}} = 7$. A simulation with $\alpha = 5$ has been performed (not presented here) showing very small difference ($< 2\%$) with the case $\alpha = 7$. However, as this value could have more impact for larger q values due to resonance condition $v_{\parallel}/qR = \omega_{GAM}$, the value $\alpha = 7$ has been preferred for the following tests. L_μ is fixed to $L_\mu = 12 T_i/B_0$ (with $B_0 = 1$). All simulations have been performed for a flat safety factor profile equal to 2 and until $t = 50000 \Omega_i^{-1}$. Flat density and temperature profiles are also considered with $\tau_e = T_e/T_i = 1$.

Parameters and results are summarized in Table 3.2. Comparisons are performed on the three quantities: (i) the radial wave number $k_r \rho_i$, (ii) the damping rate γ and (iii) frequency ω of the zonal component of the electrostatic potential ϕ_{00} . The radial wave number is computed with the following formula:

$$k_r \rho_i = \rho_i \sqrt{\sum_{i=0}^{N_r} \left(\frac{d}{dr} \phi_{00 \text{ norm}}(r_i, t) \right)^2} / \sqrt{\sum_{i=0}^{N_r} (\phi_{00 \text{ norm}}(r_i, t) - \langle \phi_{00 \text{ norm}} \rangle_r)^2} \quad (3.84)$$

with $\rho_i = \frac{\sqrt{T_i/m_i}}{\Omega_i}$ and $\phi_{00 \text{ norm}}(r_i, t) = \phi_{00}(r_i, t) / \max_{r_i} \phi_{00}(r_i, t)$. The values reported in Table 3.2 correspond to the mean values of $k_r \rho_i$ computed at times where $\log(\phi_{00}(r_p, t))$ is maximum with r_p the radial position of the maximum value of $\phi_{00}(r)$ at initial time. The damping rate is estimated by using the method of least squares also on the maximum values of $\log(\phi_{00}(r_p, t))$. γ values reported in Table 3.2 are computed with 6 maximums

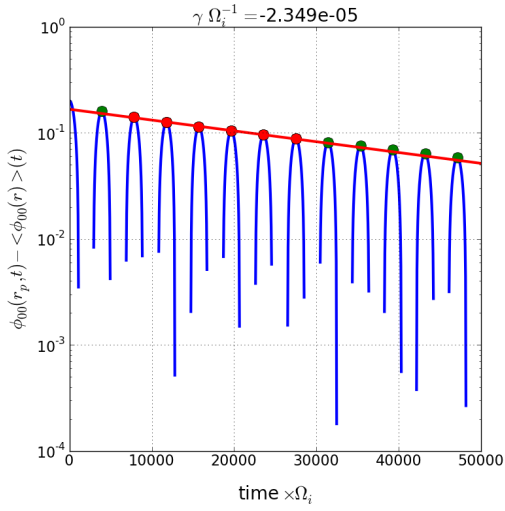


Figure 3.4: Time evolution of $\phi_{00}(r_p, t) - \langle \phi_{00}(r) \rangle_r(t)$ used to compute the damping rate. r_p is the radial position of the maximum value of $\phi_{00}(r)$ at initial time. The green points correspond to the maximum values. The 6 red points correspond to the points used for the linear interpolation (red line).

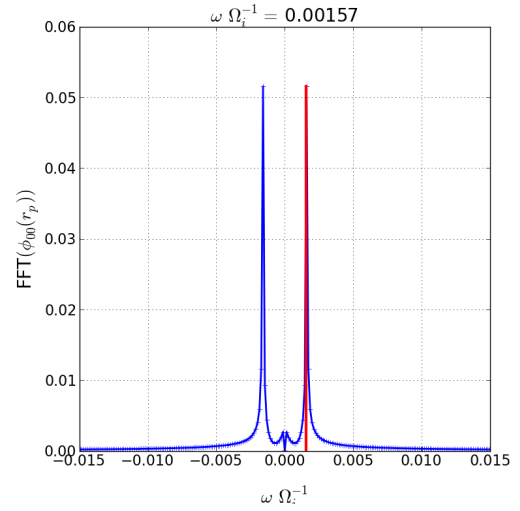


Figure 3.5: Fourier transform in time of $\phi_{00}(r = r_p)$ used to compute the frequency with r_p the radial position of the maximum value of $\phi_{00}(r)$ at initial time.

(see red circles in Figure 3.4). Four first simulations (cases 1 to 4 in Table 3.2) have been performed for the same 5D mesh of ~ 536.8 millions of points $(N_r, N_\theta, N_\varphi, N_{v_\parallel}, N_\mu) = (256, 64, 8, 128, 32)$ but with varying the time step Δt from $\Delta t = 5 \Omega_i^{-1}$ to $\Delta t = 50 \Omega_i^{-1}$. All the other simulations except the last one (cases 5 to 10) have been performed with $\Delta t \Omega_i = 25$ varying: (i) the number of points in μ direction (case 5: $N_\mu = 16$, case 6: $N_\mu = 8$); (ii) the number of points in radial direction (case 7: $N_r = 128$, case 8: $N_r = 512$); (iii) the number of points in poloidal direction (case 9: $N_r \times N_\theta = 256^2$) and (iv) finally the number of points in parallel velocity space (case 10: $N_{v_\parallel} = 64$). The last case (case 11) corresponds to a simulation where all varying parameters have been taken to their smaller tested value, namely $\Delta t = 50 \Omega_i^{-1}$, $N_r = 128$, $N_\theta = 64$, $N_{v_\parallel} = 64$ and $N_\mu = 8$.

case	N_r	N_θ	N_{v_\parallel}	N_μ	$\Delta t \Omega_i$	$k_r \rho_i$	$\gamma \Omega_i^{-1}$	$\omega \Omega_i^{-1}$
1	256	64	128	32	5.	0.05630867	0.02664329	1.81126121
2	256	64	128	32	10.	0.05630867	0.02663145	1.81126121
3	256	64	128	32	25.	0.05630868	0.02657794	1.81126121
4	256	64	128	32	50.	0.05630874	0.02653612	1.81196116
5	256	64	128	16	25.	0.05630058	0.02657711	1.81126121
6	256	64	128	8	25.	0.05601206	0.0265876	1.81126121
7	128	64	128	32	25.	0.05649958	0.0266591	1.81126121
8	512	64	128	32	25.	0.0562041	0.02655708	1.81126121
9	256	256	128	32	25.	0.05630868	0.02657654	1.81126121
10	256	64	64	32	25.	0.05630868	0.02655779	1.81196116
11	128	64	64	8	50.	0.05620426	0.02661145	1.81126121

Table 3.2: 11 simulations performed for $q = 2$ with $N_\varphi = 8$ by varying the number of points in r , θ , v_\parallel and μ directions. Results are compared for the radial wave number $k_r \rho_i$, the damping rate γ and the frequency ω of the zonal component of the electrostatic potential.

Considering case 1 as the reference case, the maximum relative error is less than 1% for $k_r \rho_i$ and ω estimations, and less than 2% for γ (see Table 3.2). In all these simulations, even the coarse grained one (case 11), are fully accurate. However, it appears that,

considering that these tests have been performed for a low value of the safety factor $q = 2$ and a small radial wave number $k_r \rho_i \sim 0.056$, those results suggest to avoid parameters where we observe a departure even small from the reference case, namely $\Delta t = 50 \Omega_i^{-1}$ and $N_\mu = 8$. Hence, more secure parameters for larger q values or larger $k_r \rho_i$ values could correspond to those of case 5, namely a mesh $(N_r, N_\theta, N_\varphi, N_{v_\parallel}, N_\mu) = (256, 64, 8, 128, 16)$ of 268.4 millions of points with a time step of $\Delta t = 25 \Omega_i^{-1}$. Such a simulation requires 2 hours on 256 cores for 2000 time iterations compared to the coarse grained simulation which takes around 1 hour on 64 cores (1000 iterations).

3.5.2 Dependence on the radial wave number $k_r \rho_i$

In the theoretical part, the radial profile of the mode is assumed to remain constant over time, during both the initial plasma reorganization phase and the damping phase of the GAM. In fact, the radial wave number k_r varies slightly due to the radial coupling induced by the quasi-neutrality equation on the potential and the need to satisfy the Neumann condition $d_r \phi = 0$ at the limits r_{min} and r_{max} of the radial domain. This modification of k_r can lead to deviations from the theoretical predictions of ω_{GAM} and γ_{GAM} seen earlier, and it should be verified that these remain valid in our simulations. Because of this problem, it is useless to try retrieving the exact theoretical dependence of ω_{GAM} and γ_{GAM} in k_r at high orders. Fig.3.6 shows the evolution over time of the potential radial profile as well as the associated radial wave number for two forms of initial perturbations :

- $\tilde{\phi}_{00}^{(1)}(r, t = 0) = \tilde{\phi}_{00,0} \sin(k_r r)$
- $\tilde{\phi}_{00}^{(2)}(r, t = 0) = \tilde{\phi}_{00,0}(1 - \cos(k_r r))$

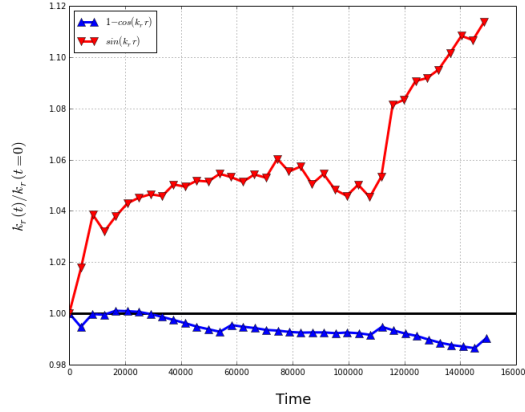


Figure 3.6: Time evolution of k_r with an initial perturbation in $1 - \cos(k_r r)$ and $\sin(k_r r)$.

To compute the value of k_r through time, the following average on r has been done :

$$\langle k_r \rangle_r(t) = \frac{\sum_r \partial_r \phi_{00}(r, t)}{\sum_r \phi_{00}(r, t)}$$

We observe that the value of k_r is less altered through time with the perturbation $1 - \cos$. This is related to the fact that this perturbation satisfies Neumann's conditions from the beginning of the simulation. As a result, the profile of the potential is less changed during the initial reorganization phase for this profile. On the contrary, in the \sin case, the profile changes quickly in the vicinity of r_{min} and r_{max} to satisfy the Neumann's condition, hence a slight increase of k_r for this profile. Consequently, the form $1 - \cos$ is preferred to the form \sin because we do not want the radial wave number k_r to change too much over time. Details on the two forms the radial profile of the density perturbation \tilde{n}_i should take are given in Appendix C.6.

3.5.3 Dependence on the mass ratio m_i/m_e

We now compare the expressions of the GAM pulsation and damping rate previously found in the theoretical study with the results obtained with numerical simulations. The dependence on mass ratio of the GAM damping rate and pulsation computed with the GYSELA code using the FKE model for $\tau_e = 1$, $q = 3.5$ is shown on Fig.3.7. Several conclusions can be drawn from these figures. First the pulsation depends weakly on m_i/m_e - this means that trapped electrons do not influence much the real part of the Lagrangian, as expected. The damping rate exhibits a characteristic $(m_i/m_e)^{-1/2}$ scaling. A best fit leads to a constant value of $\mathcal{D}(\sigma^*) = 1^4$. This indicates that the useful part of the phase space that contributes to GAM damping does not depend critically on the mass ratio, a rather surprising finding. In fact, picking up the numerical value $\Omega_0 \simeq 1.8$, it appears that Eq.(3.81) agrees well with the numerical results when choosing $\mathcal{D}(\sigma^*) = 1$. We will keep up with this value in the following. Hence Eq.(3.81) becomes:

$$\frac{R_0\gamma}{v_{Ti}} \simeq 0.34 \left(1 + \frac{2 + \tau_e}{q^2\Omega_0^2}\right)^2 q\tau_e^{1/2} \left(\frac{m_i}{m_e}\right)^{-1/2} \quad (3.85)$$

Fig.3.7 also shows a comparison of γ_{GAM} between the codes GYSELA (models FKE and AE), ORB5 and GENE [7, Biancalani 2017]. The dependency in $(m_i/m_e)^{-1/2}$ is also recovered with the codes ORB5 and GENE. It can be observed however that for $m_i/m_e = 400$ and $m_i/m_e = 1600$, the damping rate predicted with GYSELA is lower than expected. This behaviour has two consequences : first, this reinforces the idea of a coupling between the GAM and the trapped electron modes as explained in the previous theoretical model. Nevertheless, the dependency in $(m_i/m_e)^{-1/2}$ implies that the GAM damping is overevaluated at low mass ratios. Hence, a good prediction of the behaviour of GAMs must be done at realistic mass ratios, which of course requires more computer resources.

⁴The fact that $\mathcal{D}(\sigma^*)$ is a constant is not trivial, as $\sigma^* = \frac{q}{\tau_e^{1/2}\epsilon^{1/2}} \left(\frac{m_e}{m_i}\right)^{1/2}$ shows a m_i/m_e dependency. Only the results of numerical tests show that $\mathcal{D}(\sigma^*)$ is approximately independent of the mass ratio.

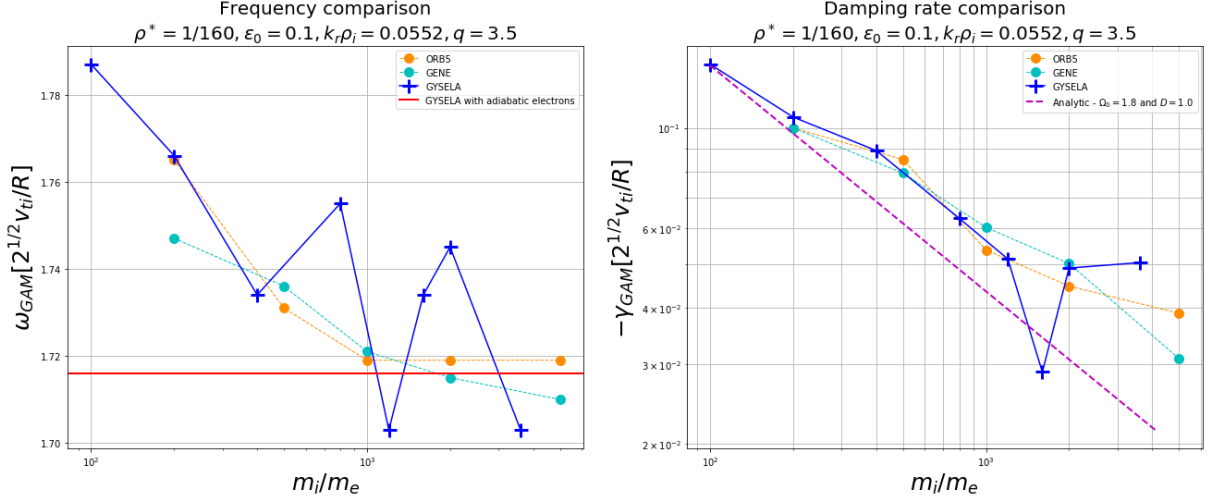


Figure 3.7: GAM pulsation and damping rate calculated with GYSELA vs ion to electron mass ratio. The damping rate is compared with the codes ORB5 and GENE [7, Biancalani 2017]. The analytic dashed line is given by Eq.(3.85).

3.5.4 Dependence on the safety factor q

We now turn to the dependence on safety factor. Results from the GYSELA code are shown on Fig.3.8 for the damping rate and pulsation - parameters are $m_i/m_e = 1600$ and $\tau_e = 1$. It appears that Ω_0 depends weakly on q , a consequence of the inequality $q^2 \Omega_0^2 \gg 1$ over most of the scan range. In this case Eq.(3.85) predicts a linear dependence on q , while a roughly inverse dependence is observed on Fig.3.8. This is a rather puzzling result. Indeed, it cannot come from a poor identification of the function $\mathcal{D}(\sigma^*)$. Indeed, an inverse dependence on q would require a function $\mathcal{D}(\sigma^*) \sim [\sigma^*]^{-2}$ since $\sigma^* = q \tau_e^{-1/2} \varepsilon^{-1/2} (m_e/m_i)^{1/2}$, but this would imply a $(m_e/m_i)^{-1/2}$ scaling of the damping rate, clearly inconsistent with the numerical results.

It can also be pointed out that Fig 3.8 shows that the deviation between the adiabatic and kinetic electron models is larger for $q > 2$ as it has already been observed with the GTC code [83, Zhang 2010]. In particular, we note that the local maxima due to the second order resonance arising from the finite orbit width effect in the adiabatic model becomes negligible compared to the damping due to trapped electrons.

3.5.5 Dependence on the temperature ratio $\tau_e = T_e/T_i$

The damping rate and pulsation calculated by GYSELA are reproduced on Fig.3.9 for the parameters are $m_i/m_e = 1600$ and $q = 3.5$. It is quite difficult to infer a monomial scaling law, but we find that the dependence in $\tau_e^{1/2}$ is well satisfied for $\tau_e > 1$. Finding the good scaling in both m_i/m_e and τ_e strongly recommends the proposed formula of

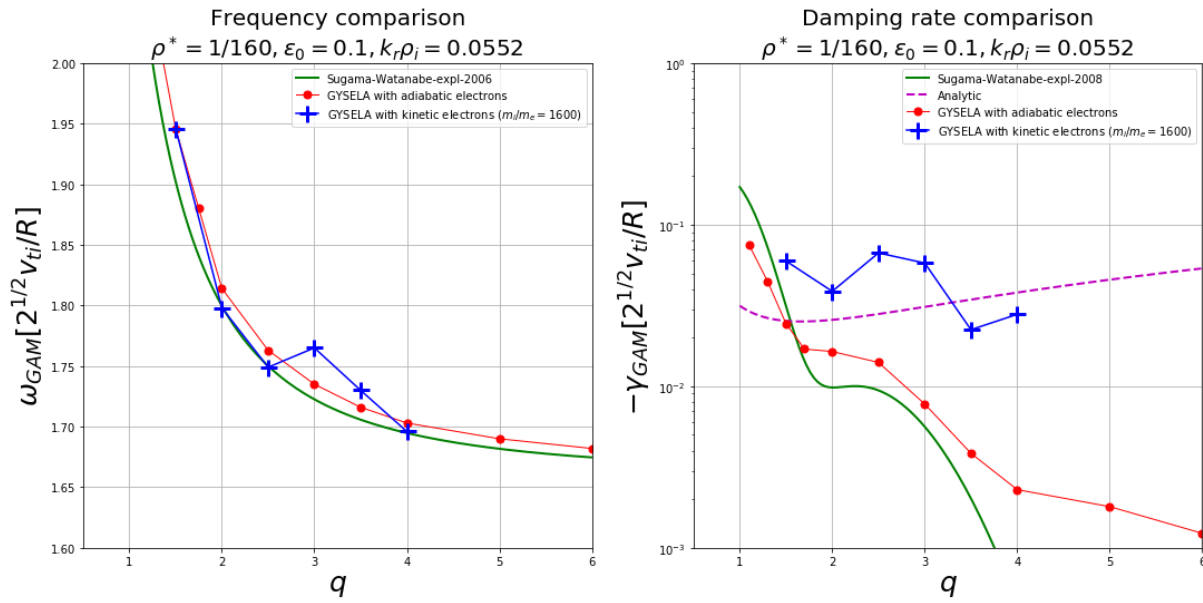


Figure 3.8: Dependence of the pulsation and damping rate with the safety factor q . The analytic dashed line is given by Eq.(3.85).

the GAM damping rate Eq.(3.85). This formula predicts indeed an over-damping due to barely trapped/passing electrons but the scaling in safety factor is not well found. Further studies should be made to understand this discrepancy.

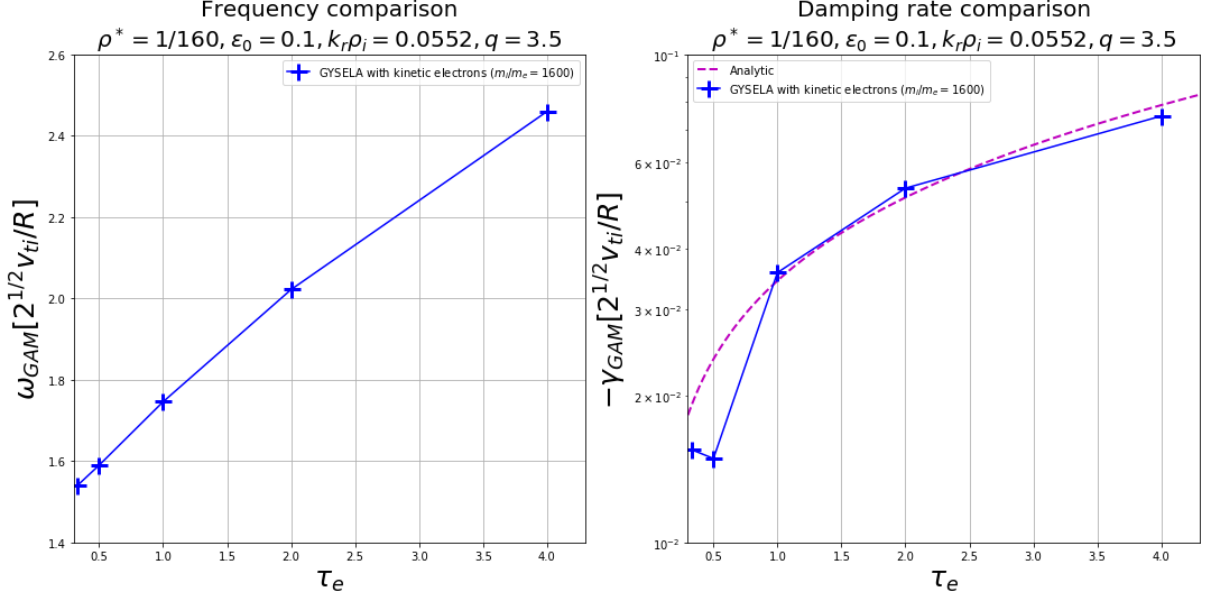


Figure 3.9: GAM pulsation and damping rate vs electron to ion temperature ratio. The analytic dashed line is given by Eq.(3.85).

3.5.6 Conclusion

In this section, several results have been verified:

- Taking into account a radial profile of the form $1 - \cos(k_r r)$ with Neumann boundary conditions provides a better conservation of the initial radial wave number than a profile in $\sin(k_r r)$. Choosing a $1 - \cos(k_r r)$ form is useful to minimize the discrepancies in the comparison between analytical and numerical results.
- Kinetic electrons have only a slight impact on the GAM pulsation, but increase the damping rate tremendously. This confirms the existence of a resonant interaction between trapped electrons and GAM.
- It is possible to recover with the FKE model the $(m_i/m_e)^{-1/2}$ scaling of the GAM damping rate due to trapped electrons by choosing a phase space weight $\mathcal{D}(\sigma^*)$ that is constant and equal to $\frac{1}{2}$. Besides, the scaling in electron to ion temperature ratio in $\tau_e^{1/2}$ is also recovered. However some discrepancies on the safety factor still need to be investigated. The scaling in mass ratio is also recovered with the local codes ORB5 and GENE.
- For low mass ratios ($m_i/m_e \sim 100$), the TKE model is found to have a behaviour close to the AE model. However, for realistic mass ratios ($m_i/m_e \sim 3600$), the GAM damping rate found with the TKE model matches the one obtained with the FKE model.

Chapter 4

Linear study and first non-linear simulations of the Ion Temperature Gradient (ITG) and Trapped Electron Mode (TEM) instabilities

The deviations from thermodynamic equilibrium, in particular density and temperature gradients, are sources of free energy which fuel the micro-instabilities of the plasma, leading to particle and energy turbulent transport. These micro-instabilities are classified according to the sources of free energy that fuel them. In particular, the ITG-TEM instabilities are created by density and temperature gradients. The ITG regime is obtained when it is mainly the ions that provide energy to the electric wave and TEM when this is the electrons which give their energy. Besides, in that particular case the instability is mainly due to the trapped electrons.

First, the linear dispersion relation of the ITG-TEM instability is given with a closer look at the pulsation and growth rate. In a second time, simulations are performed with the trapped kinetic electron model of GYSELA. This test allows us to look at the dependence of the pulsation and growth rate with different parameters and in particular the poloidal wavelength and the ionic temperature gradient. A transition between the ITG dominated regime and the TEM dominated regime is shown. Then, some simulation results where we initialize a perturbation composed of several poloidal wavelength are shown: these enable to highlight some pure electrostatic phenomena among which the so-called ω_H mode. Finally, we present the first non-linear results obtained with kinetic electrons.

4.1 The Ion Temperature Gradient and Trapped Electron Mode instability

First, a qualitative presentation on the mechanisms of the general drift wave and interchange instability is given. Then we present the dispersion relation of potential waves acknowledging for non-uniform density and temperature profiles. The case of the ITG-TEM instability is then studied and an approximated analytic expression for the pulsation and damping rate of such modes is given. This presentation is based on the following works [68, Rax 2012],[72, Sarazin 2013],[30, Garbet 2001],[10, Bourdelle 2000] for this section.

4.1.1 Drift wave and interchange mechanisms

Drift waves

Let us consider a plasma in a Cartesian base (x, y, z) with a uniform magnetic field \mathbf{B} in the z direction. Ions are assumed at rest. Thus, the density of ions is supposed constant in time, uniform in the y and z directions, with a negative uniform gradient in the x direction so that it takes the form $n_i(x) = n_i(x_0) + \partial_x n_i|_{x_0}(x - x_0)$ with $\partial_x n_i|_{x_0} < 0$ in the vicinity of the position $x \sim x_0$. An initial perturbation on the electric potential of the form $\phi(x_0, y, t = 0) = \phi_0 \sin(ky)$ at $x = x_0$ is introduced. The electron density can be decomposed as $n_e = \bar{n}_e + \tilde{n}_e$ where:

- $\bar{n}_e = \langle n_e \rangle_y$ is the density profile averaged along the coordinate y .
It comes $\bar{n}_e(x) = n_i(x) = n_i(x_0) + \partial_x n_i|_{x_0}(x - x_0)$.
- $\tilde{n}_e = n_e - n_i$ is the difference between ion and electron density due to plasma polarisation. Under the hypothesis of adiabatic electrons (see section 2.1), \tilde{n}_e is in phase with the potential and can be written as $\tilde{n}_e(x_0, y, t = 0) = \tilde{n}_{e0} \sin(ky)$ at initial time and $x = x_0$.

The shape of the electric potential and the electron density is shown on Fig.4.1 as well as the electric field \mathbf{E} and associated drift \mathbf{v}_E .

At this point, we would like to study the future of such a perturbation. Therefore, we try to establish the evolution equation of the potential so as to identify it to a particular type of wave. We start from the conservation equation of matter applied to the electrons. This equation reads:

$$\frac{\partial n_e}{\partial t} + \nabla \cdot \mathbf{\Gamma}_e = 0 \quad (4.1)$$

with $\mathbf{\Gamma}_e = n_e \mathbf{v}$ the particle flux of electrons and $\mathbf{v} = \mathbf{v}_{\parallel} + \mathbf{v}_{\perp}$. We suppose that \mathbf{v}_{\parallel} varies little in the z direction. The perpendicular velocity can be decomposed as $\mathbf{v}_{\perp} = \mathbf{v}_E + \mathbf{v}_{\text{dia}}$ where \mathbf{v}_E stands for the electric drift velocity, \mathbf{v}_{dia} stands for the diamagnetic velocity. Besides, we have $\nabla \cdot (n \mathbf{v}_{\text{dia}}) = \frac{\nabla p}{e} \cdot \nabla \wedge \left(\frac{\mathbf{B}}{B^2} \right) = 0$ in a uniform magnetic field. Therefore,

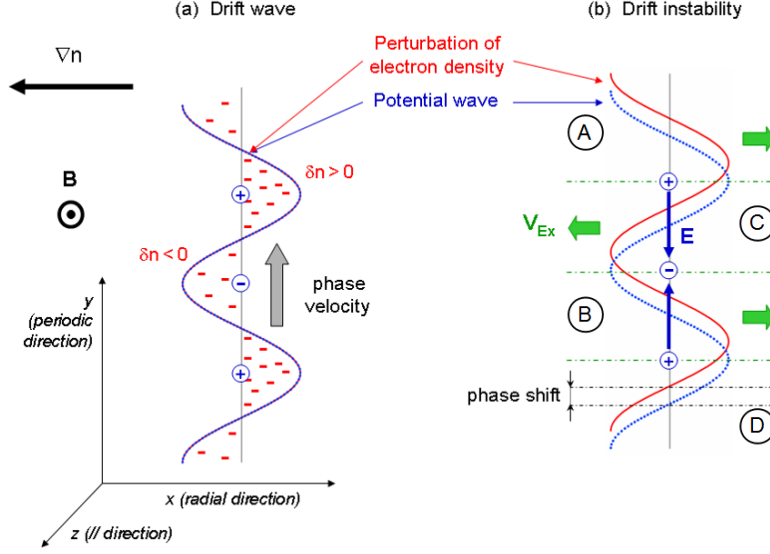


Figure 4.1: Schematic view of the drift wave (a) and drift wave instability (b) mechanisms. [72, Sarazin]

only the electric term $\mathbf{v}_E = \mathbf{E} \wedge \mathbf{B}/B^2$ is retained here. The particle flux of electrons simply reduces to:

$$\mathbf{\Gamma}_e^E = -\frac{n_e}{B} \frac{\partial \phi}{\partial y} \mathbf{e}_x$$

where \mathbf{e}_x is the unit vector of the x direction. Eq.(4.1) becomes, in the linear approximation:

$$\frac{\partial \tilde{n}_e}{\partial t} - \frac{\partial_x \tilde{n}_e}{B} \frac{\partial \phi}{\partial y} = 0 \quad (4.2)$$

Using the hypothesis of adiabatic electrons, the electron density perturbation reads $\tilde{n}_e = \frac{e \tilde{n}_e}{T_e} \phi$ ¹. Replacing \tilde{n}_e in Eq.(4.2), one eventually gets the wave equation on the electric potential:

$$\frac{\partial \phi}{\partial t} + \frac{\omega^*}{k} \frac{\partial \phi}{\partial y} = 0 \quad (4.3)$$

where $\omega^* = (kT_e/eB)(-\partial_x \tilde{n}_e)/\tilde{n}_e > 0$ is called the diamagnetic pulsation. This is the equation of a propagative wave in the direction of the $y < 0$ and of phase velocity ω^*/k . In the absence of density gradients in the x direction, this equation simply becomes $\partial_t \phi = 0$ and the wave is stationary. Physically, because of the density gradient, there are more electrons which are brought by the electric drift from the high density zones (A) and (B) on Fig.4.1 than from the low density zones (C) and (D). This causes the local

¹When $n_e = \bar{n}_e$, $\phi = \langle \phi \rangle_y = 0$.

maxima of the wave to be shifted through time. Thus, the electric drifts cause the wave to propagate and is hence called drift wave.

Besides, it is noted that in the case where \tilde{n}_e and ϕ are exactly in phase, the amplitude of the wave does not vary and there can be no instability. In the case where a phase shift between these two quantities exists, we will see that this last point is no longer true.

Drift wave instability

In the case where there is a small phase shift between the electron density perturbation and the potential, the electron density perturbation takes the form $\tilde{n}_e = \frac{e\tilde{n}_e}{T_e}(1 - i\delta)\phi$ with $|\delta| \ll 1$. Therefore, Eq.(4.3) is recast as:

$$\frac{\partial\phi}{\partial t} + \frac{\omega^*}{k}(1 - i\delta)\frac{\partial\phi}{\partial y} = 0 \quad (4.4)$$

The solution of this equation reads $\phi = \phi_0 \exp\{-i(\omega^*t - ky)\} \exp(-\delta\omega^*t)$. Two cases appear here:

- $\delta < 0$ then the wave is damped.
- $\delta > 0$ then the wave is unstable.

In the latter case, we see the appearance of a drift-wave instability. The initial phase shift between potential and electron density may have several origins among which plasma resistivity and wave-particle resonances which both cause electrons to depart from their adiabatic response. The resistive version of this instability is well described by the Hasegawa-Wakatani model, establishing the dispersion relation from matter and charge conservation ([42, Gravier], [46, Hasegawa]). The case of wave-particle resonances includes, among others, the so-called slab branches of ITG and ETG instabilities (see e.g. [18, 54, Coppi 1967, Kadomtsev 1970])

Interchange instability

We consider the same plasma with this time a gradient of magnetic field in the x direction $\partial_x B < 0$. The same initial perturbation on the electric potential $\phi(x_0, y, t = 0) = \phi_0 \sin(ky)$ at $x = x_0$ is introduced. Let us consider a region located between a minimum and a maximum of potential. The fluctuations of ϕ lead to local electric fields $\mathbf{E} = -\partial_y\phi \mathbf{e}_y$. Within the adiabatic theory, the particles are subject to velocity drifts transverse to the magnetic field lines. In the configuration plotted on Fig.4.2, we see that the combination of the electric drifts \mathbf{v}_E and the ∇B drifts $\mathbf{v}_{\nabla B}$ tend to bring ions coming from the high density region \textcircled{H} towards a maximum of potential $\textcircled{\boxplus}$ ². It is the opposite for particles coming from the low density region \textcircled{L} . There are significantly more ions and electrons coming from the high density region than from the low density region.

²and respectively to bring electrons coming from the high density region \textcircled{H} towards a minimum of potential $\textcircled{\boxminus}$

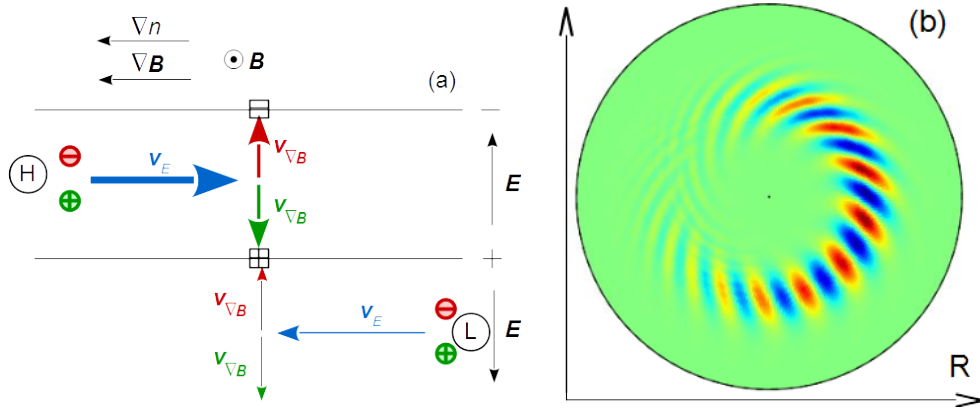


Figure 4.2: (a) Schematic view explaining the physical mechanism of the interchange instability. (b) Evidence of ballooned character of ITG linear modes (fluctuations of the electric potential, GYSELA code)

As a result, the potential perturbation increases, hence leading to an instability.

The case where the gradients of density and magnetic field are in the same direction leads to the interchange instability. Yet, when these are in opposite directions, the potential perturbation is damped and there is no instability. Consequently in tokamaks, the interchange instability appears only in the low field side region as shown on Fig.4.2.

4.1.2 Dispersion relation in presence of density and temperature gradients

The stability of a given mode of the electric potential is given by the sign of the linear growth rate γ . This information is contained via the knowledge of the dispersion relation established from the Vlasov equation coupled to the quasi-neutrality equation, in the same way as it has been done for the GAM study in chapter 3. In that case, we consider non-uniform density and temperature profiles, and we use the angle-action set of coordinates (α, \mathbf{J}) introduced in section 1.2.2, so that for $i = (1, 2, 3)$:

$$\frac{d\alpha_i}{dt} = \frac{\partial H_{eq}}{\partial J_i} = \Omega_i(\mathbf{J}) \quad (4.5)$$

$$\frac{dJ_i}{dt} = -\frac{\partial H_{eq}}{\partial \alpha_i} = 0 \quad (4.6)$$

In this derivation, we first express the Vlasov equation and its linear solutions. Then the quasi-neutrality equation is recalled and we eventually express the Lagrangian of the system by plugging the linear solutions of the Vlasov equation in the quasi-neutrality equation.

Linear solutions of the Vlasov equation

In the absence of sources and collisions, the Vlasov equation reads:

$$\partial_t F(\mathbf{x}, \mathbf{p}, t) - [H, F](\mathbf{x}, \mathbf{p}, t) = 0 \quad (4.7)$$

where H is the Hamiltonian and F the distribution function. The Poisson bracket is given in the angle-action set of coordinates by:

$$[H, F] = \frac{\partial H}{\partial \boldsymbol{\alpha}} \cdot \frac{\partial F}{\partial \mathbf{J}} - \frac{\partial H}{\partial \mathbf{J}} \cdot \frac{\partial F}{\partial \boldsymbol{\alpha}} \quad (4.8)$$

The distribution function F and the Hamiltonian H are developed in Fourier series along the coordinates $\boldsymbol{\alpha}$ and t :

$$\begin{cases} F(\boldsymbol{\alpha}, \mathbf{J}, t) &= F_{eq}(\mathbf{J}) + \sum_{\mathbf{n}\omega} f_{\mathbf{n}\omega}(\mathbf{J}) e^{i(\mathbf{n}\cdot\boldsymbol{\alpha} - \omega t)} \\ H(\boldsymbol{\alpha}, \mathbf{J}, t) &= H_{eq}(\mathbf{J}) + \sum_{\mathbf{n}\omega} h_{\mathbf{n}\omega}(\mathbf{J}) e^{i(\mathbf{n}\cdot\boldsymbol{\alpha} - \omega t)} \end{cases} \quad (4.9)$$

We note $f = F - F_{eq}$ and $h = H - H_{eq}$. Replacing these expressions in Eq.(4.7), using the fact that $\partial_t F_{eq} - [H_{eq}, F_{eq}] = 0$, it comes:

$$\partial_t f + \frac{\partial f}{\partial \boldsymbol{\alpha}} \cdot \frac{\partial H_{eq}}{\partial \mathbf{J}} - \frac{\partial F_{eq}}{\partial \mathbf{J}} \cdot \frac{\partial h}{\partial \boldsymbol{\alpha}} + \left(\frac{\partial f}{\partial \boldsymbol{\alpha}} \cdot \frac{\partial h}{\partial \mathbf{J}} - \frac{\partial f}{\partial \mathbf{J}} \cdot \frac{\partial h}{\partial \boldsymbol{\alpha}} \right) = 0$$

The source term S is supposed constant in time. Neglecting the quadratic terms, and using the Fourier development (4.9), the Vlasov equation becomes:

$$-i\omega f_{\mathbf{n}\omega} + i\mathbf{n} \cdot \boldsymbol{\Omega} f_{\mathbf{n}\omega} - i\mathbf{n} \cdot \frac{\partial F_{eq}}{\partial \mathbf{J}} h_{\mathbf{n}\omega} = 0 \quad (4.10)$$

with $\boldsymbol{\Omega} = \partial H_{eq} / \partial \mathbf{J}$. Finally, the linear solutions of the Vlasov equation can be written as:

$$f_{\mathbf{n}\omega} = \frac{-\mathbf{n} \cdot \frac{\partial F_{eq}}{\partial \mathbf{J}} h_{\mathbf{n}\omega}}{\omega - \mathbf{n} \cdot \boldsymbol{\Omega} + i0^+} \quad (4.11)$$

Taking F_{eq} as a Maxwellian distribution function of expression $F_{eq} = \frac{n}{(2\pi mT)^{3/2}} e^{-H_{eq}/T}$, Eq.(4.11) becomes after calculations:

$$f_{\mathbf{n}\omega} = -\frac{F_{eq}}{T} \left(1 - \frac{\omega - \mathbf{n} \cdot \boldsymbol{\omega}^*}{\omega - \mathbf{n} \cdot \boldsymbol{\Omega} + i0^+} \right) h_{\mathbf{n}\omega} \quad (4.12)$$

with $\boldsymbol{\omega}^* = \frac{1}{n} \frac{\partial n}{\partial \mathbf{J}} - \left(\frac{3}{2} - \frac{H_{eq}}{T} \right) \frac{1}{T} \frac{\partial T}{\partial \mathbf{J}}$ being the diamagnetic frequency. This quantity contains the influence of the gradients of density and temperature hence representing the deviations of the system from tokamak equilibrium. The term $+i0^+$ is used to remind that an analytic continuation must be done according to the Landau prescription (i.e. to ensure causality). The result is independent of 0^+ as long as 0^+ tends to 0.

Quasi-electroneutrality

The quasi-neutrality constraint can be written as $\sum_{\text{species}} e_s n_s = 0$. It is still satisfied at equilibrium. The condition $\sum_{\text{species}} e_s (n_s - n_{s,eq}) = 0$ writes:

$$\sum_{\text{species}} e_s \int d^3 \mathbf{p} f_s(\mathbf{x}, \mathbf{p}, t) = 0 \quad (4.13)$$

The quasi-neutrality constraint can be reformulated in a "weak" form ³ as:

$$\forall \phi^\dagger(\mathbf{x}, t), \int d^3 \mathbf{x} \left\{ \sum_{\text{species}} e_s \int d^3 \mathbf{p} f_s(\mathbf{x}, \mathbf{p}, t) \right\} \phi^\dagger(\mathbf{x}, t) = 0 \quad (4.14)$$

with ϕ^\dagger an arbitrary field. We introduce the functional \mathcal{L} ⁴ of ϕ^\dagger defined as:

$$\mathcal{L} = \sum_{\text{species}} e_s \int d^3 \mathbf{x} d^3 \mathbf{p} f_s(\mathbf{x}, \mathbf{p}, t) \phi^\dagger(\mathbf{x}, t) \quad (4.15)$$

We do the choice $\phi^\dagger = \phi^*$. Replacing the expression (4.12) of f for each mode ω and taking into account that for each species s , $h^s = e_s \phi$, functional (4.15) is easily recast as:

$$\mathcal{L}_\omega = - \sum_{\text{species}} \int \left\{ d^3 \mathbf{x} d^3 \mathbf{v} \frac{e_s F_{eq}^s}{T_s} \left(\sum_{\mathbf{n}\omega} \left[1 - \frac{\omega - \mathbf{n} \cdot \boldsymbol{\omega}_s^*}{\omega - \mathbf{n} \cdot \boldsymbol{\Omega} + i0^+} \right] \phi_{\mathbf{n}\omega} e^{i(\mathbf{n} \cdot \boldsymbol{\alpha} - \omega t)} \right) \left(\sum_{\mathbf{n}'\omega'} \phi_{\mathbf{n}'\omega'} e^{i(\mathbf{n}' \cdot \boldsymbol{\alpha} - \omega' t)} \right)^* \right\}$$

Since the set of angle-action variables introduced in section 1.2.2 is canonically conjugated to the variables (\mathbf{x}, \mathbf{p}) , the integration element in the phase space reads:

$$d\tau = d^3 \mathbf{x} d^3 \mathbf{p} = d^3 \boldsymbol{\alpha} d^3 \mathbf{J} \quad (4.16)$$

Noticing that $\int d^3 \boldsymbol{\alpha} e^{i\mathbf{n} \cdot \boldsymbol{\alpha}} = (2\pi)^3 \delta(\mathbf{n})$, the functional can be simplified as:

$$\boxed{\mathcal{L}_\omega = - \sum_{\text{species}} \int (2\pi)^3 d^3 \mathbf{J} \frac{e_s F_{eq}^s}{T_s} \sum_{\mathbf{n}\omega} \phi_{\mathbf{n}\omega} \phi_{\mathbf{n}\omega}^* \left(1 - \frac{\omega - \mathbf{n} \cdot \boldsymbol{\omega}_s^*}{\omega - \mathbf{n} \cdot \boldsymbol{\Omega} + i0^+} \right)} \quad (4.17)$$

The term $\mathbf{n} \cdot \boldsymbol{\Omega}$ represents all the possible resonant modes linked with one of the three motion invariants. The formulation is not yet gyrokinetic: indeed, the terms $n_1 \Omega_1$ describe the resonance of cyclotron modes, the terms $n_2 \Omega_2$ describe the resonance for the

³Let $A : \mathbb{R} \rightarrow \mathbb{R}$. Then, equation $\forall x, A(x) = 0 \Rightarrow \forall B : \mathbb{R} \rightarrow \mathbb{R}, \int A(x)B(x)dx = 0$. The last form of the equation is called the "weak" formulation of the first one.

⁴The weak formulation of the quasi-neutrality is written as Eq.(4.14) $\forall \phi^\dagger, \mathcal{L}(\phi^\dagger) = 0$ whereas the strong formulation writes as Eq.(4.13) $\frac{\partial \mathcal{L}}{\partial \phi^\dagger} = 0$. Both formulations are equivalent for a continuous functional.

bounce/passing motion, and the terms $n_3\Omega_3$ describe the resonance for the precession motion. Furthermore, as a characteristic function of the system, this Lagrangian functional contains all the information required to tackle the development of potential modes of the system, i.e. the expression of pulsation and growth rate of each mode number k .

Besides, in the absence of inhomogeneities, we have $\omega^* = 0$. In that case, the mode can only be damped: this is the Landau damping case which has been tackled in several books (see for instance [39, Goldston]). Therefore, the apparition of an instability requires to have gradients on the density and temperature profiles. These deviations from equilibrium state act as a source of free energy which can fuel the instabilities on the potential modes.

Lagrangian (4.17) can be decomposed into an adiabatic and a kinetic part. The kinetic part is the fraction on the right of the parenthesis. We see that considering a model with adiabatic electrons not only skips all electron modes, but it also modifies the growth of ion modes. We can therefore expect, with a kinetic electron model to see the appearance of electron modes, including the TEM regime, but also to see an influence of the kinetic electrons on the dynamics of ion modes and in particular the ITG.

4.1.3 Dispersion relation of ITG and TEM

A particular case of the drift wave and interchange instability

Most instabilities which govern turbulence in tokamak plasmas can be explained with the mechanisms of the drift wave and the interchange instabilities. The instability is then fuelled by the inhomogeneities of density, temperature and magnetic field. It is possible to distinguish some classes of instabilities depending on which class of particles transfers its kinetic energy into potential energy to develop the instability:

- The Ion/Electron Temperature Gradient modes (ITG/ETG) mostly involve passing ions/electrons. This instability has two branches: the slab one has the mechanism of the drift wave instability whereas the toroidal one has the mechanism of the interchange instability.
- The Trapped Ion/Electron Modes (TIM/TEM) involve trapped ions/electrons. The mechanism's type is interchange.

The resonance condition depends both on the mode wavenumber as shown on Fig.4.3, and on the density and temperature profiles. With the knowledge of these profiles, a map of the dominant instabilities function of the density and temperature gradient values of the two species can be established (see Fig.4.4).

Under the usual tokamak conditions, simulations show that the main instabilities responsible for turbulent transport are the ITG and TEM [63, Merz 2010]. Besides, theoretical kinetic models predicted quite early that this turbulent transport was impacted

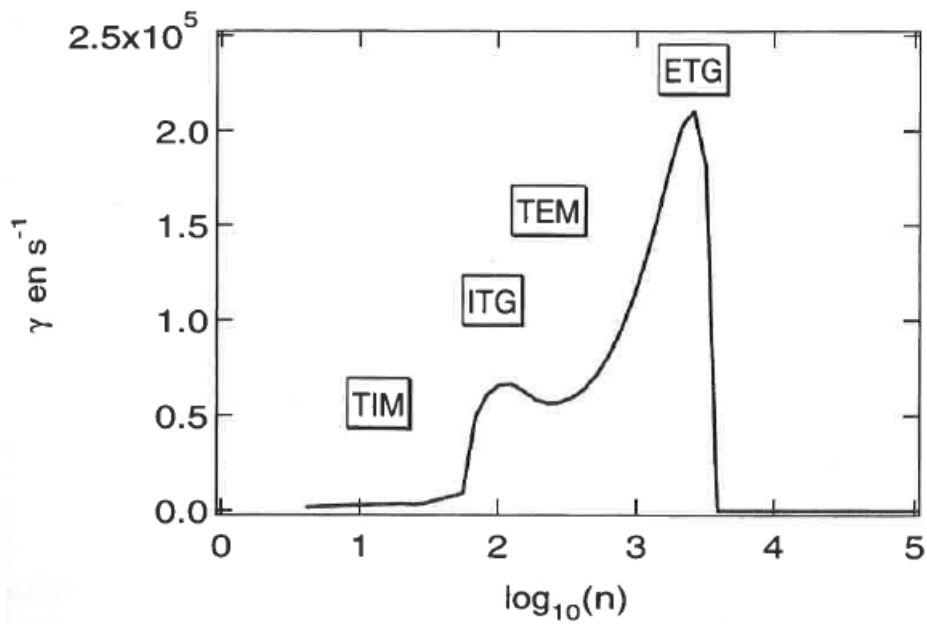


Figure 4.3: Schematic localization of different modes over a growth rate spectrum. n refers here to the toroidal wavenumber. [10, Bourdelle 2000]

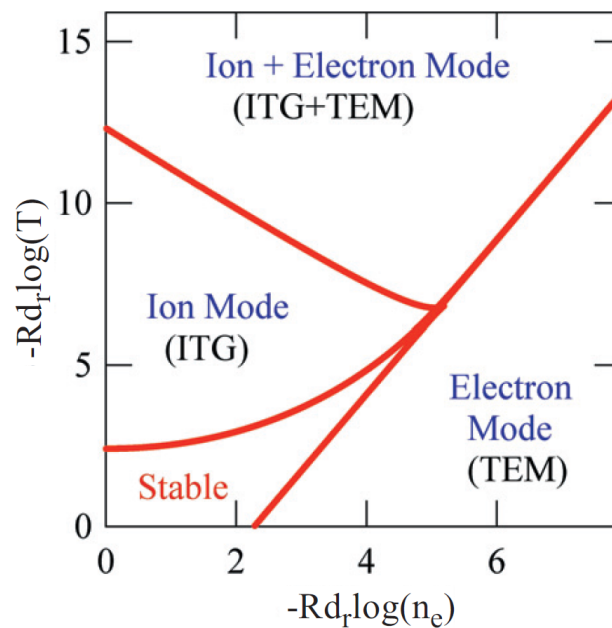


Figure 4.4: Predominance domain of the ITG-TEM instability with $T_i = T_e$ [34, Garbet].

strongly by kinetic electrons [29, Gang 1991],[79, Weiland 1992]. Consequently, the role of kinetic electrons on turbulent transport has been investigated thoroughly in the past twenty years. It has been shown by several codes that taking into account the kinetic response of trapped electrons in gyrokinetic models added the TEM turbulence but also modified strongly the level of ITG turbulence [14, 13, 15, Chen 2001-3][51, Idomura 2016]. Other important physics such as finite- β effects and collisions [9, Bottino 2011] or the generation of Zonal Flows in the case of TEM and TIM microturbulence [27, 26, 41, Drouot 2014-5, Gravier 2016] has been studied. A benchmark between several codes is made in [69, Rewoldt 2007]. Besides, the impact of kinetic passing electrons has been studied as well and these add another family of unstable modes, namely the Electron Temperature Gradient (ETG) which can create turbulent transport as well [25, Dorland 2000],[53, Jenko 2000],[77, Waltz 2007]. In addition, kinetic passing electrons modify significantly the level of the ITG and TEM turbulence as well [23, 24, Dominski 2015-7]. However, for numerical resources issues, we consider in our simulations (sections 4.2 and 4.3) only the trapped electrons kinetic because they have a stronger impact on turbulent transport than the passing ones.

Dispersion relation: simplified approach

In this section, one derives a simplified expression of the dispersion relation of ion and electron modes governed by the gyrokinetic equation Eq.(1.56) and the quasi-neutrality Eq.(2.18). Denoting $f_s(r, \theta, \varphi, v_{G\parallel}, \mu, t)$ the distribution function of the gyrocenters of a given species “ s ”, the simplified gyrokinetic equation considered here is the following:

$$\partial_t f_s + (\mathbf{v}_E + \mathbf{v}_D + \mathbf{v}_{G\parallel}) \cdot \nabla f_s + \frac{dv_{G\parallel}}{dt} \partial_{v_{G\parallel}} f_s = 0 \quad (4.18)$$

where \mathbf{v}_E and \mathbf{v}_D stand respectively for the electric and magnetic (curvature and ∇B) drifts. In this expressions, it should be noticed that the gradient operator ∇ is to be taken at constant $v_{G\parallel}$ and μ . Simplified expressions will be used in the following:

$$\begin{aligned} \mathbf{v}_E \cdot \nabla &\simeq \frac{\mathbf{B} \times \nabla J_0 \cdot \phi}{B^2} \cdot \nabla \simeq \frac{1}{rB} \{ \partial_r (J_0 \cdot \phi) \partial_\theta - \partial_\theta (J_0 \cdot \phi) \partial_r \} \\ \mathbf{v}_D \cdot \nabla &\simeq \frac{m_s v_{G\parallel}^2 + \mu B}{e_s B} \frac{\mathbf{B} \times \nabla B}{B^2} \cdot \nabla \simeq v_{D0} \left\{ \sin \theta \partial_r + \frac{\cos \theta}{r} \partial_\theta \right\} \\ v_{G\parallel} \nabla_{\parallel} &\simeq \frac{v_{G\parallel}}{R} \left\{ \partial_\varphi + \frac{1}{q} \partial_\theta \right\} \\ m_s \frac{dv_{G\parallel}}{dt} &\simeq -e_s \nabla_{\parallel} (J_0 \cdot \phi) - \mu \nabla_{\parallel} B + m_s v_{G\parallel} \mathbf{v}_E \cdot \frac{\nabla B}{B} \end{aligned}$$

with J_0 the gyro-average operator and $v_{D0} = -(m_s v_{G\parallel}^2 + \mu B)/e_s B R$. Here, B_{\parallel}^* has been approximated by B and sub-dominant components of the transverse drifts (toroidal components and finite beta contribution) have been neglected.

Let us consider a stationary equilibrium without any electric field: $\phi_{eq} = 0$. Canonical Maxwellian distribution functions are solutions of the equilibrium gyrokinetic equation: they are formed with canonical profiles of density, temperature and velocity depending on the toroidal canonical momentum [52, 2, 21, Idomura 2003, Angelino 2006, Dif-Pradalier 2008]. In the limit of small ρ_* values, these profiles can be approximated by their local limit, so that the profiles depend on the radial coordinate only. Hereafter, we consider a centered local Maxwellian as the equilibrium:

$$f_{s,eq}(r, \theta, v_{G\parallel}, \mu) = \frac{n_{eq,s}}{(2\pi T_{eq,s}/m_s)^{3/2}} \exp\left\{-\frac{\mathcal{E}_s}{T_{eq,s}}\right\} \quad (4.19)$$

where $\mathcal{E}_s = \frac{1}{2}m_s v_{G\parallel}^2 + \mu B$ is the kinetic energy and $n_{eq,s}$ and $T_{eq,s}$ depend on the radial coordinate r only.

Let us now add perturbations to this equilibrium: $\phi = \tilde{\phi}(r, \theta, \varphi, t)$ and $f_s = f_{s,eq} + \tilde{f}_s(r, \theta, \varphi, v_{G\parallel}, \mu, t)$. In the limit of small perturbations, i.e. $\tilde{f}_s/f_{s,eq} \sim e_s \tilde{\phi}/T_{eq,s} \ll 1$, Eq.(4.18) can be linearized by dropping off all nonlinear terms which are quadratic in fluctuations. The resulting equation reads as follows:

$$\begin{aligned} & \partial_t \tilde{f}_s + \mathbf{v}_D \cdot \nabla_{\perp} \tilde{f}_s + v_{G\parallel} \nabla_{\parallel} \tilde{f}_s + \mathbf{v}_E \cdot \nabla_{\perp} f_{s,eq} \\ & + \left\{ -\frac{e_s}{m_s} \nabla_{\parallel} (J_0 \cdot \tilde{\phi}) + v_{G\parallel} \mathbf{v}_E \cdot \frac{\nabla B}{B} \right\} \partial_{v_{G\parallel}} f_{s,eq} = 0 \end{aligned} \quad (4.20)$$

Here, the parallel trapping in the local mirrors of the magnetic field has been ignored (term proportional to $\mu \nabla_{\parallel} B \partial_{v_{G\parallel}} \tilde{f}_s$), which is relevant for strongly passing particles only. Further noticing that:

$$\begin{aligned} \nabla_{\perp} f_{s,eq} &= \left\{ \frac{\nabla_r n_{eq,s}}{n_{eq,s}} + \frac{\nabla_r T_{eq,s}}{T_{eq,s}} \left(\frac{\mathcal{E}_s}{T_{eq,s}} - \frac{3}{2} \right) - \frac{\mu}{T_{eq,s}} \nabla_{\perp} B \right\} f_{s,eq} \\ v_{G\parallel} \mathbf{v}_E \cdot \frac{\nabla B}{B} \partial_{v_{G\parallel}} f_{s,eq} &= \frac{m v_{G\parallel}^2}{e_s B} \frac{\mathbf{B} \times \nabla B}{B^2} \cdot \nabla_{\perp} (e_s J_0 \cdot \tilde{\phi}) \frac{f_{s,eq}}{T_{eq,s}} \end{aligned}$$

Eq.(4.20) can be recast as follows:

$$\begin{aligned} & \partial_t \tilde{f}_s + \mathbf{v}_D \cdot \nabla_{\perp} \tilde{f}_s + v_{G\parallel} \nabla_{\parallel} \tilde{f}_s \\ & + v_{Er} \left\{ \frac{\nabla_r n_{eq,s}}{n_{eq,s}} + \frac{\nabla_r T_{eq,s}}{T_{eq,s}} \left(\frac{\mathcal{E}_s}{T_{eq,s}} - \frac{3}{2} \right) \right\} f_{s,eq} \\ & + \left\{ v_{G\parallel} \nabla_{\parallel} (e_s J_0 \cdot \tilde{\phi}) + \mathbf{v}_D \cdot \nabla_{\perp} (e_s J_0 \cdot \tilde{\phi}) \right\} \frac{f_{s,eq}}{T_{eq,s}} = 0 \end{aligned} \quad (4.21)$$

with $v_{Er} = -\partial_{\theta}(J_0 \cdot \tilde{\phi})/rB$ the radial component of the electric drift.

The next step consists in projecting fluctuating fields in the Fourier space:

$$\begin{aligned} \tilde{f}_s &= \sum_{m,n,\omega} \hat{f}_{m,n,\omega} e^{i(m\theta+n\varphi-\omega t)} \\ \tilde{\phi} &= \sum_{m,n,\omega} \hat{\phi}_{m,n,\omega} e^{i(m\theta+n\varphi-\omega t)} \end{aligned}$$

In the linear regime, each of these modes turns out to be decoupled from the others, up to the toroidal coupling terms (involving \mathbf{v}_D) which couple adjacent poloidal m numbers, namely m , $m + 1$ and $m - 1$. For the sake of simplicity, the following notation will be used for these terms:

$$\mathbf{v}_D \cdot \nabla_{\perp} \rightarrow i\omega_{Ds}$$

where $\omega_D \simeq k_{\perp} v_{D0}$ actually stands for an operator. A more rigorous treatment requires using the ballooning representation, which is mentioned the next section. In Fourier space, Eq.(4.21) yields:

$$\begin{aligned} \hat{f}_{m,n,\omega} &= \frac{-\omega_s^* + \omega_D + k_{\parallel} v_{G\parallel}}{\omega - \omega_D - k_{\parallel} v_{G\parallel}} \frac{e_s J_0 \cdot \tilde{\phi}}{T_{eq,s}} f_{s,eq} \\ &= - \left\{ 1 - \frac{\omega - \omega_s^*}{\omega - \omega_D - k_{\parallel} v_{G\parallel}} \right\} \frac{e_s J_0 \cdot \tilde{\phi}}{T_{eq,s}} f_{s,eq} \end{aligned} \quad (4.22)$$

where $k_{\parallel} = (n + m/q)/R$ is the parallel wave vector and the diamagnetic frequency is defined by:

$$\omega_s^* = \omega_n^* + \omega_T^* \left(\frac{\mathcal{E}_s}{T_{eq,s}} - \frac{3}{2} \right)$$

with $\omega_X^* = (k_{\theta} \rho_s) v_{Ts} \nabla_r \log X$, $k_{\theta} = m/r$ the poloidal wave vector, $\rho_s = m_s v_{Ts} / e_s B$ the thermal gyro-radius and $v_{Ts} = \sqrt{T_{eq,s} / m_s}$ the thermal velocity.

The last step requires using the quasi-neutrality, which relates the charge densities of gyro-centers to the ion polarization densities. In the case of a single ion plasma with equal ion and electron temperatures, the final dispersion relation reads as follows:

$$2 + (k_{\perp} \rho_i)^2 - \left\langle J_0 \frac{\omega - \omega_i^*}{\omega - k_{\parallel} v_{G\parallel} - \omega_{Di}} J_0 \right\rangle_i - \left\langle \frac{\omega - \omega_e^*}{\omega - k_{\parallel} v_{G\parallel} - \omega_{De}} \right\rangle_e = 0 \quad (4.23)$$

Here, the brackets stand for the integral over the velocity space, weighted by the respective equilibrium distribution function: $\langle \dots \rangle_s = \int d^3v \dots f_{eq,s}$. In the case where the inhomogeneity of the magnetic field can be neglected, the ω_{Ds} operators should be ignored.

Dispersion relation using the ballooning representation

The full calculation of the dispersion relation (4.23) is obtained under the following assumptions:

- Hydrodynamic limit : $\omega/k \gg v_{th,i}$
- Limit of high wavelength values : $k_{\perp} \rho_i \ll 1$
- Ballooning representation [16, 70, Connor 1979, Romanelli 1993]

- Adiabatic electrons⁵

This calculation, made in [30, Garbet 2001] and verified in [36, Girardo 2015], leads to the form (Eq.(100) of [30]):

$$\left\{ \frac{\tau\omega + \omega_{ni}^*}{\omega - \omega_{pi}^*} + \frac{v_{th,i}^2}{2\omega^2 q^2 R^2} \partial_{\theta\theta} + \frac{1}{2} k_{\theta}^2 \rho_i^2 (1 + s^2 \theta^2) - \frac{\omega_{gi}}{\omega} \right\} \hat{\phi}_{n\omega}(\theta) = 0 \quad (4.24)$$

with $\tau = T_e/T_i$, $s = \frac{r}{q} \frac{dq}{dr}$, $\omega_{ni}^* = \frac{1}{n_i} \frac{\partial n_i}{\partial \mathbf{J}}$, $\omega_{Ti}^* = \frac{1}{T_i} \frac{\partial T_i}{\partial \mathbf{J}}$, $\omega_{pi}^* = \omega_{ni}^* + \omega_{Ti}^*$, $\omega_{gi} = -2T_i k_{\theta} / (e_i B R)$ and $\hat{\phi}_{n\omega}$ is the ballooning potential defined as:

$$\phi(r, \theta, \varphi, t) = \sum_{n\omega} \hat{\phi}_{n\omega}(\theta) \exp \{ in [\varphi - q(r)(\theta - \theta_k)] - i\omega t \}$$

with θ_k is a reference angle known as the ballooning angle. Likewise, Drouot and Gravier derived a linear dispersion relation valid for TIM and TEM turbulence (Eq.(12) of [26, Drouot 2015]). Neglecting the FLR effect (term in $k_{\theta} \rho_i$) and the inhomogeneities of the magnetic field (hence $\omega_g = 0$), the two last terms of Eq.(4.24) vanish. Previous simulations launched using the "Cyclone DIII-D base case parameter set" defined in [22, Dimits 2010] showed that the pulsation of a ITG or TEM mode can be expressed as:

$$\omega \sim \omega_{ns}^* \sim -\text{sign}(e_s) k_{\theta} \rho_i \frac{v_{th,s}}{L_n} \quad (4.25)$$

where $L_n = n/\nabla n$. The sign of the pulsation is negative for ITG modes and positive for TEM modes. This statement is of great use in the linear study that follows, for the knowledge of the pulsation sign enables to sort ITG from TEM modes.

⁵This hypothesis can be easily removed by doing the sum on all species.

4.2 Linear ITG-TEM simulations

The linear study carried here consists in retrieving the pulsation and growth rate of unstable modes so as to compare the values with those obtained with other codes. In fact, we prefer to do a benchmark with other codes rather than a verification with analytic results because these latter are approximated, especially for a global code such as GYSELA. In this part, we use the label (m, n) to describe a mode of poloidal wavenumber m and toroidal wavenumber n . Besides, the indice "i" is used for the type of ions in the simulations, namely deuterium, and "0" is used for normalized quantities in GYSELA, the normalisation using hydrogen ions.

4.2.1 Parameters used and type of the instability in a linear simulation

In a standard linear case, we introduce a perturbation \tilde{f} on the initial Maxwellian distribution function of ions f_0 using a single $n = n_0$ and several m . In order to keep only this toroidal mode n_0 , a filter is introduced to eliminate all the modes $n \notin \{0, n_0\}$. Thereafter, the system builds up the eigenmodes that grow exponentially. The magnitude of the initial potential perturbation is of the form $\phi_{m,n_0}(t=0) \propto \exp\{-(m/n_0 + q)^2\}$. For each chosen value n_0 , we look at the evolution of the resonant mode $(-qn_0, n_0)$. The associated wavenumber of this mode is given by $k_\theta \rho_i = -(n_0 q/r) \rho_i$. In order to do a comparison with the results obtained with kinetic electrons in the gyrokinetic code GT5D, we use the same plasma parameters as those used in [51, Idomura 2016]. We consider a collisionless deuterium plasma in a circular concentric tokamak configuration where we have taken the aspect ratio $R_0/a = 2.79$, the safety factor profile $q(r) = 0.85 + 2.18(r/a)^2$, and $\rho^* = \rho_0/a = 1/139$ with $\rho_0 = \sqrt{T_0/m_0}/\omega_{c0}$, T_0 being a normalized temperature, m_0 the hydrogen mass and ω_{c0} the cyclotron pulsation. This value of ρ^* is different from the one used by Idomura ($\rho_{GT5D}^* = 1/150$). The difference is due to normalisation issues of the ion temperature and explained in section 4.2.5. The resulting Cyclone like parameters at mid-radius $\rho_{peak} = 0.5$ where $\rho = r/a \in [0, 1]$ are $\varepsilon = r_{peak}/R_0 \simeq 0.18$, $q(r_{peak}) = 1.4$. Besides, the density and temperature profiles are let free to evolve⁶ and set at the beginning of the simulation to:

$$X(r, t = 0) = \exp \left\{ -\frac{R_0}{L_X} \delta \tanh \left(\frac{\rho - \rho_{peak}}{\delta} \right) \right\} \quad (4.26)$$

where X stands for either n , T_i or T_e . δ , R_0/L_n , R_0/L_{T_i} , R_0/L_{T_e} are parameters that can be chosen arbitrarily. Throughout this study, we set the parameters $\delta = 0.3$ and $R_0/L_n = 2.22$. The normalized densities and temperatures at mid-radius are consequently set to 1: $n_i(r_{peak}) = n_e(r_{peak}) = 1$, $T_e(r_{peak}) = T_i(r_{peak}) = 1$. In addition, we choose the mass ratio equal to $m_i/m_e = 100$ except for the convergence test carried in section 4.2.2. In this section, two temperature profiles are used:

⁶Density and temperature profiles should not evolve much in linear regime because the radial flux is negligible. However, as the initial distribution function slightly differs from the equilibrium distribution function, these profiles evolve a little anyway.

- $R_0/L_{T_i} = R_0/L_{T_e} = 6.92$ called the 'ITG-dominant' case
- $R_0/L_{T_i} = 0.01$ and $R_0/L_{T_e} = 6.92$ called the 'TEM-dominant' case

Given these parameters, the instability can be sorted into two categories, namely ITG and TEM, depending on the type of particle, ion or electron, that fuels the instability. The sign of the pulsation ω gives the nature of the dominant instability as seen in Eq.(4.25). For a ITG instability $\omega \sim \omega_{T_i}^* < 0$ and for a TEM instability $\omega \sim \omega_{T_e}^* > 0$. We verify afterwards that both methods give the same results. Experimentally, there are other ways to identify the type of the dominant instability, including reflectometry [3, Arnichand 2015].

After a series of tests explained in section 4.2.2 to determine the maximum time step that can be used for each of the three electron models, the dependency of the linear growth rate and the pulsation with the poloidal wavenumber $k_\theta \rho_i$ is studied in section 4.2.3 and we show that the ITG regime is obtained for small values of $k_\theta \rho_i$ whereas the TEM regime is obtained for large values of $k_\theta \rho_i$. With the parameters stated before, the transition appears for $k_\theta \rho_i \simeq 0.5$. Then in section 4.2.4, we make the ion radial temperature gradient R_0/L_{T_i} vary with a fixed value of the toroidal wavenumber. It is verified that for large values of R_0/L_{T_i} the ITG instability is dominant and for small values of R_0/L_{T_i} the TEM instability becomes dominant. For $k_\theta \rho_i = 0.28$, the transition appears at $R_0/L_{T_i} \simeq 5$.

4.2.2 Numerical study to determine the maximum time step

Using the GYSELA parameters introduced earlier, the 5D space $(r, \theta, \varphi, v_\parallel, \mu)$ is uniformly discretized with $N_r \times N_\theta \times N_\varphi$ points in the 3D position space and $N_{v_\parallel} \times N_\mu$ points in the 2D velocity space (with N_x the number of points in x direction). This mesh grid is fixed in time with $r \in [0, a]$, $\theta \in [0, 2\pi]$, $\varphi \in [0, 2\pi]$ (full torus), $v_\parallel \in [-\alpha_\parallel v_{T_0}, \alpha_\parallel v_{T_0}]$ and $\mu \in [0, L_\mu]$. The maximum of thermal velocities in velocity space are fixed to $\alpha_\parallel = 7$ and $L_\mu = 12 T_0/B_0$. The number of points taken in position and velocity are $N_r = 255$, $N_\theta = 256$, $N_\varphi = 128$, $N_{v_\parallel} = 64$ and $N_\mu = 32$. These values were chosen so as to resolve both the ion Larmor radius and the electron banana width spatially.

A numerical study, based on the ITG-dominant case presented earlier, is performed for the Adiabatic Electrons (AE) and Trapped Kinetic Electrons (TKE) models, introduced in chapter 2. The aim is to determine the maximum possible time step that can be used for each model without deteriorating the linear results. In Fig.4.5, the evolution of the module of the most unstable modes (m,n=14) is plotted for the two models with different time steps. It is observed that the AE model converges for much larger time steps than the TKE model. This is due to the fact that in the AE model one only needs to solve the ion dynamics, hence a required maximum time step which scales as $\Delta t_{AE} \propto R/v_{\parallel,i} \simeq R/v_{th,i}$. With kinetic electrons, one has to solve the dynamics of the electrons, i.e. a maximum time step in $\Delta t_{KE} \propto R/v_{\parallel,e}$. The parallel velocity of passing

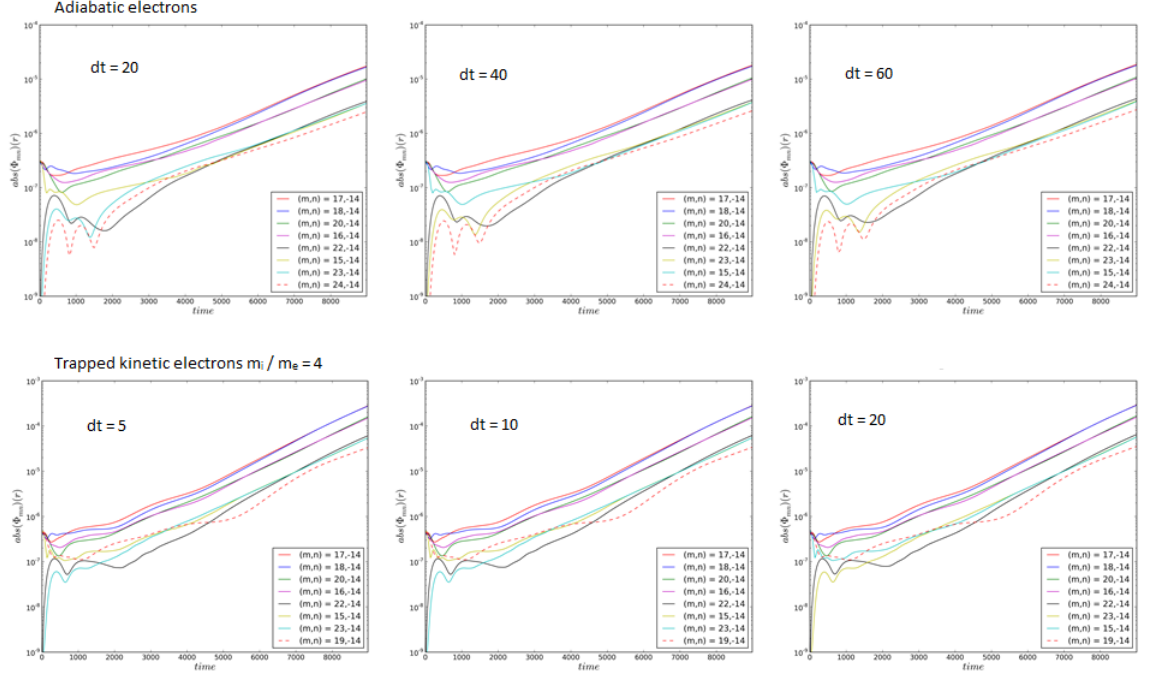


Figure 4.5: Convergence study to find the maximal time step required to resolve the AE and TKE models. We measure that the simulation is converged with $\Delta t_{AE} = 60 \omega_{c0}^{-1}$ for the AE model and $\Delta t_{TKE} = 20 \omega_{c0}^{-1}$ for the TKE model with $m_i/m_e = 4$

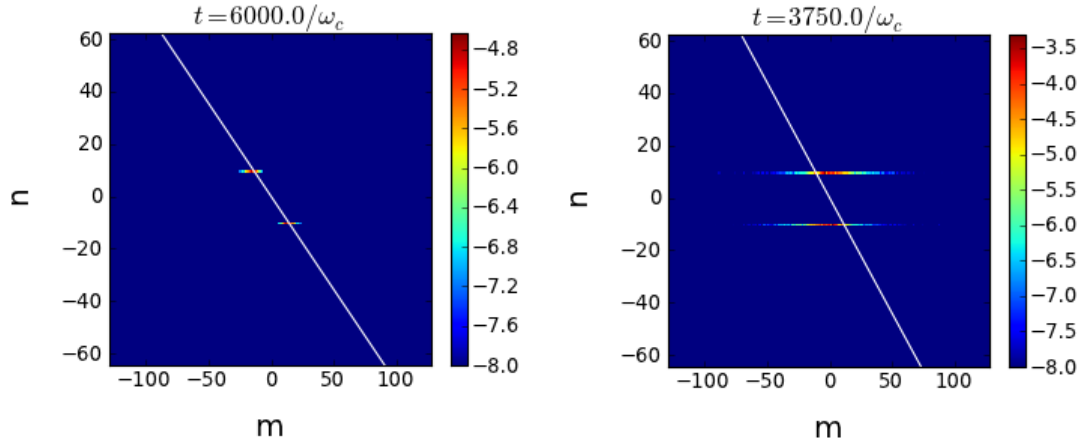


Figure 4.6: Fourier transform in (θ, φ) of the electric potential where only the toroidal mode $n = 10$ is kept. We use the trapped kinetic electron model with $m_i/m_e = 100$. The white line shows the resonant modes of equation $m = -qn$. The time step is taken as (a) $\Delta t = 2 \omega_{c0}^{-1}$: diagonal resonant modes $k_{\parallel} \sim 0$ appear, (b) $\Delta t = 10 \omega_{c0}^{-1}$: spurious modes $m \simeq 0$ appear.

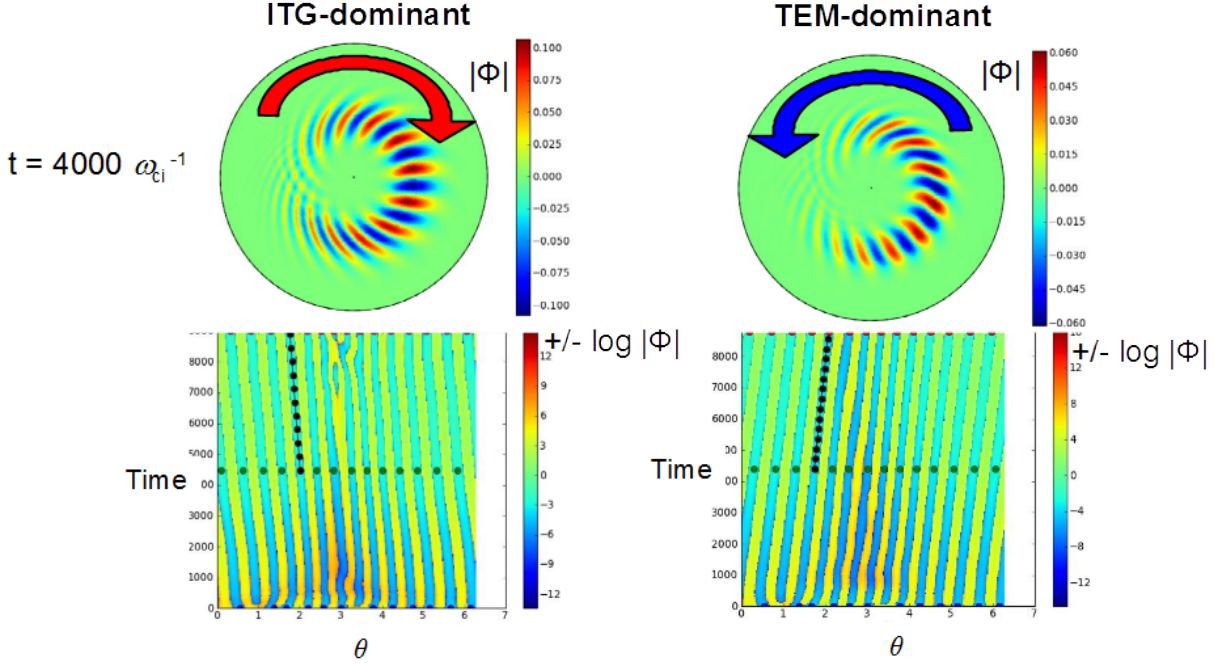


Figure 4.7: (a) Picture of the poloidal profile of the potential and (b) Evolution of the poloidal profile of $\text{sign}(\phi) \log |\phi|$ with time. The sign of $d_t \theta$ is the same as the sign of the drift wave pulsation ω .

electrons is approximately $v_{\parallel,e}^{\text{pass.}} \sim v_{th,e}$. For trapped electrons, it is $v_{\parallel,e}^{\text{trap.}} \sim \sqrt{\varepsilon} v_{th,e}$. For the aspect ratio $R_0/a = 2.79$ used in our simulations, we have $\sqrt{\varepsilon} \simeq 0.6 \sim 1$. Consequently, the minimum time step required to solve the dynamics of electrons should go as $\Delta t_{FKE} \propto \sqrt{m_e/m_i} \Delta t_{AE}$. In our case, $m_i/m_e = 4$ which implies $\Delta t_{KE} \sim \Delta t_{AE}/2$. This scaling seems to be satisfied between the AE and TKE models.

Fig.4.6 shows an example of two simulations run with the TKE model: one (on the left) has a sufficiently small time step to satisfy the criteria mentioned earlier. The other (on the right) has a time step too large to satisfy it. When the time step is too large, the modes that should be unstable are no longer dominant. We observe that other modes, with a poloidal number m close to 0, become dominant and the simulation is no longer relevant. Therefore, it must be checked that the time step is small enough to avoid this problem.

4.2.3 Dependence of the growth rate and pulsation with the toroidal wavenumber

The linear growth rate γ and pulsation ω are computed with the GYSELA code and compared to the ones found with the code GT5D that can be found in [51, Idomura 2016].

Both codes are gyrokinetic, global, full- f . The resolution scheme is different however: GT5D is eulerian whereas GYSELA is semi-lagrangian. The comparison in the case of adiabatic electrons was already made by Y. Asahi [5, Asahi 2017]. This study plus the similarities between the two codes GYSELA and GT5D encouraged us to do the same comparison with kinetic electrons. Details about the normalisation of ρ^* between the two codes are given in section 4.2.5. The parameters used in GYSELA and GT5D are explained in section 4.2.1. The type of instability, ITG or TEM, is given by the sign of ω as seen in part 4.1.3. It is therefore crucial to have access to this information. ITG and TEM being particular cases of drift waves, the pulsation can be retrieved from the poloidal mode phase velocity: $\omega = k_\theta v_\theta = -nq \, d_t \theta$. Plotting the potential with respect to time and poloidal angle shows immediately the sign of ω (see Fig.4.7).

We present in Figs.4.8 and 4.9 a comparison between both codes regarding the growth rate and pulsation in the ITG-dominant case using the Adiabatic Electrons and Trapped Kinetic Electrons models for different values of the toroidal wavenumber $k_\theta \rho_i$. This curve has the same general shape as the theoretical diagram shown in Fig.4.3: the ITG regime is expected to be obtained for the low values of $k_\theta \rho_i$ and the TEM regime for the larger ones. A good agreement is found between the two codes in the ITG regime for both the adiabatic and trapped kinetic models. However, it is unclear if the ITG/TEM transition is recovered for the same value of $k_\theta \rho_i$. Simulations were launched using larger values of $k_\perp \rho_i$ (0.6 and 0.7) but we could not retrieve the value of ω and γ : indeed, the evolutions of the modes $\phi_{m,n}$ do not exhibit an exponential growth in time at these values of m and n . This exponential growth would have been expected for this kind of instability. Since the number of points in θ and φ is unchanged for large $k_\perp \rho_i$ values, it might not be enough to resolve the mode when $n = 30$ or $n = 35$. Indeed, a number of points $N_\varphi = 128$ implies that there are roughly 4 points per period when $n = 30$. The same reasoning applies for the θ direction as $N_\theta = 256$ and $m_{\text{res}} \simeq q n_{\text{res}} \sim 60$. Low spatial discretization could explain why we were unable to retrieve the growth rate and pulsation for large values of $k_\perp \rho_i$, but this problem remains an open question. We believe on the other hand that the time step is small enough. Indeed, simulations with smaller time steps ($\Delta t = 1 \omega_{c0}^{-1}$) have been launched, but no change of behaviour has been noticed.

4.2.4 Dependence of the growth rate and the pulsation with the ion temperature gradient

In this section, the electron temperature gradient is maintained constant $R_0/L_{T_e} = 6.92$ whereas the ion temperature gradient varies within the range $R_0/L_{T_i} \in [0, 6.92]$, the two limit cases corresponding to the TEM and ITG dominant regimes introduced in section 4.2.1. The toroidal wavenumber is fixed to $n = 14$ which implies $k_\theta \rho_i = -(nq/r_{\text{peak}})\rho_i = -0.28$. The evolution of the linear growth rate γ and pulsation ω are computed using the Trapped Kinetic Electron model with the codes GYSELA and GT5D and shown on Figs.4.10 and 4.11.

The TEM regime is obtained for $R_0/L_{T_i} < 5.2$. The ITG-TEM transition is charac-

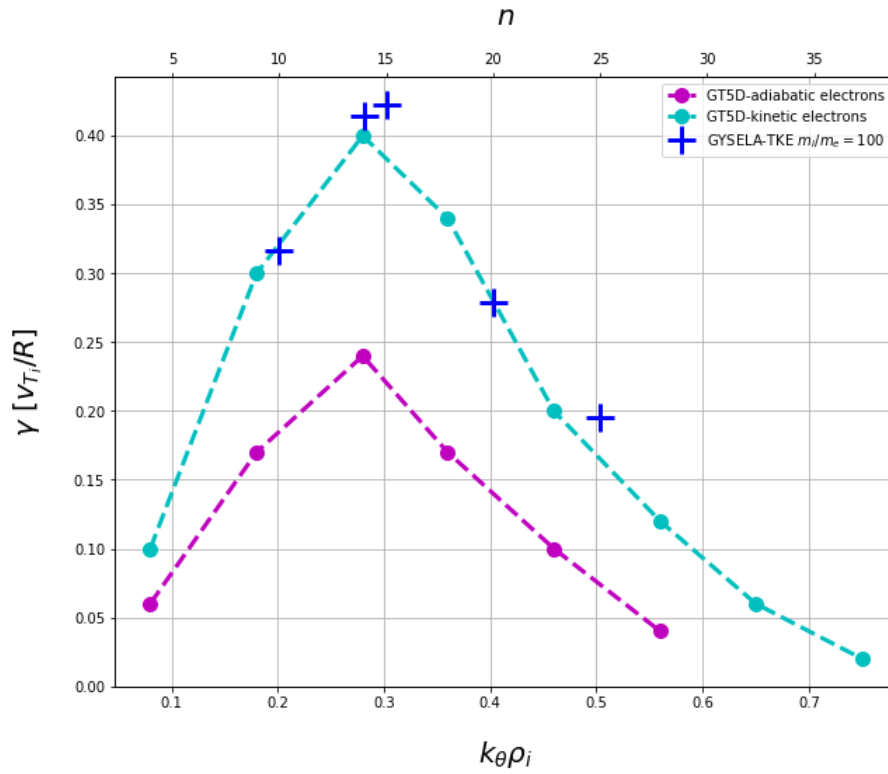


Figure 4.8: Dependence of the growth rate with the toroidal wavenumber. The ITG-dominant case used here corresponds to the parameters: $R_0/L_{T_i} = R_0/L_{T_e} = 6.92$

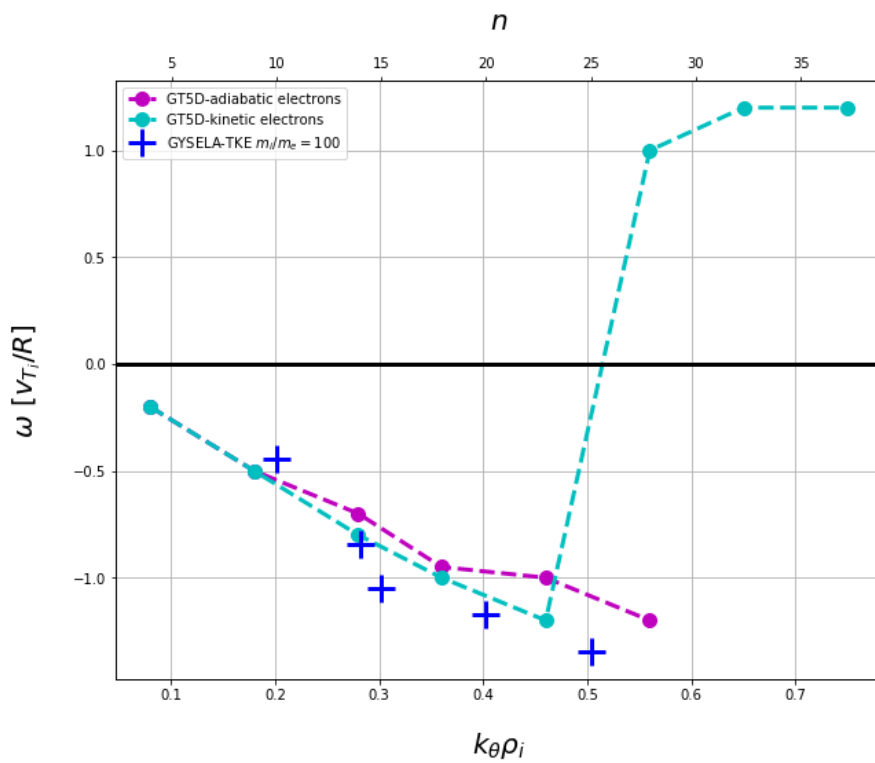


Figure 4.9: Dependence of the pulsation with the toroidal wavenumber. The ITG-dominant case used here corresponds to the parameters: $R_0/L_{T_i} = R_0/L_{T_e} = 6.92$

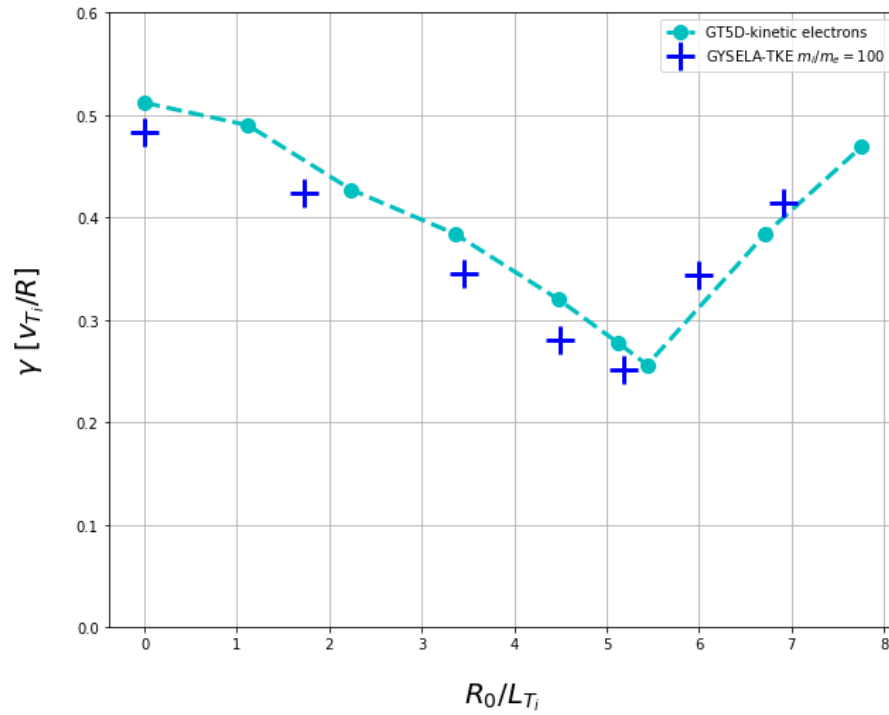


Figure 4.10: Dependence of the growth rate with the ion temperature gradient. One toroidal mode $n = 14$ has been launched with an electron temperature gradient $R_0/L_{T_e} = 6.92$

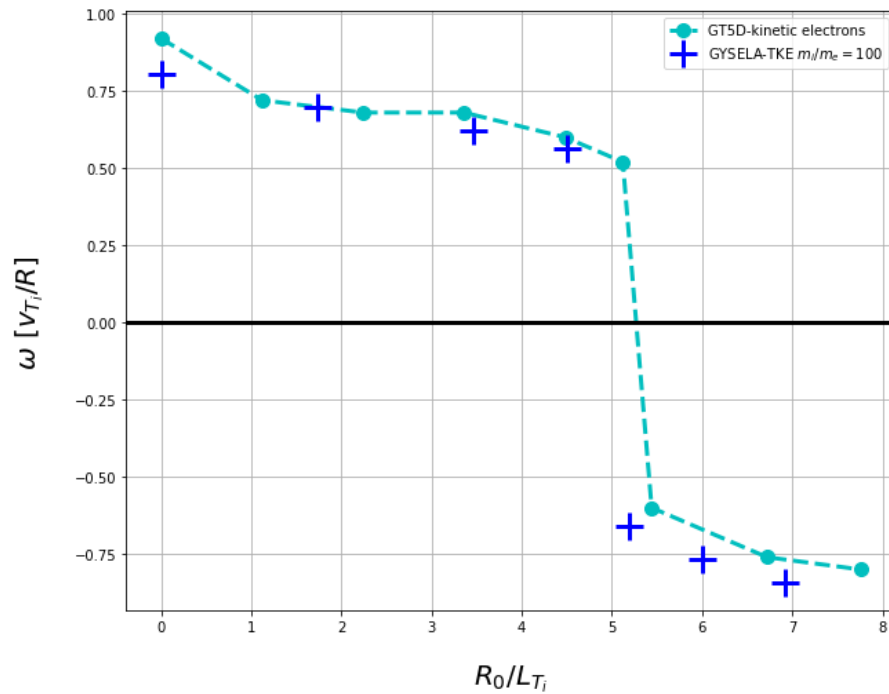


Figure 4.11: Dependence of the pulsation with the ion temperature gradient. One toroidal mode $n = 14$ has been launched with an electron temperature gradient $R_0/L_{T_e} = 6.92$

terized by a change of sign of the pulsation ω as explained earlier. Moreover we observe a change of slope in the evolution of γ characteristic of a different solution given by the linear dispersion relation. The instability is fuelled by the plasma inhomogeneities which act as sources of free energy. In the case of a low value of R_0/L_{T_i} , the instability is driven mainly by electrons and for a big value of R_0/L_{T_i} , the instability is driven mainly by ions. We observe that the ITG/TEM transition is sharp and the same with both codes. The radial temperature has a bigger impact on the type of instability than the chosen wavenumber. It can be noted that a difference appears between the two codes. This deviation can partly be explained by the fact that the value of ρ^* chosen in GYSELA must depend on the parameter R_0/L_{T_i} to be comparable to the one of GT5D as explained in section 4.2.5. The choice $\rho_{GYS}^* = 1/139$ is comparable to $\rho_{GT5D}^* = 1/150$ only for $R_0/L_{T_i} = 1.7$ and $R_0/L_{T_i} = 5.5$. In the future, it would be interesting to do this test again, using this time the good value of ρ_{GYS}^* associated with the corresponding R_0/L_{T_i} so as to get comparable ρ^* values with the two codes.

4.2.5 Normalisation of the value of ρ^* in GYSELA to fit the one in GT5D

To do the comparison between GYSELA and GT5D, we must use the same parameter ρ^* . The problem here is that ρ^* are computed differently in GYSELA and GT5D. Therefore, a given value of ρ_{GT5D}^* will correspond to a different value of ρ_{GYS}^* . We first give the expressions of ρ^* calculated with each code. Second, we give the condition between ρ_{GYS}^* and ρ_{GT5D}^* so as to have the same physical parameter. In each code, ρ^* is computed as follows:

- **GT5D**

$$\rho_{GT5D}^* = \frac{v_{th,i}^{GT5D}}{a \omega_{ci}} \quad \text{with} \quad v_{th,i}^{GT5D} = \sqrt{\frac{\langle T_i \rangle_r}{m_i}}$$

where the averaged ion temperature $\langle T_i \rangle_r$ is computed as:

$$\langle T_i \rangle_r = \frac{\int_0^a r T_i(r) dr}{\int_0^a r dr}$$

- **GYSELA**

$$\rho_{GYS}^* = \frac{v_{th,i}^{GYS}}{a \omega_{ci}} \quad \text{with} \quad v_{th,i}^{GYS} = \sqrt{\frac{T_i(r_{peak})}{m_i}}$$

The ratio of these two normalisations gives:

$$\frac{\rho_{GYS}^*}{\rho_{GT5D}^*} = \sqrt{\frac{T_i(r_{peak})}{\langle T_i \rangle_r}}$$

Therefore, to get a value of ρ^* with GYSELA identical to the one of GT5D, we must choose ρ_{GYS}^* as:

$$\rho_{GYS}^* = \sqrt{\frac{T_i(r_{peak})}{\langle T_i \rangle_r}} \rho_{GT5D}^* \quad (4.27)$$

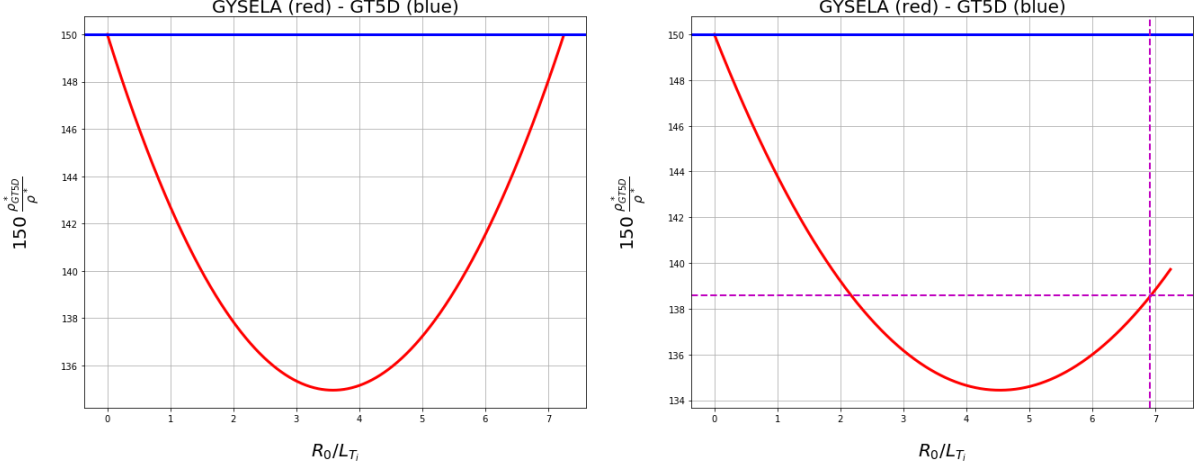


Figure 4.12: Dependence of ρ_{GYS}^* with R_0/L_{T_i} to satisfy condition (4.27) with $\rho_{GT5D}^* = 1/150$. (a) $\rho \in [0, 1]$ and $\rho_{\text{peak}} = 0.5$. (b) $\rho \in [0, 0.7]$ and $\rho_{\text{peak}} = 0.35$.

The value of $\langle T_i \rangle_r$ depends on the parameter R_0/L_{T_i} . Therefore, it is necessary to calculate for each value of R_0/L_{T_i} the corresponding value of ρ_{GYS}^* . We plot in Fig.4.12.a the value of ρ_{GYS}^* as a function of R_0/L_{T_i} to satisfy condition (4.27). The associated temperature profile is given by Eq.(4.26) with $\delta = 0.3$, $\rho \in [0, 1]$ and $\rho_{\text{peak}} = 0.5$.

In the tests launched with GYSELA, we chose $\rho_{GYS}^* = 1/139$ independently of the value of R_0/L_{T_i} . We realized recently that this value corresponds to an old normalization used for $R_0/L_{T_i} = 6.92$ with $\rho \in [0, 0.7]$ and $\rho_{\text{peak}} = 0.35$. This case corresponds to the intersection of the purple dashed lines of Fig.4.12.b. Meanwhile, these parameters were changed to $\rho \in [0, 1]$ and $\rho_{\text{peak}} = 0.5$ so as to be the same as those used in GT5D. Thus, this value of ρ_{GYS}^* does not satisfy condition (4.27) for every value of R_0/L_{T_i} . The error made on ρ^* can be estimated to approximately 7%. This could explain part of the differences observed between the two codes in Figs.4.10 and 4.11.

4.3 Implementation of a method to launch non-linear simulations

Previous linear tests have been carried out using a single toroidal mode. Fig.4.13 shows the development of the potential using the trapped kinetic electron model at $m_i/m_e = 100$ with the discretization mentioned earlier in the linear study. In such tests, the development of resonant modes at $k_{\parallel} = 0$ is observed. Yet, future studies of turbulent transport will require to launch cases with several toroidal modes for simulation times much longer than those used in the linear study. Therefore the cost of such simulations is expected to be very large. Moreover, given that the growth rate of the linear modes is substantially modified for small values of m_i/m_e (~ 1) [9, Bottino 2011], it can be expected that the transport levels will be badly predicted if a too low mass ratio is chosen. It is therefore in our best interest to find numerical methods that reduce the cost of simulations while ensuring that the evolution of turbulence is correctly predicted by doing so. The testing of such methods is done by launching a bunch of toroidal modes so as to look at the linear growth of the resonant modes satisfying $m/n = -q$.

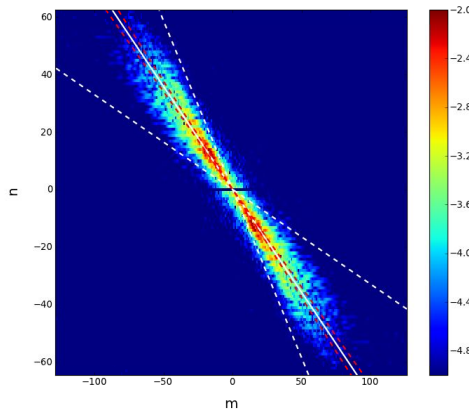


Figure 4.13: Fourier transform in (θ, φ) of the electric potential in a multimode simulation.

First, we highlight the emergence of high frequency modes when using the Full Kinetic Electron model, the so-called ω_H mode, which is characteristic of an electrostatic model. Consistently with the calculation made in section 4.3.1, ω_H modes are expected to arise due to passing particles at finite k_{\parallel} . Provided these particles are treated with an adiabatic response, as proposed by Idomura [51, Idomura 2016] (he only retains the kinetic response of passing electrons for $k_{\parallel} = 0$ modes), the simulation should be safe with respect to ω_H modes. In practice, this amounts to filtering the modes $(m, n = 0)$ with $m \neq 0$. Besides, Lee also recommend to eliminate the modes (m, n) with $m \simeq 0$ [59, Lee PFL1983]. Second, we present a method developed to reduce the numerical cost of these simulations: the aligned coordinate method ([57, Latu],[45, Hariri]). This method is particularly useful

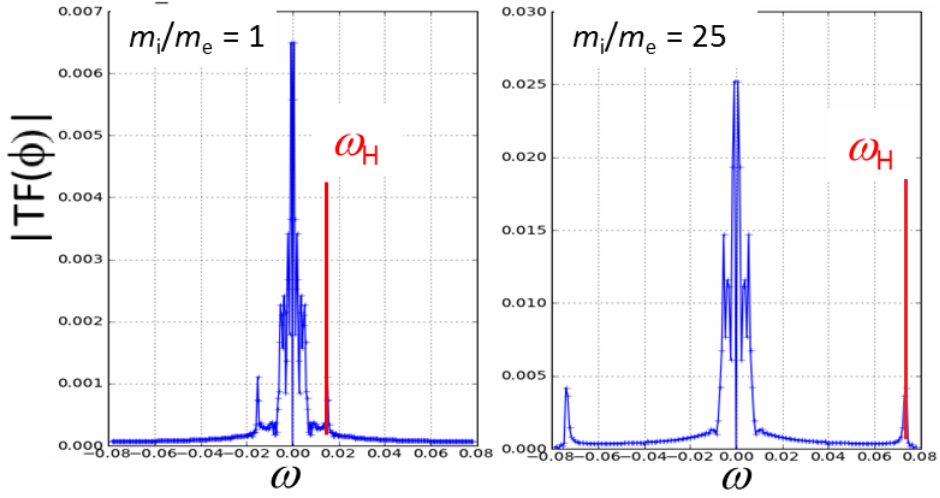


Figure 4.14: Time spectrum of a multimode ITG-like case for different mass ratios. We measure $\omega_H(m_i/m_e = 1) \simeq 0.016 \omega_{c0}$ and $\omega_H(m_i/m_e = 25) \simeq 0.076 \omega_{c0}$. We find $\omega_H(m_i/m_e = 25)/\omega_H(m_i/m_e = 1) = 4.75 \simeq 5$.

to resolve the dynamic of kinetic electrons which require higher space resolution, hence more memory.

4.3.1 The so-called ω_H mode: a signature of the electrostatic model

Using the parameters described in section 4.2.1, we place ourselves in the conditions of the ITG-like case. We introduce an initialization of the modes (m, n) with an amplitude $\phi_{m,n}(t=0) \propto \exp\{-(m/n + q)^2\}$. There is a substantial transport of matter and energy modifying the density and temperature profiles, which prevents a linear analysis from being carried out. This transport seems to be concomitant with the appearance of high frequency oscillations, attributed to the so-called ω_H mode, which are shown for different mass ratios in Fig.4.14.

The ω_H mode corresponds to the electrostatic limit $\beta \ll 1$ of the kinetic Alfvén wave [74, Scott 1997] as explained in Appendix D.2. In the case of kinetic electrons, this mode is found by looking at the resonance of the passing particles in the dispersion equation (4.23). Here, the terms $(k_\perp \rho_i)^2$ and ω_D have been neglected. Considering only the resonance of passing particles, this equation reads:

$$2 - \underbrace{\left\langle \frac{\omega - \omega_i^*}{\omega - k_\parallel v_{\parallel i}} J_0^2 \right\rangle}_{\mathcal{I}} - \underbrace{\left\langle \frac{\omega - \omega_e^*}{\omega - k_\parallel v_{\parallel e}} \right\rangle}_{\mathcal{E}} = 0 \quad (4.28)$$

where $\langle \dots \rangle = \int \dots F_{eq} d^3\mathbf{v}$ and $J_0^2 \simeq 1 - (k_\perp \rho_i)^2/2$. In the hydrodynamic limit $\omega \gg k_\parallel v_{th,e}$

and neglecting the equilibrium gradients $\omega \gg \omega_i^*, \omega_e^*$, the ion and electron terms of Eq.(4.28) become:

$$\mathcal{I} \simeq 1 - \frac{(k_{\perp} \rho_i)^2}{2} \quad ; \quad \mathcal{E} \simeq 1 + \left(\frac{k_{\parallel} v_{th,e}}{\omega} \right)^2$$

Finally, the resonant pulsation ω_H , solution of Eq.(4.28) takes the form:

$$\frac{\omega_H}{\omega_{ci}} = \frac{k_{\parallel}}{k_{\perp}} \sqrt{\frac{m_i}{m_e}} \quad (4.29)$$

This high frequency can be measured in Fig.4.14 and the dependence in $\sqrt{m_i/m_e}$ is verified. Two points can be mentioned here: on the one hand, the ω_H mode is a signature of the electrostatic model that should not appear in an electromagnetic model. On the other hand, it appears only at high frequency. Thus, two strategies can be used numerically to treat this ω_H mode:

- Either we keep these modes and the time step should be chosen small enough to resolve these modes. This solution requires a very small time step and is therefore costly numerically.
- Or we filter these modes so as not to take them into account in our study.

Choosing the second option, the question arises how to filter these modes. It should be noted that these modes are due to passing electrons and have a finite $k_{\parallel} \simeq \frac{1}{R} [n + m/q]$. We therefore choose to proceed in a way similar to what is done in GT5D [51, Idomura 2016] to eliminate the ω_H mode: on the one hand, only trapped electrons receive a kinetic treatment and on the other hand we filter the modes $n = 0$ except for the mode ($m = 0, n = 0$).

4.3.2 The aligned coordinates method: a way to reduce the toroidal discretization

In GYSELA, parallel derivatives can be computed using field-aligned coordinates [57, Latu 2018]. This allows one to use a coarser grid in a chosen direction, while still properly describing the relevant $k_{\parallel} \sim 0$ modes. The method has been initially proposed by Ottaviani [67, Ottaviani 2011], and further developed in the FENICIA code [45, Hariri 2013].

Parallel and perpendicular dynamics

The equations of motion in GYSELA state as follows, when considering dominant contributions only:

$$\begin{aligned}\frac{dr}{dt} &= v_{Er} + v_{Dr} \\ \frac{d\theta}{dt} &= \frac{v_{E\theta} + v_{D\theta}}{r} + \frac{v_{\parallel}}{qR} \\ \frac{d\varphi}{dt} &= \frac{v_{\parallel}}{R}\end{aligned}\tag{4.30}$$

In this scheme, we numerically solve a 2D advection in (r, θ) given by the two first equations of the system (4.30), a 1D advection in φ given by the last equation and the advection in v_{\parallel} . One can notice that this motion of the gyrocentres can be decomposed in two independent dynamics:

- a dynamics **parallel** to the magnetic field lines described by the equations:

$$\begin{cases} \frac{d\theta}{dt} = v_{\parallel}/qR \\ \frac{d\varphi}{dt} = v_{\parallel}/R \end{cases}\tag{4.31}$$

- a dynamics **perpendicular** to the magnetic field lines described by the equations:

$$\begin{cases} \frac{dr}{dt} = v_{Er} + v_{Dr} \\ \frac{d\theta}{dt} = (v_{E\theta} + v_{D\theta})/r \end{cases}\tag{4.32}$$

The aligned coordinate method ([57, Latu 2018],[45, Hariri 2013]) consists in solving the 2×2D advectons (4.31) and (4.32) and the advection in v_{\parallel} . This so-called Strang splitting is therefore more demanding in numerical resources for a given discretization. However, the gradients in the parallel direction are much smaller than those in the transverse directions, roughly in the ratio $k_{\parallel}qR \sim k_{\perp}\rho_i$. Therefore the aligned coordinates method enables to use a discretization in the parallel direction much coarser than that used to describe the transverse directions. It is then possible to greatly reduce the discretization in one of the three spatial dimensions with little loss of accuracy in the description of plasma physics. The idea of this method is detailed below.

In practice, small grid steps (large number of grid points) are used in the radial r and poloidal θ directions and a coarse mesh in the toroidal direction φ . Let us consider a function G of the 2 space coordinates θ and φ . Let (θ^*, φ^*) be the footpoint of the trajectory, i.e. the point at which a 2-dimensional interpolation is required. The field-aligned method proceeds in 2 steps for this interpolation. Before all, one identifies the magnetic field line which intersects (θ^*, φ^*) . The intersections of this field line with the toroidal grid mesh are marked with blue crosses on Fig.4.15. The first step consists in interpolating the value of G on each of these crosses by using the refined mesh in the

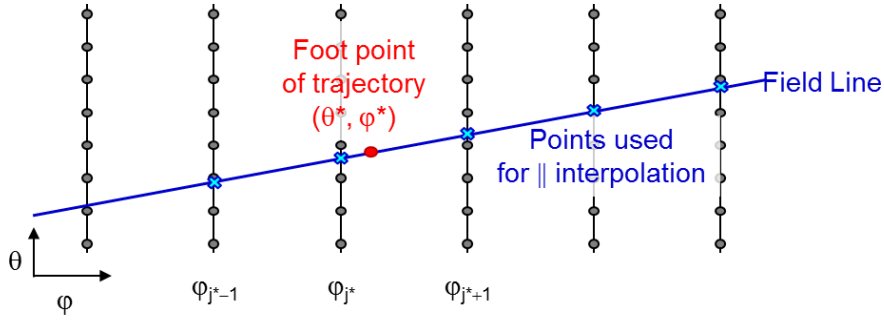


Figure 4.15: Discretization of a magnetic field line using the aligned coordinate method.

poloidal direction. For the second and last step, the value of G at (θ^*, φ^*) is computed by performing an interpolation along the field line, by using the values computed at step 1 on the blue crosses. Also, parallel gradients (which govern the equation computing $d_t v_{\parallel}$) are computed with finite differences along the field line.

Comparison aligned versus not aligned

In the adiabatic electrons model, we launch two series of simulations, one using the aligned coordinates scheme and the other using the classical coordinates scheme. We compare the evolution of the higher amplitude modes with and without aligned coordinates for different numbers of toroidal points N_{φ} (see Fig.4.16). We see that the non-aligned case with $N_{\varphi} = 32$ has not converged so we did not show the case $N_{\varphi} = 16$. Conversely, the aligned case $N_{\varphi} = 128$ has totally converged so we did not show the case $N_{\varphi} = 256$.

It is found that the two cases have converged at identical levels from a toroidal discretization $N_{\varphi} = 32$ for the aligned case and $N_{\varphi} = 256$ for the non-aligned case. The aligned coordinates enabled a reduction of spatial discretization (here by a factor 8) while obtaining similar results. The resulting effective cost in terms of computation time is summed up in Tab.4.1. Due to issues related to the Strang splitting explained earlier, aligned cases are more costly than non-aligned ones at a given N_{φ} . This saving is particularly valuable for the launch of nonlinear cases with kinetic electrons for which the evolution times are long and therefore very expensive in terms of numerical resources.

N_{φ}	256	128	32	16
Not aligned	108 653	53 746	14 187	-
Aligned	-	118 899	23 112	11 432

Table 4.1: Cost in CPU seconds of a similar case for different toroidal discretization with the aligned and not-aligned methods.

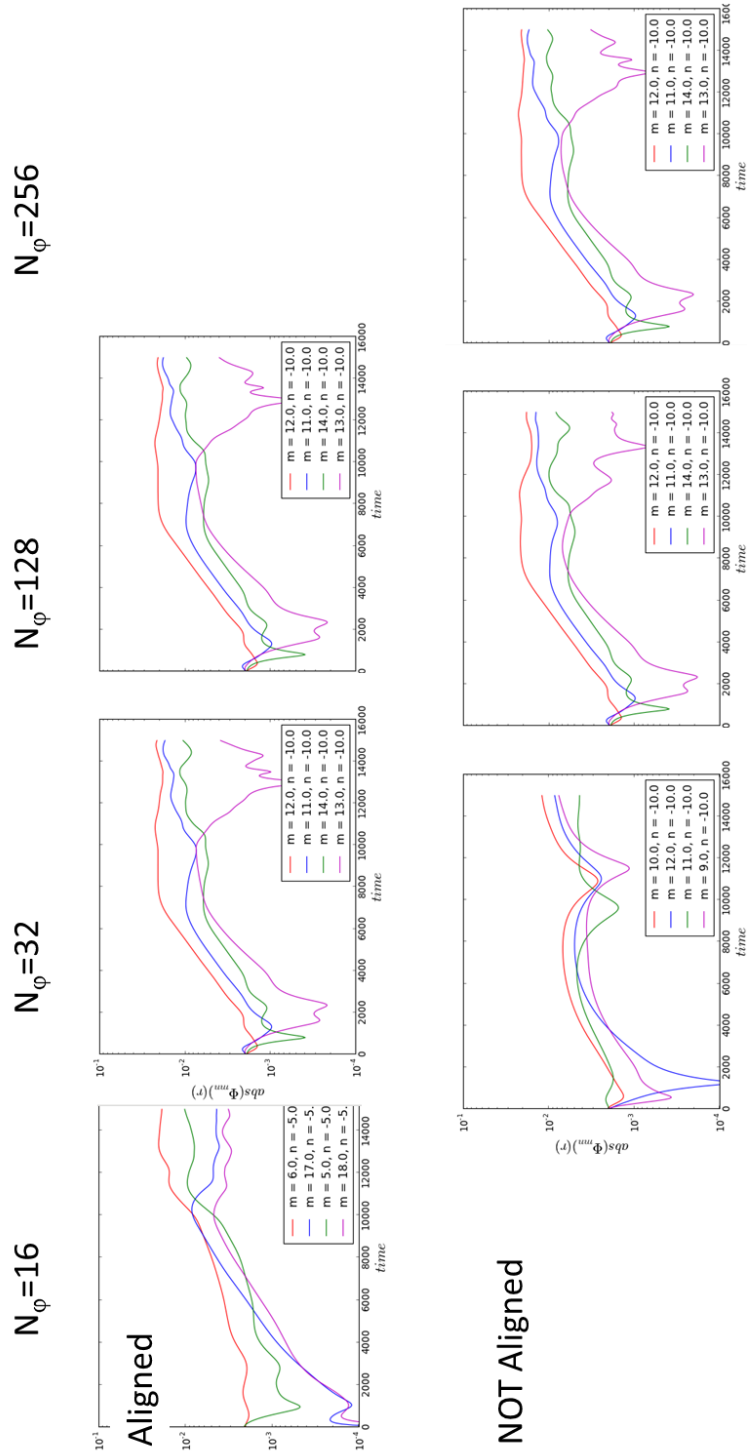


Figure 4.16: Evolution of the absolute value of the four dominant modes at $t = 16000\omega_{c0}^{-1}$. In particular, it can be noted that the simulation converges with less toroidal points in the aligned scheme ($N_\varphi = 32$ with the aligned coordinates versus $N_\varphi = 256$ without).

Expression of the effective parallel wave vector

It has been seen that the aligned method gives, for a reduced numerical cost, similar growth rate values for resonant modes as the ones obtained without using this method. However, we want to check whether the (m, n) values of resonant modes are the same with both methods. To do so, we recall the reasoning made in [45, Hariri 2013] to compute the effective parallel wave vector in the aligned method, the resonant modes being the ones such satisfying $k_{\parallel} \sim 0$. The reasoning is the following. The parallel gradient of any 3D field ϕ can be computed by finite differences along the parallel direction s . At second order, it reads:

$$R\nabla_{\parallel}^{FA}\phi(r, \xi, s) \approx \frac{\phi(r, \xi, s + \Delta s) - \phi(r, \xi, s - \Delta s)}{2\Delta s} \quad (4.33)$$

where R is the major radius and the superscript FA stands for field-aligned coordinates. $\Delta s = \Delta\varphi = 2\pi/N_{\varphi}$ is the increment in the parallel direction (N_{φ} being the number of toroidal grid points), and ξ denotes the second coordinate orthogonal to the magnetic field \mathbf{B} (typically, $\xi = \theta - \varphi/q(r)$). In terms of poloidal and toroidal Fourier modes (using the change of variables $(\xi, s) \rightarrow (\theta, \varphi)$, with $\theta = \xi + \varphi/q$ and $\varphi = s$), such an expression leads to:

$$\begin{aligned} R\nabla_{\parallel}^{FA}\phi(r, \xi, s) &= \frac{1}{2\Delta s} \sum_{m,n} \hat{\phi}_{m,n}(r, t) \\ &\quad \left\{ e^{im[\xi+(s+\Delta s)/q]+in(s+\Delta s)} - e^{im[\xi+(s-\Delta s)/q]+in(s-\Delta s)} \right\} \\ &= \sum_{m,n} \hat{\phi}_{m,n}(r, t) e^{i(m\theta+n\varphi)} \frac{e^{i\Delta\varphi(n+m/q)} - e^{-i\Delta\varphi(n+m/q)}}{2\Delta\varphi} \\ &= \sum_{m,n} \hat{\phi}_{m,n}(r, t) e^{i(m\theta+n\varphi)} \frac{i \sin[(n+m/q)\Delta\varphi]}{\Delta\varphi} \end{aligned} \quad (4.34)$$

It turns out that the normalized effective parallel wave vector then reads:

$$k_{\parallel}^{FA} = \frac{\sin(Rk_{\parallel}\Delta\varphi)}{R\Delta\varphi} = k_{\parallel} \text{sinc}(Rk_{\parallel}\Delta\varphi) \quad (4.35)$$

where k_{\parallel} stands for the actual parallel wave vector at this resolution:

$$Rk_{\parallel} = n + \frac{m}{q}$$

In this framework, the resonant modes are such that their effective parallel wave number is vanishing $k_{\parallel}^{FA} = 0$. This leads to the following relationship:

$$k_{\parallel}^{FA} = 0 \Leftrightarrow n_{res} = -\frac{m}{q} + \frac{\ell\pi}{\Delta\varphi} = -\frac{m}{q} + \frac{\ell N_{\varphi}}{2} \quad (\text{with } \ell \in \mathbb{Z}) \quad (4.36)$$

In this case, even large m modes can be coupled to “resonant” (i.e. such that $k_{\parallel}^{FA} = 0$) low n modes. As a matter of fact, given a maximum poloidal wave number m_{max} which needs

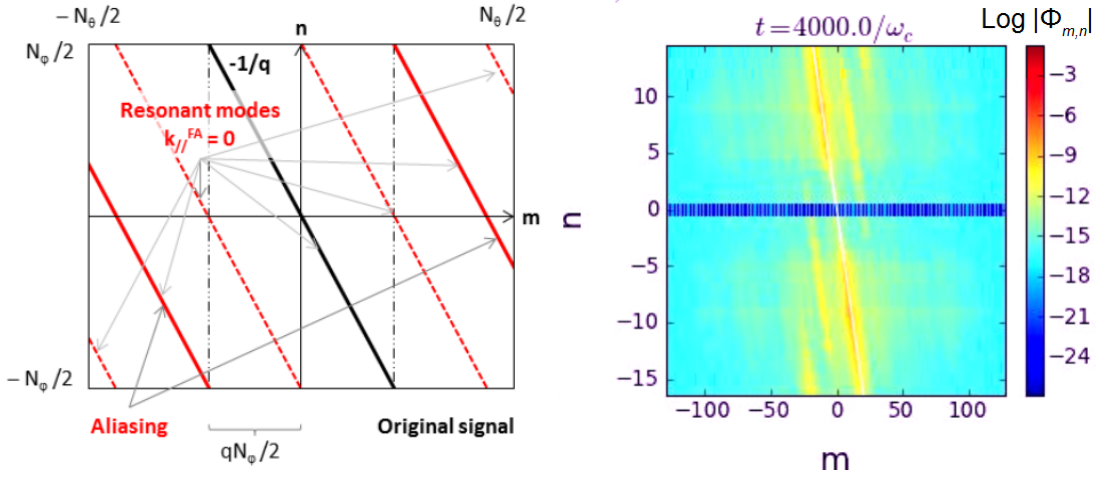


Figure 4.17: (a) Expected and (b) obtained 2D Fourier spectrum (m, n) of any fluctuating field $\phi(r, \theta, \varphi)$ using the aligned coordinate scheme. Fig.(b) has been obtained with the trapped kinetic electron model. Fig.(a) shows three kind of modes: the resonant (in black), folded (in red) and spurious (in dashed red) modes.

to be resolved, there is no need to go up to $n_{max} = -m_{max}/q$ in order to properly account for resonant modes at this small transverse scale: the toroidal n_{ℓ} modes characterized by $n_{\ell} = -m_{max}/q + \ell\pi/\Delta\varphi$ will already do the job.

Aliasing and resonances

Let us now consider the case of an under resolved simulation in φ using field aligned coordinates to compute parallel derivatives. By under resolved, we mean that resonant modes such that $m + nq = 0$ will still have a large magnitude at the smallest resolved scale in φ , namely for $(m, n) = (\mp qN_{\varphi}/2, \pm N_{\varphi}/2)$. Aliasing (see Appendix D.3) will result in the appearance of off-diagonal modes in the 2D (m, n) Fourier spectrum of the signal, depicted by the red-solid lines on Fig. 4.17.a. These modes will still be treated as resonant by the code (although $m+nq \neq 0$) since their effective parallel wave vector k_{\parallel}^{FA} is vanishing. However, these are not the only modes which are considered as resonant within the field-aligned approach. Indeed, Eq.(4.36) shows that additional off-diagonal bands are also to be considered as resonant (dashed-red lines on Fig. 4.17.a). In a GYSELA simulation, after a reorganization phase, we observe on Fig.4.17.b the appearance of the three types of modes mentioned earlier:

- The **resonant** modes satisfying $m/n = -q$ (black line of Fig.4.17.a).
- The **"folded"** modes due to aliasing and corresponding in fact to the modes such that $|n| > N_{\varphi}/2$ (red lines of 4.17.a).
- Other **"spurious"** modes that are resonant in the field-aligned approach but which

are neither the ones satisfying $m/n = -q$ nor the ones explained by aliasing which are considered (dashed-red lines on Fig. 4.17.a).

In our case, $N_\varphi = 32$ and the modes $n > 16$ (resp. $n < -16$) will appear at the toroidal frequencies $n - N_\varphi$ (resp. $N_\varphi - n$). We take the ITG-like case in which we initially excite the set of resonant modes for $n \in [-10, 10]$. In order to launch non-linear tests, it is necessary to ensure that the folded and spurious modes do not interfere with the resonant modes with a m/n value close to $-q$. If the value of N_φ is too small, the resonant modes and the spurious modes overlap. This could alter the predictions of turbulent transport and should therefore be avoided. To circumvent this problem, we add a "diagonal filter" which retains only the diagonal band $m = -nq$ and those corresponding to folded modes. The width Δm of these bands must be chosen both to retain these modes while eliminating the spurious modes. The gap in m between the spurious modes and the original signal being $qN_\varphi/2$, a possible choice is to retain only the modes $m \in [-qn - \Delta m/2; -qn + \Delta m/2]$ with $\Delta m = qN_\varphi/2$.

4.4 First results of non-linear simulations

Using the strategy described in section 4.3, some first non-linear simulations were launched with the trapped kinetic electron model. In this section, we present some results to validate the trapped kinetic electron model. To do so, we compare the results obtained with the 2 limit cases ITG-dominant and TEM-dominant mentioned earlier. We use the same parameters as those described in section 4.2.1. We use Neumann boundary conditions without any source of particle or energy. The initial potential perturbation is taken as $\phi_{m,n_0}(t=0) = 10^{-5} \exp\{-(m/n_0 + q)^2\}$ in normalized units. Besides, we use a mass ratio $m_i/m_e = 100$ and we recall the form of density and temperature profiles given by Eq.(4.26):

$$X(r, t=0) = \exp\left\{-\frac{R_0}{L_X} \delta \tanh\left(\frac{\rho - \rho_{peak}}{\delta}\right)\right\}$$

where X stands for either n , T_i or T_e . We have $\delta = 0.3$, $R_0/L_n = 2.22$ and $R_0/L_{T_e} = 6.92$ in both cases. Besides, we choose (i) $R_0/L_{T_i} = 6.92$ in the ITG-dominant case and (ii) $R_0/L_{T_i} = 0.5$ in the TEM-dominant case. Furthermore, we use the aligned coordinates method described in section 4.3.2. We also introduce in both cases the same initialization as the one used in part 4.3.1. In particular, we use the same filter to eliminate the modes $(m, n=0)$ with $m \neq 0$. The discretization used in these simulations is $N_r = 255$, $N_\theta = 256$, $N_\varphi = 32$, $N_{v_\parallel} = 127$ and $N_\mu = 15$ and the time step is $\Delta t = 2\omega_{c0}^{-1}$. Both cases were launched using the Marconi machine on the Broadwell partition. Each case made 15000 iterations on 4608 processors for a total computational time of 200 000 CPU hours. It should be stressed that the two simulations presented here are at the minimum possible resolution in terms of time step, spatial and μ discretization. The discretization should be increased for future non-linear tests. The cost of such simulations would be rather 1 million CPU hours. The following study aims to show that some simple physical statements can be verified with this kinetic electron model.

First, we look at the evolution and structure of the potential. Then we study the energy transfer from the electric wave to particles in order to verify which species is responsible for the instability in each case. Finally, we check that the conservation of energy is well satisfied using our model.

4.4.1 Potential structure

Fig.4.18 shows the evolution of the modes (m, n) of the electric potential which are dominant at $t = 30000\omega_{c0}^{-1}$. We recognize up to $t \simeq 17000\omega_{c0}^{-1}$ the linear growth phase of the resonant modes seen in the linear analysis and then the saturation of these modes at their maximum level during the non-linear phase that follows. It can be noted here that the mode ϕ_{00} grows very fast and independently with other modes. This mode is not only due to turbulence: it also participates to the radial force balance $E_r = \frac{1}{e}\nabla_r p - v_\theta B_\varphi + v_\varphi B_\theta$. It is possible that it is this contribution which appears very early, before the turbulence contributes to it. Besides, an "accident" seems to appear in both cases ($t = 20000$ for

the ITG case, $t = 15000$ for the TEM case). One should keep in mind that what is plotted corresponds to the value of ϕ_{00} at a given radius (r_{peak}). However ϕ_{00} has a radial structure, which oscillates around 0. If these oscillations move slightly, ϕ_{00} may change sign in r_{peak} , passing through 0. This is probably the case in the accident at $t = 20000$. Thereafter, we choose to explore the potential structure in the non-linear phase at the two times $t = 20000 \omega_{c0}^{-1}$ and $t = 25000 \omega_{c0}^{-1}$.

Fig.4.20 shows the poloidal profiles of the potential fluctuations $\phi - \phi_{00}$ in the non-linear phase at the times mentioned earlier. We recognize a ballooned structure, i.e. the fluctuations are greater in the low field side than in the high field side. This is a characteristic of an interchange-type instability. It can be noted here that in Fig.4.18 the case ITG-dominant seems to enter the non-linear phase before the TEM-dominant case. This explains that potential poloidal profile in Fig.4.20 seems to have a more advanced structure in the ITG-dominant case than in the TEM-dominant one. Besides, the potential structures seem to be larger in the TEM-dominant case than in the ITG-dominant one. In certain ranges of plasma parameters, zonal flows are known to be less efficient to stabilize TEM turbulence than ITG turbulence [4, 62, Asahi 2014, Merz 2008], hence letting potential structures to become larger in the TEM-dominant case. If we look at the $d_r \phi_{00}$ profiles on Fig.4.19 at the final time, the shears seem to be of the same order of magnitude ($\sim 3.10^{-3}$) and present similar profiles, with a large layer of central shear ($\rho \sim 0.5 - 0.6$) and not much elsewhere. The history is quite difficult to compare because of differences in color scale, but shear levels do not seem to differ greatly between the two simulations ITG-dominant and TEM-dominant. In fact, the shear seems to be almost the same in both situations but its effect on turbulence is different: differences in radial scales observed on potential fluctuations (Fig.4.20) could result from the fact that TEMs are less sensitive to a given shear than the ITGs. That would be consistent with the literature.

We show on Fig.4.21 the Fourier transform in (θ, φ) of the previous potential profiles in the non-linear phase at the same times as before. The blue horizontal band $n = 0$ corresponds to the modes ($m \neq 0, n = 0$) which were removed here as said earlier. We verify that in the non-linear phase, the resonant modes (m, n) satisfying $k_{\parallel} = 0$ remain dominant in the non-linear phase. We also notice the presence of the folded modes mentioned in section 4.3.2. Besides, we see that the spurious modes, presented in the same section, appear in the ITG-dominant case.

4.4.2 Energy conservation

We now want to check that the energy conservation equation established in Appendix D.1 is verified in the non-linear phase for the two cases: ITG-dominant and TEM-dominant. The energy conservation for a given species reads as follows:

$$V \partial_t \langle \mathcal{E} \rangle_{FS} + \partial_{\chi} (V \langle Q^x \rangle_{FS}) = -e \left\langle \int d^3v (\mathbf{v}_{\parallel} + \mathbf{v}_E + \mathbf{v}_D) \cdot \nabla \bar{\phi} \bar{f} \right\rangle_{FS} \quad (4.37)$$

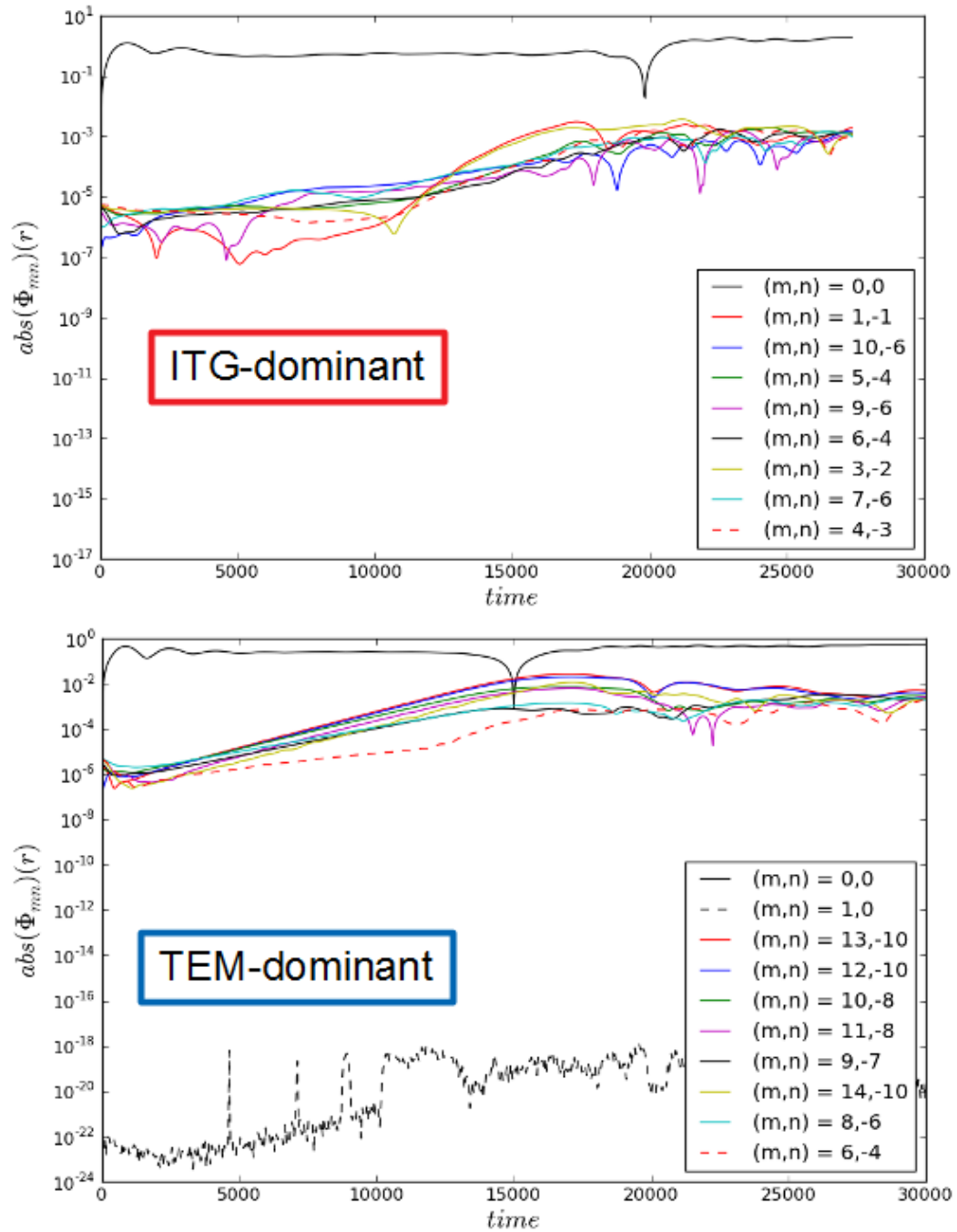


Figure 4.18: Evolution of resonant modes for the ITG-dominant and TEM-dominant cases.

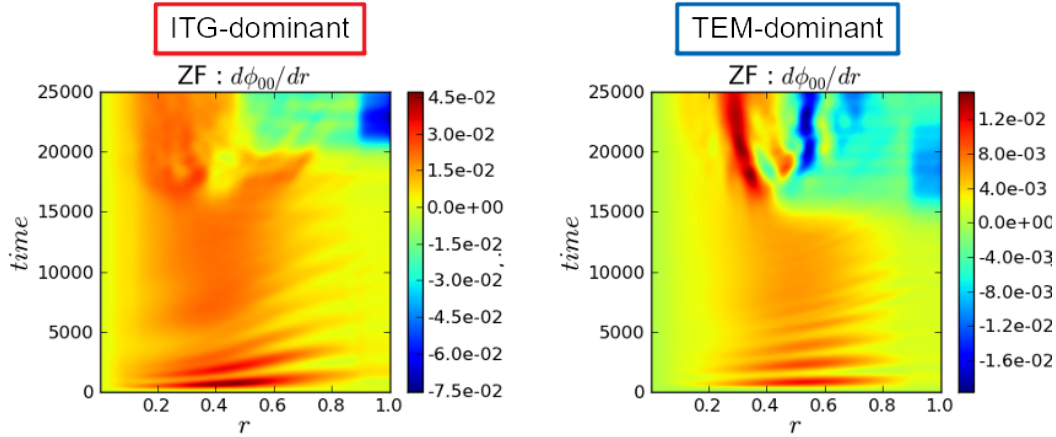


Figure 4.19: Evolution of the radial profile of $d_r \phi_{00}$ for the ITG-dominant and TEM-dominant cases.

where the flux surface average has been defined as $\langle \dots \rangle_{FS} = V^{-1} \int d\theta d\varphi \sqrt{g} \dots$ with $V = \int d\theta d\varphi \sqrt{g}$ and $\sqrt{g} = Rr \frac{dr}{dx}$ the Jacobian in position coordinates. The term $V \partial_t \langle \mathcal{E} \rangle_{FS}$ stands for the time variation of the kinetic energy of the considered species. The term $\partial_\chi (V \langle Q^x \rangle_{FS})$ represents the radial energy transport within the tokamak. The right hand side corresponds to the energy transferred from the electric wave to particles, also written $\int \mathbf{J}_s \cdot \mathbf{E} d^3v$ where \mathbf{E} stands for the electric field and $\mathbf{J}_s = e_s (\mathbf{v}_\parallel + \mathbf{v}_E + \mathbf{v}_{Ds}) \bar{f}_s$, \mathbf{v}_\parallel , \mathbf{v}_E , \mathbf{v}_D being respectively the parallel velocity, the electric and magnetic drifts and \bar{f} the gyrokinetic distribution function of the considered species. This term has a particular significance and is studied in more details in the next section.

Fig.4.22 shows the radial profiles of the different terms involved in the energy conservation equation (4.37) for the two species. Figs.4.23 and 4.24 shows the same diagnostic for each species. We observe that the energy conservation is well satisfied for ions and electrons. Besides, we can notice that the terms $\partial_\chi \langle Q_E \rangle_{FS}$ and $\partial_\chi \langle Q_D \rangle_{FS}$ are opposite [32, Garbet 2016]. It is interesting to note that the exchanged energy between wave and particles $e\bar{\phi}\partial_t n$ in green in Figs.4.23 and 4.24 is much lower than the other terms involved in the conservation equation.

4.4.3 Energy transfer between the electric wave and particles

The method mentioned in section 4.2.3 to determine the nature of the instability is difficult to use during the non-linear phase because the potential profile is very heckled. However, we can look at the energy transferred to the wave by the ions and electrons of the plasma. We expect that in an ITG turbulence it is mainly the ions that supply the energy to the wave and conversely that it is the electrons that provide the energy to the wave in a TEM turbulence. In Appendix D.1.2, this energy transfer is derived and reads as $\int \mathbf{J}_s \cdot \mathbf{E} d^3v$ as mentioned in section 4.4.2. It is shown in particular that the energy

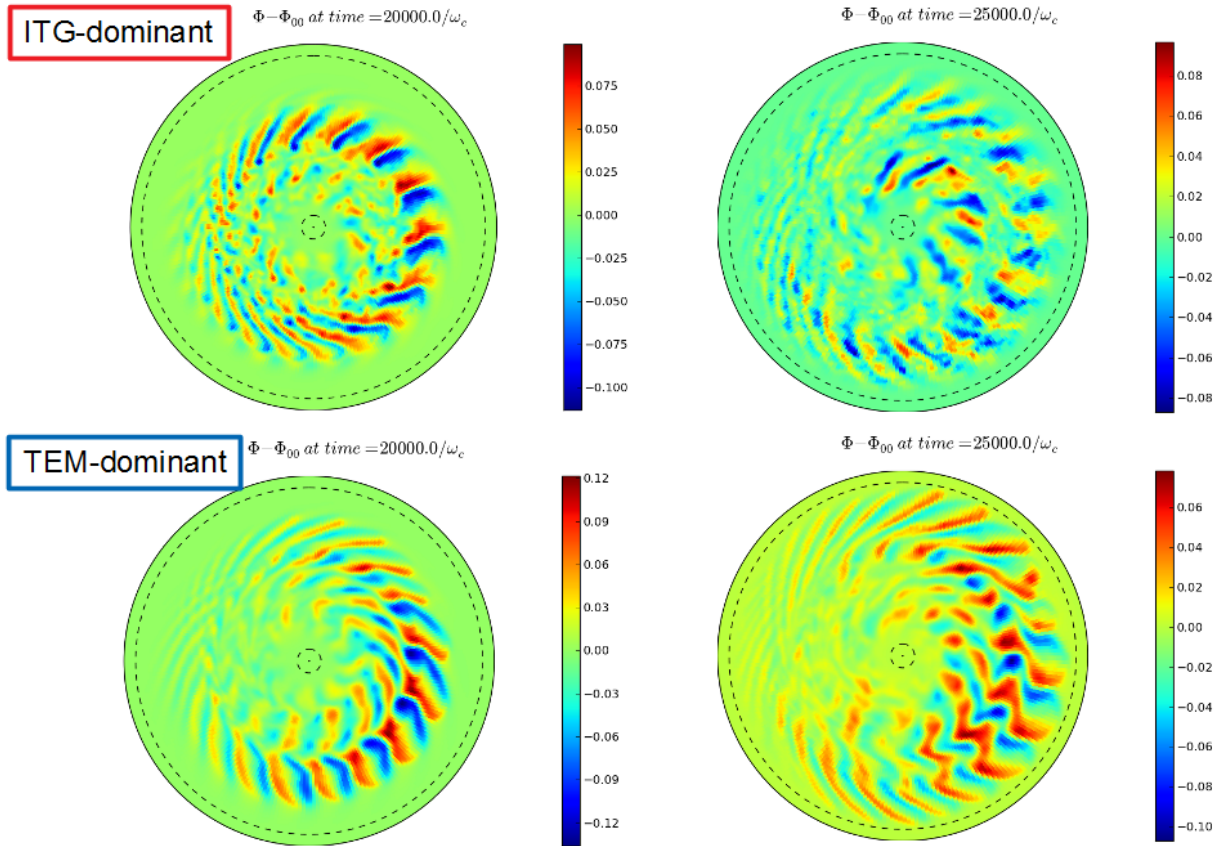


Figure 4.20: Poloidal profile of the potential fluctuations $\phi - \phi_{00}$ at the times $t = 20000 \omega_{c0}^{-1}$ and $t = 25000 \omega_{c0}^{-1}$ for the ITG-dominant and TEM-dominant cases. $t = 20000 \omega_{c0}^{-1}$ corresponds to the beginning of the non-linear phase.

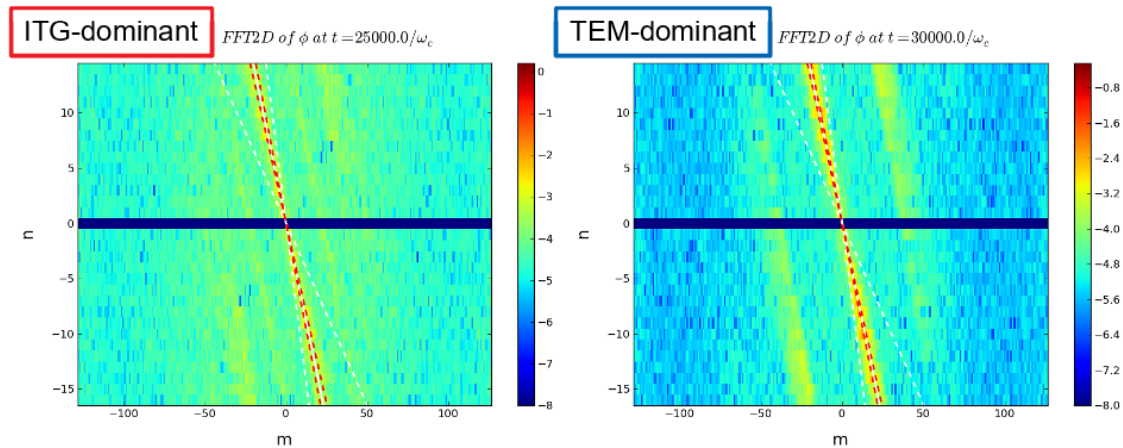


Figure 4.21: Fourier transform of the poloidal profile of the potential for the ITG-dominant and TEM-dominant cases.

transfer associated to the electric drift is vanishing and that the term associated to the parallel drift is negligible compared to the one due to the gradients and curvature of the magnetic field. This is consistent with the fact that the instability is of the "interchange" type, i.e. governed by the inhomogeneity of B (as well as the inhomogeneities of n and T). Consequently, the energy transfer term reduces to $\int \mathbf{J}_D \cdot \mathbf{E} d^3v$ where $\mathbf{J}_D = e\mathbf{v}_D \bar{f}$. We show on Fig.4.25 the energy transfer wave to particle from $t = 0$ to $t = 25000\omega_{c0}^{-1}$ with GYSELA.

We find that in the ITG-dominant case, it is indeed the ions that give energy to the electric wave. For the TEM-dominant case, both species participate in the instability. We can see on both plots that the radial profiles are perturbed. The high variations between neighbouring points observed in the ITG-dominant case are typical of a too low resolution. It is known that the radial step is too small to fully resolve our simulations and this could explain these profiles. In the TEM-dominant case however, the perturbations seem to have a larger radial period. It is therefore unclear whether these corrugations observed on the energy transfer profiles are a kinetic signature of electrons as explained in Appendix D.4 or a mere consequence of a low spatial resolution. Future simulations would require decreasing the radial step to check this last point.

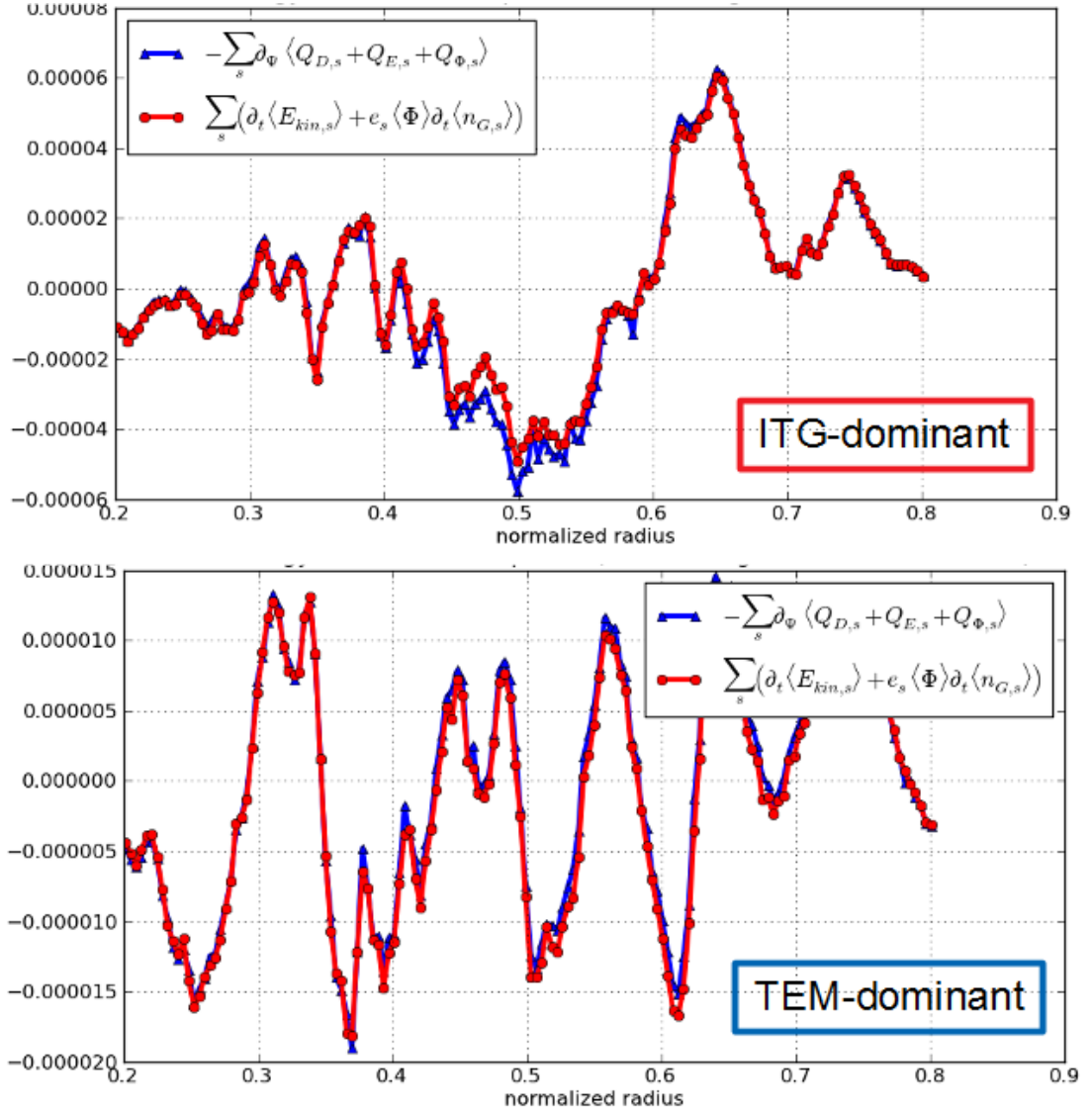


Figure 4.22: Local energy balance for all species at time $t = 20000 \omega_{c0}^{-1}$ for the ITG-dominant case and $t = 25000 \omega_{c0}^{-1}$ for the TEM-dominant case.

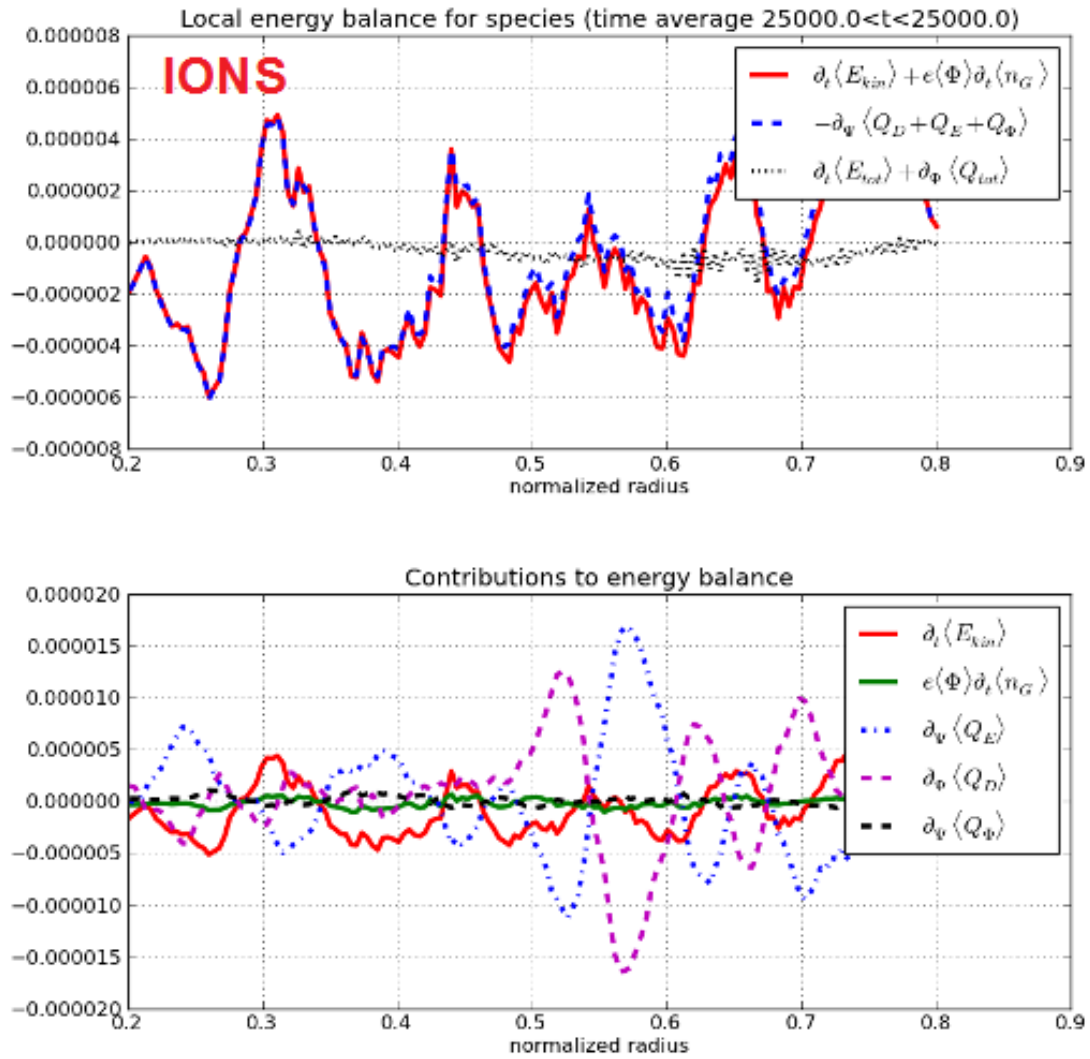


Figure 4.23: Local energy balance for ions at time $t = 25000 \omega_{c0}^{-1}$ for the TEM-dominant case.

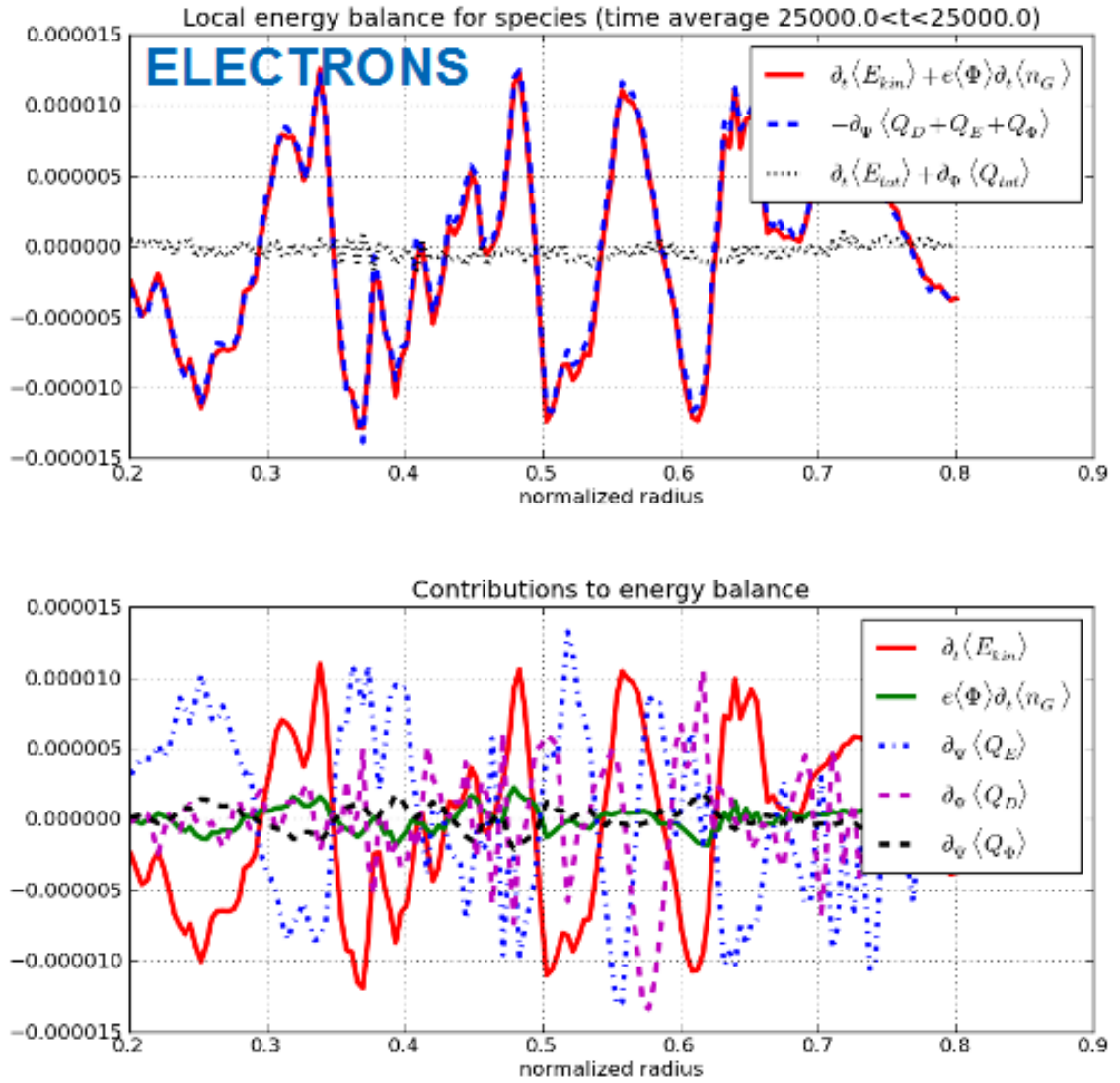


Figure 4.24: Local energy balance for electrons at time $t = 25000 \omega_{c0}^{-1}$ for the TEM-dominant case.

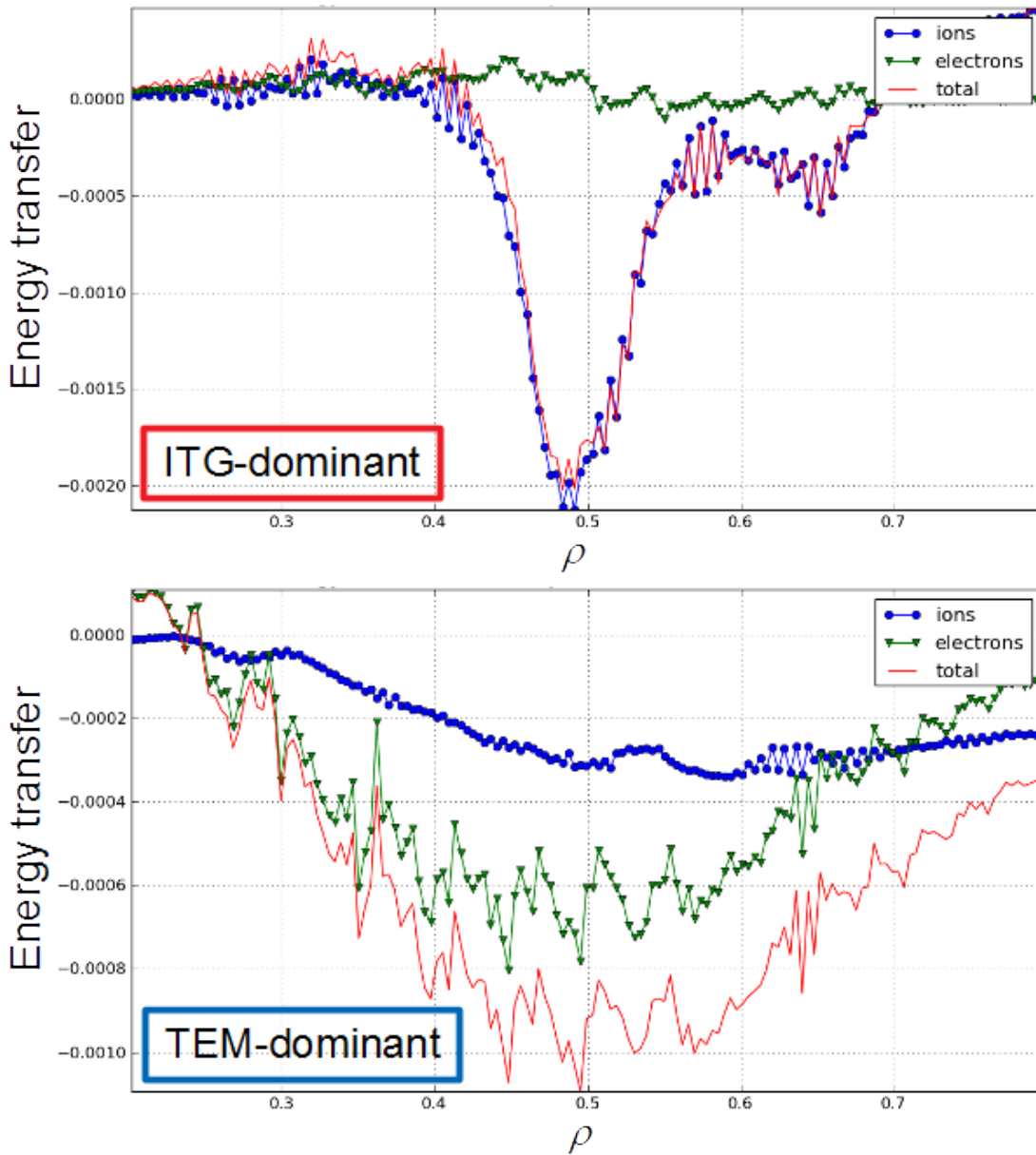


Figure 4.25: Energy transfer normalized to T_0 from the electric wave to particles from $t = 0$ to $t = 25000 \omega_{c0}^{-1}$ on the radial domain. A negative value means that particles give energy to the wave.

4.5 Conclusion

In this chapter, several results have been seen:

- The ITG instability is recovered for large values of R_0/L_{T_i} and the TEM instability for small values of R_0/L_{T_i} while keeping the parameter R_0/L_{T_e} constant.
- The linear behaviour of the codes GYSELA and GT5D is similar. The deviations observed between the two codes are less than 10%. These may be due to the low discretization used in GYSELA and/or to the differences of simulation parameters (in particular ρ^*).
- One should remove the modes ($m \neq 0, n = 0$) to avoid the apparition of the so-called ω_H mode. This mode appears here because the model is electrostatic and it should not be present in an electromagnetic simulation.
- The aligned coordinates method enables to reduce the number of points in the toroidal direction by a factor 4 to 8, hence reducing the overall cost of simulations. So far, this method requires the use of a diagonal filter in the Fourier space so as to remove spurious modes specific to that method.
- In the first non-linear simulations, we saw on the one hand, that the potential structure shows a ballooned shape with the resonant modes $k_{\parallel} = 0$ which become dominant as expected. On the other hand, the energy transfer diagnostic indicates that ions give energy to the wave in the case of an ITG instability and that both ions and electrons participate to the growth of the considered TEM instability, the role of electrons being dominant. Moreover, the energy conservation seems to be globally satisfied for both species.

Conclusion

Providing an adiabatic treatment to electrons is not an unreasonable assumption for a turbulence dominated by ions. In this case, the structures of the modes are made at large scales and evolve over times much longer than the evolution times of electrons. Indeed, the fast parallel dynamics of the electrons allows them to stay in phase with ion turbulence structures, hence leading to an adiabatic response of the electrons. Nevertheless, this approach misses some important physical issues:

- Near the resonance surfaces $k_{\parallel} = 0$, the response of electrons is non-adiabatic.
- In an adiabatic electron model, the turbulent particle transport is almost vanishing.
- The turbulence carried by electrons is not taken into account when electrons are adiabatic.

Accessing this physics thus requires to go beyond the frame of adiabatic electrons. Some codes have already taken this step and the aim of this thesis is to do the same for the GYSELA code. A kinetic electron model has been developed in which a gyrokinetic equation is added to describe the temporal evolution of the electron distribution function on the one hand and in which the quasi-neutrality equation is modified to take into account the new kinetic form of the electron density on the other hand. The high cost of such full kinetic simulations has led us to develop a third hybrid model between the adiabatic electron model and the kinetic electron model in which only the trapped electrons are treated kinetically. This intermediate model has the advantage of allowing less expensive simulations by artificially reducing the mass ratio m_i/m_e while still recovering some of the physics of the trapped electrons. Eventually, we end up with three different models to treat electrons:

- The **Adiabatic Electron (AE)** model where all electrons have an adiabatic response.
- The **Full Kinetic Electron (FKE)** model where all electrons are described by a kinetic distribution function.
- The **Trapped Kinetic Electrons (TKE)** model in which it is possible to give a kinetic response only to a part of the electrons (usually the trapped ones) and to treat the rest adiabatically.

First, we have looked at the impact of kinetic electrons on the damping of Geodesic Acoustic Modes (GAM). The damping of GAMs is part of the Rosenbluth-Hinton test which is a well known test to benchmark and verify gyrokinetic codes. The comparison between simulations run with the Adiabatic Electron model and the Full Kinetic Electron model showed that the GAM pulsation remains almost unchanged in the presence of kinetic electrons in agreement with theoretical predictions. Conversely, the GAM damping rate is increased for large values of the safety factor. The theory to predict the pulsation and damping rate of GAMs existed only for adiabatic electrons models. In this thesis, the contribution of electrons to GAM damping has been derived. It appears that this contribution is usually not negligible thanks to a resonance between barely trapped/passing electrons bounce/transit frequency and the mode pulsation. Damping is estimated via the computation of the energy exchanged between the mode and electrons. This expression appears to be quite intricate as it involves a quadruple integral over the phase space and poloidal angles. A more tractable expression is obtained by assuming a strong weight of trapped particle bounce points in this integral. The ratio between the exact result and the approximate is a weight function that depends only on a dimensionless number, which characterises the ratio of the mode to trapped electrons bounce frequencies. This weight function thus measures the number of resonant electrons that participate in mode damping. Comparison with available data in the literature suggests that this weight function is nearly constant and close to 1, thus confirming a prominent role of barely trapped particles. In addition, under suitable assumptions, the model recovers that the damping rate evolves with the mass ratio as $(m_i/m_e)^{-1/2}$, in agreement with three gyrokinetic codes, namely GYSELA, ORB5 and GENE [7, Biancalani 2017].

This work also enabled to look at the impact of kinetic electrons on the linear growth of the Ion Temperature Gradient (ITG) and Trapped Electron Mode (TEM) instabilities. We use the Trapped Kinetic Electron model at low mass ratio $m_i/m_e = 100$ to save numerical resources and we look at both the sign of the poloidal pulsation and the energy transfer from the electric wave to the ions and electrons of the plasma to determine the type of instability, ITG or TEM. It appears that temperature gradients have a very big impact on the type of instability in presence : a high electron temperature gradient implies the trapped electrons provide energy to the electric wave, whereas a high ion temperature gradient implies the ions excite the wave. Besides the transition between ITG and TEM dominated regimes is clearly observed while changing the radial gradient of the ion temperature for a fixed electron temperature profile. However, we did not recover the transition when increasing the value of the wavevector of the mode, interpreted as a result of a too coarse mesh grid, constrained by numerical resources. Finally, we set up the frame for future simulations to build non linear cases that could enable to study the influence of kinetic electrons on turbulent transport. First, it is important to filter the modes of poloidal number $m = 0$ and those of toroidal number $n = 0$ except for the zonal flow $(m, n) = (0, 0)$. This operation eliminates the ω_H mode which is the low β response of the kinetic Alfvén wave and appears only in electrostatic simulations. The appearance of this mode is accompanied by a radial particle and energy transport

that should not occur in the electromagnetic case. Therefore, this mode has been safely filtered out. Second, the aligned coordinate method developed in [45, 57, Hariri 2013, Latu 2018] is to be preferred since it gives results similar to the non-aligned method for a much lower numerical cost. It should be used in conjunction with a diagonal filter to avoid the growth of spurious non-resonant modes.

The first step to continue this work would be to measure the transport coefficients with and without kinetic electrons. This study should provide a first glimpse of the impact of kinetic electrons on turbulent transport. To complete this first study, one should add the possibility of using the particle source that has been discussed in the end of chapter 2 and treat the collision term electron-ion that is not implemented in the current version of the code although it is of the same order of magnitude as the collision term ion-ion. Finally, one should get rid of the electrostatic hypothesis by adding the Ampere equation to the gyrokinetic system in order to solve the evolution of the magnetic field. This electromagnetic model would thus take into account all the magnetic modes.

Appendices

Appendix A

Appendices of chapter 1

A.1 Expression of the intrinsic angle θ^*

We are looking for the expression of θ^* as a function of the poloidal geometric angle θ , and the poloidal flux ψ . In particular, the ratio $d\theta^*/d\theta$ will be computed.

We introduce \mathbf{A} as the vector potential. Assuming that there is no radial current, \mathbf{A} can be developed in a suitable base $(\nabla\psi, \nabla\theta^*, \nabla\varphi)$ as:

$$\mathbf{A} = \Psi_T \nabla\theta^* + \Psi_P \nabla\varphi$$

where Ψ_T and Ψ_P are for now undetermined quantities depending of ψ only. It is then possible to compute $\mathbf{B} = \nabla \wedge \mathbf{A}$:

$$\mathbf{B} = \nabla\Psi_T \wedge \nabla\theta^* + \nabla\Psi_P \wedge \nabla\varphi$$

The projection of \mathbf{B} on the vectors of the contravariant basis yields:

$$\begin{aligned} \mathbf{B} \cdot \nabla\psi &= 0 \quad \text{by definition, } \mathbf{B} \text{ is tangent to magnetic surfaces} \\ \mathbf{B} \cdot \nabla\theta^* &= -J \frac{d\Psi_P}{d\psi} \quad \text{with } J = \nabla\psi \cdot (\nabla\theta^* \wedge \nabla\varphi) \\ \mathbf{B} \cdot \nabla\varphi &= J \frac{d\Psi_T}{d\psi} \end{aligned} \tag{A.1}$$

It can be shown that by averaging the quantities Ψ_T , Ψ_P on the magnetic surfaces of the tokamak, we see that they correspond up to a factor 2π , to the toroidal and poloidal flux values respectively ([68, Rax 2012] p.165).

The safety factor expression can be found by noticing that:

$$q(\psi) \equiv \left. \frac{d\varphi}{d\theta^*} \right|_{LC} = - \frac{d\Psi_T}{d\Psi_P} = \frac{\mathbf{B} \cdot \nabla\varphi}{\mathbf{B} \cdot \nabla\theta^*} \tag{A.2}$$

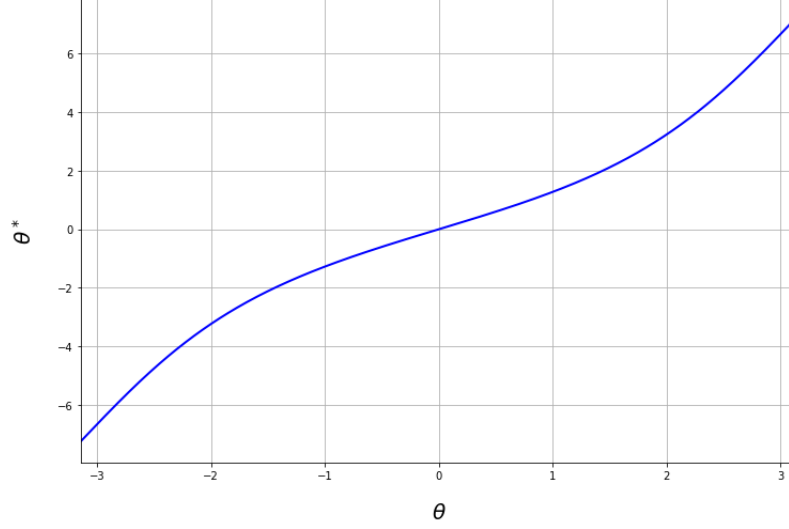


Figure A.1: Evolution of the intrinsic angle θ^* depending on the poloidal angle θ as predicted by Eq.(A.4). Here, we have chosen $\varepsilon = 0.3$, $q = 2$ and $\Delta = 0.01$.

In order to find the relation $\theta^*(\psi, \theta)$, let us compute the ratio $d\theta^*/d\theta$:

$$\frac{d\theta^*}{d\theta} = \frac{\mathbf{B} \cdot \nabla \theta^*}{\mathbf{B} \cdot \nabla \theta} = \frac{\mathbf{B} \cdot \nabla \varphi}{q\mathbf{B} \cdot \nabla \theta}$$

Hence it comes

$$\theta^*(\psi, \theta) = \int_0^\theta d\vartheta \frac{\mathbf{B} \cdot \nabla \varphi}{q(\psi)\mathbf{B} \cdot \nabla \vartheta} \quad (\text{A.3})$$

with $\mathbf{B} \cdot \nabla \varphi = \frac{B_\varphi}{R}$ and $\mathbf{B} \cdot \nabla \theta = \frac{B_\theta}{r}$ with R and r being resp. the major and minor radius of the position. Ampere's law implies $B_\varphi R = B_{\varphi 0} R_0$ with R_0 the major radius at the center of the tokamak, $B_{\varphi 0}$ the toroidal field B_φ at R_0 . As an approximation, one can choose for the expression of the poloidal field: $B_\theta = B_{\theta 0} \left(1 + \Delta \frac{r}{R_0} \cos \theta\right)$ with Δ the Shafranov shift and $B_{\theta 0}$ a function of ψ . Knowing moreover, that $R = R_0 \left(1 + \frac{r}{R_0} \cos \theta\right)$, equation (A.3) becomes:

$$\theta^*(\psi, \theta) = \int_0^\theta d\vartheta \frac{r B_{\varphi 0} R_0}{R_0^2 B_{\theta 0}} \left(1 + \frac{r}{R_0} \cos \vartheta\right)^{-2} \left(1 + \Delta \frac{r}{R_0} \cos \vartheta\right)^{-1} \quad (\text{A.4})$$

Fig.A.1 shows the evolution of θ^* when θ varies.

A.2 Change of coordinates from particle to gyrocentre

A.2.1 Canonical change of coordinates for \bar{f} : $(\mathbf{q}_{gy}, \mathbf{p}_{gy})$ to $(\mathbf{q}_{GC}, \mathbf{p}_{GC})$

Introduction of the gyro-centre

To define correctly the gyrocentre, we first write the Hamiltonians describing a particle and its guiding centre, and second we choose a good form of the Hamiltonian of the gyrocentre, with the constraint that it should be independent of the gyroangle φ_c .

The Hamiltonian associated with a particle of mass m , charge e at coordinates (\mathbf{q}, \mathbf{p}) is given by:

$$H(\mathbf{q}, \mathbf{p}, t) = \frac{1}{2}mv_{\parallel}^2 + \mu B + e\phi(\mathbf{x}, t) \quad (\text{A.5})$$

The magnetic moment is an adiabatic invariant. At leading order, the value of μB calculated at the position of the guiding centre can be approximated by μB calculated at the position of the particle. The Hamiltonian of the guiding centre associated to the coordinates $(\mathbf{q}_{GC}, \mathbf{p}_{GC})$ is then given by:

$$H_{GC}(\mathbf{q}_{GC}, \mathbf{p}_{GC}, t) = \frac{1}{2}mv_{GC\parallel}^2 + \mu B + e\phi_{GC}(\mathbf{x}_{GC}, t)$$

where $\phi_{GC}(\mathbf{x}_{GC}, t)$ is the potential observed by a given guiding centre at the position \mathbf{x}_{GC} . For each couple guiding centre-particle, the same potential is observed. Thus, it comes the relation $\phi(\mathbf{x}, t) = \phi_{GC}(\mathbf{x}_{GC}, t)$. Indeed, the same physical reality is seen from the point of view of the particle and the guiding centre, in the same way as for the distribution functions (cf. Eq.(1.63)). To express $\phi_{GC}(\mathbf{x}_{GC}, t)$ as a function of ϕ at point \mathbf{x}_{GC} , it is needed to process a change of coordinates from \mathbf{x} to \mathbf{x}_{GC} which consists in making a limited development in $\mathbf{x} - \mathbf{x}_{GC} = \boldsymbol{\rho}_c$. Let F be a function of \mathbf{x}_{GC} that we want to express in \mathbf{x} . This can be written as:

$$F(\mathbf{x}_{GC}) = F(\mathbf{x}) - (\mathbf{x} - \mathbf{x}_{GC}) \cdot \nabla F|_{\mathbf{x}} + \dots \text{ with } \mathbf{x} - \mathbf{x}_{GC} = \boldsymbol{\rho}_c$$

which can also be written as:

$$F(\mathbf{x}_{GC}) = e^{-\boldsymbol{\rho}_c \cdot \nabla} F(\mathbf{x}) \quad (\text{A.6})$$

Thus, it is possible to write $\phi_{GC}(\mathbf{x}_{GC}, t)$ as:

$$\phi_{GC}(\mathbf{x}_{GC}, t) = \phi(\mathbf{x}, t) = \phi(\mathbf{x}_{GC} + \boldsymbol{\rho}_c, t) = e^{\boldsymbol{\rho}_c \cdot \nabla} \phi(\mathbf{x}_{GC}, t)$$

It is then possible to derive the final form of $H_{GC}(\mathbf{q}_{GC}, \mathbf{p}_{GC}, t)$:

$$H_{GC}(\mathbf{q}_{GC}, \mathbf{p}_{GC}, t) = \frac{1}{2}mv_{GC\parallel}^2 + \mu B + ee^{\boldsymbol{\rho}_c \cdot \nabla} \phi(\mathbf{x}_{GC}, t) \quad (\text{A.7})$$

The fundamental point to notice here is that, due to the variations of the value of the local electric field on scales of the Larmor radius, H_{GC} **depends of the gyroangle**

φ_c even when considered at the position of the guiding centre (cf. [11, Brizard 2007] p. 423). The dependency in φ_c comes from the fact that in the expression of H_{GC} , the Larmor radius vector $\boldsymbol{\rho}_c$ depends on the gyroangle. Indeed, for different values of φ_c , the electric field seen by the particle is not the same, and this results in a modification of the Hamiltonian H_{GC} . To simplify our problem, a physical object, the gyrocentre, at coordinates noted $(\mathbf{q}_{gy}, \mathbf{p}_{gy})$, is introduced, and defined by its Hamiltonian, $\bar{H}(\mathbf{q}_{gy}, \mathbf{p}_{gy}, t)$, taken as the gyroaverage on the gyroangle of $H_{GC}(\mathbf{q}_{GC}, \mathbf{p}_{GC}, t)$:

$$\begin{aligned}\bar{H}(\mathbf{q}_{gy}, \mathbf{p}_{gy}, t) &= \int \frac{d\varphi_c}{2\pi} \{H_{GC}(\mathbf{q}_{GC}, \mathbf{p}_{GC}, t)\} \\ &= \frac{1}{2}mv_{GC\parallel}^2 + \mu B + e\bar{\phi}(\mathbf{x}_{gy}, t)\end{aligned}\quad (\text{A.8})$$

with $\bar{\phi}$ being the averaged value of ϕ on the gyroangle:

$$\bar{\phi}(\mathbf{x}_{gy}, t) = \left\{ \int \frac{d\varphi_c}{2\pi} \mathbf{e}^{\rho_c \cdot \nabla} \right\} \phi(\mathbf{x}_{GC}, t) \equiv J.\phi(\mathbf{x}_{GC}, t) \quad (\text{A.9})$$

As J involves only terms of even order, it is then possible to write equivalently $J = \left\{ \int \frac{d\varphi_c}{2\pi} \mathbf{e}^{-\rho_c \cdot \nabla} \right\}$. It will be useful to keep in mind that due to the construction of \bar{H} :

$$\partial_{\varphi_c} \bar{H}(\mathbf{q}_{gy}, \mathbf{p}_{gy}, t) = 0 \quad (\text{A.10})$$

Use of the generating function S from guiding-centres to gyrocentres

The old canonical coordinates $(\mathbf{q}_{GC}, \mathbf{p}_{GC})$ – that of the guiding centre – and the new ones $(\mathbf{q}_{gy}, \mathbf{p}_{gy})$ – those of the gyro-centre – only differ by infinitesimal quantities of order $\varepsilon \sim \rho_*$. They are related to each other by some infinitesimal canonical transform. In such a case, they can be shown to be related, at first order in the small parameter ε , by the generating function $\varepsilon S(\mathbf{q}_{GC}, \mathbf{p}_{GC})$ ¹ as follows (see [38, Goldstein 2002]):

$$\begin{cases} \mathbf{q}_{gy} - \mathbf{q}_{GC} &= \varepsilon \partial_{\mathbf{p}_{gy}} S \\ \mathbf{p}_{gy} - \mathbf{p}_{GC} &= -\varepsilon \partial_{\mathbf{q}_{gy}} S \end{cases}$$

At this point, the generating function εS remains to be determined. As explained later, it can be deduced from the expressions of the Hamiltonians associated with the old (guide centres) and the new (gyrocentres) coordinates (and the constraints put on their structures).

Using Taylor expansion at first order, any field F evaluated at the position $(\mathbf{q}_{GC}, \mathbf{p}_{GC})$ can then be expressed in terms of its value at $(\mathbf{q}_{gy}, \mathbf{p}_{gy})$:

$$F(\mathbf{q}_{GC}, \mathbf{p}_{GC}) = F(\mathbf{q}_{gy}, \mathbf{p}_{gy}) - \varepsilon [F, S]_{\mathbf{q}_{GC}, \mathbf{p}_{GC}} + O(\varepsilon^2) \quad (\text{A.11})$$

¹ Rigorously speaking, the generating function G is of the second kind: $G = G_2(\mathbf{q}_{GC}, \mathbf{p}_{gy}) - q_{gyro,i} p_{gyro,i}$, with $G_2 = q_{GC,i} p_{gyro,i} + \varepsilon S(\mathbf{q}_{GC}, \mathbf{p}_{gy}, t)$. Here, $(q_{GC,i} p_{gyro,i} - q_{gyro,i} p_{gyro,i})$ acts as the identity transform. The function S depends a priori on $S(\mathbf{q}_{GC}, \mathbf{p}_{gy}, t)$. At leading order in ε however, it can also be considered as a function of either $(\mathbf{q}_{GC}, \mathbf{p}_{GC})$ or $(\mathbf{q}_{gy}, \mathbf{p}_{gy})$, equivalently.

This is especially true for the Hamiltonian H_{GC} :

$$H_{GC}(\mathbf{q}_{GC}, \mathbf{p}_{GC}, t) = H_{GC}(\mathbf{q}_{gy}, \mathbf{p}_{gy}, t) - \varepsilon [H_{GC}, S]_{\mathbf{q}_{GC}, \mathbf{p}_{GC}} + O(\varepsilon^2) \quad (\text{A.12})$$

Here, $H_{GC}(\mathbf{q}_{gy}, \mathbf{p}_{gy}, t)$ stands for the *old* Hamiltonian (for which $(\mathbf{q}_{GC}, \mathbf{p}_{GC})$ are canonically conjugated), with \mathbf{q}_{GC} (resp. \mathbf{p}_{GC}) replaced by \mathbf{q}_{gy} (resp. \mathbf{p}_{gy}). A priori, it differs from the *new* Hamiltonian, $\bar{H}(\mathbf{q}_{gy}, \mathbf{p}_{gy}, t)$, for which $(\mathbf{q}_{gy}, \mathbf{p}_{gy})$ are canonically conjugated. The theory of canonical transformations ensures that H_{GC} and \bar{H} are related by the following relation:

$$\bar{H}(\mathbf{q}_{gy}, \mathbf{p}_{gy}, t) = H_{GC}(\mathbf{q}_{GC}, \mathbf{p}_{GC}, t) + \varepsilon \partial_t S + O(\varepsilon^2) \quad (\text{A.13})$$

On the other hand, the total time derivative of S reads: $d_t S = \partial_t S - [H_{GC}, S]$. By injecting Eq.(A.12) in Eq.(A.13), it readily appears that:

$$\bar{H}(\mathbf{q}_{gy}, \mathbf{p}_{gy}, t) = H_{GC}(\mathbf{q}_{gy}, \mathbf{p}_{gy}, t) + \varepsilon \frac{dS}{dt} + O(\varepsilon^2)$$

As will be checked a posteriori, the considered generating function εS evolves slowly enough so that $\varepsilon d_t S$ is actually of second order in ε . Therefore, at the first order of the development that is considered here, it should be neglected:

$$\bar{H}(\mathbf{q}_{gy}, \mathbf{p}_{gy}, t) = H_{GC}(\mathbf{q}_{gy}, \mathbf{p}_{gy}, t) + O(\varepsilon^2) \quad (\text{A.14})$$

In this case only, equation (A.12) can be safely replaced by:

$$H_{GC}(\mathbf{q}_{GC}, \mathbf{p}_{GC}, t) \simeq \bar{H}(\mathbf{q}_{gy}, \mathbf{p}_{gy}, t) - \varepsilon [\bar{H}, S]_{\mathbf{q}_{GC}, \mathbf{p}_{GC}} \quad (\text{A.15})$$

Let us use the set of angle-anction canonical coordinates $(\boldsymbol{\alpha}, \mathbf{J})$ defined in section 1.2.2. As far as the gyrokinetic theory is concerned, the transformation acts on the first pair of conjugate coordinates (α_1, J_1) , with $\alpha_1 = \varphi_c$ the gyro-phase and $J_1 = -m_s \mu_s / e_s$ (see [31, Garbet 2009]). From Eq.(A.15), it comes:

$$\begin{aligned} H_{GC}(\mathbf{q}_{GC}, \mathbf{p}_{GC}, t) &= \bar{H}(\mathbf{q}_{gy}, \mathbf{p}_{gy}, t) - \varepsilon [\bar{H}, S]_{\varphi_c, J_1} \\ &= \bar{H}(\mathbf{q}_{gy}, \mathbf{p}_{gy}, t) + \varepsilon (\omega_{cs} \partial_{\varphi_c} S - \partial_{\varphi_c} \bar{H} \partial_{J_1} S) \end{aligned} \quad (\text{A.16})$$

with $\dot{\varphi}_c \equiv \omega_{cs} = \partial_{J_1} \bar{H}$ the cyclotron frequency. The canonical structure of the transformation implies that the Poisson bracket is unchanged, and its calculation is then easy.

Determination of S

As said previously in equation A.10, $\bar{H}(\mathbf{q}_{gy}, \mathbf{p}_{gy}, t)$ should not depend on the gyro-angle φ_c . In this case, the last term on the right hand side of Eq.(A.16) vanishes. This allows

one to express the generating function S^2 as function of the old and new Hamiltonian:

$$\begin{aligned}\varepsilon S(\mathbf{q}_{GC}, \mathbf{p}_{GC}, t) &= \int \frac{d\varphi_c}{\omega_{cs}} \{H_{GC}(\mathbf{q}_{GC}, \mathbf{p}_{GC}, t) - \bar{H}(\mathbf{q}_{gy}, \mathbf{p}_{gy}, t)\} \\ &= \int \frac{m_s d\varphi_c}{B} \{e^{\rho_c \cdot \nabla} \phi(\mathbf{x}_{GC}, t) - \bar{\phi}(\mathbf{x}_{gy}, t)\} \\ &= \int \frac{m_s d\varphi_c}{B} \{\phi(\mathbf{x}, t) - \bar{\phi}(\mathbf{x}_{gy}, t)\}\end{aligned}\quad (\text{A.17})$$

A.2.2 Particle versus gyrocentre distribution functions

The problem that occurs here is that the quasi-neutrality equation is a constraint on the particle densities of the different species s of the plasma, which can be expressed as integrals of the different f_s . But the gyrokinetic approach uses and computes only the distribution function of gyrocentres \bar{f}_s . Thus it is necessary to insert a link between the values of f and \bar{f} evaluated at the same point. Another point to state is that in the end, the physical quantities, like density, should be expressed in the real space \mathbf{x} . This fixes the choice of coordinates used when the link between both distribution functions is made.

Let us recall equation (A.11) applied to \bar{f} .

$$\bar{f}(\mathbf{x}_{GC}, \mathbf{v}_{GC}) = \bar{f}(\mathbf{x}_{gy}, \mathbf{v}_{gy}) - \varepsilon [\bar{f}, S]_{\varphi_c, J_1} + O(\varepsilon^2) \quad (\text{A.18})$$

Knowing that, by construction, $\partial_{\varphi_c} \bar{f} = 0$, it comes:

$$\bar{f}(\mathbf{x}_{gy}, \mathbf{v}_{gy}) = \bar{f}(\mathbf{x}_{GC}, \mathbf{v}_{GC}) - \varepsilon \left(\frac{e_s}{m_s} \partial_{\varphi_c} S \right) \partial_{\mu} \bar{f}(\mathbf{x}_{GC}, \mathbf{v}_{GC}) \quad (\text{A.19})$$

Injecting the expression of S (Eq.(A.17)), the relation becomes:

$$\bar{f}(\mathbf{x}_{gy}, \mathbf{v}_{gy}, t) = \bar{f}(\mathbf{x}_{GC}, \mathbf{v}_{GC}, t) + \frac{e}{B} \{\phi(\mathbf{x}, t) - \bar{\phi}(\mathbf{x}_{gy}, t)\} \partial_{\mu} \bar{f}(\mathbf{x}_{GC}, \mathbf{v}_{GC}) \quad (\text{A.20})$$

Knowing that $\bar{f}(\mathbf{x}_{gy}, \mathbf{v}_{gy}, t) = f(\mathbf{x}, \mathbf{v}, t)$ (Eq.(1.63)), and by making a limited development in $\mathbf{x} - \mathbf{x}_{GC} = \rho_c$ on all the \mathbf{x}_{GC} dependant terms, according to Eq.(A.6), we can write:

$$f(\mathbf{x}, \mathbf{v}, t) = e^{-\rho_c \cdot \nabla} \bar{f}(\mathbf{x}, \mathbf{v}_{GC}, t) + \frac{e}{B} \{\phi(\mathbf{x}, t) - \bar{\phi}(\mathbf{x}_{gy}, t)\} e^{-\rho_c \cdot \nabla} \partial_{\mu} \bar{f}(\mathbf{x}, \mathbf{v}_{GC}) \quad (\text{A.21})$$

It is now possible to express the density of particle using only the distribution function of gyrocentres.

² From its expression Eq.(A.17), it is clear that the partial time derivative of εS typically involves frequencies $\partial_t S \sim \omega S$ which are much smaller than the cyclotron one: $\omega/\omega_{cs} \ll 1$. As a result, the ratio $(\varepsilon \partial_t S)/H$, with $H \sim e\phi$ the fluctuating part of the Hamiltonian, turns out to be of the order of $(\varepsilon \partial_t S)/H \sim (\omega/\omega_{cs}) \varepsilon \sim O(\varepsilon^2)$.

A.3 Expression of the polarization density $n_{s,pol}$

This calculation was first made in J. Abiteboul's thesis [1, Abiteboul 2012] and extended to the case where only trapped particles are kept.

General case

Notice that the Larmor radius itself depends on spatial location via its B dependence. More precisely, when moving from one position to another $\mathbf{x} \leftrightarrow \mathbf{x}_G$, the following relations hold:

$$\mathbf{x} \rightarrow \mathbf{x}_G : \quad \mathbf{x} = \mathbf{x}_G + \boldsymbol{\rho}_s(\mathbf{x}) \quad (\text{A.22})$$

$$\mathbf{x}_G \rightarrow \mathbf{x} : \quad \mathbf{x}_G = \mathbf{x} - \boldsymbol{\rho}_s(\mathbf{x}_G) \simeq \mathbf{x} - \boldsymbol{\rho}_s(\mathbf{x}) + (\boldsymbol{\rho}_s \cdot \nabla) \boldsymbol{\rho}_s \quad (\text{A.23})$$

Then it comes, with the convention that $\boldsymbol{\rho}_s$ stands for $\boldsymbol{\rho}_s(\mathbf{x})$ hereafter:

$$e^{\boldsymbol{\rho}_s \cdot \nabla} \simeq 1 + \boldsymbol{\rho}_s \cdot \nabla + \frac{1}{2} (\boldsymbol{\rho}_s \cdot \nabla)^2 \quad (\text{A.24})$$

$$e^{-\boldsymbol{\rho}_s \cdot \nabla} \simeq 1 - \boldsymbol{\rho}_s \cdot \nabla + [(\boldsymbol{\rho}_s \cdot \nabla) \boldsymbol{\rho}_s] \cdot \nabla + \frac{1}{2} (\boldsymbol{\rho}_s \cdot \nabla)^2 \quad (\text{A.25})$$

With these expressions, and at second order in $k_\perp \rho_s$, eq. 1.67 reads as follows:

$$\begin{aligned} n_{s,pol}(\mathbf{x}, t) \simeq & \int \mathcal{J}_v d\mu dv_{G\parallel} \frac{e_s}{B} \int_0^{2\pi} \frac{d\varphi_c}{2\pi} (1 - \boldsymbol{\rho}_s \cdot \nabla) \partial_\mu f_{s,eq}(\mathbf{x}, \mathbf{v}) \\ & \left\{ 1 - \left[1 - \boldsymbol{\rho}_s \cdot \nabla + ((\boldsymbol{\rho}_s \cdot \nabla) \boldsymbol{\rho}_s) \cdot \nabla + \frac{1}{2} (\boldsymbol{\rho}_s \cdot \nabla)^2 \right] \right. \\ & \left. \left\langle 1 + \boldsymbol{\rho}_s \cdot \nabla + \frac{1}{2} (\boldsymbol{\rho}_s \cdot \nabla)^2 \right\rangle \right\} \phi(\mathbf{x}, t) \end{aligned}$$

The gyro-radius vector $\boldsymbol{\rho}_s$ can be written $\boldsymbol{\rho}_s = \rho_s (\cos \varphi_c \mathbf{e}_x + \sin \varphi_c \mathbf{e}_y)$ where $\mathbf{e}_x, \mathbf{e}_y$ are the two vectors of the cartesian basis. It follows:

$$\begin{aligned} \langle \boldsymbol{\rho}_s \cdot \nabla \rangle &= 0 \\ \langle (\boldsymbol{\rho}_s \cdot \nabla)^2 \rangle &= \frac{1}{2} \rho_s \nabla_\perp \cdot (\rho_s \nabla_\perp) \end{aligned} \quad (\text{A.26})$$

with $\rho_s = |\boldsymbol{\rho}_s|$ the norm of the gyro-radius. Keeping terms up to the second order in $k_\perp \rho_s$ only, one gets:

$$\begin{aligned}
n_{s,pol}(\mathbf{x}, t) &\simeq \int \mathcal{J}_v d\mu dv_{G\parallel} \frac{e_s}{B} \int_0^{2\pi} \frac{d\varphi_c}{2\pi} (1 - \boldsymbol{\rho}_s \cdot \nabla) \partial_\mu f_{s,eq}(\mathbf{x}, \mathbf{v}) \\
&\quad \left\{ 1 - \left[1 - \boldsymbol{\rho}_s \cdot \nabla + ((\boldsymbol{\rho}_s \cdot \nabla) \boldsymbol{\rho}_s) \cdot \nabla + \frac{1}{2} \boldsymbol{\rho}_s \cdot \nabla (\boldsymbol{\rho}_s \cdot \nabla) \right. \right. \\
&\quad \left. \left. + \frac{1}{4} \boldsymbol{\rho}_s \nabla_\perp \cdot (\boldsymbol{\rho}_s \nabla_\perp) \right] \right\} \phi(\mathbf{x}, t) \\
&= - \int \mathcal{J}_v d\mu dv_{G\parallel} \frac{e_s}{B} \left\langle \left[\frac{1}{2} (\boldsymbol{\rho}_s \cdot \nabla (\boldsymbol{\rho}_s \cdot \nabla)) \right. \right. \\
&\quad \left. \left. + ((\boldsymbol{\rho}_s \cdot \nabla) \boldsymbol{\rho}_s) \cdot \nabla + \frac{1}{4} \boldsymbol{\rho}_s \nabla_\perp \cdot (\boldsymbol{\rho}_s \nabla_\perp) \right] \phi \frac{\partial f_{s,eq}}{\partial \mu} \right. \\
&\quad \left. + (\boldsymbol{\rho}_s \cdot \nabla \phi) \left(\boldsymbol{\rho}_s \cdot \nabla \frac{\partial f_{s,eq}}{\partial \mu} \right) \right\rangle
\end{aligned} \tag{A.27}$$

Three brackets remain to be calculated. The first one has already been computed (cf. eq. A.26). The two others read as follows:

$$\begin{aligned}
\langle ((\boldsymbol{\rho}_s \cdot \nabla) \boldsymbol{\rho}_s) \cdot \nabla \rangle &= \frac{1}{4} (\nabla_\perp \rho_s^2) \cdot \nabla_\perp \\
\langle (\boldsymbol{\rho}_s \cdot \nabla \phi) (\boldsymbol{\rho}_s \cdot \nabla \partial_\mu f_{s,eq}) \rangle &= \frac{1}{2} \rho_s^2 \nabla_\perp \phi \cdot \nabla_\perp \partial_\mu f_{s,eq}
\end{aligned}$$

It then comes, further noticing that $\boldsymbol{\rho}_s \nabla_\perp \cdot (\boldsymbol{\rho}_s \nabla_\perp \phi) = \frac{1}{2} (\nabla_\perp \rho_s^2) \cdot \nabla_\perp \phi + \rho_s^2 \nabla_\perp^2 \phi$:

$$\begin{aligned}
n_{s,pol}(\mathbf{x}, t) &\simeq - \int \mathcal{J}_v d\mu dv_{G\parallel} \frac{e_s}{B} \left[\frac{1}{2} (\nabla_\perp \rho_s^2) \cdot \nabla_\perp \phi + \frac{1}{2} \rho_s^2 \nabla_\perp^2 \phi \right. \\
&\quad \left. + \frac{1}{2} \rho_s^2 \nabla_\perp \phi \cdot \nabla_\perp \right] \partial_\mu f_{s,eq} \\
&= \int \mathcal{J}_v d\mu dv_{G\parallel} \frac{e_s}{2B} \partial_\mu \left[(\nabla_\perp \rho_s^2) \cdot \nabla_\perp \phi + \rho_s^2 \nabla_\perp^2 \phi \right. \\
&\quad \left. + \rho_s^2 \nabla_\perp \phi \cdot \nabla_\perp \right] f_{s,eq}
\end{aligned}$$

At this point, notice that $B^{-1} \partial_\mu = (m_s v_\perp)^{-1} \partial_{v_\perp}$ commutes with the operator in configuration space ∇_\perp . For the same reason, $\int \mathcal{J}_v d\mu$ also commutes with the operator ∇_\perp . Since $B^{-1} \partial_\mu \rho_s^2 = 2m_s / (e_s B)^2$, one finally obtains the following expression for the polarization density:

$$\begin{aligned}
n_{s,pol}(\mathbf{x}, t) &\simeq \int \mathcal{J}_v d\mu dv_{G\parallel} \nabla_\perp \cdot \left(\frac{m_s}{e_s B^2} f_{s,eq} \nabla_\perp \phi \right) \\
&= \nabla_\perp \cdot \left(\int \mathcal{J}_v d\mu dv_{G\parallel} \frac{m_s}{e_s B^2} f_{s,eq} \nabla_\perp \phi \right) \\
&= \nabla_\perp \cdot \left(\frac{m_s n_{s,eq}}{e_s B^2} \nabla_\perp \phi(\mathbf{x}, t) \right)
\end{aligned} \tag{A.28}$$

Trapped particles only

Expressing the density $n_{s,eq}$ as an integral in velocity space, Eq.(A.28) recasts as:

$$n_{s,pol}(\mathbf{x}, t) \simeq \nabla_{\perp} \cdot \left(\frac{m_s}{e_s B^2} \left[\int \mathcal{J}_v d\mu dv_{G\parallel} f_{s,eq}(\mathbf{x}, \mathbf{v}) \right] \nabla_{\perp} \phi(\mathbf{x}, t) \right)$$

The same calculation is carried out when considering trapped particles only. However, the integration domain of $f_{s,eq}$ is changed. Therefore, the polarisation density for trapped particles $n_{s,pol}^{trap.}$ simply expresses as:

$$\begin{aligned} n_{s,pol}^{trap.}(\mathbf{x}, t) &\simeq \nabla_{\perp} \cdot \left(\frac{m_e}{e_e B^2} \left[\int_{trap.} \mathcal{J}_v d\mu dv_{G\parallel} f_{s,eq}(\mathbf{x}, \mathbf{v}) \right] \nabla_{\perp} \phi(\mathbf{x}, t) \right) \\ &= \nabla_{\perp} \cdot \left(\frac{m_e}{e_e B^2} n_{s,eq}^{trap.} \nabla_{\perp} \phi \right) \\ &= \nabla_{\perp} \cdot \left(\frac{m_e}{e_e B^2} \alpha_t n_{s,eq} \nabla_{\perp} \phi \right) \end{aligned} \tag{A.29}$$

where $\alpha_t = n_{s,eq}^{trap.} / n_{s,eq}$ is the fraction of trapped particles.

Appendix B

Appendices of chapter 2

B.1 Adiabatic particle transport

The turbulent radial transport of particles is given by Eq.(2.15) and using the notations introduced in part 2.1.2, it reads:

$$\Gamma_r = -\frac{en_{e,eq}}{rT_e} \frac{1}{\iint \frac{d\varphi d\theta}{\mathbf{B} \cdot \nabla \theta}} \iint \frac{d\varphi d\theta}{\mathbf{B} \cdot \nabla \theta} (\phi - \langle \phi \rangle_{FS}) \frac{\partial \theta \phi}{B}$$

One notes $A = \iint \frac{d\varphi d\theta}{\mathbf{B} \cdot \nabla \theta} (\phi - \langle \phi \rangle_{FS}) \frac{\partial \theta \phi}{B}$. The magnetic field can be expressed as:

$$\mathbf{B} = I(\psi) \nabla \varphi + \nabla \varphi \wedge \nabla \psi \quad \rightarrow \quad \mathbf{B} \cdot \nabla \theta = (\nabla \psi \wedge \nabla \theta) \cdot \nabla \varphi$$

Then it comes:

$$\begin{aligned} B^2 &= I^2 |\nabla \varphi|^2 + (\nabla \varphi \wedge \nabla \psi) \cdot (\nabla \varphi \wedge \nabla \psi) \\ &= \left(\frac{I}{R}\right)^2 + |\nabla \psi|^2 |\nabla \varphi|^2 = \frac{I^2 + |\nabla \psi|^2}{R^2} \end{aligned}$$

Besides:

$$q(\psi) = \frac{\mathbf{B} \cdot \nabla \varphi}{\mathbf{B} \cdot \nabla \theta} \quad \Rightarrow \quad \mathbf{B} \cdot \nabla \theta = \frac{1}{q} \mathbf{B} \cdot \nabla \varphi = \frac{I}{qR^2}$$

Thus, the expression of A becomes:

$$\begin{aligned} A &= \iint d\varphi d\theta (\phi - \langle \phi \rangle_{FS}) \partial_{\theta} \phi \frac{qR^2}{I} \frac{R}{\sqrt{I^2 + |\nabla \psi|^2}} \\ &= \frac{q}{I \sqrt{I^2 + |\nabla \psi|^2}} \iint d\varphi d\theta R^3 (\phi - \langle \phi \rangle_{FS}) \partial_{\theta} \phi \\ &= \frac{qR_0^3}{I \sqrt{I^2 + |\nabla \psi|^2}} \iint d\varphi d\theta (1 + \varepsilon \cos \theta)^3 (\phi - \langle \phi \rangle_{FS}) \partial_{\theta} \phi \end{aligned}$$

Moreover, due to the periodicity in θ of ϕ we have:

$$\iint d\varphi d\theta (\phi - \langle \phi \rangle_{FS}) \partial_{\theta} \phi = \int d\varphi \left\{ \left[\frac{\phi^2}{2} \right]_0^{2\pi} - [\langle \phi \rangle_{FS} \phi]_0^{2\pi} \right\} = 0$$

Therefore, A can be recast as:

$$A = \frac{\varepsilon q R_0^3}{I \sqrt{I^2 + |\nabla \psi|^2}} \iint d\varphi d\theta [3 \cos \theta + 3\varepsilon \cos^2 \theta + \varepsilon^2 \cos^3 \theta] (\phi - \langle \phi \rangle_{FS}) \partial_{\theta} \phi$$

The calculation of $\iint \frac{d\varphi d\theta}{\mathbf{B} \cdot \nabla \theta}$ gives:

$$\iint \frac{d\varphi d\theta}{\mathbf{B} \cdot \nabla \theta} = \frac{qR_0^2}{I} \iint d\varphi d\theta (1 + \varepsilon \cos \theta)^2 = \frac{4\pi^2 q R_0^2}{I} \left(1 + \frac{\varepsilon^2}{2}\right)$$

Eventually, the development of the turbulent radial transport of particles Γ_r in ε reads:

$$\Gamma_r = -\frac{en_{e,eq}}{rT_e} \frac{R_0}{4\pi^2 \sqrt{I^2 + |\nabla \psi|^2}} \frac{\varepsilon}{1 + \frac{\varepsilon^2}{2}} \iint d\varphi d\theta [3 \cos \theta + 3\varepsilon \cos^2 \theta + \varepsilon^2 \cos^3 \theta] (\phi - \langle \phi \rangle_{FS}) \partial_{\theta} \phi$$

B.2 Computation of $n_{e\mathcal{R}}$

Two strategies can be adopted to compute $n_{e\mathcal{R}}$ in the case we suppose $J_{0e} \neq 1$:

- either replacing J_{0e} by its Padé approximation. In this case, $n_{e\mathcal{R}}$ is the solution of an ordinary differential equation, which can be easily solved numerically by inverting a tridiagonal matrix.
- or using an iterative procedure from an initial guess. This latter method has the advantage of considering the actual gyroaverage operator which is used in GYSELA. Its drawback is that the convergence cannot be guaranteed for simulation arbitrary parameters.

In the future, we believe the former method should be implemented in GYSELA for the convergence issue mentioned in the iterative procedure.

Differential equation

Admitting that all profiles have gradient lengths larger than the Larmor radii, the gyroaverage operator J_0 can then be approximated by its long wave length limit given by the Padé development Eq.(2.13). In this case ¹:

$$\int J_{0e} \cdot f_{e\mathcal{R}} \, d^3v \approx \int \left[f_{e\mathcal{R}} + \frac{A_e}{2r} \partial_r \{ r \partial_r (\mu f_{e\mathcal{R}}) \} \right] d^3v$$

Using Eq.(2.21) and (2.24) to compute the integrals, it comes:

$$\left\langle \int J_{0e} \cdot f_{e\mathcal{R}} \, d^3v \right\rangle_{FS} \approx n_{e\mathcal{R}} + \frac{A_e}{2r} \partial_r \{ r \partial_r (n_{e\mathcal{R}} T_{\perp e, eq}) \} = \alpha(r) n_{e\mathcal{R}} + \beta(r) n'_{e\mathcal{R}} + \gamma(r) n''_{e\mathcal{R}}$$

with

$$\begin{aligned} \alpha(r) &= 1 + \frac{A_e}{2} \left[\frac{T'_{\perp e, eq}(r)}{r} + T''_{\perp e, eq}(r) \right] \\ \beta(r) &= A_e \left[\frac{T_{\perp e, eq}(r)}{2r} + T'_{\perp e, eq}(r) \right] \\ \gamma(r) &= \frac{A_e}{2} T_{\perp e, eq}(r) \end{aligned}$$

Here the prime “'” denotes the radial derivative. The radial range $r \in [0, a]$ is discretized in the values r_j with $j \in [1, N_r]$ and the notation X_j is used instead of $X(r_j)$, where X is a given function of r . A numerical way to retrieve $n_{e\mathcal{R}}$ is to invert the following tridiagonal system (in the case where the derivatives in the radial direction are computed with finite differences at second order in Δr). For $j \in [2, N_r - 1]$ this system reads:

$$L_j n_{e\mathcal{R}, j-1} + D_j n_{e\mathcal{R}, j} + U_j n_{e\mathcal{R}, j+1} = \mathcal{R}_j \quad (\text{B.1})$$

¹Here, d^3v is approximated by $d^3v \approx 2\pi B \, d\mu \, dv_{\parallel}$, i.e. $B_{\parallel e}^*$ is replaced by B . Also, the radial derivatives of the magnetic field B can be safely neglected because they are of higher order.

with

$$L_j = -\frac{\beta_j}{2\Delta r} + \frac{\gamma_j}{\Delta r^2} ; \quad D_j = \alpha(r_j) - \frac{2\gamma_j}{\Delta r^2} ; \quad U_j = \frac{\beta_j}{2\Delta r} + \frac{\gamma_j}{\Delta r^2} \quad (\text{B.2})$$

The values of $n_{e\mathcal{R}}$ for $j = 1$ and N_r are set by the Neumann constraint $d_r n_{e\mathcal{R}}|_j = 0$, which takes the form numerically:

$$n_{e\mathcal{R},1} = n_{e\mathcal{R},2} ; \quad n_{e\mathcal{R},N_r} = n_{e\mathcal{R},N_r-1}$$

Iterative procedure

Let us define the normalized Maxwellian $\hat{f}_{e\mathcal{R}} = f_{e\mathcal{R}}/n_{e\mathcal{R}}$. Then condition (??) reads as follows:

$$\int J_{0e} \cdot (n_{e\mathcal{R}} \hat{f}_{e\mathcal{R}}) \, d^3v = \mathcal{R} \quad (\text{B.3})$$

where the electron gyro-average operator J_{0e} has been added. A first approximation for $n_{e\mathcal{R}}$ can be readily obtained by assuming that it commutes with the gyroaverage operator J_{0e} . This is equivalent to neglecting terms of the order of $(\rho_e/L_n)^k$, with k a strictly positive integer and $L_n^k = n_{e\mathcal{R}}/(\partial^k n_{e\mathcal{R}}/\partial r^k)$. This value of $n_{e\mathcal{R}}$ constitute the initial guess of the iterative procedure. Let us call it $n_{e\mathcal{R}}^0$:

$$n_{e\mathcal{R}}^0 = \frac{\mathcal{R}}{\int d^3v J_{0e} \cdot \hat{f}_{e\mathcal{R}}} \quad (\text{B.4})$$

The difference $\Delta n_{e\mathcal{R}} = n_{e\mathcal{R}} - n_{e\mathcal{R}}^0$ between $n_{e\mathcal{R}}^0$ and the exact solution $n_{e\mathcal{R}}$ of eq.(B.3) is a measure of the error. It simply reads:

$$\int J_{0e} \cdot (\Delta n_{e\mathcal{R}} \hat{f}_{e\mathcal{R}}) \, d^3v = \mathcal{R} - \int J_{0e} \cdot (n_{e\mathcal{R}}^0 \hat{f}_{e\mathcal{R}}) \, d^3v$$

which is the same equation as eq.(B.3) with a different right hand side. Using the same assumption as previously, $\Delta n_{e\mathcal{R}}$ can be approximated by neglecting its radial derivatives, so that it would commute with J_{0e} . Denoting $\Delta n_{e\mathcal{R}}^0$ this approximate quantity, one obtains:

$$\Delta n_{e\mathcal{R}}^0 = \frac{\mathcal{R} - \int J_{0e} \cdot (n_{e\mathcal{R}}^0 \hat{f}_{e\mathcal{R}}) \, d^3v}{\int J_{0e} \cdot \hat{f}_{e\mathcal{R}} \, d^3v} \quad (\text{B.5})$$

This method can be further iterated. The iterative procedure then takes the form:

$$\begin{aligned} n_{e\mathcal{R}}^0 &= \frac{\mathcal{R}}{\int J_{0e} \cdot \hat{f}_{e\mathcal{R}}} \, d^3v \\ n_{e\mathcal{R}}^{k+1} &= n_{e\mathcal{R}}^k + \frac{\mathcal{R} - \int J_{0e} \cdot (n_{e\mathcal{R}}^k \hat{f}_{e\mathcal{R}}) \, d^3v}{\int J_{0e} \cdot \hat{f}_{e\mathcal{R}} \, d^3v} \quad \forall k \in \mathbb{N} \end{aligned} \quad (\text{B.6})$$

The iteration is then stopped at iteration $k = K$ as soon as a predefined convergence condition is fulfilled. Such a condition requires that the difference between \mathcal{R} and

$\int J_{0e} \cdot (n_{e\mathcal{R}}^K \hat{f}_{e\mathcal{R}}) d^3v$ remains much smaller than the ion polarization term, typically in the ratio ρ_* . A possible condition can then read as follows:

$$\frac{\max_r \left\{ \mathcal{R} - \int J_{0e} \cdot (n_{e\mathcal{R}}^K \hat{f}_{e\mathcal{R}}) d^3v \right\}}{\max_{r,i} \{ \nabla_r \cdot (A_i n_{i0} \nabla_r \phi_{00}) \}} \leq \min_{r,i} \{ \rho_i^* \}$$

with $\rho_i^* = \sqrt{A_i T_{i0}} / (a Z_i)$ and where the extrema are to be taken on the radial profile and on all active (i.e. non-trace) ion species. Alternatively, it could be replaced by the following condition:

$$\max_r \left\{ \mathcal{R} - \int J_{0e} \cdot (n_{e\mathcal{R}}^K \hat{f}_{e\mathcal{R}}) d^3v \right\} \leq \min_{r,i} \{ \rho_i^{*2} \} \min_r \{ \mathcal{R} \}$$

Because the iterative procedure presents the risk of not converging, we should employ the former method in GYSELA, i.e. the inversion of the tridiagonal system Eq.(B.1).

B.3 Normalized quasi-neutrality equation for adiabatic electrons

In this appendix, the symbol $\hat{\cdot}$ refers to normalized quantities in the GYSELA code. The normalized quasi-neutrality equation in the case of adiabatic electrons can be written:

$$-\frac{1}{\hat{n}_{e0}} \sum_i \hat{A}_i \hat{\nabla}_\perp \cdot \left(\frac{\hat{n}_{i0}}{\hat{B}_0} \hat{\nabla}_\perp \hat{\phi} \right) + \frac{1}{Z_0^2 \hat{T}_e} \left[\hat{\phi} - \langle \hat{\phi} \rangle_{\text{FS}} \right] = \frac{1}{\hat{n}_{e0}} \sum_i \hat{Z}_i [\hat{n}_{G_i} - \hat{n}_{G_i, \text{eq}}] \quad (\text{B.7})$$

where the normalized electron density \hat{n}_{e0} is defined as $\hat{n}_{e0} = \sum_i Z_0 \hat{Z}_i \hat{n}_{i0}$. In the following, i symbol stands for ion species while the e symbol stands for electrons. The s symbol will be used when no distinction between both ion and electron species is required. Notice that, in the polarization term (first term of eq. (B.7)), \hat{B} has been replaced by $\hat{B}_0 = 1$. The integral $\langle \hat{\phi} \rangle_{\text{FS}}$ represents the flux surface average of $\hat{\phi}$ where for all $g(\hat{r}, \theta, \varphi)$ function:

$$\langle g \rangle_{\text{FS}}(\hat{r}) = \int g \hat{\mathcal{J}}_x \, d\theta \, d\varphi / \int \hat{\mathcal{J}}_x \, d\theta \, d\varphi \quad (\text{B.8})$$

with $\hat{\mathcal{J}}_x = 1/(\hat{B} \cdot \hat{\nabla}\theta)$ the normalized jacobian space. The normalized guiding-center density \hat{n}_{G_s} of species s is given by:

$$\hat{n}_{G_s} = \int d\hat{\mu}_s \int \hat{\mathcal{J}}_v \, d\hat{v}_{G\parallel s} \hat{J}_{0_s} \cdot \hat{f}_s \quad (\text{B.9})$$

with the normalized jacobian in velocity equal to $\hat{\mathcal{J}}_v = 2\pi \hat{B}_{\parallel s}^*$. The correction term $\hat{n}_{G_s, \text{eq}}$ in the right hand side is defined as follows:

$$\hat{n}_{G_s, \text{eq}} = \int d\hat{\mu}_s \int \hat{\mathcal{J}}_v \, d\hat{v}_{G\parallel s} \hat{J}_{0_s} \cdot \hat{f}_{s, \text{eq}} \quad (\text{B.10})$$

where the normalized equilibrium distribution function is defined as:

$$\hat{f}_{s, \text{eq}} = c_s \frac{\hat{n}_{s0}}{(2\pi \hat{T}_s)^{3/2}} \exp \left[-\frac{(\hat{v}_{G\parallel s}^2/2 + \hat{\mu}_s \hat{B})}{\hat{T}_s} \right] \quad (\text{B.11})$$

represents the equilibrium part of the distribution function. The concentration c_i is such that $\sum_i c_i Z_0 \hat{Z}_i = 1$. The normalized gyro-average operator \hat{J}_{0_s} approximated by Padé corresponds to:

$$\hat{J}_{0_s} \approx 1 + \frac{1}{2} \frac{\hat{A}_s}{\hat{Z}_s^2} \frac{\hat{\mu}_s}{\hat{B}} \hat{\nabla}_\perp^2 \quad (\text{B.12})$$

where, as in the quasi-neutrality equation, \hat{B} is replaced by $\hat{B}_0 = 1$ in the code. Let us notice that in the code, to avoid the expensive gyro-average operation for each value of $v_{G\parallel}$ —which occur for the computation of the RHS of the quasi-neutrality equation (B.7)—we use the definition of $\hat{B}_{\parallel s}^*$

$$\hat{\mathbf{b}}_s^* = \frac{1}{\hat{B}_{\parallel s}^*} \left(\hat{\mathbf{B}} + \frac{\sqrt{\hat{A}_s}}{\hat{Z}_s} \frac{\hat{v}_{G\parallel s}}{\hat{B}} \hat{\mathbf{J}} \right) \quad \text{and} \quad \hat{B}_{\parallel s}^* = \hat{B} + \frac{\sqrt{\hat{A}_s}}{\hat{Z}_s} \frac{\hat{v}_{G\parallel s}}{\hat{B}} \mathbf{b} \cdot \hat{\mathbf{J}} \quad (\text{B.13})$$

and therefore the fact that the term $\hat{n}_{G_s} - \hat{n}_{G_s,eq}$ can be expressed as:

$$\hat{n}_{G_s} - \hat{n}_{G_s,eq} = 2\pi \int d\hat{\mu}_s \left(\hat{B} \hat{J}_{0_s} \cdot I_0(\hat{r}, \theta, \varphi, \hat{\mu}_s) + \frac{\sqrt{\hat{A}_s} \hat{v}_{G\parallel s}}{\hat{Z}_s \hat{B}} \mathbf{b} \cdot \hat{\mathbf{J}} \hat{J}_{0_s} \cdot I_1(\hat{r}, \theta, \varphi, \hat{\mu}_s) \right)$$

where the integrals I_0 and I_1 are defined by:

$$I_0(\hat{r}, \theta, \varphi, \hat{\mu}_s) = \int (\hat{f}_s - \hat{f}_{s,eq}) d\hat{v}_{G\parallel s} \quad \text{and} \quad I_1(\hat{r}, \theta, \varphi, \hat{\mu}_s) = \int \hat{v}_{G\parallel s} (\hat{f}_s - \hat{f}_{s,eq}) d\hat{v}_{G\parallel s}$$

B.3.1 How to overcome the difficulty due to $\langle \phi \rangle_{\text{FS}}$ term ?

In this section, we explain the particular treatment performed to overcome the problem of the flux surface average term $\langle \dots \rangle_{\text{FS}}$ appearing in quasi-neutrality equation (B.7). For more readability the hat symbols will be omitted for normalized quantities in the following. Let us consider a disk Ω of radius $r = r_{\text{max}}$, i.e

$$\Omega = \{(r, \theta) : 0 < r \leq r_{\text{max}} ; 0 \leq \theta < 2\pi\} \quad (\text{B.14})$$

As φ plays the role of a parameter in equation (B.7), it can be written as a set of 2D Poisson equations in polar coordinates as:

$$\mathcal{L}^{\text{AE}} \phi + \frac{1}{Z_0^2 T_e(r)} [\phi - \langle \phi \rangle_{\text{FS}}] = \rho(r, \theta, \varphi) \quad \forall (r, \theta) \in \Omega \quad \text{and} \quad 0 \leq \varphi < 2\pi \quad (\text{B.15})$$

where the differential operator of second order \mathcal{L}^{AE} (where AE symbol stands for adiabatic electrons) is defined as:

$$\begin{aligned} \mathcal{L}^{\text{AE}} &= -\frac{1}{n_{e0}(r)} \sum_i A_i \nabla_{\perp} \cdot (n_{i0}(r) \nabla_{\perp}) \\ &= -\frac{1}{n_{e0}(r)} \sum_i A_i n_{i0}(r) \left\{ \frac{\partial^2}{\partial r^2} + \left[\frac{1}{r} + \frac{1}{n_{i0}(r)} \frac{dn_{i0}(r)}{dr} \right] \frac{\partial}{\partial r} + \frac{1}{r^2} \frac{\partial^2}{\partial \theta^2} \right\} \end{aligned}$$

and the right hand side reads

$$\rho(r, \theta, \varphi) = \frac{1}{n_{e0}(r)} \sum_s Z_s [n_{G_s}(r, \theta, \varphi) - n_{G_s,eq}(r, \theta)] \quad (\text{B.16})$$

where n_{G_s} and $n_{G_s,eq}$ are respectively defined by equations (B.9) and (B.10). One difficulty of equation (B.15) is the treatment of polar coordinates singularity. As discussed later, the first idea was to treat the problem of a corona, i.e $r_{\text{min}} \leq r \leq r_{\text{max}}$ with $r_{\text{min}} > 1.e^{-2}$. But more recently the strategy proposed by Lai [56] to overcome this singularity has been used. This will be described more in details in the next section.

Concerning the treatment of $\langle \phi \rangle_{\text{FS}}$ in Eq.(B.15), let us first define for all function g , $\langle g \rangle_{\theta, \varphi}$ the radial function equal to

$$\langle g \rangle_{\theta, \varphi}(r) = \frac{1}{L_{\theta} L_{\varphi}} \int \int g(r, \theta, \varphi) d\theta d\varphi$$

By applying the integration $\frac{1}{L_\theta L_\varphi} \int \int \cdot d\theta d\varphi$ to previous equation (B.15) and by using the fact that $\langle \langle \phi \rangle_{\theta, \varphi} \rangle_{\text{FS}} = \langle \phi \rangle_{\text{FS}}$ then:

$$\mathcal{L}^{\text{AE}} \langle \phi \rangle_{\theta, \varphi} + \frac{1}{Z_0^2 T_e} [\langle \phi \rangle_{\theta, \varphi} - \langle \phi \rangle_{\text{FS}}] = \langle \rho \rangle_{\theta, \varphi} \quad (\text{B.17})$$

Let $\tilde{\phi}$ be defined as

$$\tilde{\phi} = \phi - \langle \phi \rangle_{\theta, \varphi} \quad (\text{B.18})$$

Then, by subtracting (B.17) to (B.15),

$$\left(\mathcal{L}^{\text{AE}} + \frac{1}{Z_0^2 T_e} \right) \tilde{\phi}(r, \theta, \varphi) = \tilde{\rho}(r, \theta, \varphi) \quad \text{with} \quad \tilde{\rho} = \rho - \langle \rho \rangle_{\theta, \varphi} \quad \forall (r, \theta, \varphi) \in \mathbb{R}^3 \quad (\text{B.19})$$

According to (B.18), $\langle \tilde{\phi} \rangle_{\text{FS}} = \langle \phi \rangle_{\text{FS}} - \langle \phi \rangle_{\theta, \varphi}$. Then $\langle \phi \rangle_{\text{FS}}$ replaced by $\langle \tilde{\phi} \rangle_{\text{FS}} + \langle \phi \rangle_{\theta, \varphi}$ in equation (B.17) gives

$$\mathcal{L}^{\text{AE}} \langle \phi \rangle_{\theta, \varphi} + \frac{1}{Z_0^2 T_e} \langle \phi \rangle_{\theta, \varphi} = \langle \rho \rangle_{\theta, \varphi} \quad (\text{B.20})$$

To summarize, the solving of equation system (B.15) can be replaced by the solving of two simpler equations (B.19) and (B.20) and the electrostatic potential deduced by $\phi = \tilde{\phi} + \langle \phi \rangle_{\theta, \varphi}$ (due to relation (B.18)). Indeed, equation (B.20) is a differential equation only depending on the radial direction. Besides, in (B.19) the variable φ plays the role of a parameter, then the discretization of the equation can be performed by projecting in Fourier space in θ direction and by using finite differences in the radial direction as described in the following paragraph.

B.3.2 Numerical solving of the quasi-neutrality equation

Global algorithm for the quasi-neutrality solver

Boundary conditions are periodic in θ and φ while Dirichlet boundary conditions are applied in the radial direction. To avoid the polar coordinate singularity in $r = 0$, equation (B.15) is not solved on the disk domain Ω (Eq. (B.14)) in poloidal cross-section but on a corona $\Omega_{r_{\min}}$ defined as

$$\Omega_{r_{\min}} = \{(r, \theta) : r_{\min} \leq r \leq r_{\max} ; 0 \leq \theta < 2\pi\} \quad (\text{B.21})$$

So including boundary conditions, Eq. (B.15) on $\Omega_{r_{\min}} \times [0, L_\varphi]$ becomes:

$$\left\{ \begin{array}{ll} \mathcal{L}^{\text{AE}}\phi + \frac{1}{Z_0^2 T_e(r)} [\phi - \langle \phi \rangle_{\text{FS}}] = \rho(r, \theta, \varphi) & \forall (r, \theta) \in \Omega_{r_{\min}} ; 0 \leq \varphi < L_\varphi \\ \phi(r_{\min}, \theta, \varphi) = \phi(r_{\max}, \theta, \varphi) = 0 & 0 \leq \theta < 2\pi ; 0 \leq \varphi < L_\varphi \\ \phi(r, 0, \varphi) = \phi(r, 2\pi, \varphi) & r_{\min} \leq r \leq r_{\max} ; 0 \leq \varphi < L_\varphi \\ \phi(r, \theta, 0) = \phi(r, \theta, L_\varphi) & \forall (r, \theta) \in \Omega_{r_{\min}} \end{array} \right. \quad (\text{B.22})$$

Then the different steps for solving (B.22) and obtaining ϕ are the following:

1. Compute $\rho(r, \theta, \varphi)$ given by Eq.(B.16) and $\langle \rho \rangle_{\theta, \varphi}(r)$.
2. Compute $\tilde{\rho}(r, \theta, \varphi) = \rho(r, \theta, \varphi) - \langle \rho \rangle_{\theta, \varphi}(r)$ the RHS of equation (B.19).
3. Solve for each $\varphi \in [0, L_\varphi[$ the 2D following system (B.23) (deduced from (B.19)) to obtain $\tilde{\phi}(r, \theta, \varphi)$:

$$\left\{ \begin{array}{ll} \left(\mathcal{L}^{\text{AE}} + \frac{1}{Z_0^2 T_e} \right) \tilde{\phi}(r, \theta, \varphi) = \tilde{\rho}(r, \theta, \varphi) \quad \text{with} \quad \tilde{\rho} = \rho - \langle \rho \rangle_{\theta, \varphi} & \forall (r, \theta) \in \Omega_{r_{\min}} \\ \tilde{\phi}(r_{\min}, \theta, \varphi) = \tilde{\phi}(r_{\max}, \theta, \varphi) = 0 & 0 \leq \theta < 2\pi \\ \tilde{\phi}(r, 0, \varphi) = \tilde{\phi}(r, 2\pi, \varphi) & r_{\min} \leq r \leq r_{\max} \end{array} \right. \quad (\text{B.23})$$

And applied the periodic boundary conditions in φ direction to compute $\tilde{\phi}(r, \theta, \varphi = L_\varphi)$.

4. Compute $\langle \rho \rangle_{\theta, \varphi}$.
5. Solve the 1D system (B.24) to obtain $\langle \phi \rangle_{\theta, \varphi}(r)$.

$$\left\{ \begin{array}{ll} \left(\mathcal{L}^{\text{AE}} + \frac{1}{Z_0^2 T_e} \right) \langle \phi \rangle_{\theta, \varphi}(r) = \langle \rho \rangle_{\theta, \varphi} & \forall r \in [r_{\min}, r_{\max}] \\ \langle \phi \rangle_{\theta, \varphi}(r_{\min}) = \langle \phi \rangle_{\theta, \varphi}(r_{\max}) = 0 \end{array} \right. \quad (\text{B.24})$$

6. Finally, compute $\phi(r, \theta, \varphi)$ by using (B.18), i.e $\phi(r, \theta, \varphi) = \tilde{\phi}(r, \theta, \varphi) + \langle \phi \rangle_{\theta, \varphi}(r)$.

Let us notice that radial boundary conditions imposed in (B.23) and (B.24) ensure radial Dirichlet boundary conditions for ϕ (because $\phi(r_{\min}, \theta, \varphi) = \tilde{\phi}(r_{\min}, \theta, \varphi) + \langle \phi \rangle_{\theta, \varphi}(r_{\min}) = 0$ and the same for $\phi(r_{\max}, \theta, \varphi) = 0$).

Solving of the equation system (B.23)

As described in the following, the matrix system (B.23) (where φ plays the role of a parameter) is solved with finite differences in radial direction and Fourier projections in θ . Let $\tilde{\phi}$ and $\tilde{\rho}$ be represented in terms of the Fourier expansion as

$$\begin{cases} \tilde{\phi}(r, \theta, \varphi) = \sum_m \tilde{\phi}^m(r, \varphi) \exp(im\theta) \\ \tilde{\rho}(r, \theta, \varphi) = \sum_m \tilde{\rho}^m(r, \varphi) \exp(im\theta) \end{cases}$$

then the equation (B.23) can be rewritten in the wave number representation, for each poloidal mode m and for each independent value of φ , as the following differential equation:

$$\left(\mathcal{L}_m^{\text{AE}} + \frac{1}{Z_0^2 T_e(r)} \right) \tilde{\phi}^m(r, \varphi) = \tilde{\rho}^m(r, \varphi) \quad (\text{B.25})$$

with the operator $\mathcal{L}_m^{\text{AE}}$ defined as

$$\mathcal{L}_m^{\text{AE}} = -\frac{1}{n_{e0}(r)} \sum_{s \neq e} A_s n_{s0}(r) \left\{ \frac{\partial^2}{\partial r^2} + \left[\frac{1}{r} + \frac{1}{n_{s0}(r)} \frac{dn_{s0}(r)}{dr} \right] \frac{\partial}{\partial r} - \frac{m^2}{r^2} \right\} \quad (\text{B.26})$$

and where $\tilde{\phi}^m$ (resp. $\tilde{\rho}^m$) is the Fourier transform in θ of $\tilde{\phi}$ (resp. $\tilde{\rho}$). Let us define,

$$K_s(r) = \frac{A_s n_{s0}(r)}{n_{e0}(r)} \quad ; \quad \beta(r) = \sum_{s \neq e} K_s(r) \quad \text{and} \quad \alpha(r) = \sum_{s \neq e} K_s(r) \left(\frac{1}{r} + \frac{1}{n_{s0}(r)} \frac{dn_{s0}(r)}{dr} \right) \quad (\text{B.27})$$

then the differential operator $\mathcal{L}_m^{\text{AE}}$ can be written

$$\mathcal{L}_m^{\text{AE}} = - \left[\beta(r) \frac{\partial^2}{\partial r^2} + \alpha(r) \frac{\partial}{\partial r} - \beta(r) \frac{m^2}{r^2} \right] \quad (\text{B.28})$$

Let us defined the radial discrete domain $[r_{\min}, r_{\max}]$ by N_1 points $r_i = r_{\min} + (i-1)\Delta r$, $\forall i = 1, \dots, N_1$ with the discretization step $\Delta r = L_r / (N_1 - 1)$ where $L_r = r_{\max} - r_{\min}$ represents the domain length. For the following, let us defined the notations $\tilde{\phi}_i^m = \tilde{\phi}^m(r_i, \varphi)$, $\tilde{\rho}_i^m = \tilde{\rho}^m(r_i, \varphi)$, $\beta_i = \beta(r_i)$ and $\alpha_i = \alpha(r_i)$. Then up to second order in Δr , equations (B.23) can be written as the following set of equations $\forall i = 1, \dots, N_1$

$$-\beta_i \left(\frac{\tilde{\phi}_{i-1}^m - 2\tilde{\phi}_i^m + \tilde{\phi}_{i+1}^m}{2\Delta r^2} \right) - \alpha_i \left(\frac{\tilde{\phi}_{i+1}^m - \tilde{\phi}_{i-1}^m}{2\Delta r} \right) + \beta_i \frac{m^2}{r_i^2} \tilde{\phi}_i^m + \frac{1}{Z_0^2 T_e(r_i)} \tilde{\phi}_i^m = \tilde{\rho}_i^m$$

which is equivalent to $\forall i = 1, \dots, N_1$

$$-\left(\frac{\beta_i}{\Delta r^2} - \frac{\alpha_i}{2\Delta r} \right) \tilde{\phi}_{i-1}^m + \left(\frac{2\beta_i}{\Delta r^2} + \frac{\beta_i m^2}{r_i^2} + \frac{1}{Z_0^2 T_e(r_i)} \right) \tilde{\phi}_i^m - \left(\frac{\beta_i}{\Delta r^2} + \frac{\alpha_i}{2\Delta r} \right) \tilde{\phi}_{i+1}^m = \tilde{\rho}_i^m \quad (\text{B.29})$$

Concerning boundary conditions, Dirichlet conditions are applied in r_{\max} , i.e. $\tilde{\phi}_{N_1}^m = \tilde{\phi}^m(r_i = r_{\max}, \varphi) = 0$, then for $i = N_1 - 1$ equation (B.29) becomes

$$-\left(\frac{\beta_{N_1-1}}{\Delta r^2} - \frac{\alpha_{N_1-1}}{2\Delta r}\right)\tilde{\phi}_{N_1-2}^m + \left(\frac{2\beta_{N_1-1}}{\Delta r^2} + \frac{\beta_{N_1-1}m^2}{r_{N_1-1}^2} + \frac{1}{Z_0^2 T_e(r_{N_1-1})}\right)\tilde{\phi}_{N_1-1}^m = \tilde{\rho}_{N_1-1}^m \quad (\text{B.30})$$

For inner boundary conditions ($r = r_{\min}$), two choices are possible, depending on if: (i) $r_{\min} > \Delta r/2$ (for a corona case), or (ii) $r_{\min} = \Delta r/2$. For the first case ($r_{\min} > \Delta r/2$), Dirichlet conditions are applied, i.e. $\tilde{\phi}_1^m = \tilde{\phi}^m(r_i = r_{\min}, \varphi) = 0$. For the second case ($r_{\min} = \Delta r/2$), we use the same strategy than the one proposed by Lai [56] to overcome the $1/r$ singularity on the axis. This strategy is simply based on the fact that if r_{\min} is chosen equal to $\Delta r/2$, the term $(\frac{1}{\Delta r^2} - \frac{1}{r\Delta r})$ which appear for a standard Poisson equation is equal to 0. In our case, this strategy is applicable if and only if the radial derivative of the density profiles n_{i_0} is null at $r = r_{\min}$. Indeed, in this case the term behind $\tilde{\phi}_0^m$ in equation (B.29) for $i = 1$ is equal to $\sum_{s \neq e} K_s(r_1) (\frac{1}{\Delta r^2} - \frac{1}{r\Delta r}) = 0$, such that

$$\left[\beta_1 \left(\frac{2}{\Delta r^2} + \frac{m^2}{r_1^2}\right) + \frac{1}{Z_0^2 T_e(r_1)}\right]\tilde{\phi}_1^m - \left(\frac{\beta_1}{\Delta r^2} + \frac{\alpha_1}{2\Delta r}\right)\tilde{\phi}_2^m = \tilde{\rho}_1^m \quad (\text{B.31})$$

Then solving (B.29) leads to solve the tridiagonal $(N_1 - 1) \times (N_1 - 1)$ system

$$\begin{pmatrix} d_1^m & u_1 & 0 & \cdots & 0 \\ l_2 & d_2^m & u_2 & 0 & \\ 0 & l_3 & d_3^m & u_3 & 0 \\ \vdots & 0 & \ddots & \ddots & \ddots \\ & & 0 & l_{N_1-2} & d_{N_1-2}^m & u_{N_1-2} \\ 0 & & & 0 & l_{N_1-1} & d_{N_1-1}^m \end{pmatrix} \begin{pmatrix} \tilde{\phi}_1^m \\ \tilde{\phi}_2^m \\ \vdots \\ \tilde{\phi}_{N_1-2}^m \\ \tilde{\phi}_{N_1-1}^m \end{pmatrix} = \begin{pmatrix} \tilde{\rho}_1^m \\ \tilde{\rho}_2^m \\ \vdots \\ \tilde{\rho}_{N_1-2}^m \\ \tilde{\rho}_{N_1-1}^m \end{pmatrix} \quad (\text{B.32})$$

where for each $i \in [1, N_1 - 1]$

$$\begin{cases} l_i = -\left(\frac{\beta_i}{\Delta r^2} - \frac{\alpha_i}{2\Delta r}\right) \\ d_i^m = \beta_i \left(\frac{2}{\Delta r^2} + \frac{m^2}{r_i^2}\right) + \frac{1}{Z_0^2 T_e(r_i)} \\ u_i = -\left(\frac{\beta_i}{\Delta r^2} + \frac{\alpha_i}{2\Delta r}\right) \end{cases} \quad \text{with} \quad \begin{cases} \alpha_i = \sum_s K_s(r_i) \left(\frac{1}{r_i} + \frac{1}{n_{s_0}(r_i)} \frac{dn_{s_0}(r_i)}{dr}\right) \\ \beta_i = \sum_s K_s(r_i) \text{ and } K_s(r_i) = A_s \frac{n_{s_0}(r_i)}{n_{e_0}(r_i)} \end{cases} \quad (\text{B.33})$$

with $\tilde{\rho}_i^m$ the poloidal wave vector of $\tilde{\rho}_i$ defined as

$$\tilde{\rho}_i = \rho_i - \langle \rho_i \rangle_{\theta, \varphi} \quad \text{with} \quad \rho_i = \frac{1}{n_{e_0}(r_i)} \sum_{s \neq e} [n_{G_s}(r_i, \theta, \varphi) - n_{G_s, \text{eq}}(r_i, \theta)]$$

and with $\tilde{\phi}_{N_1}^m = 0$.

Let us notice that for the first case, where inner Dirichlet boundary conditions are applied, the matrix system to solve is a $(N_1 - 2) \times (N_1 - 2)$ tridiagonal system equivalent to (B.32) where first line and first column are deleted and replaced by the condition $\tilde{\phi}_1^m = 0$.

Solving of the equation system (B.24)

The system (B.24), also solved with finite differences, can be rewritten as:

$$\begin{cases} \left(\mathcal{L}^{\text{AE}} + \frac{1}{Z_0^2 T_e(r_i)} \right) \langle \phi \rangle_{\theta, \varphi}(r_i) = \Gamma(r_i) & \text{for each } r_i \in [r_1, r_{N_1}] \\ \langle \phi \rangle_{\theta, \varphi}(r_{\min}) = \langle \phi \rangle_{\theta, \varphi}(r_{\max}) = 0 \end{cases}$$

with $\Gamma_i = \Gamma(r_i) = \langle \rho \rangle_{\theta, \varphi}(r_i)$ which is equivalent (by using the same notation than for the previous matrix system (B.32)) to

$$\begin{pmatrix} d_1 & u_1 & 0 & \cdots & 0 \\ l_2 & d_2 & u_2 & 0 & \\ 0 & l_3 & d_3 & u_3 & 0 \\ \vdots & 0 & \ddots & \ddots & \ddots \\ & & 0 & l_{N_1-2} & d_{N_1-2} & u_{N_1-2} \\ 0 & & & 0 & l_{N_1-1} & d_{N_1-1} \end{pmatrix} \begin{pmatrix} \langle \phi \rangle_{\theta, \varphi}(r_1) \\ \langle \phi \rangle_{\theta, \varphi}(r_2) \\ \vdots \\ \langle \phi \rangle_{\theta, \varphi}(r_{N_1-2}) \\ \langle \phi \rangle_{\theta, \varphi}(r_{N_1-1}) \end{pmatrix} = \begin{pmatrix} \Gamma_1 \\ \Gamma_2 \\ \vdots \\ \Gamma_{N_1-2} \\ \Gamma_{N_1-1} \end{pmatrix} \quad (\text{B.34})$$

where for each $i \in [1, N_1 - 1]$, l_i and u_i are defined by (B.33) and

$$\begin{cases} d_i = \frac{2}{\Delta r^2} \beta_i + \frac{1}{Z_0^2 T_e(r_i)} = d_i^0 & \text{with } d_i^0 \text{ given by (B.33)} \\ \Gamma_i = \langle \rho \rangle_{\theta, \varphi}(r_i) \end{cases}$$

Appendix C

Appendices of chapter 3

C.1 Saturation limit

The mixing length theory

With the notations used in part 3.1, f , g are of the same order as $F_H - F_{eq}$. Knowing equation (3.8), this difference can be linked to the potential ϕ :

$$F_H - F_{eq} = F_{eq} \left[-\frac{e}{T}\phi + o\left(\frac{e\phi}{T}\right) \right]$$

Dividing by F_{eq} , it comes:

$$\frac{g}{F_{eq}} \sim \frac{e\phi}{T}$$

Moreover we have :

$$\frac{g}{F_{eq}} \sim \frac{\delta n}{n_{eq}}$$

The mixing length theory states that the saturation, which corresponds to the long time limit that we are interested in, is obtained when the condition $|\nabla\delta n| \simeq |\nabla n_{eq}|$ is satisfied. It is possible to evaluate $|\nabla\delta n| \simeq k_{\perp}\delta n$ with $1/k_{\perp} = \rho_i$ the scale of ion instabilities, and $|\nabla n_{eq}| \simeq n_{eq}/L_n$ with $L_n \sim a$ the tokamak scale. Thus, the saturation limit corresponds to the condition :

$$\frac{\delta n}{n_{eq}} \sim \frac{\rho_i}{a} = \rho^* \ll 1$$

Thus it comes :

$$\frac{g}{F_{eq}} \sim \frac{e\phi}{T} \sim \rho^* \ll 1$$

Justification of the linear approximation

Let us introduce the Poisson brackets of two functionals \mathcal{F} and \mathcal{G} in the gyrokinetics coordinates (Eq.(159) of [11, Brizard 2007]) :

$$\{\mathcal{F}, \mathcal{G}\} \simeq \left(\nabla_{\parallel} \mathcal{F} \frac{\partial \mathcal{G}}{\partial p_{\parallel}} - \frac{\partial \mathcal{F}}{\partial p_{\parallel}} \nabla_{\parallel} \mathcal{G} \right) - \frac{\mathbf{b}}{eB} \cdot (\nabla \mathcal{F} \times \nabla \mathcal{G})$$

with \parallel standing for the direction of the magnetic field, p the momentum, B the magnetic field, \mathbf{b} the magnetic field unit vector and e the charge of the considered particle. It is possible to evaluate the two Poisson brackets $\{H_{eq}, g\}$ and $\{e\phi, g\}$ using the notations of part 3.1 :

$$\begin{aligned}\{H_{eq}, g\} &\sim \left| \frac{\partial H_{eq}}{\partial p_{\parallel}} \frac{\partial g}{\partial x_{\parallel}} \right| \sim v_{\parallel} k_{\parallel} g \\ \{e\phi, g\} &\sim \frac{1}{eB} \left| \frac{e\partial\phi}{\partial r} \frac{\partial g}{r\partial\theta} \right| \sim \frac{1}{B} k_r \phi k_{\theta} g\end{aligned}$$

with $v_{\parallel} \sim \sqrt{T/m}$ the velocity parallel to the magnetic field lines, k_x a typical wave number in the x direction (in particular $k_{\parallel} \sim 1/qR$), r the radial coordinate, θ the poloidal angle. Calculating the ratio $\{e\phi, g\} / \{H_{eq}, g\}$, it comes :

$$\frac{\{e\phi, g\}}{\{H_{eq}, g\}} \sim \frac{k_r k_{\theta} \phi}{B v_{\parallel} k_{\parallel}} \sim qR\rho_L k_r k_{\theta} \frac{e\phi}{T}$$

with ρ_L the Larmor radius of the ions. We see that the ratio $\{e\phi, g\} / \{H_{eq}, g\}$ depends of the radial and poloidal structure of the plasma via $k_r k_{\theta}$. Hence, the saturation limit $e\phi/T \ll 1$ is not enough to state that the ratio $\{e\phi, g\} / \{H_{eq}, g\} \ll 1$. However, in the case of GAMs, $k_r \sim a^{-1}$ and $k_{\theta} \sim a^{-1}$ with a the small radius of the tokamak. The ratio becomes in that case :

$$\frac{\{e\phi, g\}}{\{H_{eq}, g\}} \sim \frac{qR\rho_L}{a^2} \frac{e\phi}{T} \ll 1 \text{ in the case } \frac{e\phi}{T} \ll 1$$

C.2 Angle action variables

Using parity arguments, the bounce/transit average be reduced to an average over an upper quadrant in α_2

$$\frac{2}{\pi} \int_0^{\frac{\pi}{2}} d\alpha_2 \dots = \begin{cases} \frac{1}{\tau} \frac{2}{\pi} \int_0^{\frac{\pi}{2}} \frac{d\delta}{\sqrt{1-\kappa^2 \sin^2 \delta}} \dots & \text{if } 0 \leq \kappa < 1 \text{ (passing)} \\ \frac{1}{\kappa\tau} \frac{2}{\pi} \int_0^{\frac{\pi}{2}} \frac{d\delta}{\sqrt{1-\frac{1}{\kappa^2} \sin^2 \delta}} \dots & \text{if } 1 < \kappa < +\infty \text{ (trapped)} \end{cases} \quad (\text{C.1})$$

where it is reminded that

$$\tau(\kappa) = \frac{2}{\pi} \begin{cases} \mathbb{K}(\kappa^2) & \text{if } 0 \leq \kappa < 1 \text{ (passing)} \\ \frac{1}{\kappa} \mathbb{K}\left(\frac{1}{\kappa^2}\right) & \text{if } 1 < \kappa < +\infty \text{ (trapped)} \end{cases} \quad (\text{C.2})$$

As expected, the bounce/transit period becomes very large near the passing/trapped boundary $\kappa = 1$ since $\mathbb{K}(\kappa) \simeq -\frac{1}{2} \ln |1 - \kappa|$ for $|1 - \kappa| \ll 1$. A useful expression of $\alpha_2(\delta)$

in the upper quadrant $0 \leq \delta \leq \frac{\pi}{2}$, $0 \leq \alpha_2 \leq \frac{\pi}{2}$ is

$$\alpha_2 = \begin{cases} \pi \frac{\mathbb{F}\left(\frac{\theta}{2}, \kappa^2\right)}{\mathbb{F}\left(\frac{\pi}{2}, \kappa^2\right)} & \text{if } 0 \leq \kappa < 1 \text{ (passing)} \\ \frac{\pi}{2} \frac{\mathbb{F}\left(\sin^{-1}\left[\kappa \sin\left(\frac{\theta}{2}\right)\right], \frac{1}{\kappa^2}\right)}{\mathbb{F}\left(\frac{\pi}{2}, \frac{1}{\kappa^2}\right)} & \text{if } 1 < \kappa < +\infty \text{ (trapped)} \end{cases} \quad (\text{C.3})$$

where $F(\varphi, k)$ is the incomplete elliptical function of the first kind defined as

$$\mathbb{F}(\delta, m) = \int_0^\delta \frac{d\delta'}{\sqrt{1 - m \sin^2 \delta'}} \quad (\text{C.4})$$

This relation can be formally inverted to provide a link between the guiding-center poloidal angle θ and the angular variable α_2 . It is also interesting to construct this link for all values of the angles α_2 and θ . Using the property $\mathbb{K}(k) = \mathbb{F}\left(\frac{\pi}{2}, k\right)$, the relation Eq.(C.3) can be rephrased as

$$\begin{aligned} \sin\left(\frac{\theta}{2}\right) &= \text{sn}\left(\frac{\tau\alpha_2}{2}, \kappa^2\right) & \text{if } 0 \leq \kappa < 1 \text{ (passing)} \\ \sin\left(\frac{\theta}{2}\right) &= \frac{1}{\kappa} \text{sn}\left(\kappa\tau\alpha_2, \frac{1}{\kappa^2}\right) & \text{if } 1 < \kappa < +\infty \text{ (trapped)} \end{aligned} \quad (\text{C.5})$$

valid for all α_2, θ . The function $\text{sn}(\delta, k)$ is the Jacobian elliptic function that coincides with the trigonometric $\sin \delta$ function for $k \ll 1$. One recovers that $\theta = \alpha_2 + \frac{1}{4}\kappa^2 \sin(\alpha_2)$ for deeply passing particles $\kappa \rightarrow 0$. For deeply trapped particles $\kappa \rightarrow \infty$, $\theta = \theta_0 \sin \alpha_2$ where θ_0 is the bounce angle, $\sin\left(\frac{\theta_0}{2}\right) = \frac{1}{\kappa}$. Note that the Jacobi sn function differs significantly from a sinusoidal function for barely trapped or passing particles $\kappa \sim 1$.

Eqs.(C.1, C.3) also provide a useful expression of the derivative $\frac{d\alpha_2}{d\theta}$, which reads for passing particles

$$\tau(\kappa) d\alpha_2 = \frac{d\theta}{\sqrt{1 - \kappa^2 \sin^2 \frac{\theta}{2}}} \quad (\text{C.6})$$

while for trapped particles

$$2\tau(\kappa) d\alpha_2 = \epsilon_{\parallel} \frac{d\theta}{\sqrt{1 - \kappa^2 \sin^2 \frac{\theta}{2}}} \quad (\text{C.7})$$

where $\epsilon_{\parallel} = 1$, when $-\frac{\pi}{2} < \alpha_2 < \frac{\pi}{2}$ and $\epsilon_{\parallel} = -1$ when $-\pi < \alpha_2 < -\frac{\pi}{2}$ or $\frac{\pi}{2} < \alpha_2 < \pi$. The factor 2 comes from the period doubling when crossing the passing/trapped boundary. The parameter ϵ_{\parallel} is readily interpreted as the sign of the particle parallel velocity. When $\epsilon_{\parallel} = 1$, a trapped particle moves from $-\theta_0$ ($\alpha_2 = -\frac{\pi}{2}$) to θ_0 ($\alpha_2 = \frac{\pi}{2}$), while it moves back from θ_0 to $-\theta_0$ for $\epsilon_{\parallel} = -1$. Note also that $\theta = 0$ for $\alpha_2 = \pi$, $\alpha_2 = 0$ and $\alpha_2 = -\pi$.

C.3 Electron Lagrangian expressed with angular variables

Eq.(3.49) is recalled:

$$\bar{\mathcal{L}}_{res,e} = - \sum_{n_2=-\infty}^{+\infty} \int d\zeta F_M \frac{\Omega}{\Omega - n_2 \frac{\Omega_b}{\sigma} + i0^+} |\tilde{h}_{n_2\omega}|^2$$

Using Eq.(3.52) the Lagrangian is recast as follows:

$$\bar{\mathcal{L}}_{res,e} = i\sigma\Omega \int d\zeta \frac{F_M}{|\Omega_b|} \int_0^{+\infty} ds \exp \left\{ i\sigma \frac{\Omega}{\Omega_b} \varepsilon_{\parallel} s \right\} \underbrace{\sum_{n_2=-\infty}^{+\infty} e^{-in_2\varepsilon_{\parallel}s} |\tilde{h}_{n_2\omega}|^2}_A$$

The term A can be calculated by replacing $\tilde{h}_{n_2\omega}$ by its expression given by Eq.(3.51). It becomes:

$$A = \oint \frac{d\alpha_2}{2\pi} \tilde{h}_{\omega}(\alpha_2) \oint \frac{d\alpha'_2}{2\pi} \tilde{h}_{\omega}^*(\alpha'_2) \sum_{n_2=-\infty}^{+\infty} e^{in_2(\alpha'_2 - \alpha_2 - \varepsilon_{\parallel}s)}$$

Using Eq.(3.53), A becomes:

$$A = \oint \frac{d\alpha_2}{2\pi} \tilde{h}_{\omega}(\alpha_2) \oint \frac{d\alpha'_2}{2\pi} \tilde{h}_{\omega}^*(\alpha'_2) \sum_{p=-\infty}^{+\infty} 2\pi\delta(\alpha'_2 - \alpha_2 - \varepsilon_{\parallel}s - 2\pi p)$$

Replacing the expression of A in $\bar{\mathcal{L}}_{res,e}$, it comes:

$$\bar{\mathcal{L}}_{res,e} = 2i\pi\sigma\Omega \sum_{p=-\infty}^{+\infty} \int d\zeta \frac{F_M}{|\Omega_b|} \oint \frac{d\alpha_2}{2\pi} \tilde{h}_{\omega}(\alpha_2) \oint \frac{d\alpha'_2}{2\pi} \tilde{h}_{\omega}^*(\alpha'_2) \underbrace{\int_0^{+\infty} ds \exp \left\{ i\sigma \frac{\Omega}{\Omega_b} \varepsilon_{\parallel} s \right\} \delta(\alpha'_2 - \alpha_2 - \varepsilon_{\parallel}s - 2\pi p)}_B$$

Two cases appear now:

- if $s_0 = \frac{1}{\varepsilon_{\parallel}}(\alpha'_2 - \alpha_2 + 2\pi p) = \varepsilon_{\parallel}(\alpha'_2 - \alpha_2 + 2\pi p)$, ($\varepsilon_{\parallel} = \pm 1$) is negative, then the dirac function is zero in the integration domain $[0; +\infty[$ and $B = 0$.
- if $s_0 = \varepsilon_{\parallel}(\alpha'_2 - \alpha_2 + 2\pi p)$ is positive, then it is in the integration domain $[0; +\infty[$ and $B = \exp \left\{ i\sigma \frac{\Omega}{\Omega_b} (\alpha'_2 - \alpha_2 + 2\pi p) \right\}$

This can be dealt with by the introduction of an Heaviside function Θ ($\Theta(x) = 1$ for $x > 0$, 0 otherwise) and doing the integral over s , the Lagrangian finally takes the shape of Eq.(3.54):

$$\bar{\mathcal{L}}_{res,e} = 2i\pi\sigma\Omega \sum_{p=-\infty}^{+\infty} \int d\zeta \frac{F_M}{|\Omega_b|} \oint \frac{d\alpha_2}{2\pi} \tilde{h}_{\omega}(\alpha_2) \oint \frac{d\alpha'_2}{2\pi} \tilde{h}_{\omega}^*(\alpha'_2) \Theta[\varepsilon_{\parallel}(\alpha'_2 - \alpha_2 + 2\pi p)] \exp \left\{ i\sigma \frac{\Omega}{\Omega_b} (\alpha'_2 - \alpha_2 + 2\pi p) \right\}$$

We consider $\varepsilon_{\parallel} = 1$. The Heaviside function in Eq.(3.54) is equal to:

$$\Theta(\alpha'_2 - \alpha_2 + 2p\pi) = \begin{cases} 1 & \text{if } p > 0 \\ \Theta(\alpha'_2 - \alpha_2) & \text{if } p = 0 \\ 0 & \text{if } p < 0 \end{cases}$$

Therefore, the Lagrangian Eq.(3.54) becomes:

$$\begin{aligned} \bar{\mathcal{L}}_{res,e} = & 2i\pi\sigma\Omega \int d\varsigma \frac{F_M}{|\Omega_b|} \int_{-\pi}^{\pi} \frac{d\alpha_2}{2\pi} \int_{-\pi}^{\pi} \frac{d\alpha'_2}{2\pi} \tilde{h}_{\omega}(\alpha_2) \tilde{h}_{\omega}^*(\alpha'_2) \exp\left\{i\sigma \frac{\Omega}{\Omega_b}(\alpha'_2 - \alpha_2)\right\} \\ & \left\{ \Theta(\alpha'_2 - \alpha_2) + \sum_{p=1}^{+\infty} \exp\left\{i\sigma \frac{\Omega}{\Omega_b} 2\pi p\right\} \right\} \end{aligned}$$

Besides, the geometrical sum can be rewritten as:

$$\sum_{p=1}^{+\infty} \exp\left\{i\sigma \frac{\Omega}{\Omega_b} 2\pi p\right\} = \sum_{p=0}^{+\infty} \exp\left\{i\sigma \frac{\Omega}{\Omega_b} 2\pi p\right\} - 1 = \frac{1 - \exp\left\{i\sigma \frac{\Omega}{\Omega_b} 2\pi\right\}^{\infty}}{1 - \exp\left\{i\sigma \frac{\Omega}{\Omega_b} 2\pi\right\}} - 1$$

In fact, we earlier removed the term " $i0^+$ " that appeared in Eq.(3.52) for simplification. Taking this term into account, the expression $\exp\left\{i\sigma \frac{\Omega}{\Omega_b} 2\pi\right\}^{\infty}$ should be rewritten $\exp\left\{i\left(\sigma \frac{\Omega}{\Omega_b} 2\pi + i0^+\right)\right\}^{\infty}$ hence becoming zero. The sum is then recast as:

$$\sum_{p=1}^{+\infty} \exp\left\{i\sigma \frac{\Omega}{\Omega_b} 2\pi p\right\} = \frac{1}{\exp\left\{-2i\pi\sigma \frac{\Omega}{\Omega_b}\right\} - 1}$$

The Lagrangian then takes the shape of Eq.(3.55):

$$\begin{aligned} \bar{\mathcal{L}}_{res,e} = & 2i\pi\sigma\Omega \int d\varsigma \frac{F_M}{|\Omega_b|} \int_{-\pi}^{\pi} \frac{d\alpha_2}{2\pi} \int_{-\pi}^{\pi} \frac{d\alpha'_2}{2\pi} \tilde{h}_{\omega}(\alpha_2) \tilde{h}_{\omega}^*(\alpha'_2) \exp\left\{i\sigma \frac{\Omega}{\Omega_b}(\alpha'_2 - \alpha_2)\right\} \\ & \left\{ \Theta(\alpha'_2 - \alpha_2) + \frac{1}{\exp\left\{-2i\pi\sigma \frac{\Omega}{\Omega_b}\right\} - 1} \right\} \end{aligned}$$

C.4 Trapped electron Lagrangian

C.4.1 Trapped electron Lagrangian for a $\sin \theta$ GAM perturbation

The harmonic $m = 1$ of the GAM corresponds to a $\tilde{h}_\omega(\alpha_2) = \eta \sin[\theta(\alpha_2)]$ perturbation. The corresponding Lagrangian reads

$$\bar{L}_{res,e} = 8i\sqrt{2\pi}\varepsilon^{1/2}\eta^2 \int_1^{+\infty} \frac{\kappa d\kappa}{\Lambda^{3/2}(\kappa)} \tau(\kappa) \int_0^{+\infty} dv v^2 \exp(-v^2) \mathcal{I}(\kappa, v)$$

where

$$\begin{aligned} \mathcal{I}(\kappa, v) &= \bar{\sigma} \int_{-\pi}^{\pi} \frac{d\alpha}{2\pi} \int_{-\pi}^{\pi} \frac{d\alpha'}{2\pi} \sin[\theta(\alpha)] \sin[\theta(\alpha')] \\ &\quad \exp\{i\bar{\sigma}(\alpha' - \alpha)\} \left\{ \Theta(\alpha' - \alpha) + \frac{1}{\exp(-2i\pi\bar{\sigma}) - 1} \right\} \end{aligned}$$

where $\bar{\sigma} = \sigma^* \frac{\tau(\kappa)}{v} \Lambda^{1/2}(\kappa)$. It is reminded that $\frac{\partial\theta}{\partial\alpha} = 2\epsilon_{\parallel}\tau(\kappa)\sqrt{1 - \kappa^2 \sin^2 \frac{\theta}{2}}$ (see Eq.(C.7) in Appendix C.2), where $\epsilon_{\parallel} = 1$ when θ goes from $-\theta_0$ to $+\theta_0$ and $\epsilon_{\parallel} = -1$ on the way back, i.e. from $+\theta_0$ to $-\theta_0$. It then appears that $\frac{\partial^2\theta}{\partial\alpha^2} = -\tau^2(\kappa)\kappa^2 \sin \theta$, and

$$\begin{aligned} \mathcal{I}(\kappa, v) &= \frac{1}{\tau^4 \kappa^4} \bar{\sigma} \int_{-\pi}^{\pi} \frac{d\alpha}{2\pi} \frac{\partial^2\theta}{\partial\alpha^2} \int_{-\pi}^{\pi} \frac{d\alpha'}{2\pi} \frac{\partial^2\theta}{\partial\alpha'^2} \\ &\quad \exp\{i\bar{\sigma}(\alpha' - \alpha)\} \left\{ \Theta(\alpha' - \alpha) + \frac{1}{\exp(-2i\pi\bar{\sigma}) - 1} \right\} \end{aligned}$$

We now expand Eq.(C.8) in power laws in $\bar{\sigma}$. We note that

$$\lim_{\bar{\sigma} \rightarrow 0} \bar{\sigma} \exp\{i\bar{\sigma}(\alpha' - \alpha)\} = \bar{\sigma} + i\bar{\sigma}^2(\alpha' - \alpha) + o(\bar{\sigma}^3) \quad (\text{C.8})$$

$$\begin{aligned} \lim_{\bar{\sigma} \rightarrow 0} \frac{\bar{\sigma} \exp\{i\bar{\sigma}(\alpha' - \alpha)\}}{\exp(-2i\pi\bar{\sigma}) - 1} &= -\frac{1}{2i\pi} \left\{ 1 + i\bar{\sigma}(\pi + \alpha' - \alpha) + \bar{\sigma}^2 \left[\frac{\pi^2}{6} \right. \right. \\ &\quad \left. \left. - \pi(\alpha' - \alpha) - \frac{1}{2}(\alpha' - \alpha)^2 \right] + o(\bar{\sigma}^3) \right\} \quad (\text{C.9}) \end{aligned}$$

The $o(\bar{\sigma}^0)$ term in Eq.(C.9) does not contribute to $\mathcal{I}(\kappa, v)$ because it involves integrals of second derivatives $\frac{\partial^2\theta}{\partial\alpha^2}$ over a period, which obviously vanish. The $o(\bar{\sigma})$ term comes from both Eq.(C.8) and Eq.(C.9). Hence the function $\mathcal{I}(\kappa, v)$ can be decomposed in two corresponding parts $\mathcal{I} = \mathcal{I}_1 + \mathcal{I}_2$. The first one reads

$$\begin{aligned} \mathcal{I}_1(\kappa, v) &= \bar{\sigma} \frac{1}{\tau^4 \kappa^4} \int_{-\pi}^{\pi} \frac{d\alpha}{2\pi} \frac{\partial^2\theta}{\partial\alpha^2} \int_{\alpha}^{\pi} \frac{d\alpha'}{2\pi} \frac{\partial^2\theta}{\partial\alpha'^2} \\ &= -\bar{\sigma} \frac{1}{\tau^4 \kappa^4} \frac{1}{4\pi} \int_{-\pi}^{\pi} \frac{d\alpha}{2\pi} \frac{\partial}{\partial\alpha} \left[\frac{\partial\theta}{\partial\alpha} \right]^2 \\ &= 0 \end{aligned}$$

The second contribution \mathcal{I}_2 is such that

$$\begin{aligned}\mathcal{I}_2(\kappa, v) &= -\frac{\bar{\sigma}}{2\pi} \frac{1}{\tau^4 \kappa^4} \int_{-\pi}^{\pi} \frac{d\alpha}{2\pi} \frac{\partial^2 \theta}{\partial \alpha^2} \int_{-\pi}^{\pi} \frac{d\alpha'}{2\pi} \frac{\partial^2 \theta}{\partial \alpha'^2} (\pi + \alpha' - \alpha) \\ &= 0\end{aligned}$$

This comes from the fact that each term in $(\pi + \alpha' - \alpha)$ taken separately involves again a second derivative of θ integrated over a period. This implies that the $o(\bar{\sigma})$ contribution to $\bar{L}_{res,e}$ cancels.

Let us now determine the $o(\bar{\sigma})^2$ contribution to $\bar{L}_{res,e}$. Terms from both Eq.(C.8) and Eq.(C.9) matter. However a close inspection of these contribution shows that they are all pure imaginary numbers, and therefore do not contribute to damping since they exclusively contribute to the real part of the Lagrangian. Hence the imaginary part of the Lagrangian must scale as $[\bar{\sigma}]^3$ when $\bar{\sigma} \rightarrow 0$. It is stressed however that $\bar{\sigma} = \sigma^* \frac{\tau(\kappa)}{v} \Lambda^{1/2}(\kappa)$ is a function of κ and v . Therefore even if σ^* is a small number, there exists regions of the phase where the condition $\bar{\sigma} \rightarrow 0$ breaks down. These regions provide the largest contribution to the Lagrangian, and therefore to damping.

C.4.2 Explicit calculation of the electron Lagrangian

We consider the Lagrangian Eq.(3.68) as formulated in Appendix C.4.1,

$$\bar{L}_{res,e} = 8i\sqrt{2\pi\varepsilon}^{1/2} \int_1^{+\infty} \frac{\kappa d\kappa}{\Lambda^{3/2}(\kappa)} \tau(\kappa) \int_0^{+\infty} dv v^2 \exp(-v^2) \mathcal{I}(\kappa, v)$$

where

$$\begin{aligned}\mathcal{I}(\kappa, v) &= \bar{\sigma} \int_{-\pi}^{\pi} \frac{d\alpha}{2\pi} \int_{-\pi}^{\pi} \frac{d\alpha'}{2\pi} \tilde{h}_\omega(\alpha) \tilde{h}_\omega^*(\alpha') \\ &\quad \exp\{i\bar{\sigma}(\alpha' - \alpha)\} \left[\Theta(\alpha' - \alpha) + \frac{1}{\exp(-2i\pi\bar{\sigma}) - 1} \right]\end{aligned}\quad (\text{C.10})$$

where $\bar{\sigma} = \sigma^* \frac{\tau(\kappa)}{v} \Lambda^{1/2}(\kappa)$. The largest contribution must come from the domain in the phase space where $\bar{\sigma} > 1$, since it was shown in Appendix C.4.1 that regions where $\bar{\sigma} \ll 1$ bring a negligible $o(\bar{\sigma}^3)$ contribution to its imaginary part. We split $\mathcal{I}(\kappa, v)$ in two parts $\mathcal{I} = \mathcal{I}_1 + \mathcal{I}_2$, which correspond to the two terms in the bracket [] (second line of Eq.(C.10)). The first one reads

$$\begin{aligned}\mathcal{I}_1(\kappa, v) &= \bar{\sigma} \int_{-\pi}^{\pi} \frac{d\alpha}{2\pi} \int_{-\pi}^{\pi} \frac{d\alpha'}{2\pi} \tilde{h}_\omega(\alpha) \tilde{h}_\omega^*(\alpha') \\ &\quad \exp\{i\bar{\sigma}(\alpha' - \alpha)\} \Theta(\alpha' - \alpha)\end{aligned}$$

The integrand is assumed to be dominated by the turning points $\alpha = \pm\frac{\pi}{2}$, where $\theta = \pm\theta_0$. Let us detail this delicate point. For any function $h(\theta)$ even in θ , one has the identity

$$\int_{-\pi}^{\pi} \frac{d\alpha}{2\pi} h(\alpha) = \frac{\int_{-\theta_0}^{\theta_0} \frac{d\theta}{\sqrt{1-\kappa^2 \sin^2 \frac{\theta}{2}}} h(\theta)}{\int_{-\theta_0}^{\theta_0} \frac{d\theta}{\sqrt{1-\kappa^2 \sin^2 \frac{\theta}{2}}}}\quad (\text{C.11})$$

where $h(\alpha)$ must be understood as $h(\alpha) = h[\theta(\alpha)]$. If $h(\theta)$ is a smooth function, the integral on the r.h.s of Eq.(C.11) can be approximated by $h(\theta_0)$, assuming that most of the integration will be weighted by the turning point $\theta = \pm\theta_0$. The (integrable) singularity at the turning points does not appear explicitly when using the variable α , because it is then hidden in the function $h(\alpha)$, which is built from $h(\theta)$ by using the change of variable $\theta \rightarrow \alpha$. It is recovered by changing $h(\alpha)$ by $h(\theta_0)\pi \left\{ \delta\left(\alpha - \frac{\pi}{2}\right) + \delta\left(\alpha + \frac{\pi}{2}\right) \right\}$ whenever it is integrated over α , where $h(\theta_0)$ is the value of h at the turning point. A calculation of Eq.(C.11) using this approximation when $\bar{\sigma} \rightarrow 0$ shows that $\Re(\mathcal{I}_1)$ scales as $\bar{\sigma}^3$, as already found via an exact calculation in Appendix C.4.1. This is no longer true when $\bar{\sigma} \sim o(1)$. Indeed in that case, the oscillating function $\exp\{i\bar{\sigma}(\alpha' - \alpha)\}$ introduce a phase term $\exp(\pm i\pi\bar{\sigma})$ when $\alpha = \frac{\pi}{2}, \alpha' = -\frac{\pi}{2}$ or $\alpha = -\frac{\pi}{2}, \alpha' = \frac{\pi}{2}$. Once integrated over the phase space, this phase term is averaged down to a small number. Hence most of the contribution comes from the neighborhood of $\alpha = \alpha' = \frac{\pi}{2}$ and $\alpha = \alpha' = -\frac{\pi}{2}$. One must then be careful that the Heaviside function introduces a factor $\frac{1}{2}$ since the integral of a δ function over a half-space is half-unity. The integral Eq.(C.11) can then be upper bounded by the following (rough) estimate

$$\mathcal{I}_1(\kappa, v) \leq \frac{\bar{\sigma}}{4} \left| \tilde{h}_\omega(\theta_0) \right|^2 \quad (\text{C.12})$$

The second piece reads

$$\mathcal{I}_2(\kappa, v) = \bar{\sigma} \sum_{p=1}^{+\infty} \int_{-\pi}^{\pi} \frac{d\alpha}{2\pi} \int_{-\pi}^{\pi} \frac{d\alpha'}{2\pi} \tilde{h}_\omega(\alpha) \tilde{h}_\omega^*(\alpha') \exp\{i\bar{\sigma}(\alpha' - \alpha + 2p\pi)\}$$

where a prior version of the Lagrangian, namely Eq.(3.54) (before summation over the index p), was used. Using the same trick as before, it appears that the region of the phase space where $\bar{\sigma} > 1$ contributes weakly, because the phase terms $\exp\{i2p\pi\bar{\sigma}\}$ average out to small numbers after integration over the phase space. The resulting Lagrangian then reads

$$\bar{L}_{res,e} = 2i\sqrt{2\pi}\varepsilon^{1/2}\sigma^*\mathcal{D}(\sigma^*) \int_1^{+\infty} \frac{\kappa d\kappa}{\Lambda(\kappa)} \tau^2(\kappa) \int_0^{+\infty} dv v \exp(-v^2) \left| \tilde{h}_\omega(\theta_0(\kappa)) \right|^2$$

which leads to Eq.(3.69) after integration over the velocity modulus v . The function $\mathcal{D}(\sigma^*)$ measures the weight of the region in the phase space (κ, v) where $\bar{\sigma} \geq 1$. The function $\mathcal{D}(\sigma^*)$ is presumably smaller than 1. The complementary part of the phase space where $\bar{\sigma} \leq 1$ was shown in Appendix C.4.1 to produce a small $o(\bar{\sigma}^3)$ contribution to imaginary part of $\bar{L}_{res,e}$. Hence $\mathcal{D}(\sigma^*) = 1$ can be considered as an upper bound of the Lagrangian.

C.5 Damping rate estimation

The notations \mathcal{D}_r and \mathcal{D}_i are used respectfully for the real and imaginary parts of the dispersion relation. The solutions of the equation $\mathcal{D}(\Omega) = 0$ are characterized by the complex pulsation $\Omega = \Omega_0 - i\Gamma$ with Ω_0 the normalized resonance pulsation and Γ the normalized damping rate. Close to the GAM resonance, $\Omega \simeq \Omega_0$ and $|\Gamma/\Omega_0| \ll 1$. Developing the dispersion relation $\mathcal{D}(\Omega) = \mathcal{D}_r(\Omega) + i\mathcal{D}_i(\Omega) = 0$ around Ω_0 gives:

$$\mathcal{D}(\Omega) \simeq \underbrace{\mathcal{D}_r(\Omega_0)}_0 + i\mathcal{D}_i(\Omega_0) + \underbrace{(\Omega - \Omega_0)}_{-i\Gamma} \partial_\Omega (\mathcal{D}_r + i \underbrace{\mathcal{D}_i}_{\ll \mathcal{D}_r})|_{\Omega_0} = 0$$

and Γ can be recast as:

$$\Gamma \simeq \frac{\mathcal{D}_i(\Omega_0)}{\partial_\Omega \mathcal{D}_r(\Omega_0)}$$

Taking the real part of dispersion relation of the form $\mathcal{D}_r(\Omega) = 1 - \frac{\Omega_0^2}{\Omega^2}$, we have $\partial_\Omega \mathcal{D}_r(\Omega_0) = \frac{2}{\Omega_0}$. Taking now the imaginary part of the dispersion relation due to electrons in Eq.(3.76), namely $\mathcal{D}_i(\Omega) = G(q, \tau_e) \mathcal{D}(\sigma^*) \left(\frac{m_e}{m_i}\right)^{1/2} q \tau_e^{1/2} \Omega$, the normalized damping rate yields to Eq.(3.79):

$$\Gamma \simeq \frac{1}{2} G(q, \tau_e) \mathcal{D}(\sigma^*) \left(\frac{m_e}{m_i}\right)^{1/2} q \tau_e^{1/2} \Omega_0^2$$

C.6 Form of the density perturbation to get a sinusoidal potential

We decompose the initial distribution function profile into a Maxwellian plus a perturbation $g(r)$. This perturbation triggers an initial potential profile of the form $\phi(r) = \tilde{\phi} \sin(kr)$ with k the spatial frequency of the oscillations. We consider only one ion species, the electrons response is adiabatic, and the gyroaverage operator is approximated by a Padé form, which reads :

$$J_0 = \frac{1}{1 - \frac{\rho^2}{4} \nabla_{\perp}^2} \sim 1 + \frac{\rho^2}{4} \nabla_{\perp}^2$$

with ρ the Larmor radius, and $\nabla_{\perp}^2 = \frac{1}{r} \partial_r (r \partial_r) + \frac{1}{r^2} \partial_{\theta}^2$. Since all quantities considered are independent of θ at the initial time, we will take $\nabla_{\perp}^2 = \frac{1}{r} \partial_r (r \partial_r)$.

In this framework, the equation of quasi-neutrality at the initial time reads :

$$\int d^3v J_0 \cdot g(r) + \nabla_{\perp} \cdot \left(\frac{mn_0(r)}{ZeB^2} \nabla_{\perp} \phi \right) = \frac{e}{T_e(r)} (\phi(r) - \langle \phi(r) \rangle_{FS})$$

$$\int d^3v J_0 \cdot g(r) + \frac{1}{r} \partial_r \left(r \frac{mn_0(r)}{ZeB^2} \partial_r \phi \right) = 0$$

with $n_0(r) = \int d^3v J_0 \cdot f_0$ the initial density and f_0 the initial Maxwellian profile of the distribution function. In our case, it is assumed that f_0 (and hence n_0) and the magnetic field B are independent of r and that $J_0 = 1$. After developing the polarization term, we find:

$$\int d^3v \{g(r) + K(r)\} = 0 \quad (\text{C.13})$$

where

$$K(r) = M f_0 \left[\frac{1}{r} (\partial_r \phi + r \partial_r^2 \phi) \right] \quad (\text{C.14})$$

By choosing a perturbation of the distribution function $g(r) = -K(r)$, Eq.(C.13) is satisfied.

- For $\phi(r) = \tilde{\phi} \sin(kr)$, choosing $\tilde{\phi} = 1/M f_0$ implies

$$g(r) = -\frac{1}{r} [k \cos(kr) - k^2 r \sin(kr)] \quad (\text{C.15})$$

- For $\phi(r) = \tilde{\phi} (1 - \cos(kr))$, choosing $\tilde{\phi} = 1/M f_0$ implies

$$g(r) = -\frac{1}{r} [k \sin(kr) + k^2 r \cos(kr)] \quad (\text{C.16})$$

Appendix D

Appendices of chapter 4

D.1 Conservation equations

Conservation equations in GYSELA are tackled in J. Abiteboul's thesis [1, Abiteboul 2012]. We here do a similar derivation with the particular objective of getting an expression of the energy transfer from the electric wave to particles. We first retrieve the particle and energy conservation equation for gyrocentres by integrating the gyrokinetic equation in velocity space. The gyrokinetic equation takes the form:

$$\frac{\partial \bar{f}}{\partial t} + \frac{1}{B_{\parallel}^*} \nabla_z \left(\dot{z} B_{\parallel}^* \bar{f} \right) = 0 \quad (\text{D.1})$$

with $z = (\mathbf{x}, \mathbf{v})$ referring to the position and velocity coordinates and $B_{\parallel}^* = B + \frac{m}{q} v_{G,\parallel} \mathbf{b} \cdot \nabla \wedge \mathbf{b}$. First, the matter conservation equation is derived and then the energy conservation equation for gyrocentres.

We note: \mathbf{x} the position, \mathbf{v} the velocity, v_{\parallel} the projection of the velocity on the magnetic field direction, μ the magnetic moment, F the distribution function, J_0 the gyroaverage operator, ϕ the electric potential, \mathbf{E} the electric field, \mathbf{B} the magnetic field, \mathbf{J} the electric current, ε_0 the dielectric permittivity of vacuum, μ_0 the dielectric permeability of vacuum, n the density, m the mass, e the charge. \bar{X} refers to the quantity X applied for gyrocentres.

D.1.1 Matter conservation

The conservation equation of particles is obtained by integrating equation (D.1) in velocity space, it comes:

$$\int \frac{\partial \bar{f}}{\partial t} d^3v + \int \frac{1}{B_{\parallel}^*} \nabla_z \left(\dot{z} B_{\parallel}^* \bar{f} \right) d^3v = 0$$

with $d^3v = \mathcal{J}_v dv_{\parallel} d\mu$ where $\mathcal{J}_v = 2\pi B_{\parallel}^*$ stands for the jacobian between particle and gyrocentres in velocity phase space.

- The calculation of the first integral I_1 gives $I_1 = \frac{\partial n}{\partial t}$ where n stands for the density of gyrocentres.
- The calculation of the second integral I_2 reads:

$$I_2 = \int \frac{d^3v}{B_{\parallel}^*} \left[\nabla \cdot (\dot{\mathbf{x}} B_{\parallel}^* \bar{f}) + \partial_{v_{\parallel}} (\dot{v}_{\parallel} B_{\parallel}^* \bar{f}) + \partial_{\mu} (\dot{\mu} B_{\parallel}^* \bar{f}) \right]$$

The magnetic moment is conserved through time, thus $\dot{\mu} = 0$. Since $d^3v/B_{\parallel}^* = 2\pi dv_{\parallel} d\mu$, the integral of the second term reads:

$$\int \frac{d^3v}{B_{\parallel}^*} \partial_{v_{\parallel}} (\dot{v}_{\parallel} B_{\parallel}^* \bar{f}) = \int 2\pi d\mu \left[\dot{v}_{\parallel} B_{\parallel}^* \bar{f} \right]_{v_{\parallel}=-\infty}^{v_{\parallel}=\infty} = 0$$

because \bar{f} becomes 0 when $|v|$ becomes infinite. As d^3v/B_{\parallel}^* is independent of the position coordinate \mathbf{x} , the integral I_2 then reduces to:

$$I_2 = \int \frac{d^3v}{B_{\parallel}^*} \nabla \cdot (\dot{\mathbf{x}} B_{\parallel}^* \bar{f}) = \nabla \cdot \int d^3v \dot{\mathbf{x}} \bar{f} = \nabla \cdot \mathbf{\Gamma}$$

where $\mathbf{\Gamma} = \int d^3v \dot{\mathbf{x}} \bar{f}$ stands for the particle flux.

Consequently, the conservation equation for particle takes the form:

$$\frac{\partial n}{\partial t} + \nabla \cdot \mathbf{\Gamma} = 0 \quad (\text{D.2})$$

In a set of coordinates (x^i) , the expression of the gradient becomes:

$$\nabla \cdot \mathbf{\Gamma} = \frac{1}{\sqrt{g}} \sum_i \partial_{x^i} (\sqrt{g} \Gamma_i)$$

where \sqrt{g} stands for the Jacobian of the set of coordinates (x^i) . In the case of the usual tokamak coordinates (χ, θ, φ) , we have $\sqrt{g} = Rr \frac{dr}{d\chi}$. With this formulation, equation (D.2) becomes:

$$\partial_t (\sqrt{g} n) + \partial_{\chi} (\sqrt{g} \Gamma^{\chi}) + \frac{1}{r} \partial_{\theta} (\sqrt{g} \Gamma^{\theta}) + \frac{1}{R} \partial_{\varphi} (\sqrt{g} \Gamma^{\varphi}) = 0 \quad (\text{D.3})$$

Averaging this equation on (θ, φ) , the last two terms disappear: $\int_0^{2\pi} d\theta \partial_{\theta} (\sqrt{g} \Gamma^{\theta}) = \sqrt{g} \Gamma^{\theta}(\theta = 2\pi) - \sqrt{g} \Gamma^{\theta}(\theta = 0) = 0$ because $\sqrt{g} \Gamma^{\theta}$ is periodic in θ . The same can be done for Γ^{φ} . Therefore, it comes:

$$\partial_t \left(\int d\theta d\varphi \sqrt{g} n \right) + \partial_{\chi} \left(\int d\theta d\varphi \sqrt{g} \Gamma^{\chi} \right) = 0$$

Defining $\langle \dots \rangle_{FS} = V^{-1} \int d\theta d\varphi \sqrt{g} \dots$ with $V = \int d\theta d\varphi \sqrt{g}$ the flux surface average, it comes:

$$V \partial_t \langle n \rangle_{FS} + \partial_{\chi} (V \langle \Gamma^{\chi} \rangle_{FS}) = 0 \quad (\text{D.4})$$

NB: If we work with the spatial coordinates (r, θ, φ) , then $\sqrt{g} = rR$ and the conservation equation becomes:

$$V \partial_t \langle n \rangle_{FS} + \partial_r (V \langle \Gamma^r \rangle_{FS}) = 0$$

D.1.2 Energy conservation

The conservation equation of energy is obtained by replacing \bar{f} by $\bar{f}\bar{H}$ in equation (D.1) where $\bar{H} = \frac{1}{2}mv_{\parallel}^2 + \mu B + e\bar{\phi}$ stands for the hamiltonian with $\bar{\phi} = J_0\phi$, J_0 being the gyroaverage operator. We then integrate this equation in velocity space. It comes:

$$\int \frac{\partial \bar{f}}{\partial t} \bar{H} d^3v + \int \frac{1}{B_{\parallel}^*} \nabla_z \left(\dot{z} B_{\parallel}^* \bar{f} \bar{H} \right) d^3v = 0$$

- The calculation of the first integral I_1 gives:

$$\begin{aligned} I_1 &= \frac{\partial}{\partial t} \int \bar{f} \bar{H} d^3v - \int e \bar{f} \partial_t \bar{\phi} d^3v \\ &= \frac{\partial \mathcal{E}}{\partial t} + \int e \bar{\phi} \partial_t \bar{f} d^3v \\ &= \frac{\partial \mathcal{E}}{\partial t} + e \bar{\phi} \partial_t n \end{aligned}$$

where $\mathcal{E} = \frac{1}{2}mv_{\parallel}^2 + \mu B$ stands for the total energy of gyrocentres.

- The calculation of the second integral I_2 gives:

$$I_2 = \int \frac{d^3v}{B_{\parallel}^*} \left[\nabla \cdot \left(\dot{\mathbf{x}} B_{\parallel}^* \bar{f} \bar{H} \right) + \partial_{v_{\parallel}} \left(\dot{v}_{\parallel} B_{\parallel}^* \bar{f} \bar{H} \right) + \partial_{\mu} \left(\dot{\mu} B_{\parallel}^* \bar{f} \bar{H} \right) \right]$$

Like the conservation of particle, the two last terms are equal to 0. The integral I_2 then reduces to:

$$I_2 = \nabla \cdot \int d^3v \dot{\mathbf{x}} \bar{f} \left(\frac{1}{2}mv^2 + e\bar{\phi} \right) = \nabla \cdot \mathbf{Q} + \nabla \cdot (e\bar{\phi}\mathbf{\Gamma})$$

where $\mathbf{Q} = \frac{1}{2}m \int d^3v \dot{\mathbf{x}} v^2 \bar{f}$ stands for the kinetic energy flux.

Consequently, the conservation equation for energy takes the form:

$$\frac{\partial \mathcal{E}}{\partial t} + \nabla \cdot \mathbf{Q} + e\bar{\phi} \partial_t n + \nabla \cdot (e\bar{\phi}\mathbf{\Gamma}) = 0 \quad (\text{D.5})$$

Besides, $\nabla \cdot (e\bar{\phi}\mathbf{\Gamma}) = e\mathbf{\Gamma} \cdot \nabla \bar{\phi} + e\bar{\phi} \nabla \cdot \mathbf{\Gamma} = e\mathbf{\Gamma} \cdot \nabla \bar{\phi} - e\bar{\phi} \partial_t n$ due to matter conservation (D.2). Thus, the conservation equation of energy writes:

$$\begin{aligned} \frac{\partial \mathcal{E}}{\partial t} + \nabla \cdot \mathbf{Q} &= -e\mathbf{\Gamma} \cdot \nabla \bar{\phi} \\ &= -e \int d^3v (\mathbf{v}_{\parallel} + \mathbf{v}_E + \mathbf{v}_D) \cdot \nabla \bar{\phi} \bar{f} \end{aligned} \quad (\text{D.6})$$

where $v_{G\parallel}$ is the parallel gyrocentre velocity, v_E is the electric gyrocentre drift, v_D is the magnetic gyrocentre drift, J_0 is the gyroaverage operator. Averaging this equation on a flux surface in the same way it has been made for matter conservation, it comes:

$$V \partial_t \langle \mathcal{E} \rangle_{FS} + \partial_{\chi} (V \langle Q^{\chi} \rangle_{FS}) = -e \left\langle \int d^3v (\mathbf{v}_{\parallel} + \mathbf{v}_E + \mathbf{v}_D) \cdot \nabla \bar{\phi} \bar{f} \right\rangle_{FS} \quad (\text{D.7})$$

The right hand side term can also be written as $+\int \mathbf{J} \cdot \mathbf{E} d^3v$ using the notations $\mathbf{J} = e\mathbf{v}$ and $\mathbf{E} = -\nabla\bar{\phi}$. This term, computed as the opposite of the time derivative of the electromagnetic potential energy, corresponds to the power transferred from the electric wave to the particles. Three contributions to this term can be identified:

- The parallel contribution $\int \mathbf{J}_{\parallel} \cdot \mathbf{E} d^3v$
- The electric contribution $\int \mathbf{J}_E \cdot \mathbf{E} d^3v$
- The magnetic contribution $\int \mathbf{J}_D \cdot \mathbf{E} d^3v$

Of these three contributions, only the $\mathbf{J}_D \cdot \mathbf{E}$ term is retained, the others being negligible as shown below.

Electric contribution

The electric term appearing in the right hand side of Eq.(D.7) reads:

$$\begin{aligned} \int \mathbf{J}_E \cdot \mathbf{E} d^3v &= -e \int d^3v \mathbf{v}_E \cdot \nabla\bar{\phi} \bar{f} \\ &= e \int d^3v \frac{\nabla\bar{\phi} \wedge \mathbf{B}}{B^2} \cdot \nabla\bar{\phi} \bar{f} = 0 \end{aligned}$$

Therefore, the electric contribution is always vanishing.

Parallel contribution

The right hand side of equation (D.7) can be written as:

$$\int \mathbf{J} \cdot \mathbf{E} d^3v = \int \mathbf{J}_{\parallel} \cdot \mathbf{E} d^3v + \int \mathbf{J}_{\perp} \cdot \mathbf{E} d^3v$$

We want to know which of the parallel or the perpendicular contributions is dominant. The parallel and transverse electric field can be evaluated as:

$$\begin{aligned} E_{\parallel} &= -\nabla_{\parallel}\phi \simeq k_{\parallel}\rho^* \frac{T}{e} \\ \|\mathbf{E}_{\perp}\| &= \|\nabla_{\perp}\phi\| \simeq k_{\perp}\rho^* \frac{T}{e} \end{aligned}$$

where $k_{\parallel} \sim 1/qR$ is the parallel wave vector, k_{\perp} is the transverse wave vector, ρ_L being the Larmor radius, $\rho^* = \rho_i/a \sim e\phi/T$ is the ratio between the ion Larmor radius and the small tokamak ratio and T is the temperature supposed isotropic. The parallel and transverse velocity can be evaluated as:

$$\begin{aligned} v_{\parallel} &\rightarrow M_{\parallel}v_{th} \\ v_{\perp} &\rightarrow v_D \simeq \frac{p}{eBR} \simeq \rho^* \frac{a}{R} v_{th} \end{aligned}$$

with M_{\parallel} the Mach number in the parallel direction and $p \simeq m v_{th}^2$ the pressure. Thus, the ratio between the parallel and transverse contribution to the right hand side of equation (D.7) is:

$$\frac{\int \mathbf{J}_{\parallel} \cdot \mathbf{E} d^3v}{\int \mathbf{J}_{\perp} \cdot \mathbf{E} d^3v} \simeq \frac{M_{\parallel} v_{th} E_{\parallel}}{\rho^*(a/R) v_{th} E_{\perp}} \simeq \frac{M_{\parallel}}{\rho^*(a/R)} \frac{1/qR}{k_{\perp}} = \frac{M_{\parallel}}{q k_{\perp} \rho_i} \ll 1$$

This ratio is small enough to neglect the parallel contribution compared to transverse one.

Removing the electric and parallel contributions, Eq.(D.7) eventually reads:

$$V \partial_t \langle \mathcal{E} \rangle_{FS} + \partial_{\chi} (V \langle Q^{\chi} \rangle_{FS}) = -e \left\langle \int d^3v \mathbf{v}_D \cdot \nabla \bar{\phi} \bar{f} \right\rangle_{FS} \quad (\text{D.8})$$

D.2 The ω_H mode and the kinetic Alfvén wave

In the absence of perpendicular gradients, the dispersion relation giving the real pulsation of the kinetic Alfvén wave reads [74, Scott 1997]:

$$\Omega^2 = \kappa_{\parallel}^2 \frac{1 + \kappa_{\perp}^2}{\hat{\beta} + \hat{\mu} \kappa_{\perp}^2}$$

$$\text{where } \begin{cases} \hat{\beta} &= 4\pi \frac{nT_e}{B^2} \left(\frac{qR}{L_{\perp}}\right)^2 = \left(\frac{c_s/L_{\perp}}{v_A/qR}\right)^2 \\ \hat{\mu} &= \frac{nT_e}{B^2} \left(\frac{qR}{L_{\perp}}\right)^2 = \left(\frac{c_s/L_{\perp}}{v_{th,e}/qR}\right)^2 \\ \kappa_{\perp} &= k_{\perp} \rho_s \quad \kappa_{\parallel} = qR k_{\parallel} \quad \Omega = \omega \frac{L_{\perp}}{c_s} \end{cases}$$

where L_{\perp} is a characteristic wavelength perpendicular to the magnetic field. Using non-normalized notations the pulsation of the kinetic Alfvén wave is recast as:

$$\omega^2 = k_{\parallel}^2 v_A^2 \frac{1 + k_{\perp}^2 \rho_i^2}{1 + k_{\perp}^2 \delta_e^2} \quad (\text{D.9})$$

where the Alfvén velocity v_A and the electron skin depth δ_e have been defined as:

$$v_A = \frac{B}{\sqrt{\mu_0 n m_i}} \quad ; \quad \delta_e = \frac{c_s}{\omega_{pe}} = \sqrt{\frac{m_e}{\mu_0 n e^2}}$$

In the electrostatic limit $\beta = nT/(B^2/2\mu_0) \ll 1$, it comes:

$$k_{\perp}^2 \delta_e^2 = 2k_{\perp}^2 \rho_s^2 \frac{m_e}{m_i} \frac{1}{\beta} \gg 1 \quad (\text{D.10})$$

In that case, the dispersion relation Eq.(D.9) becomes:

$$\omega^2 \simeq \left(\frac{k_{\parallel}}{k_{\perp}}\right)^2 \left(\frac{v_A}{\delta_e}\right)^2 (1 + k_{\perp}^2 \rho_i^2) \quad \text{where} \quad \left(\frac{v_A}{\delta_e}\right)^2 = \left(\frac{v_{th,e}}{\rho_s}\right)^2 = \frac{e^2 B^2}{m_e m_i}$$

The solution of the dispersion relation of kinetic Alfvén modes in the electrostatic limit is the so-called ω_H mode:

$$\omega_H^2 = \omega_{ci}^2 \left(\frac{k_{\parallel}}{k_{\perp}}\right)^2 \frac{m_i}{m_e} (1 + k_{\perp}^2 \rho_i^2) \quad (\text{D.11})$$

However, we notice that the condition (D.10) on β is rarely satisfied in tokamaks. As a consequence, taking into account the electromagnetic effects at finite β ($\gtrsim k_{\perp}^2 \rho_i^2 m_e/m_i \sim 5 \cdot 10^{-5}$) naturally eliminates this mode ω_H and replaces it with the kinetic Alfvén wave.

D.3 Aliasing and Nyquist frequency

Let's consider a continuous signal of time t , $x(t)$, characterized by a bounded frequency Fourier spectrum $\hat{x}(f)$ (see Fig. D.1):

$$|\hat{x}(f)| \equiv \left| \int_{-\infty}^{+\infty} dt x(t) e^{2i\pi ft} \right| = 0 \quad \text{for } |f| > f_{max}$$

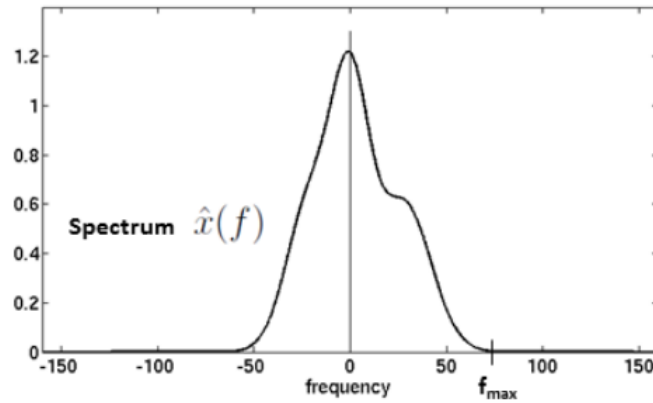


Figure D.1: Fourier spectrum of the continuous signal $x(t)$: $\hat{x}(f)$.

The signal is now sampled at the frequency $f_s = \tau^{-1}$, so that the sampled signal $x_s(t)$ reads as follows:

$$x_s(t) = x(t) \sum_{n=-\infty}^{+\infty} \tau \delta(t - n\tau)$$

It follows that the Fourier transform (denoted FT) $\hat{x}_s(f)$ of the sampled signal is the convolution of $\hat{x}(f)$ by the Fourier transform of the Dirac comb:

$$\begin{aligned} \hat{x}_s(f) &= \hat{x}(f) \star \text{FT} \left[\sum_{n=-\infty}^{+\infty} \tau \delta(t - n\tau) \right] \\ &= \hat{x}(f) \star \sum_{k=-\infty}^{+\infty} \delta(f - kf_s) \\ &= \sum_{k=-\infty}^{+\infty} \hat{x}(f - kf_s) \end{aligned}$$

It readily appears that, in between the frequencies $-f_{max}$ and $+f_{max}$, the two spectra $\hat{x}(f)$ and $\hat{x}_s(f)$ will differ from each other if the sampling frequency f_s is smaller than $2f_{max}$. In other words, any frequency component of the original signal above $f_s/2$ is indistinguishable from a lower frequency component, called an alias, associated with one of the copies (blue dashed curves on Fig. D.2). $f_s/2$ is called the Nyquist frequency.

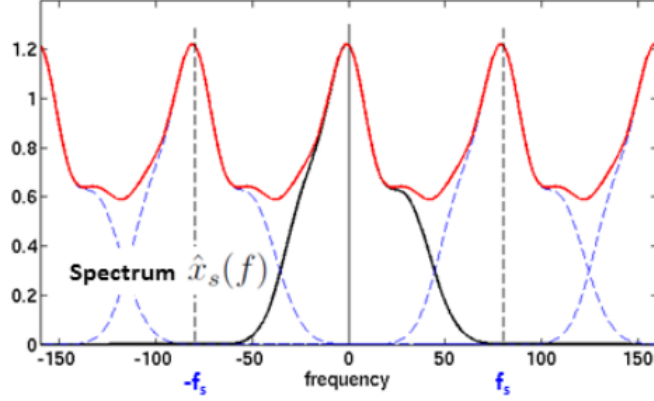


Figure D.2: Red curve: Fourier spectrum of the discretized signal $x_s(t)$: $\hat{x}_s(f)$. Blue dashed curves: copies (aliases) of the original spectrum, shifted by kf_s ($k \in \mathbb{Z}$).

Remark: The reason for such a statement can be understood easily. Let's consider the signal sampled at the frequency $f_s = 1/\tau$. Then $x_{s1}(n\tau) = x_1(n\tau) = \hat{x} \sin(2\pi f_1 n\tau + \varphi)$ with $n \in \mathbb{Z}$. Let $x_2(t)$ be a signal of same amplitude and phase as $x_1(t)$, but of frequency f_2 such that $f_2 = f_1 + kf_s$ with $k \in \mathbb{Z}$: $x_2(t) = \hat{x} \sin(2\pi f_2 t + \varphi)$. When sampled at frequency f_s , $x_2(t)$ will then be indistinguishable from $x_1(t)$, sampled at the same frequency. Indeed, $x_{s2}(n\tau) = x_2(n\tau) = \hat{x} \sin(2\pi f_1 n\tau + \varphi + 2\pi nk)$.

D.4 Kinetic response of electrons close to resonance surfaces

We want to show that the behaviour of kinetic electrons close to resonance surfaces $k_{\parallel} = 0$ is different from the one with adiabatic electrons. The idea here is to determine the position of the resonance due to the kinetic part in the electron density. The fluctuation of the electron density $\tilde{n}_e = n_e - n_{e,eq}$, calculated from Eq.(4.22), can be evaluated as:

$$\left(\frac{\widehat{\tilde{n}_e}}{n_e} \right) \simeq \frac{e\widehat{\phi}}{T} \left[1 - \underbrace{\left\langle \frac{\omega - \omega_e^*}{\omega - k_{\parallel} v_{\parallel e} - \omega_{De}} \right\rangle}_{\text{non-adiabatic part}} \right] \quad (\text{D.12})$$

where $\widehat{\dots}$ stands for the Fourier transform in action-angle variables and $\langle \dots \rangle = \int d^3v \dots F_{eq}$ with F_{eq} a Maxwellian distribution function and $\omega_{De} \sim \mathbf{k}_{\perp} \cdot \mathbf{v}_{De}$ is a pulsation linked with the magnetic drifts. The pulsation for an ion turbulence reads:

$$\omega \sim \omega_i^* = (k_{\perp} \rho_i) \frac{v_{th,i}}{L_T} \sim k_{\parallel} v_{th,i}$$

where L_T is a characteristic length of temperature gradients. Besides, we have:

$$\begin{aligned} \omega_e^* &= (k_\perp \rho_e) \frac{v_{th,e}}{L_T} \sim \omega_i^* \quad \text{since} \quad \rho_s v_{th,s} = \frac{T_s}{e_s B} \\ k_\parallel v_{th,e} &= k_\parallel v_{th,i} \sqrt{\frac{m_i}{m_e}} \gg k_\parallel v_{th,i} \end{aligned} \quad (\text{D.13})$$

At this point, two cases can be distinguished depending of the radial position:

- Far from resonance surfaces: $k_\parallel \neq 0$. The term $k_\parallel v_{th,e}$ is greater than ω and the non adiabatic part of Eq.(D.12) vanishes:

$$\frac{\omega - \omega_e^*}{\omega - k_\parallel v_{\parallel e} - \omega_{De}} \sim \frac{\omega_i^*}{k_\parallel v_{th,e}} \sim 0$$

Thus, the adiabatic behaviour is retrieved.

- Close to the resonance surfaces $q \simeq -m/n$: $k_\parallel = \frac{1}{R}(n + m/q) \rightarrow 0$. Therefore, k_\parallel changes from a very high value to zero and there is a particular radial position $r_{m,n} + \delta r_{m,n}$ close to the resonance surface $r_{m,n}$ such that the denominator of the non adiabatic part of Eq.(D.12) vanishes, thus causing the fluctuations of the electron density \tilde{n}_e to diverge.

This last divergence condition is recast as $k_\parallel(r_{m,n} + \delta r_{m,n}) v_{th,e} = \omega_i^* - \omega_{De} \simeq \omega_i^* \sim \omega_e^*$. It is possible from this relation to give an approximated expression of $\delta r_{m,n}$. Developing k_\parallel around the position $r_{m,n}$, it comes:

$$k_\parallel(r_{m,n} + \delta r_{m,n}) = k_\parallel(r_{m,n}) + \delta r_{m,n} \left. \frac{dk_\parallel}{dr} \right|_{r_{m,n}}$$

Since $k_\parallel(r_{m,n}) = 0$ and using the expression of ω_e^* Eq.(D.13), the resonance condition reads:

$$\delta r_{m,n} \left. \frac{dk_\parallel}{dr} \right|_{r_{m,n}} \simeq (k_\perp \rho_e) \frac{v_{th,e}}{L_T}$$

The radial derivative of k_\parallel reads $d_r k_\parallel \simeq -\frac{m}{qR} \frac{dq}{q dr} = k_\theta s / (qR)$ with $s = r d_r q / q$ is the magnetic shear. Therefore, the radial extension of the zone around a resonance surface where the response of electrons is kinetic reads as:

$$|\delta r_{m,n}| \simeq \left| \frac{k_\perp}{k_\theta} \right| \frac{q}{s} \frac{R}{L_T} \rho_e \simeq \frac{q}{s} \frac{R}{L_T} \rho_e$$

We have $L_T \sim a$ and $q/s \sim 1$ in the core plasma. This causes $\delta r_{m,n} \sim \rho_e$. Thus, in a kinetic electron model, the kinetic effects of electrons are expected to be localized near the resonance surfaces and to have a width of the order of a few ρ_e . An analysis of these fine radial structures in the GENE code can be found in [23, Dominski 2015]. It should be pointed out that this kinetic signature can be explained only if the ratio m_i/m_e is big enough. However, as the TEM resonance does not depend on the mass ratio, simulated plasmas using small mass ratio $m_i/m_e = 100$ can still show some physical behaviour.

Bibliography

- [1] Jérémie Abiteboul. Transport turbulent et néoclassique de quantité de mouvement toroidale dans les plasmas de tokamak. PhD thesis, Université d'Aix-Marseille, 2012.
- [2] P. Angelino, A. Bottino, and R. Hatzky *et al.* On the definition of a kinetic equilibrium in global gyrokinetic simulations. Physics of Plasmas, 13:052304, 2006.
- [3] Hugo Arnichand. Identification of Trapped Electron Modes in Frequency Fluctuation Spectra of fusion plasmas. PhD thesis, Université d'Aix-Marseille, 2015.
- [4] Y. Asahi, A. Ishizawa, T.-H. Watanabe, H. Tsutsui, and S. Tsuji-Iio. Regulation of electron temperature gradient turbulence by zonal flows driven by trapped electron modes. Physics of Plasmas, 21(5):052306, 2014.
- [5] Yuuichi Asahi, Virginie Grandgirard, Yasuhiro Idomura, Xavier Garbet, Guillaume Latu, Yanick Sarazin, Guilhem Dif-Pradalier, Peter Donnel, and Charles Ehrlacher. Benchmarking of flux-driven full-f gyrokinetic simulations. Physics of Plasmas, 24(10):102515, 2017.
- [6] ITER Physics Basis. Chapter 2: Plasma confinement and transport. Nuclear Fusion, 47(S18), 2007.
- [7] A. Biancalani, A. Bottino, C. Ehrlacher, V. Grandgirard, G. Merlo, I. Novikau, Z. Qiu, E. Sonnendrücker, X. Garbet, T. Görler, S. Leerink, F. Palermo, and D. Zarzoso. Cross-code gyrokinetic verification and benchmark on the linear collisionless dynamics of the geodesic acoustic mode. Physics of Plasmas, 24(6):062512, 2017.
- [8] A. Bottino, B. Scott, S. Brunner, B.F. McMillan, T.M. Tran, T. Vernay, L. Villard, S. Jolliet, R. Hatzky, and A.G. Peeters. Global nonlinear electromagnetic simulations of tokamak turbulence. Plasma Science, IEEE Transactions on, 38(9):2129 –2135, 2010.
- [9] A Bottino, T Vernay, B Scott, S Brunner, R Hatzky, S Jolliet, B F McMillan, T M Tran, and L Villard. Global simulations of tokamak microturbulence: finite-beta effects and collisions. PPCF, 53(12):124027, 2011.
- [10] Clarisse Bourdelle. Analyse de stabilité de plasmas de tokamak. PhD thesis, 2000.

- [11] A.J. Brizard and T.S. Hahm. Foundations of nonlinear gyrokinetic theory. Rev. Mod. Phys., 79(2):421–468, Apr 2007.
- [12] J. Candy and R.E. Waltz. An eulerian gyrokinetic-maxwell solver. JOCP, 186(2):545–581, 2003.
- [13] Y. Chen, S.E. Parker, B.I. Cohen, A.M. Dimits, W.M. Nevins, D. Shumaker, V.K. Decyk, and J.N. Leboeuf. Simulations of turbulent transport with kinetic electrons and electromagnetic effects. Nuclear Fusion, 43(10):1121, 2003.
- [14] Yang Chen and Scott Parker. Gyrokinetic turbulence simulations with kinetic electrons. Physics of Plasmas, 8(5):2095–2100, 2001.
- [15] Yang Chen and Scott E. Parker. A π particle method for gyrokinetic simulations with kinetic electrons and electromagnetic perturbations. Journal of Computational Physics, 189(2):463 – 475, 2003.
- [16] J. W. Connor, R. J. Hastie, and J. B. Taylor. High mode number stability of an axisymmetric toroidal plasma. Proceedings of the Royal Society of London A: Mathematical, Physical and Engineering Sciences, 365(1720):1–17, 1979.
- [17] G. D. Conway, C. Angioni, F. Ryter, P. Sauter, and J. Vicente. Mean and oscillating plasma flows and turbulence interactions across the $l-h$ confinement transition. Phys. Rev. Lett., 106:065001, Feb 2011.
- [18] B. Coppi, M. N. Rosenbluth, and R. Z. Sagdeev. Instabilities due to temperature gradients in complex magnetic field configurations. The Physics of Fluids, 10(3):582–587, 1967.
- [19] Tilman Dannert and Frank Jenko. Gyrokinetic simulation of collisionless trapped-electron mode turbulence. Physics of Plasmas, 12(7):072309, 2005.
- [20] Richard E. Denton and M. Kotschenreuther. Δf algorithm. Journal of Computational Physics, 119(2):283–294, 1995.
- [21] G. Dif-Pradalier, V. Grandgirard, Y. Sarazin, X. Garbet, Ph. Ghendrih, and P. Angelino. On the influence of initial state on gyrokinetic simulations. Physics of Plasmas, 15(4):042315, 2008.
- [22] Andris M. Dimits. Gyrokinetic equations in an extended ordering. Physics of Plasmas, 17(5):055901, 2010.
- [23] J. Dominski, S. Brunner, T. Görler, F. Jenko, D. Told, and L. Villard. How non-adiabatic passing electron layers of linear microinstabilities affect turbulent transport. Physics of Plasmas, 22(6):062303, 2015.

- [24] J. Dominski, B. F. McMillan, S. Brunner, G. Merlo, T.-M. Tran, and L. Villard. An arbitrary wavelength solver for global gyrokinetic simulations. application to the study of fine radial structures on microturbulence due to non-adiabatic passing electron dynamics. Physics of Plasmas, 24(2):022308, 2017.
- [25] W. Dorland, F. Jenko, M. Kotschenreuther, and B.N. Rogers. Electron temperature gradient turbulence. Physics Review Letters, (85):5579–5582, 2000.
- [26] T. Drouot, E. Gravier, T. Reveille, M. Sarrat, M. Collard, P. Bertrand, T. Cartier-Michaud, P. Ghendrih, Y. Sarazin, and X. Garbet. Global gyrokinetic simulations of trapped-electron mode and trapped-ion mode microturbulence. Physics of Plasmas, 22(8):082302, 2015.
- [27] Thomas Drouot, Etienne Gravier, Thierry Reveille, Alain Ghizzo, Pierre Bertrand, Xavier Garbet, Yanick Sarazin, and Thomas Cartier-Michaud. A gyro-kinetic model for trapped electron and ion modes. The European Physical Journal D, 68(10):280, Oct 2014.
- [28] Damien Estève. Etude gyrocinétique du transport multi-espèces néoclassique et turbulent dans un plasma de fusion. PhD thesis, Université d’Aix-Marseille, 2015.
- [29] F. Y. Gang, P. H. Diamond, and M. N. Rosenbluth. A kinetic theory of trapped?electron?driven drift wave turbulence in a sheared magnetic field. Physics of Fluids B: Plasma Physics, 3(1):68–86, 1991.
- [30] X Garbet. Instabilités, turbulence et transport dans un plasma magnétisé. Habilitation dissertation, University of Marseille, France, 2001.
- [31] X. Garbet, G. Dif-Pradalier, C. Nguyen, Y. Sarazin, V. Grandgirard, and P. Ghendrih. Neoclassical equilibrium in gyrokinetic simulations. PoP, 16(6):062503, 2009.
- [32] X. Garbet, P. Donnel, C. Ehrlacher, E. Caschera, R. Dumont, M. Faganello, V. Grandgirard, P. Ghendrih, M. Idouakass, M. Lesur, Y. Sarazin, and D. Zarzoso. On the relationship between residual zonal flows and bump-on tail saturated instabilities. Journal of Physics: Conference Series, 775(1):012004, 2016.
- [33] X. Garbet, L. Garzotti, P. Mantica, H. Nordman, M. Valovic, H. Weisen, and C. Angioni. Turbulent particle transport in magnetized plasmas. Phys. Rev. Lett., 91:035001, Jul 2003.
- [34] X Garbet, P Mantica, C Angioni, E Asp, Y Baranov, C Bourdelle, R Budny, F Crisanti, G Cordey, L Garzotti, N Kirneva, D Hogeweyj, T Hoang, F Imbeaux, E Joffrin, X Litaudon, A Manini, D C McDonald, H Nordman, V Parail, A Peeters, F Ryter, C Sozzi, M Valovic, T Tala, A Thyagaraaja, I Voitsekhovitch, J Weiland, H Weisen, A Zabolotsky, and the JET EFDA Contributors. Physics of transport in tokamaks. Plasma Physics and Controlled Fusion, 46(12B):B557, 2004.
- [35] P. Ghendrih. Cours de Master 2 - Plasmas de Bords. 2014.

- [36] Jean-Baptiste Girardo. Control of instabilities and turbulence by fast particles in fusion plasmas. PhD thesis, Ecole Polytechnique, 2015.
- [37] James Glanz. Turbulence may sink titanic reactor. Science, 274(5293):1600, 1996.
- [38] H. Goldstein, C. Poole, and J. Safko. Classical Mechanics. Addison-Wesley, San Francisco, 3rd edition, 2002.
- [39] Robert J Goldston and Paul Harding Rutherford. Introduction to plasma physics. CRC Press, 1995.
- [40] V. Grandgirard, J. Abiteboul, J. Bigot, T. Cartier-Michaud, N. Crouseilles, G. Dif-Pradalier, Ch. Ehrlacher, D. Esteve, X. Garbet, Ph. Ghendrih, G. Latu, M. Mehrenberger, C. Norscini, Ch. Passeron, F. Rozar, Y. Sarazin, E. Sonnendrücker, A. Strugarek, and D. Zarzoso. A 5d gyrokinetic full-f global semi-lagrangian code for flux-driven ion turbulence simulations. Computer Physics Communications, 207:35 – 68, 2016.
- [41] E. Gravier, M. Lesur, T. Reveille, and T. Drouot. Stimulated zonal flow generation in the case of tem and tim microturbulence. Physics of Plasmas, 23(9):092507, 2016.
- [42] Etienne Gravier. Etude expérimentale des régimes dynamiques des ondes de dérive dans un plasma magnétisé de laboratoire. Contrôle du chaos spatio-temporel. PhD thesis, Université de Lorraine, 1999.
- [43] Martin Greenwald. Density limits in toroidal plasmas. Plasma Physics and Controlled Fusion, 44(8):R27, 2002.
- [44] G W Hammett, M A Beer, W Dorland, S C Cowley, and S A Smith. Developments in the gyrofluid approach to tokamak turbulence simulations. Plasma Physics and Controlled Fusion, 35(8):973, 1993.
- [45] F. Hariri and M. Ottaviani. A flux-coordinate independent field-aligned approach to plasma turbulence simulations. Computer Physics Communications, 184(11):2419 – 2429, 2013.
- [46] Akira Hasegawa and Masahiro Wakatani. Plasma edge turbulence. Phys. Rev. Lett., 50:682–686, Feb 1983.
- [47] R.D. Hazeltine and J.D. Meiss. Plasma confinement. Dover publication, 2003.
- [48] P Helander, C D Beidler, T M Bird, M Drevlak, Y Feng, R Hatzky, F Jenko, R Kleiber, J H E Proll, Yu Turkin, and P Xanthopoulos. Stellarator and tokamak plasmas: a comparison. Plasma Physics and Controlled Fusion, 54(12):124009, 2012.
- [49] P. Helander and D.J. Sigmar. Collisional Transport in Magnetized Plasmas. Cambridge university press, 2002.
- [50] S. Ichimaru. Basic Principles of Plasma Physics. Frontiers in physics, 1973.

- [51] Y. Idomura. A new hybrid kinetic electron model for full-f gyrokinetic simulations. Journal of Computational Physics, 313:511 – 531, 2016.
- [52] Y. Idomura, S. Tokuda, and Y. Kishimoto. Global gyrokinetic simulation of ion temperature gradient driven turbulence in plasmas using a canonical maxwellian distribution. Nuclear Fusion, 43(4):234, 2003.
- [53] F. Jenko, W. Dorland, M. Kotschenreuther, and B. N. Rogers. Electron temperature gradient driven turbulence. Physics of Plasmas, 7(5):1904–1910, 2000.
- [54] B. B. Kadomtsev and O. P. Pogutse. Turbulence in Toroidal Systems, volume 5, page 249. Springer US, Boston, MA, 1970.
- [55] M. D. Kruskal and R. M. Kulsrud. Equilibrium of a magnetically confined plasma in a toroid. The Physics of Fluids, 1(4):265–274, 1958.
- [56] Ming-Chih Lai. A note on finite difference discretizations for poisson equation on a disk. Numerical Methods for Partial Differential Equations, 17(3):199–203, 2001.
- [57] Guillaume Latu, Michel Mehrenberger, Yaman Güçlü, Maurizio Ottaviani, and Eric Sonnendrücker. Field-aligned interpolation for semi-lagrangian gyrokinetic simulations. Journal of Scientific Computing, 74(3):1601–1650, Mar 2018.
- [58] J D Lawson. Some criteria for a power producing thermonuclear reactor. Proceedings of the Physical Society. Section B, 70(1):6, 1957.
- [59] W. W. Lee. Gyrokinetic approach in particle simulation. Physics of Fluids, 26(2):556–562, 1983.
- [60] Paulett C. Liewer. Measurements of microturbulence in tokamaks and comparisons with theories of turbulence and anomalous transport. Nuclear Fusion, 25(5):543, 1985.
- [61] Robert G. Littlejohn. Variational principles of guiding centre motion. Journal of Plasma Physics, 29(1):111–125, 1983.
- [62] F. Merz and F. Jenko. Nonlinear saturation of trapped electron modes via perpendicular particle diffusion. Phys. Rev. Lett., 100:035005, Jan 2008.
- [63] F. Merz and F. Jenko. Nonlinear interplay of tem and itg turbulence and its effect on transport. Nuclear Fusion, 50(5):054005, 2010.
- [64] C. Nguyen, X. Garbet, and A. I. Smolyakov. Variational derivation of the dispersion relation of kinetic coherent modes in the acoustic frequency range in tokamaks. Physics of Plasmas, 15(11):112502, 2008.
- [65] Christine Nguyen. Magneto-hydrodynamic activity and energetic particles : application to Beta Alfvén Eigenmodes. PhD thesis, 2009. Thèse de doctorat dirigée par Garbet, Xavier Physique des plasmas Palaiseau, Ecole polytechnique 2009.

- [66] D. R. Nicholson. Introduction to Plasma Theory. Wiley, 1983.
- [67] M. Ottaviani. An alternative approach to field-aligned coordinates for plasma turbulence simulations. Physics Letters A, 375(15):1677 – 1685, 2011.
- [68] J.-M. Rax. Physique des Tokamaks. Les Editions de l'Ecole Polytechnique - Ellipses, 2012.
- [69] G. Rewoldt, Z. Lin, and Y. Idomura. Linear comparison of gyrokinetic codes with trapped electrons. Computer Physics Communications, 177(10):775 – 780, 2007.
- [70] F. Romanelli and F. Zonca. The radial structure of the ion-temperature-gradient-driven mode. Physics of Fluids B: Plasma Physics, 5(11):4081–4089, 1993.
- [71] M.N. Rosenbluth and F.L. Hinton. Poloidal flow driven by ion-temperature-gradient turbulence in tokamaks. Physical Review Letters, 80(4), 1998.
- [72] Y. Sarazin. Cours de Master 2 - Turbulence et Transport. 2013.
- [73] Y. Sarazin, V. Grandgirard, J. Abiteboul, S. Allfrey, X. Garbet, Ph. Ghendrih, G. Latu, A. Strugarek, G. Dif-Pradalier, P.H. Diamond, S. Ku, C.S. Chang, B.F. McMillan, T.M. Tran, L. Villard, S. Jolliet, A. Bottino, and P. Angelino. Predictions on heat transport and plasma rotation from global gyrokinetic simulations. Nuclear Fusion, 51(10):103023, 2011.
- [74] B Scott. Three-dimensional computation of drift alfvén turbulence. Plasma Physics and Controlled Fusion, 39(10):1635, 1997.
- [75] H. Sugama and T.H. Watanabe. Collisionless damping of geodesic acoustic modes. Journal of Plasma Physics, 74(1):139–140, 2006.
- [76] H. Sugama and T.H. Watanabe. Collisionless damping of geodesic acoustic modes. Journal of Plasma Physics, 74(1):139–140, 2008.
- [77] R. E. Waltz, J. Candy, and M. Fahey. Coupled ion temperature gradient and trapped electron mode to electron temperature gradient mode gyrokinetic simulations. Physics of Plasmas, 14(5):056116, 2007.
- [78] R. E. Waltz, G. D. Kerbel, and J. Milovich. Toroidal gyro-landau fluid model turbulence simulations in a nonlinear ballooning mode representation with radial modes. Physics of Plasmas, 1(7):2229–2244, 1994.
- [79] J. Weiland and A. Hirose. Electromagnetic and kinetic effects on the ion temperature gradient mode. Nuclear Fusion, 32(1):151, 1992.
- [80] Niels Winsor, John L. Johnson, and John M. Dawson. Geodesic acoustic waves in hydromagnetic systems. The Physics of Fluids, 11(11):2448–2450, 1968.

- [81] D. Zarzoso, X. Garbet, Y. Sarazin, R. Dumont, and V. Grandgirard. Fully kinetic description of the linear excitation and nonlinear saturation of fast-ion-driven geodesic acoustic mode instability. Physics of Plasmas, 19(2):022102, 2012.
- [82] D. Zarzoso, Y. Sarazin, X. Garbet, R. Dumont, A. Strugarek, J. Abiteboul, T. Cartier-Michaud, G. Dif-Pradalier, Ph. Ghendrih, V. Grandgirard, G. Latu, C. Passeron, and O. Thomine. Impact of energetic-particle-driven geodesic acoustic modes on turbulence. Phys. Rev. Lett., 110:125002, Mar 2013.
- [83] H. S. Zhang and Z. Lin. Trapped electron damping of geodesic acoustic mode. Physics of Plasmas, 17(7):072502, 2010.
- [84] F. Zonca and L. Chen. Radial structures and nonlinear excitation of geodesic acoustic modes. EPL (Europhysics Letters), 83(3):35001, 2008.
- [85] Fulvio Zonca, Liu Chen, and Robert A Santoro. Kinetic theory of low-frequency alfvén modes in tokamaks. Plasma Physics and Controlled Fusion, 38(11):2011, 1996.

Titre : Contribution des électrons cinétiques dans les plasmas de Tokamak

Mots clés : Plasmas, Tokamak, Gyrocinétique

Résumé : Les plasmas de fusion par confinement magnétique sont le siège d'instabilités qui développent des structures turbulentes d'échelles milli- à centi-métriques. Le transport qui en résulte contrôle le temps de confinement de l'énergie et, in fine, les performances énergétiques.

Dans les régimes de confinement non améliorés, c'est une turbulence à l'échelle ionique qui domine ce transport. Cette turbulence est portée par les ions, mais également par une certaine classe d'électrons, ceux qui sont piégés dans les miroirs locaux du champ magnétique. Il est de fait important de prendre en compte leur dynamique, d'autant plus qu'ils sont également responsables du transport de matière.

L'objectif de la thèse consiste à étudier l'impact des électrons d'une part, sur l'amortissement des "Geodesic Acoustic Modes" (GAM) d'une part, et sur la croissance linéaire des modes de turbulence "Ion Temperature Gradients" (ITG) et "Trapped Electron Modes" (TEM) d'autre part.

Title : Contribution of kinetic electrons in Tokamak plasmas

Keywords : Plasmas, Tokamak, Gyrokinetic

Abstract : Instabilities, within fusion plasmas by magnetic confinement, develop turbulent structures with milli-centimetric scales. The resulting transport impacts the energy confinement time and, ultimately, the energy performance.

In unimproved confinement regimes, ion-scale turbulence generally dominates this transport. This turbulence is carried by the ions, but also by a certain class of electrons, those trapped in the local mirrors of the magnetic field. Taking into account their dynamics is important, especially since they are also responsible for particle transport.

The aim of this thesis is to study the impact of electrons on the damping of "Geodesic Acoustic Modes" (GAM) on the one hand and the linear growth of the turbulence modes "Ion Temperature Gradients" (ITG) and "Trapped Electron Modes" (TEM) on the other hand.